Dispersion-theoretical analysis of $\pi\pi$ and $\pi\eta$ rescattering effects in strong three-body decays

Dissertation

zur

Erlangung des Doktorgrades (Dr. rer. nat.)

der

Mathematisch-Naturwissenschaftlichen Fakultät

der

Rheinischen Friedrich-Wilhelms-Universität Bonn

vorgelegt von

Tobias Isken

aus

Köln

Bonn, Juli 2021

Angefertigt mit Genehmigung der
Mathematisch-Naturwissenschaftlichen Fakultät der
Rheinischen Friedrich-Wilhelms-Universität Bonn

Diese Dissertation ist auf dem Hochschulschriftenserver der ULB Bonn unter
`https://bonndoc.ulb.uni-bonn.de/xmlui/` elektronisch publiziert.

Promotionskommission

1. PD Dr. Bastian Kubis
2. Prof. Dr. Dr. h.c. Ulf-G. Meißner
3. Prof. Dr. Ulrike Thoma
4. Prof. Dr. Alexander C. Filippou

Tag der Prüfung
29.09.2021

Erscheinungsjahr
2021

Abstract

Employing dispersion theory to analyse hadronic three-body decays is a classic subject. Based on the fundamental physical principles of analyticity and unitarity, dispersion relations exploit basic theorems of complex analysis to provide a mathematical toolkit that describes the analytic structure of the amplitude in terms of integral equations. Since the resummation of the leading final-state rescattering effects among the three decay products is implemented by construction, an application is of particular interest for processes of the strong interaction at low energies, where a perturbative expansion of quantum chromodynamics fails. In this thesis we present a dispersion-theoretical analysis of hadronic three-body decays based on integral equations of the Khuri–Treiman type.

The $\eta' \to \pi\pi\eta$ decay offers several features of interest: due to the small available phase space it can be used to constrain $\pi\eta$ rescattering at low energies, in the soft-pion limit current algebra predicts two Adler zeros in the unphysical region, and the neutral $\eta' \to \pi^0\pi^0\eta$ Dalitz-plot distribution is expected to show a cusp effect at the $\pi^+\pi^-$ threshold. Restricting ourselves to the dominant S-wave discontinuities, our dispersive representation of $\eta' \to \pi\pi\eta$ is based solely on the $\pi\pi$ and $\pi\eta$ S-wave scattering phase shifts. Isospin symmetry dictates that both the charged and neutral decay modes $\eta' \to \pi^+\pi^-\eta/\pi^0\pi^0\eta$ are given in terms of the same amplitude. The subtraction constants contained in the dispersion relation are determined by a fit to experimental data of the $\eta' \to \pi^+\pi^-\eta$ Dalitz-plot distribution from the VES and BESIII collaborations. In accordance with the soft-pion theorem our amplitude exhibits two Adler zeros. We compare the dispersive representation to variants of chiral perturbation theory and provide a prediction for the cusp effect in the $\eta' \to \pi^0\pi^0\eta$ Dalitz-plot distribution.

Patterns of C- and CP-violation from mirror symmetry breaking in the Dalitz-plot distribution of the $\eta \to \pi^+\pi^-\pi^0$ decay offer an ideal arena in the search for physics beyond the standard model. Effects of this kind are particularly interesting as they are not directly constrained by limits on electric dipole moments. Determined by the isospin coupling of the three pions in the final state, the amplitude can be decomposed into an isoscalar, isovector, and isotensor structure. Based on the dispersive framework, we present a consistent description of these isospin amplitudes allowing for contributions of $\pi\pi$ S- and P-waves to the discontinuities. We compare the dispersive representation to experimental data of the $\eta \to \pi^+\pi^-\pi^0/3\pi^0$ Dalitz-plot distributions from the KLOE-2 and A2 collaborations as well as constraints of standard chiral perturbation theory. Furthermore, our dispersion relation allows us to give bounds on effective coupling strengths of the underlying operators beyond the standard model.

Decays of light isoscalar vector mesons into three pions provide an ideal test case for dispersion relations. Due to Bose symmetry only odd partial waves are allowed to contribute, so neglecting discontinuities of F- and higher partial waves, the decay is fully described by the $\pi\pi$ P-wave rescattering effects. In the context of two-body resonances, like the $\rho(770)$, unitarized versions of chiral perturbation theory offer a way to investigate

resonance properties and their quark-mass dependence. Three-body resonances like the $\omega(782)$ cannot be accessed in such a formalism. We study the quark-mass dependence of $\omega \to 3\pi$ decays within the dispersive framework, relying on the $\pi\pi$ P-wave scattering phase shift extracted from unitarized chiral perturbation theory. The described formalism may be used as an extrapolation tool for lattice QCD studies of three-pion decays, for which $\omega \to 3\pi$ serves as a paradigm case.

Parts of this thesis have been published in the following articles:

- T. Isken, B. Kubis, S. P. Schneider and P. Stoffer, *Dispersion relations for $\eta' \to \eta\pi\pi$,* Eur. Phys. J. C **77**, 489 (2017) [arXiv:1705.04339 [hep-ph]].
- M. Dax, T. Isken and B. Kubis, *Quark-mass dependence in $\omega \to 3\pi$ decays,* Eur. Phys. J. C **78**, 859 (2018) [arXiv:1808.08957 [hep-ph]].

Moreover, parts of the material presented in this thesis and their extensions will be published in the forthcoming articles:

- T. Isken, B. Kubis, A. Kupść, and P. Stoffer, *Strong three-body decays of η and η' mesons,* in preparation.
- H. Akdag, T. Isken and B. Kubis, *Patterns of C- and CP-violation in hadronic η and η' three-body decays,* in preparation.

Excerpts of the above have also been published in the following conference proceedings:

- T. Isken, *Dispersion relations for mesonic three-body decays,* PoS **CD2018**, 068 (2019).

Contents

Introduction

Ever since the existence of humanity, the description and prediction of natural phenomena from cosmological scales to the quantum level has been at the heart of our aspiration. In our strive to discover the elementary building blocks of matter and understand the fundamental laws of nature we pushed physics to smaller and smaller dimensions, corresponding to ever increasing energy scales at which theory has to be probed by experiment.

At present it is believed that the fundamental forces mediating interactions between the elementary particles fall into four categories differentiated by their strength: *strong*, *weak*, *electromagnetic*, and *gravity*. Since its formulation in the second half of the 20th century the standard model (SM) of particle physics [1–5] has become the accepted theory unifying three of the fundamental forces (strong, weak, and electromagnetic interactions, excluding gravity) and classifying all known elementary particles. Verified by direct and indirect experimental searches over an energy range of many orders of magnitude, the SM has proven to be extremely successful in describing particle physics processes of the strong and electroweak interactions. By now, it is regarded as one of the best tested theories in physics. However, the SM does not explain gravity and so far a consistent unification with general relativity at the quantum level has not been achieved. Further caveats like the hierarchy problem or its inconsistency with the Lambda-CDM model of cosmology indicate that the SM may only be a part of a more fundamental yet to unravel theory of everything.

As a locally Poincaré and gauge invariant quantum field theory of the underlying symmetry group

$$\mathrm{SU}(3)_C \times \mathrm{SU}(2)_L \times \mathrm{U}(1)_{Y_\mathrm{W}}\,, \tag{1}$$

the SM is founded on the principles of special relativity and quantum mechanics. Each kind of elementary particle is described in terms of its corresponding dynamical field that pervades space-time. These fields lie in different representations of the various symmetry groups of the SM, which define their fundamental properties. The dynamics of the fields are controlled by the Lagrangian of the SM. In its most general form this Lagrangian depends on 19 *a priori* unknown parameters not fixed by theory, whose numerical values have to be determined by experiment.

The matter content of the SM consists of twelve spin-$\frac{1}{2}$ fields (Fermions) obeying the Fermi–Dirac statistics, which can be grouped into six *quark* fields (charged under $\mathrm{SU}(3)_C$, *i.e.*, they interact strongly) and six *lepton* fields (singlets of $\mathrm{SU}(3)_C$, *i.e.*, they do not interact strongly). While all quarks also interact weakly and electromagnetically, the leptons can be further subdivided into electrically charged leptons and neutrinos (they do not carry electric charge, thus they only participate in weak interactions). Both quarks

and leptons are pairwise grouped into three generations or families, with the second and third being an exact copy of the first concerning all quantum numbers except for increasing masses. Each quark and lepton has a corresponding antiparticle.

Apart from the FERMIONIC matter content the SM also contains five elementary fields with integer spin (BOSONS), which respect the BOSE–EINSTEIN statistics. Four spin-1 gauge fields act as carriers of the fundamental forces mediating the interactions of the FERMIONS: the gluon (strong), the W and Z (weak), and the photon (electromagnetic). An auxiliary YUKAWA-type interaction is mediated by the spin-0 HIGGS field, the only elementary scalar field of the SM. Note that BOSONS do not only interact with FERMIONS, but also among themselves.

Due to gauge invariance of the SM, an explicit inclusion of mass terms for the gauge fields is forbidden. Thus, the gluon, the W and Z, as well as the photon are required to be massless. However, it is known from experiment that the W- and Z-BOSONS not only have mass, but are even among the heaviest particles of the SM. This puzzle has been solved by the BROUT–ENGLERT–HIGGS mechanism formulated in 1964 [6–8]. According to this mechanism the masses of the quarks, the electrically charged leptons, as well as the W-, Z-, and HIGGS BOSONS are all generated through the spontaneous breaking of electroweak symmetry

$$\mathrm{SU}(2)_L \times \mathrm{U}(1)_{Y_\mathrm{W}} \to \mathrm{U}(1)_{\mathrm{e.m.}}\,, \tag{2}$$

induced by the non-vanishing vacuum expectation value of the HIGGS field. As its last missing essential piece, the HIGGS particle was experimentally discovered by the ATLAS and CMS collaborations at CERN's Large Hadron Collider in 2012 confirming the SM prediction [9, 10].

The focus of this thesis is on aspects of quantum chromodynamics (QCD) as the theory describing strong interactions. While in the electroweak sector of the SM the framework of perturbation theory allows for precise predictions in the experimentally accessible energy region, the dynamics of strong interactions are still insufficiently understood at low energies as its running coupling constant becomes too large for a perturbative description. At these energies a spectrum of composite *hadrons* emerges, replacing the quarks and gluons as the relevant degrees of freedom of the theory. In order to describe the dynamics of strong interactions in the realm of hadrons alternative solution methods have been developed. Besides the effective field theory approach or simulating QCD on discretized space-time lattices, dispersion theory is one of these alternatives. Founded on the fundamental principles of analyticity and unitarity, dispersion theory exploits the analytic structure of scattering processes and relates them to holomorphic functions of complex variables that can be obtained by solving integral equations. As we will demonstrate exemplarily in this thesis, the three methods mentioned above are not mutually exclusive but are particularly strong in their interplay.

As decay and scattering processes of hadrons allow us to uncover essential information on the structure of QCD and the SM, much has been learned and will be learned by further investigation of these processes in experiment and theory. In this thesis we employ a dispersion-theoretical approach to study hadronic three-body decays. Contrary to two-body decays where the kinematical variables are completely fixed by energy-momentum conservation, the kinematical structure in three-body decays is more involved, making

these decays an ideal testing ground for the dynamics of strong interactions at low energies. In order to obtain a sensible description in the physical decay region of the heavy state, an accurate control over the final-state interactions of the three light decay products is of paramount importance. This can be achieved in a dispersive treatment based on integral equations of the KHURI–TREIMAN type [11]. One of its main virtues is the fact that the most important final-state interactions among the three light decay products are fully taken into account, hence analyticity and two-body unitarity are respected exactly. This becomes the more important, the higher the mass of the decaying heavy particle, and therefore the higher the possible energies of the lighter decay products in the final-state two-body subsystems get.

The outline of this thesis is as follows: in ch. 1 we review the structure of strong interactions at low energies in more detail. This is followed by a short introduction into S-matrix theory and its application in scattering processes discussed in ch. 2. We display the basic concepts of the dispersion-theoretical framework for functions with one cut in ch. 3, and extend it to functions with two cuts in ch. 4. Applications of these dispersive techniques to hadronic three-body decays in terms of KHURI–TREIMAN-type equations are presented in the final three chapters. In ch. 5 we study the $\eta' \to \pi\pi\eta$ DALITZ-plot distributions and compare our dispersive representation with experimental data, a low-energy theorem, as well as variants of chiral effective theories. We analyze mirror symmetry breaking C- and CP-violating effects of the $\eta \to \pi^+\pi^-\pi^0$ DALITZ-plot distribution in ch. 6 and show how the interference of the underlying isospin amplitudes affect these patterns. A study of the quark-mass dependence of $\omega \to 3\pi$ decays based on the dispersion-theoretical framework is presented in ch. 7. The thesis closes with a short summary and outlook.

Part I

Foundations

Chapter 1

Theory of the strong interaction

QCD as the theory of strong interactions and one of the pillars of the SM is formulated in terms of a non-Abelian Yang–Mills gauge theory of the underlying $SU(3)_C$ symmetry group [5,12,13]. Its fundamental degrees of freedom are the quarks (massive spin-$\frac{1}{2}$ matter fields) and the gluon (massless spin-1 gauge field). The quark fields can be grouped into six different *flavors*: up (u), down (d), strange (s), charm (c), bottom (b), and top (t). Contrary to the theory of quantum electrodynamics (QED), where the uncharged photons mediate the interactions between electrically charged particles, the quarks and gluons are carriers of a $SU(3)_C$ *color charge* (the QCD analog to the electric charge of QED). While free quarks or gluons have never been observed in nature, a spectrum of colorless bound states, so-called hadrons, emerges at low energies, which take the place as relevant degrees of freedom of the strong interaction, *cf.* fig. 1.1.

The mechanism behind this property of QCD is called *color confinement*: the strong force between two color charges does not decrease with distance as one would expect *e.g.* from electromagnetic interactions. Thus the energy required to separate two quarks within a hadron ever increases until a quark–anti-quark pair is spontaneously produced out of the vacuum, resulting in two hadrons instead of an isolated color charge. This mechanism renders QCD strongly coupled at low energies, and thus a perturbative description of interactions between quarks and gluons fails. Although color confinement has not been rigorously proved mathematically, it is well established by lattice QCD simulations and experimental measurements [15]. Its pending analytical proof is one of the seven Millennium Prize Problems stated by the Clay Mathematics Institute [16].

Another peculiarity of QCD is *asymptotic freedom*: the coupling strength of strong interactions between quarks and gluons decreases as the energy scale increases, *i.e.*, the β-function of QCD is negative [17–22]. At very high energies (small distances) the strong interaction becomes weak, thus quarks and gluons start to behave like free particles. For their discovery of asymptotic freedom Gross, Politzer, and Wilczek have been awarded the 2004 Nobel Prize in physics.

Since strong interactions are not discriminating between different quark flavors (the strong force is flavor blind), QCD exhibits a *chiral flavor symmetry* in the limit of massless quarks. In nature the *scale separation* of QCD dictates that this symmetry is only meaningful for the three light-quark flavors u, d, and s whose masses are small compared to the

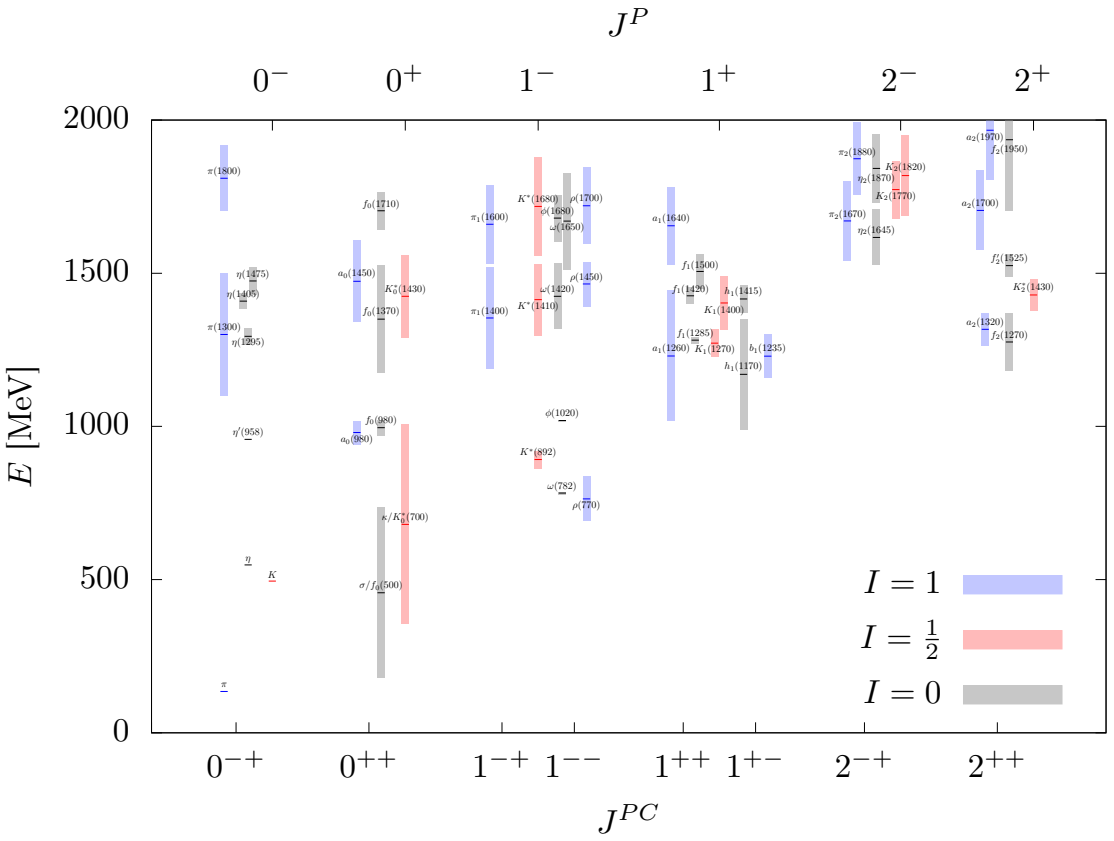

Fig. 1.1: Mass spectrum of all established states in the light-meson sector up to 2 GeV labelled according to the PDG nomenclature [14]. The states are classified by their spin J, parity P, charge conjugation C, and isospin I quantum numbers: isospin singlets (black), doublets (red), and triplets (blue). The decay widths of the states are marked by the boxes.

hadronic scale $\Lambda_{\text{hadr.}} \sim 1\,\text{GeV}$ (*e.g.* the lightest *baryons*, *i.e.*, the nucleons, have a mass of $m_N \sim 939\,\text{MeV}$),[#1] while the heavy-quark flavors c, b, and t are integrated out at low energies. However, chiral flavor symmetry is spontaneously broken by the non-vanishing vacuum expectation value of the chiral quark condensate $\langle\bar{q}q\rangle$, which results in the emergence of eight massless Nambu–Goldstone Bosons [32–35] that can be identified with the *pseudoscalar octet* of pions, kaons, and the η [36–41]. Since the physical values of light-quark masses will cause an additional explicit breaking of chiral symmetry, these *mesons* actually acquire a finite mass, but are still significantly lighter than the other states in the hadron spectrum, *cf.* fig. 1.1. The Nobel Prize in physics has been awarded to Gell-Mann in 1969 for his work on classifying the ground-state hadron spectrum and Nambu in 2008 for the discovery of the mechanism of spontaneously broken symmetry.

[#1] In fact the trace anomaly of the QCD energy-momentum tensor causes the nucleon to stay massive even in the limit of vanishing quark masses [23–27]. Moreover, the by far biggest bulk of nucleon mass is generated by self-interactions of the gluon field, while the light-quark masses turn out to cause only tiny corrections [28–31].

The outline of this chapter is as follows: in sec. 1.1 we discuss QCD and its global symmetries in the chiral limit. We study the main mathematical features of the chiral $\mathrm{SU}(3)_V \times \mathrm{U}(1)_V$ flavor symmetry group and its realization in the physical properties of the pseudoscalar meson nonet in sec. 1.2. A discussion of the mass generation due to explicit chiral flavor symmetry breaking is given in sec. 1.3. For further details on QCD and general aspects of chiral flavor symmetry presented in this chapter we refer to [42–48].

1.1 The Lagrangian of quantum chromodynamics

The dynamics of the quarks and gluons are controlled by the QCD LAGRANGIAN that is given by

$$\mathcal{L}_{\mathrm{QCD}} = \bar{q}\,(i\not{D} - \mathcal{M})\,q - \frac{1}{2}\mathrm{tr}(F_{\mu\nu}F^{\mu\nu}) + \theta\,\frac{g^2}{16\pi^2}\,\mathrm{tr}(F_{\mu\nu}\tilde{F}^{\mu\nu})\,, \tag{1.1}$$

where $q = (u, d, s, ...)^T$ contains the quark fields transforming under the *fundamental representation* **3** of $\mathrm{SU}(3)_C$ and $\mathcal{M} = \mathrm{diag}(m_u, m_d, m_s, ...)$ denotes the quark-mass matrix. Of course, each component of q introduced here will be the usual four-dimensional DIRAC-spinor under the LORENTZ group. The adjoint quark field $\bar{q} = q^\dagger\gamma_0$ will transform under the *conjugate representation* $\bar{\mathbf{3}}$ of $\mathrm{SU}(3)_C$. Since we are interested in strong interactions at low energies, we will drop the contributions of the heavy-quark flavors c, b, and t to eq. (1.1) from now on. The vector potential $G^\mu = \frac{1}{2}\lambda^a\,G^\mu_a$, which lies in the *adjoint representation* **8** of $\mathrm{SU}(3)_C$, describes the gluon field. It enters through the covariant derivative

$$D^\mu = \partial^\mu - ig\,G^\mu\,, \tag{1.2}$$

and the field-strength tensor

$$F^{\mu\nu} = \partial^\mu G^\nu - \partial^\nu G^\mu - ig\,[G^\mu, G^\nu]\,, \tag{1.3}$$

where g is the coupling constant of QCD, λ^a are the complex 3×3 GELL-MANN matrices and the trace relations in eq. (1.1) have to be evaluated in color space, *cf.* app. A.1. For completeness, we also included the θ-term of QCD, which involves the dual field-strength tensor $\tilde{F}_{\mu\nu} = \frac{1}{2}\epsilon_{\mu\nu\alpha\beta}F^{\alpha\beta}$ and is related to strong P- and CP-violation. However, careful estimations indicate that the θ-term is extremely small [49], and therefore we will neglect it in the following calculations by setting $\theta = 0$.

1.1.1 Accidental chiral $\mathrm{U}(3)_L \times \mathrm{U}(3)_R$ flavor symmetry

Rewriting the QCD LAGRANGIAN in terms of left- and right-handed chiral fields

$$q_{L/R} = \frac{\mathbb{1} \mp \gamma_5}{2}\,q\,, \tag{1.4}$$

the DIRAC part in eq. (1.1) decomposes into

$$\bar{q}\,(i\not{D} - \mathcal{M})\,q = \bar{q}_L\,i\not{D}\,q_L + \bar{q}_R\,i\not{D}\,q_R - \bar{q}_L\,\mathcal{M}\,q_R - \bar{q}_R\,\mathcal{M}\,q_L\,. \tag{1.5}$$

In the limit of vanishing light-quark masses ($m_u = m_d = m_s = 0$) it becomes manifest that the left- and right-handed chiral fields in eq. (1.5) decouple. Accordingly, the QCD LAGRANGIAN becomes invariant under the transformations

$$q_L \mapsto U_L\, q_L\,, \qquad q_R \mapsto U_R\, q_R\,, \qquad U_{L/R} \in \mathrm{U}(3)_{L/R} \tag{1.6}$$

of global $\mathrm{U}(3)_L \times \mathrm{U}(3)_R$ flavor symmetry in the so-called *chiral limit*. Obviously, the mass term in eq. (1.5) mixes left- and right-handed fields. Consequently, chiral flavor symmetry is explicitly broken by the light-quark masses.

The chiral $\mathrm{U}(3)_L \times \mathrm{U}(3)_R$ flavor symmetry group can be factorized in terms of

$$\mathrm{SU}(3)_L \times \mathrm{SU}(3)_R \times \mathrm{U}(1)_V \times \mathrm{U}(1)_A\,, \tag{1.7}$$

where we have introduced vector $V = L + R$ and axial vector $A = L - R$ transformations. According to NOETHER's theorem the symmetry group in eq. (1.7) is related to a total number of 18 currents given by

$$\begin{aligned} V^\mu &= \bar{q}\gamma^\mu q\,, & A^\mu &= \bar{q}\gamma^\mu\gamma_5 q\,, \\ V_a^\mu &= \bar{q}\gamma^\mu \frac{\lambda^a}{2} q\,, & A_a^\mu &= \bar{q}\gamma^\mu\gamma_5 \frac{\lambda^a}{2} q\,, \end{aligned} \tag{1.8}$$

which are all conserved at the classical level. Under parity the currents V^μ, V_a^μ and A^μ, A_a^μ transform like vector and axial vectors, respectively. After quantization it turns out that the singlet axial-vector current A^μ is anomalous and thus not conserved [50–54]

$$\partial_\mu A^\mu = \frac{3g^2}{8\pi^2}\,\mathrm{tr}(F_{\mu\nu}\tilde{F}^{\mu\nu})\,, \tag{1.9}$$

which is known as the $\mathrm{U}(1)_A$ anomaly of QCD.[#2] The transformation corresponding to A^μ is therefore not a symmetry of the chiral QCD LAGRANGIAN. However, all the other currents defined in eq. (1.8) are still conserved at the quantum level. Thus the symmetry group that leaves the chiral QCD LAGRANGIAN invariant is reduced to

$$\mathrm{SU}(3)_L \times \mathrm{SU}(3)_R \times \mathrm{U}(1)_V\,. \tag{1.10}$$

In the presence of the quark-mass term the divergences of the currents defined in eq. (1.8) are given by

$$\begin{aligned} \partial_\mu V^\mu &= 0\,, & \partial_\mu A^\mu &= 2i\bar{q}\,\mathcal{M}\gamma_5\, q + \frac{3g^2}{8\pi^2}\,\mathrm{tr}(F_{\mu\nu}\tilde{F}^{\mu\nu})\,, \\ \partial_\mu V_a^\mu &= i\bar{q}\left[\frac{\lambda^a}{2}, \mathcal{M}\right] q\,, & \partial_\mu A_a^\mu &= i\bar{q}\left\{\frac{\lambda^a}{2}, \mathcal{M}\right\}\gamma_5\, q\,, \end{aligned} \tag{1.11}$$

with $[\cdot,\cdot]$, $\{\cdot,\cdot\}$ being the commutator and anticommutator, respectively. Hence, only the singlet vector current V^μ is conserved, implying that the massive QCD LAGRANGIAN

[#2] Since the strong coupling constant behaves like $g^2 \sim N_C^{-1}$ with N_C being the number of colors, the singlet axial-vector current will be conserved in the limit of $N_C \to \infty$.

possesses only a $\mathrm{U}(1)_V$ symmetry.[#3] By means of eq. (A.10) the quark-mass matrix can be spit into

$$\mathcal{M} = \frac{m_u + m_d + m_s}{\sqrt{6}}\,\lambda^0 + \frac{m_u - m_d}{2}\,\lambda^3 + \frac{\hat{m} - m_s}{\sqrt{3}}\,\lambda^8\,, \tag{1.12}$$

with $\hat{m} = \frac{1}{2}(m_u + m_d)$ combining the up- and down-quark masses. We note that the term proportional to λ^0 in this decomposition acts as identity in flavor space, while the latter two terms proportional to λ^3 and λ^8 measure the strength of isospin SU(2) and flavor SU(3) symmetry breaking, *cf.* sec. 1.2.1. If the contributions of λ^3 and λ^8 are neglected, *i.e.*, in the limit of equal light-quark masses $m_u = m_d = m_s$, the octet vector currents V_a^μ will again be conserved. Contrary, for the conservation of the octet axial-vector currents A_a^μ the anticommutation relations in eq. (1.11) require all three structures proportional to λ^0, λ^3, and λ^8 to vanish, *i.e.*, the chiral limit.

Since the physical values of the light-quark masses $m_u \sim 2\,\mathrm{MeV}$, $m_d \sim 5\,\mathrm{MeV}$, and $m_s \sim 93\,\mathrm{MeV}$ are small compared to $\Lambda_{\mathrm{hadr.}} \sim 1\,\mathrm{GeV}$, nature is not too far from the chiral limit.[#4] Thus (approximate) chiral flavor symmetry of the QCD Lagrangian is only an accidental consequence of the smallness of the three light-quark masses, but not a fundamental symmetry at all. One would expect that the hadron spectrum at low energies is organized in degenerate multiplets corresponding to the symmetry group of the chiral QCD Lagrangian given in eq. (1.10). Indeed, the conservation of the *baryon number* B, which corresponds to the $\mathrm{U}(1)_V$ symmetry group, induces an ordering principle of the hadrons: the spectrum can be grouped into states with $B = 0$ and integer spin (*mesons*) as well as states with $B = 1$ and half-integer spin (*baryons*). Hence, we are left with the question whether the remaining chiral $\mathrm{SU}(3)_L \times \mathrm{SU}(3)_R$ symmetry group is realized in the Wigner–Weyl mode [55, 56], *i.e.*, the hadron spectrum is arranged in degenerated parity multiplets (parity doubling), or in the Nambu–Goldstone mode [32–35], *i.e.*, a multiplet of spin-0 massless excitations emerges in the hadron spectrum corresponding to the generators of the spontaneously broken symmetry (Nambu–Goldstone Bosons).

Phenomenologically, we find the hadron spectrum ordered in (approximate) multiplets of the $\mathrm{SU}(3)_V$ symmetry group, while parity doubling is not observed in nature (*e.g.* the hadron spectrum at low energies does not contain a baryon octet of negative parity degenerate with the lowest-lying positive-parity one). Furthermore, the masses of the ground-state pseudoscalar meson octet, *i.e.*, the states with spin-0 and negative parity ($J^P = 0^-$), turn out to be exceptionally light ($M_\pi \sim 138\,\mathrm{MeV}$, $M_K \sim 496\,\mathrm{MeV}$, and $M_\eta \sim 548\,\mathrm{MeV}$) in comparison to those of the corresponding $J^P = 1^-$ vector mesons, *cf.* fig. 1.1. In accordance with these observations, the Vafa–Witten theorem [57] demands the pattern of spontaneous symmetry breaking (SSB) to be

$$\mathrm{SU}(3)_L \times \mathrm{SU}(3)_R \xrightarrow{\mathrm{SSB}} \mathrm{SU}(3)_V\,. \tag{1.13}$$

The eight Nambu-Goldstone Bosons corresponding to the broken generators of $\mathrm{SU}(3)_A$

[#3] Note that the conservation of the singlet vector current for any value of the quark masses is a direct consequence of flavor blindness of the strong interaction.

[#4] As the quarks are color confined, it is impossible to treat them as free asymptotic states. Accordingly, their masses turn out to be scale-dependent quantities, which cannot be measured directly. The running masses quoted here are fixed in the $\overline{\mathrm{MS}}$-scheme at a renormalization scale of 2 GeV [14].

should be pseudoscalars, and therefore can be identified with the octet of pions, kaons, and the η. Note that the $\mathrm{U}(1)_V$ symmetry is untouched by the chiral SSB, and therefore is still preserved. Moreover, the mass gap to the much heavier η' meson (interpreted as the corresponding pseudoscalar singlet state with $M_{\eta'} \sim 958\,\mathrm{MeV}$), can be explained by the $\mathrm{U}(1)_A$ anomaly of QCD (1.9), which gives rise to a non-vanishing mass even in the chiral limit.

1.2 Multiplets of chiral $\mathrm{SU}(3)_V$ flavor symmetry

As explained in the previous section, the ordering principle of the hadron spectrum at low energies is directly related to the chiral $\mathrm{SU}(3)_V \times \mathrm{U}(1)_V$ flavor symmetry group. While the classification into mesons and baryons according to the conserved baryon quantum number of $\mathrm{U}(1)_V$ symmetry is obvious, the identification of the states within multiplets of $\mathrm{SU}(3)_V$ is less clear. In the following we want to present the mathematical basis to classify the states of the pseudoscalar meson nonet.

We begin with three orthonormal vectors $|e_i\rangle$ with components defined by

$$e^k{}_{(i)} \equiv \langle e_k | e_i \rangle = \delta_{ik}\,, \tag{1.14}$$

where the indices i, k run from 1 to 3. In the three-dimensional flavor space spanned by these basis vectors the contravariant components $q^i = \langle e_i | q \rangle$ of the quark field transform under the fundamental **3** representation of $\mathrm{SU}(3)_V$ according to

$$q^i \mapsto U^i{}_k\, q^k\,, \qquad U = \exp\left(i\epsilon_a L^a\right) \tag{1.15}$$

with $U \in \mathrm{SU}(3)_V$, where the real parameters ϵ_a define the infinitesimal generalized angles and the summation index a runs from 1 to 8. The eight linearly independent generators $L^a \equiv \frac{1}{2}\lambda^a$ fulfill the Lie algebra commutation relations (*cf.* app. A.1)

$$\left[L^a, L^b\right] = i f_{abc}\, L^c\,. \tag{1.16}$$

Contrary, the Hermitian adjoint covariant components $\bar{q}_i$ of the quark field transform under the conjugate $\overline{\mathbf{3}}$ representation of $\mathrm{SU}(3)_V$ like

$$\bar{q}_i \mapsto \bar{q}_k\, (U^\dagger)^k{}_i\,, \qquad U^\dagger = \exp\left(i\epsilon_a\, \bar{L}^a\right), \tag{1.17}$$

where the set of generators is given by $\bar{L}^a \equiv -\frac{1}{2}(\lambda^a)^*$. These conjugate generators $\bar{L}^a$ fulfill the same commutation relations as the L^a do in eq. (1.16):

$$\left[\bar{L}^a, \bar{L}^b\right] = i f_{abc}\, \bar{L}^c\,. \tag{1.18}$$

Introducing a ninth generator $L^0 = \frac{1}{2}\lambda^0$ the transformation $U \in \mathrm{U}(1)_V$ of the quark fields is given in analogy to eqs. (1.15) and (1.17). Since the $\mathrm{U}(1)_V$ symmetry is flavor blind, λ^0 has to act like the identity in flavor space and may be given in terms of the Casimir element of $\mathrm{SU}(3)_V$

$$8\,\lambda^0\lambda^0 \equiv \lambda^a\lambda^a\,, \tag{1.19}$$

where the summation index a runs from 1 to 8. Taking this choice the identities in eq. (A.8) will hold for all nine λ^a. As already discussed in sec. 1.1.1 the baryon number B is the conserved additive quantum number of U(1)$_V$, which we identify with the operator

$$B = \sqrt{\tfrac{2}{3}} L^0 \,. \tag{1.20}$$

Accordingly, the basis vectors of the quark field in the fundamental representation take the eigenvalues $B = \frac{1}{3}$, while the eigenvalues of basis vectors of the adjoint representation are found to be $B = -\frac{1}{3}$ (anti-quarks). Note that the scalar product $\langle \bar{q} q \rangle$ with $B = 0$ is an invariant of LORENTZ as well as chiral SU(3)$_V \times$ U(1)$_V$ flavor transformations, *cf.* eqs. (1.15) and (1.17).

1.2.1 SU(2) subspaces and classification of the light-quark states

Considering the explicit representation of the generators of SU(3)$_V$ in the fundamental representation (A.1) we directly recognize that the operators L^3 and L^8 are diagonal at the same time. Additionally, in the two-dimensional subspace spanned by the vectors $|e_1\rangle$ and $|e_2\rangle$ the matrices λ^1, λ^2, and λ^3 act like the PAULI matrices σ^1, σ^2, and σ^3 of SU(2). Thus, we identify $|e_1\rangle$ and $|e_2\rangle$ as the two components of an *isospin doublet*, while $|e_3\rangle$ will be considered as the corresponding *isospin singlet*. Consequently, the first additive quantum number we introduce in this scheme is the eigenvalue of the third isospin component I_3, which can be taken as coincident with the generator L^3. A second useful quantum number connected to the eigenvalues of the other diagonal operator will be the *hypercharge* $Y = \frac{2}{\sqrt{3}} L^8$.[#5]

Taking the eigenvalues of the operators (I_3, Y) acting on $|e_i\rangle$ as components of a two-dimensional vector in *weight space* spans an equilateral triangle.[#6] The components of these weights are interpreted as the quantum numbers suited to identify the basis vectors uniquely with the light-quark flavor states $|u\rangle$, $|d\rangle$, and $|s\rangle$. A weight diagram of the fundamental representation is depicted in fig. 1.2. For the conjugate representation the weight diagram can be obtained by reflecting the weights of the fundamental representation with respect to the origin, *cf.* fig. 1.2. Accordingly, the basis vectors of the conjugate representation are interpreted as corresponding anti-quark states $|\bar{u}\rangle$, $|\bar{d}\rangle$, and $|\bar{s}\rangle$.

Besides the already discussed diagonal operators I_3 and Y, we want to construct ladder operators that allow for a transition between different basis states of the SU(3)$_V$ representation. These will be given by

$$I^{\pm} = L^1 \pm i L^2 \,, \qquad V^{\pm} = L^4 \pm i L^5 \,, \qquad U^{\pm} = L^6 \pm i L^7 \,. \tag{1.21}$$

From these definitions we note that three SU(2) sub-algebras are embedded in the SU(3)$_V$

[#5] Note that strong interactions will always preserve hypercharge, since it is directly related to the baryon and strangeness quantum numbers $Y = B + S$.

[#6] Using the eigenvalues of (I_3, Y) instead of (L^3, L^8) the weight diagram loses its fundamental symmetry character. However, for physical applications it is more natural to introduce the operator Y instead of L^8. In order to preserve the symmetry in the (I_3, Y) diagrams, different scales of the I_3- and Y-axes are used.

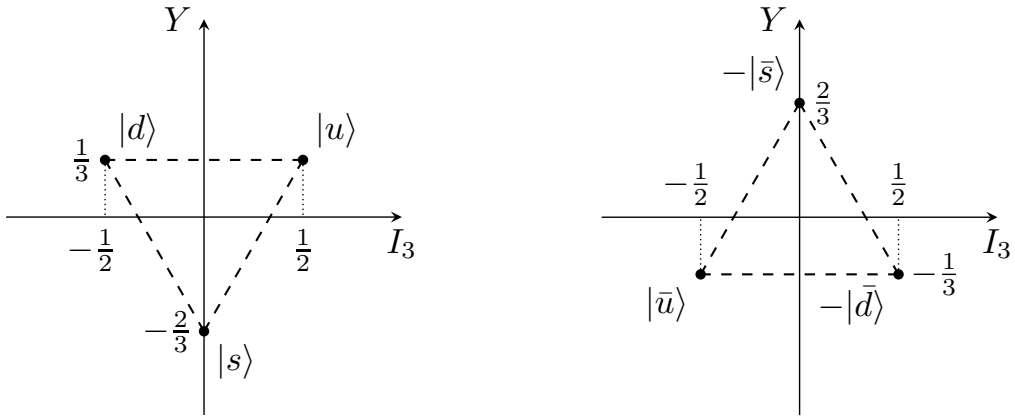

Fig. 1.2: Weight diagrams of the fundamental **3** (left) and conjugate $\overline{\mathbf{3}}$ (right) representations of chiral $\mathrm{SU}(3)_V$ flavor symmetry in the (I_3, Y) plane. The identification with the light quark and anti-quark states follows the DE SWART phase convention [58].

representation [59]: the I-spin algebra

$$[I^+, I^-] = 2I_3\,, \qquad [I_3, I^\pm] = \pm I^\pm\,, \tag{1.22}$$

the V-spin algebra

$$[V^+, V^-] = 2V_3\,, \qquad [V_3, V^\pm] = \pm V^\pm\,, \tag{1.23}$$

and the U-spin algebra

$$[U^+, U^-] = 2U_3\,, \qquad [U_3, U^\pm] = \pm U^\pm\,. \tag{1.24}$$

The diagonal operators V_3 and U_3 defined in the above equations are combinations of I_3 and Y given by

$$V_3 = \tfrac{1}{2}I_3 + \tfrac{3}{4}Y\,, \qquad U_3 = -\tfrac{1}{2}I_3 + \tfrac{3}{4}Y\,. \tag{1.25}$$

Among the different $\mathrm{SU}(2)$ subspaces the ladder operators fulfill the commutation relations

$$[I^\pm, V^\mp] = \mp U^\mp\,, \qquad [I^\pm, U^\pm] = \pm V^\pm\,, \qquad [V^\pm, U^\mp] = \pm I^\pm\,. \tag{1.26}$$

In each of these sub-algebras an additional combination of I_3 and Y plays the role of a scalar operator for that respective sub-algebra. In case of the I-spin we already know that Y is this generator, since

$$[I^\pm, Y] = 0\,, \qquad [I_3, Y] = 0\,. \tag{1.27}$$

We conclude that states belonging to the same isospin multiplet share the same hypercharge quantum number and the ladder operators $I^\pm$ obey the selection rule $\Delta Y = 0$, *cf.* fig. 1.2. For this reason the U-spin is of particular interest, since the scalar operator in this case can be identified with the electric charge operator[#7]

$$Q = I_3 + \tfrac{1}{2}Y\,. \tag{1.28}$$

[#7]The quarks are the only particles in the SM whose electric charges are not integer multiples of the elementary charge e.

Accordingly, the quark-charge matrix reads $\mathcal{Q} = e\,\mathrm{diag}(\frac{2}{3}, -\frac{1}{3}, -\frac{1}{3})$. Equation (1.28) is known as the GELL-MANN–NAKANO–NISHIJIMA formula [60–62]. States belonging to the same U-spin multiplet have the same electric charge Q given that

$$[U^{\pm}, Q] = 0\,, \qquad [U_3, Q] = 0\,. \tag{1.29}$$

Thus the $U^{\pm}$ ladder operators fulfill the selection rule $\Delta Q = 0$. Finally, the scalar operator Q_V of the V-spin is defined by

$$Q_V = I_3 - \tfrac{1}{2}Y\,. \tag{1.30}$$

Apart from any immediate deeper physical meaning this operator fulfills

$$[V^{\pm}, Q_V] = 0\,, \qquad [V_3, Q_V] = 0\,, \tag{1.31}$$

thus states in the same V-spin multiplet share the same value of Q_V. However, strangeness-changing weak transitions occur inside V-spin multiplets, as they obey the $\Delta Y = \Delta Q$ selection rule like the $V^{\pm}$ ladder operators.

The previous definitions classify the basis states according to their I-, U-, or V-spin content. Obviously the classification of a state in terms of $|I_3, Y\rangle$, $|U_3, Q\rangle$, or $|V_3, Q_V\rangle$ is an equally good choice. Indeed, the choice is immaterial for the states in the fundamental or conjugate representation, since each state can be unambiguously identified by its respective weight.[#8] Hence, we are in the position to define the matrix elements of the ladder operators in the SU(2) subspaces:

$$I^{\pm}\,|I_3, Y\rangle = |I_3 \pm 1, Y\rangle\,, \quad U^{\pm}\,|U_3, Q\rangle = \pm|U_3 \pm 1, Q\rangle\,, \quad V^{\pm}\,|V_3, Q_V\rangle = |V_3 \pm 1, Q_V\rangle\,. \tag{1.32}$$

The relative phases within these multiplets are chosen according to the DE SWAT convention [58], requiring real non-negative coefficients in all I- and V-spin matrix elements. This directly fixes the coefficients of the remaining U-spin multiplets uniquely by the commutation relations given in eq. (1.26).

1.2.2 The pseudoscalar meson nonet

So far we discussed the properties of the three light-quark flavors in the fundamental **3** and their anti-quark counterparts in the conjugate $\bar{\mathbf{3}}$ representation. In the next step we want to consider states composed out of a quark and an anti-quark, *i.e.*, mesons with $B = 0$, and study their behaviour within SU(3)$_V$ symmetry. Given that $\mathbf{3} \otimes \bar{\mathbf{3}} = \mathbf{1} \oplus \mathbf{8}$ we can form nine different orthogonal combinations, *i.e.* one flavor singlet state and eight states forming a flavor octet. The quantum numbers I_3 and Y are additive, thus the quantum numbers of mesons can be calculated by vector addition of the respective fundamental and conjugate weights. The associated weight diagrams of the $\mathbf{1} \oplus \mathbf{8}$ representation can be found by placing a $\bar{\mathbf{3}}$ diagram with its (I_3, Y) origin once at each corner of the **3** diagram

[#8] The fundamental and conjugate representations contain only *simple weights*. This does not need to be the case when dealing with states in higher SU(3) representations. Considering a state belonging to a *multiple weight*. In such a case a definite I-spin eigenstate will be an admixture of every U- (or V-) spin eigenstate belonging to that weight.

and adding up the weight vectors, *cf.* fig. 1.3. It follows immediately that three states will be located at the (I_3, Y) origin, hence this point is a *multiple weight*. One of these states can be identified with the singlet representation which contains only a single point. The other two states have to be in the octet representation, thus the quantum numbers I_3 and Y are not sufficient to identify the basis states uniquely within this multiplet. In order to remove this degeneracy we have to introduce an additional new quantum number. We may choose the square of the total isospin operator

$$\boldsymbol{I}^2 = \tfrac{1}{2}\{I^+, I^-\} + I_3^2\,, \tag{1.33}$$

as an additional quantum number, which fulfills the constraints

$$[\boldsymbol{I}^2, I_3] = 0 \qquad [\boldsymbol{I}^2, Y] = 0\,. \tag{1.34}$$

Any generic state $|I, I_3, Y\rangle$ of a given irreducible representation is uniquely characterised by the set of eigenvalues belonging to the operators $\boldsymbol{I}^2$, I_3, and Y.[#9] The flavor singlet will be assigned with $|0,0,0\rangle$ and identified with the $|\eta_1\rangle$ state. In case of the flavor octet the degeneracy is now lifted by choosing the respective basis states $|\pi^0\rangle$ and $|\eta_8\rangle$ as $|1,0,0\rangle$ and $|0,0,0\rangle$.[#10]

Starting from these states, the repeated application of the ladder operators defined in eq. (1.21) allows us to construct all basis states within the octet, *cf.* fig. 1.3. These states can be grouped according to their behavior under isospin transformations: the states $|\pi^+\rangle$, $|\pi^0\rangle$, and $|\pi^-\rangle$ form an isospin triplet, two doublets are consisting of $|K^+\rangle$ and $|K^0\rangle$ as well as $|\bar{K}^0\rangle$ and $|K^-\rangle$, and an isospin singlet given by the $|\eta_8\rangle$ state. In some cases it might be more convenient to work in the HERMITIAN *basis* of the generators L^a instead of the introduced *physical basis*, *cf.* eqs. (1.21) and (A.1). For such a change of basis the matrix elements of the generators and the basis states have to be known. When dealing with the *regular* **8** representation of $\mathrm{SU}(3)_V$ these matrix elements are immediately known, since they are given by the structure constants of $\mathrm{SU}(3)_V$. In order to include the $|\eta_1\rangle$ singlet state of the **1** representation in this scheme, we have to extend the symmetry back to $\mathrm{SU}(3)_V \times \mathrm{U}(1)_V$ by introducing the ninth generator L^0, *cf.* app. A.1. Labelling the HERMITIAN basis states by $|\varphi^a\rangle$ we find

$$L^a\,|\varphi^b\rangle = i f_{abc}\,|\varphi^c\rangle\,. \tag{1.35}$$

[#9] As discussed already earlier, the classification of the basis states according to the transformation properties under the operations of I-spin subgroup is arbitrarily chosen. In general the sets of the V-spin operators V^2, V_3, and Q_V or the U-spin operators U^2, U_3, and Q would be an equally good choice. The benefit of I-spin states comes from physical considerations, given the fact that isospin is a good quantum number when dealing with strong interactions.

[#10] Note that the physical mass eigenstates $|\eta\rangle$ and $|\eta'\rangle$ are considered as linear combinations of the flavor octet $|\eta_8\rangle$ and singlet $|\eta_1\rangle$ states according to

$$|\eta\rangle = \cos\theta\,|\eta_8\rangle - \sin\theta\,|\eta_1\rangle\,, \qquad |\eta'\rangle = \cos\theta\,|\eta_1\rangle + \sin\theta\,|\eta_8\rangle\,.$$

In general the mixing angle introduced here is considered to be small $\theta \approx -10° \ldots -20°$, thus the physical mass eigenstates can be identified with $|\eta\rangle \sim |\eta_8\rangle$ and $|\eta'\rangle \sim |\eta_1\rangle$, respectively [63].

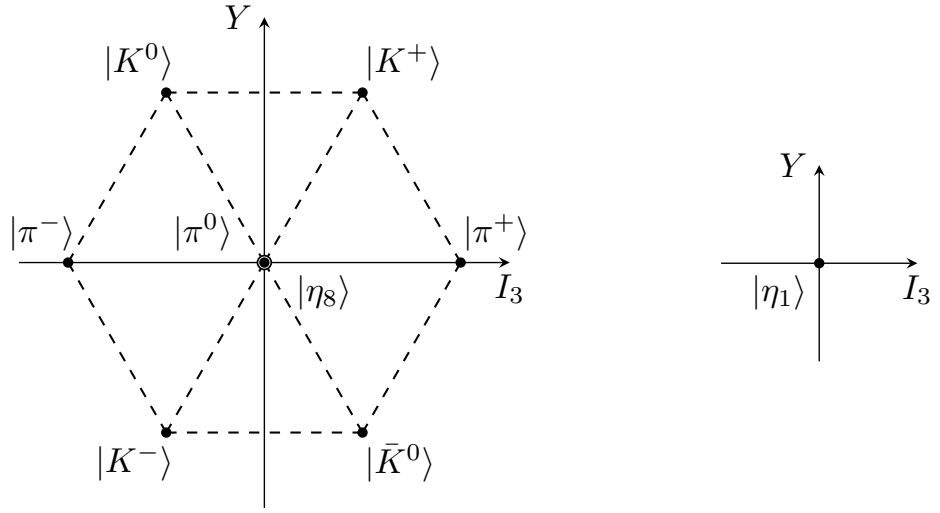

Fig. 1.3: Weight diagrams of the **8** (left) and **1** (right) representations of SU(3) in the (I_3, Y) plane. Note that the scales of the I_3- and Y-axes are chosen differently to preserve the symmetric structure. The identification with the pseudoscalar meson nonet follows the DE SWART-phase convention [58].

Of course we want to identify the HERMITIAN with the physical states. We start with the assumption $|\pi^0\rangle = |\varphi^3\rangle$, suggested by physics. Making repeated use of the ladder operators (1.21) according to eq. (1.35) leads to the identification

$$
\begin{aligned}
|\pi^+\rangle &= -\frac{1}{\sqrt{2}}|\varphi^1 + i\varphi^2\rangle\,, \qquad |\pi^0\rangle = |\varphi^3\rangle\,, \qquad |\pi^-\rangle = \frac{1}{\sqrt{2}}|\varphi^1 - i\varphi^2\rangle\,,\\
|K^+\rangle &= -\frac{1}{\sqrt{2}}|\varphi^4 + i\varphi^5\rangle\,, \qquad |K^-\rangle = \frac{1}{\sqrt{2}}|\varphi^4 - i\varphi^5\rangle\,,\\
|K^0\rangle &= -\frac{1}{\sqrt{2}}|\varphi^6 + i\varphi^7\rangle\,, \qquad |\bar{K}^0\rangle = -\frac{1}{\sqrt{2}}|\varphi^6 - i\varphi^7\rangle\,,\\
|\eta_8\rangle &= |\varphi^8\rangle\,, \qquad |\eta_1\rangle = |\varphi^0\rangle\,.
\end{aligned}
\tag{1.36}
$$

It might also be of interest to study the quark–anti-quark content of the constructed meson nonet. Starting at the left edge of the octet weight diagram we identify $|\pi^-\rangle = |d\bar{u}\rangle$ in fig. 1.3. Again using the ladder operators (1.21) repeatedly on this state we can generate the whole octet basis. The missing singlet state can then be found by demanding orthogonality to all other states. This procedure yields

$$
\begin{aligned}
|\pi^+\rangle &= -|u\bar{d}\rangle\,, \qquad |\pi^0\rangle = \frac{1}{\sqrt{2}}|u\bar{u} - d\bar{d}\rangle\,, \qquad |\pi^-\rangle = |d\bar{u}\rangle\,,\\
|K^+\rangle &= -|u\bar{s}\rangle\,, \qquad |K^0\rangle = -|d\bar{s}\rangle\,, \qquad |\bar{K}^0\rangle = -|s\bar{d}\rangle\,, \qquad |K^-\rangle = |s\bar{u}\rangle\,,\\
|\eta_8\rangle &= \frac{1}{\sqrt{6}}|u\bar{u} + d\bar{d} - 2s\bar{s}\rangle\,, \qquad |\eta_1\rangle = \frac{1}{\sqrt{3}}|u\bar{u} + d\bar{d} + s\bar{s}\rangle\,.
\end{aligned}
\tag{1.37}
$$

Hence, the flavorless physical states $|\pi^0\rangle$, $|\eta_8\rangle$, and $|\eta_1\rangle$ are realised as three orthogonal linear combinations of the *light quarkonium states* $|u\bar{u}\rangle$, $|d\bar{d}\rangle$, and $|s\bar{s}\rangle$.

Since the representations **1** as well as **8** are self-conjugate, the DE SWAT-phase convention demands

$$|I, I_3, Y\rangle^* = (-)^Q |I, -I_3, -Y\rangle \,, \tag{1.38}$$

as link between an arbitrary eigenstate and its conjugate counterpart. This relation can be interpreted as the charge conjugation operator C acting on the eigenstate $|I, I_3, Y\rangle$. Considering an isospin rotation with respect to the I_2-axis another useful relation can be found

$$\exp(i\pi I_2)|I, I_3, Y\rangle = (-)^{I+I_3}|I, -I_3, Y\rangle \,. \tag{1.39}$$

Thus the isospin triplet $|\pi\rangle$ as well as the two isospin singlets $|\eta_8\rangle$ and $|\eta_1\rangle$ are eigenstates of the G-parity operator defined by $G = C\exp(i\pi I_2)$ with

$$G\,|\pi\rangle = -|\pi\rangle \,, \qquad G\,|\eta_8\rangle = |\eta_8\rangle \,, \qquad G\,|\eta_1\rangle = |\eta_1\rangle \,. \tag{1.40}$$

1.3 Current algebra and low-energy theorems

The spontaneous breakdown of approximate chiral flavor symmetry (*cf.* sec. 1.1.1) does not only require the occurrence of eight NAMBU–GOLDSTONE BOSONS (the pions, kaons, and the η), but also governs their dynamical properties. In particular, the analytic structure of QCD at low energies is dominated by the pole contributions of these mesons. One way to access the physics of the strong interaction at low energies is provided by statements of *current algebra* [64–68]. The resulting *low-energy theorems*, first studied in the days when the QCD LAGRANGIAN was unknown, are exclusively based on the symmetry principles of the hadronic currents in the limit where the involved four-momenta vanish.

According to WEINBERG's conjecture [69–71] the low-energy structure of QCD can also be analyzed in terms of an effective field theory (EFT). The standard version of this EFT, known as *chiral perturbation theory* (ChPT), exploits chiral flavor symmetry and provides a systematic description of QCD at low energies [72, 73]. Hence, the effective LAGRANGIAN of ChPT contains the pseudoscalar octet fields as its basic degrees of freedom, which are organized in a series of operators suppressed by higher and higher powers in the expansion of the light-quark masses and involved four-momenta. Moreover, the fundamental symmetries that ChPT is based on dictate the structure of these operators, but the strength of their couplings is *a priori* unconstrained and encoded in so-called *low-energy constants* (LECs). Thus the low-energy theorems formulated in current algebra can be understood as leading-order expressions in the chiral expansion.

1.3.1 PCAC hypothesis and the meson decay constant

We start by considering the two-point function generated by the time-ordered product of two flavor octet axial-vector currents (1.8) acting on the QCD vacuum $|0\rangle$. Separating

the pole contribution of the involved pseudoscalar meson state (1.36), the LEHMANN–SYMANZIK–ZIMMERMANN (LSZ) reduction formula [74] yields

$$i\int \mathrm{d}^4x\, \exp(ipx)\, \langle 0|T\{A_a^\mu(x)\, A_b^\nu(0)\}|0\rangle = -\frac{p^\mu p^\nu}{p^2 - M_{\mathrm{GB}}^2}\, F_0^2\, \delta^{ab} + \dots\,, \tag{1.41}$$

where $T\{...\}$ refers to the time-ordering operator, M_{GB} to the mass of the octet state and p the four-momentum flow through the currents. LORENTZ invariance determines the structure of eq. (1.41) up to an unknown LEC denoted by F_0. Moreover, the residue in eq. (1.41) defines the non-vanishing matrix element of the axial-vector current between the vacuum and an octet state

$$\langle 0|A_a^\mu(x)|\varphi^b(p)\rangle = i\, p^\mu F_0\, \delta^{ab}\, \exp(-ipx) \tag{1.42}$$

in terms of F_0, which is therefore referred to as the meson decay constant in the chiral limit.[#11] Thus the octet axial-vector current acts as a so-called *interpolating field* for the octet state $|\varphi^a(p)\rangle$. From eq. (1.42) follows directly that a non-zero value of F_0 is a necessary and sufficient criterion for spontaneous chiral flavor symmetry breaking (lattice QCD determines $F_0 \sim 86\,\mathrm{MeV}$ [75]). Taking the divergence on both sides of eq. (1.42) results in

$$\langle 0|\partial_\mu A_a^\mu(x)|\varphi^b(p)\rangle = F_0\, M_{\mathrm{GB}}^2\, \delta^{ab}\, \exp(-ipx)\,. \tag{1.43}$$

Since the octet axial-vector current given in eq. (1.11) is a conserved quantity in the chiral limit, it becomes immediately clear that M_{GB} is required to vanish (provided that F_0 is finite) and the octet states become massless in this limit. Accordingly, the octet axial-vector currents reveal a kind of partial conservation related to the small masses of the octet states, also known as *partial conservation of the axial currents* (PCAC) hypothesis.

1.3.2 The Gell-Mann–Oakes–Renner relation

In the next step we want to extend eq. (1.41) to

$$i\int \mathrm{d}^4x\, \mathrm{d}^4y\, \exp(ip_1x)\, \exp(ip_2y)\, \langle 0|T\{A_a^\mu(x)\, A_b^\nu(y)\, \mathcal{H}(0)\}|0\rangle\,, \tag{1.44}$$

by adding an external field $\mathcal{H}$. Using the LSZ reduction formula and the PCAC hypothesis we find the low-energy theorem

$$\lim_{p_1,p_2\to 0}\langle \varphi^b(p_2)|\mathcal{H}(0)|\varphi^a(p_1)\rangle = -\frac{1}{F_0^2}\, \langle 0|[Q_A^a,[Q_A^b,\mathcal{H}(0)]]|0\rangle\,, \tag{1.45}$$

where Q_A^a is the octet axial-charge operator defined by

$$Q_A^a = \int \mathrm{d}^3\mathbf{x}\, A_a^0(0,\mathbf{x})\,. \tag{1.46}$$

[#11] This identification follows from the fact that eq. (1.42) is responsible for the weak $\pi^+ \to l^+\nu_l$ decay.

Identifying the external field with the quark-mass term of the QCD LAGRANGIAN (1.1), the commutator on the right-hand side of eq. (1.45) simplifies to

$$[Q_A^a, [Q_A^b, \bar{q}\mathcal{M}q]] = \frac{1}{4}\bar{q}\{\lambda^a, \{\lambda^b, \mathcal{M}\}\}q\,. \tag{1.47}$$

On the other hand, the FEYNMAN–HELLMANN theorem [76–79] relates the diagonal elements ($a = b$) the on left-hand side of eq. (1.45) to the QCD mass eigenvalue $\hat{M}_{\mathrm{GB}}$ of the respective octet state

$$m_q \frac{\partial \hat{M}_{\mathrm{GB}}^2}{\partial m_q} = \lim_{p_1,p_2\to 0} \langle \varphi^a(p_2)|\bar{q}\mathcal{M}q|\varphi^a(p_1)\rangle\,, \tag{1.48}$$

where the derivative has to be taken with respect to the three light-quark masses m_q. Thus, the QCD mass squares[#12] of the eight NAMBU–GOLDSTONE BOSONS scale linearly in m_q according to

$$\hat{M}_{\mathrm{GB}}^2 = -\frac{1}{4F_0^2}\,\langle 0|\bar{q}\{\lambda^a, \{\lambda^a, \mathcal{M}\}\}q|0\rangle\,, \tag{1.49}$$

which is known as the GELL-MANN–OAKES–RENNER (GMOR) relation [80]. Note that this relation only holds up to corrections of order m_q^2 in the expansion of light-quark masses.

Using the identification for the physical basis of the pseudoscalar octet states given in eq. (1.36) the GMOR relation yields

$$\hat{M}_\pi^2 = 2B_0\,\hat{m}\,, \quad \hat{M}_{K^+}^2 = B_0\,(m_u + m_s)\,, \quad \hat{M}_{K^0}^2 = B_0\,(m_d + m_s)\,, \quad \hat{M}_\eta^2 = \frac{2}{3}B_0\,(\hat{m} + 2m_s)\,, \tag{1.50}$$

where B_0 is another LEC related to the scalar quark condensate $\langle\bar{q}q\rangle$ in the chiral limit

$$B_0 = -\frac{\langle\bar{q}q\rangle}{3F_0^2}\,, \qquad \langle\bar{q}q\rangle \equiv 3\langle\bar{u}u\rangle = 3\langle\bar{d}d\rangle = 3\langle\bar{s}s\rangle\,. \tag{1.51}$$

Note that a non-zero value of B_0 or $\langle\bar{q}q\rangle$ is a sufficient, but in contrast to a non-vanishing value of F_0 not a necessary, condition for the spontaneous breakdown of chiral flavor symmetry. Moreover, we find the octet states to become massless in the chiral limit, which is in agreement with eq. (1.43).

In the derivation of eq. (1.49) we only considered the diagonal elements of eq. (1.47), but actually we find one pair of non-vanishing off-diagonal elements

$$-\frac{1}{4F_0^2}\,\langle 0|\bar{q}\{\lambda^3, \{\lambda^8, \mathcal{M}\}\}q|0\rangle = -\frac{1}{4F_0^2}\,\langle 0|\bar{q}\{\lambda^8, \{\lambda^3, \mathcal{M}\}\}q|0\rangle = \frac{1}{\sqrt{3}}B_0\,(m_u - m_d)\,, \tag{1.52}$$

which generates an isospin breaking mixing of the flavorless triplet $|\varphi^3\rangle$ and singlet $|\varphi^8\rangle$ states. Note that this term will vanish in the isospin limit, *i.e.*, for equal up- and down-quark masses. However, in general we have to perform a rotation of the flavorless states given by

$$|\pi^0\rangle = \cos\epsilon\,|\varphi^3\rangle - \sin\epsilon\,|\varphi^8\rangle\,, \qquad |\eta\rangle = \sin\epsilon\,|\varphi^3\rangle + \cos\epsilon\,|\varphi^8\rangle\,, \tag{1.53}$$

[#12] Any contribution to the masses of the NAMBU–GOLDSTONE BOSONS has to be generated by terms that break chiral flavor symmetry explicitly. Since all terms of the QCD LAGRANGIAN (1.1) that involve the gluon field respect chiral flavor symmetry, their contribution to $\hat{M}_{\mathrm{GB}}$ vanishes.

in order to diagonalize of the $\pi^0\eta$ mass matrix. At leading order in $m_u - m_d$ the isospin-breaking $\pi^0\eta$ mixing angle ϵ is found to be

$$\epsilon = \frac{\sqrt{3}}{4}\,\frac{m_u - m_d}{\hat{m} - m_s}\,. \tag{1.54}$$

Moreover, the QCD mass eigenvalues of the flavorless states receive leading corrections

$$\hat{M}^2_{\pi^0} = 2B_0\,\hat{m} + \frac{8}{3}B_0\,(\hat{m} - m_s)\,\epsilon^2\,, \qquad \hat{M}^2_{\eta} = \frac{2}{3}B_0\,(\hat{m} + 2m_s) - \frac{8}{3}B_0\,(\hat{m} - m_s)\,\epsilon^2 \tag{1.55}$$

at order ϵ^2. Accordingly, the GMOR relation states that pion triplet is mass degenerate in QCD up to effects of second order in isospin breaking. Since these shifts are tiny, we can safely ignore them in the following.

However, eq. (1.50) reveals another quantity that is sensitive to the up- and down-quark mass difference. The degeneracy of the kaon doublets is already lifted at first order in isospin breaking. More precisely, the QCD kaon mass splitting reads

$$\hat{M}^2_{K^+} - \hat{M}^2_{K^0} = B_0\,(m_u - m_d)\,. \tag{1.56}$$

Therefore one commonly defines the combined charged and neutral kaon mass, *i.e.*, the kaon mass in the isospin limit, according to

$$\hat{M}^2_{K} = B_0\,(\hat{m} + m_s)\,. \tag{1.57}$$

Combining eqs. (1.50) and (1.57) we recover the Gell-Mann–Okubo mass formula [36, 81, 82], which relates the QCD mass eigenvalues of the pseudoscalar octet states by

$$4\hat{M}^2_{K} = 3\hat{M}^2_{\eta} + \hat{M}^2_{\pi}\,. \tag{1.58}$$

The light-quark masses appearing in the GMOR relations are fundamental parameters of QCD, thus their values must be known for a complete understanding of the strong interaction. However, the unknown LEC B_0 in eq. (1.50) prevents us from a direct determination of the light-quark masses. But we can turn to an indirect method in which B_0 cancels: originally proposed by Weinberg, we are can form two light-quark mass ratios solely fixed by the QCD mass eigenvalues of the pseudoscalar octet [83–88]

$$\frac{m_u}{m_d} = \frac{\hat{M}^2_{K^+} - \hat{M}^2_{K^0} + \hat{M}^2_{\pi}}{\hat{M}^2_{K^0} - \hat{M}^2_{K^+} + \hat{M}^2_{\pi}}\,, \qquad \frac{m_s}{m_d} = \frac{\hat{M}^2_{K^+} + \hat{M}^2_{K^0} - \hat{M}^2_{\pi}}{\hat{M}^2_{K^0} - \hat{M}^2_{K^+} + \hat{M}^2_{\pi}}\,. \tag{1.59}$$

1.3.3 Dashen's theorem

In the previous section we have studied the masses of the pseudoscalar octet states within pure QCD. Since the light quarks carry different electric charges (1.28), chiral flavor symmetry is also explicitly violated by electromagnetic interactions. Accordingly, virtual photons are allowed to generate non-vanishing contributions to the self-energies of the pseudoscalar octet states. Similarly to the derivation of the GMOR relation (1.49), we want to study the leading electromagnetic effect that yields a non-vanishing contribution

to the mass eigenvalues of the pseudoscalar octet states. Therefore we can identify the external field in eq. (1.44) with

$$\mathcal{H}_{\text{QED}}(0) = e^2 \int \mathrm{d}^4x\, T\{J_\mu(x)\, J_\nu(0)\}\, D^{\mu\nu}(x)\,, \tag{1.60}$$

where $D^{\mu\nu}$ denotes the photon propagator and the electromagnetic current J_μ of the light-quark fields is defined by

$$J_\mu = V_\mu^3 + \tfrac{1}{\sqrt{3}} V_\mu^8\,. \tag{1.61}$$

Here V_μ^3 and V_μ^8 refer to the flavor-diagonal octet vector currents (1.8).

Inserting $\mathcal{H}_{\text{QED}}$ into eq. (1.45) the self-energies for the neutral states $|\pi^0\rangle$, $|K^0\rangle$, $|\bar{K}^0\rangle$, and $|\eta\rangle$ will vanish, since any electrically neutral Q_A^a commutes with J_μ. Moreover, there is no contribution to an off-diagonal element that would be relevant for electromagnetic $\pi^0\eta$ mixing. The question remains how self-energies of the charged pseudoscalar states relate to each other. Since the positively charged states $|\pi^+\rangle$ and $|K^+\rangle$ belong to the same U-spin multiplet (similarly for $|\pi^-\rangle$ and $|K^-\rangle$), eq. (1.29) demands their electromagnetic self-energies to be the same

$$M_{\pi^\pm}^2\big|_{\text{QED}} = M_{K^\pm}^2\big|_{\text{QED}} = \frac{2e^2\, C_0}{F_0^2}\,. \tag{1.62}$$

The electromagnetic LEC C_0 can be expressed as an integral over the difference of the vector and axial-vector spectral functions [89]. Accordingly, Dashen's theorem [90] states that in the chiral limit the QED mass splittings of the pion triplet and the kaon doublets are equal

$$M_{K^+}^2 - M_{K^0}^2\big|_{\text{QED}} = M_{\pi^+}^2 - M_{\pi^0}^2\big|_{\text{QED}}\,. \tag{1.63}$$

Note that this relation is valid up to corrections of order $e^2 m_q$.

Using eqs. (1.50), (1.57), and (1.63) we are now able to remove the QED contributions from the physical masses of the pseudoscalar octet and define the QCD mass eigenvalues

$$\hat{M}_\pi^2 = M_{\pi^0}^2\,, \qquad \hat{M}_K^2 = \frac{1}{2}\big(M_{K^+}^2 + M_{K^0}^2 - M_{\pi^+}^2 + M_{\pi^0}^2\big)\,, \qquad \hat{M}_\eta^2 = M_\eta^2\,, \tag{1.64}$$

which are valid up to corrections of $\mathcal{O}(m_q^2, \epsilon^2, e^2 m_q)$. Moreover, the Gell-Mann–Okubo mass formula (1.65) explicitly written in terms of the physical masses reads

$$2M_{K^+}^2 + 2M_{K^0}^2 = 3M_\eta^2 + 2M_{\pi^+}^2 - M_{\pi^0}^2\,, \tag{1.65}$$

and is found to be fulfilled to approximately 7% accuracy in nature. Finally, we find the improved light-quark mass ratios free of QED effects to be given by

$$\frac{m_u}{m_d} = \frac{M_{K^+}^2 - M_{K^0}^2 - M_{\pi^+}^2 + 2M_{\pi^0}^2}{M_{K^0}^2 - M_{K^+}^2 + M_{\pi^+}^2} \sim 0.56\,, \qquad \frac{m_s}{m_d} = \frac{M_{K^+}^2 + M_{K^0}^2 - M_{\pi^+}^2}{M_{K^0}^2 - M_{K^+}^2 + M_{\pi^+}^2} \sim 20\,. \tag{1.66}$$

Chapter 2

Theory of scattering processes

The renormalization procedure in QED dealing with divergences arising in the perturbative approach to quantum field theories has been established at the end of the 1940s [91–99]. However, the application of renormalization in QCD was not successful until the 1970s [17–22]. In the meantime an alternative approach to strong interactions was developed, namely the S-matrix theory [100–105]. Since these two concepts are not in conflict with each other, both can be used to describe the phenomena of the strong interaction. The link between the S-matrix and perturbation theory is given by the LSZ-reduction formula [74]. In view of applications to scattering processes in the low-energy regime, which is the problematic region of QCD (*cf.* ch. 1), dispersion theory based on the concepts of the S-matrix approach can be seen as superior to perturbation theory, *cf.* chs. 3 and 4. Historically, the S-matrix theory played also a role in the early days of string theory [106].

The S-matrix can be considered as the scattering operator evolving an arbitrary initial state in the infinite past into a final state in the infinite future regardless of the number of interacting particles or precise kind of interaction. Accordingly the S-matrix elements define the transition amplitudes of a given scattering process without the direct need of quantum fields or a LAGRANGIAN of the underlying quantum field theory, avoiding the disadvantages of perturbation theory. For further details on the presented concepts of scattering theory involving the S-matrix we recommend [107–110].

The discussion of this chapter is organized as follows: in sec. 2.1 we review the consequences of unitarity, analyticity, and crossing symmetry for general S-matrix elements. A detailed treatment of generic $2 \to 2$ scattering processes is presented in sec. 2.2. Finally, we derive the elastic $\pi\pi$ and $\pi\eta$ scattering amplitudes in sec. 2.3.

2.1 The S-matrix

In order to define transition amplitudes in this framework consistently, some basic properties need to be satisfied by the S-matrix [107]:

- the *superposition principle* of quantum mechanics rendering the S-matrix linear;

- the requirements of *special relativity* demanding LORENTZ invariance of the S-matrix elements;
- the *conservation of probability* implying that the S-matrix is *unitary*;
- the *short-range character of the interaction* leading to *free* and *stable* particles in the initial and final *asymptotic states*;[#1]
- and *causality* implemented in the S-matrix element as the real boundary of a complex-valued *analytic* function.

The initial and final states can be specified in general by the momenta of particles forming the state together with a set of discrete quantum numbers, *e.g.* spin or isospin. To keep the notation as simple as possible, in the following incoming asymptotic states will be labelled by $|i;\text{in}\rangle$ and outgoing asymptotic states by $|f;\text{out}\rangle$ where i, f account for the respective initial $p_1, p_2, ...$ and final state $q_1, q_2, ...$ four-momenta as well as possible other quantum numbers $\alpha_1, \alpha_2, ...$ and $\beta_1, \beta_2, ...$ of the individual particles. These states are postulated to satisfy the orthonormality and completeness relations given by

$$\langle f;\text{in}|i;\text{in}\rangle = (2\pi)^3\,\delta_{\alpha_1\beta_1}\,2p_1^0\,\delta^{(3)}(\mathbf{q}_1-\mathbf{p}_1)\,...\,, \qquad \sum\!\!\!\!\!\!\int_n |n;\text{in}\rangle\langle n;\text{in}| = \mathbb{1}\,, \tag{2.1}$$

for the incoming states and accordingly for the outgoing states. In eq. (2.1) the sum is meant to run over all possible configurations of multi-particle states while carrying out an integration over the respective momenta.

The LORENTZ-invariant S-matrix element $\mathcal{S}_{fi}$ is defined as the probability amplitude for the transition of an arbitrary initial state into an arbitrary final state given by

$$\langle f;\text{out}|i;\text{in}\rangle = \langle f;\text{in}|S|i;\text{in}\rangle \equiv (2\pi)^4\,\delta^{(4)}(p_i-q_f)\,\mathcal{S}_{fi}(p_1,p_2,...,q_1,q_2,...)\,. \tag{2.2}$$

Due to POINCARÉ invariance the total four-momenta of the incoming p_i and outgoing states q_f are conserved, which is assured by the delta function. The S-matrix in eq. (2.2) evolves an incoming into an outgoing asymptotic state by

$$\langle f;\text{in}|S = \langle f;\text{out}|\,. \tag{2.3}$$

Given the fact that incoming and outgoing states form complete sets, the S-matrix cannot be singular. Accordingly, its inverse must exist transforming an outgoing into an incoming asymptotic state like

$$\langle f;\text{out}|S^{-1} = \langle f;\text{in}|\,. \tag{2.4}$$

Using the orthonormality and completeness relations (2.1) together with eqs. (2.3) and (2.4) we find

$$S = \sum\!\!\!\!\!\!\int_n |n;\text{in}\rangle\langle n;\text{out}|\,, \qquad S^{-1} = \sum\!\!\!\!\!\!\int_n |n;\text{out}\rangle\langle n;\text{in}|\,, \tag{2.5}$$

[#1] An extension of this framework to decay processes is addressed at the end of sec. 2.2.2.

which implies that the S-matrix is unitary

$$S^\dagger S = S S^\dagger = \mathbb{1}\,. \tag{2.6}$$

Likewise to eqs. (2.3) and (2.4) the unitarity condition of the S-matrix can be used to relate incoming and outgoing asymptotic states according to

$$\begin{aligned} \langle f;\text{in}|S &= \langle f;\text{out}|\,, & S^\dagger|i;\text{in}\rangle &= |i;\text{out}\rangle\,, \\ \langle f;\text{out}|S^\dagger &= \langle f;\text{in}|\,, & S|i;\text{out}\rangle &= |i;\text{in}\rangle\,. \end{aligned} \tag{2.7}$$

It follows directly that S-matrix elements expressed in terms of incoming or outgoing states are equivalent

$$\langle f;\text{in}|S|i;\text{in}\rangle = \langle f;\text{out}|S|i;\text{out}\rangle\,. \tag{2.8}$$

Thus we are allowed to omit the labels for the incoming and outgoing states safely whenever calculating S-matrix elements. In the following we will account for this by labelling the initial and final states simply by their momenta $|p_1, p_2, ...\rangle$ and $|q_1, q_2, ...\rangle$, respectively.

2.1.1 Consequences of unitarity and the scattering amplitude

Commonly the S-matrix is split into a trivial and non-trivial part

$$S = \mathbb{1} + iT\,, \tag{2.9}$$

where the latter part containing the T-matrix describes the interactions among the particles. According to eq. (2.9) the S-matrix element decomposed into

$$\langle q_1, q_2, ...|S|p_1, p_2, ...\rangle = \langle q_1, q_2, ...|p_1, p_2, ...\rangle + \langle q_1, q_2, ...|iT|p_1, p_2, ...\rangle\,, \tag{2.10}$$

defines the LORENTZ-invariant scattering amplitude given by the T-matrix element

$$\langle q_1, q_2, ...|iT|p_1, p_2, ...\rangle = i\,(2\pi)^4\,\delta^{(4)}(p_i - q_f)\,\mathcal{T}_{fi}(p_1, p_2, ..., q_1, q_2, ...)\,. \tag{2.11}$$

A diagrammatic sketch of eq. (2.10) is depicted in fig. 2.1. Combining eq. (2.9) with eq. (2.6) implies the unitarity condition for the T-matrix

$$i(T^\dagger - T) = T^\dagger T = T\,T^\dagger\,. \tag{2.12}$$

On the amplitude level, the left-hand side of the unitarity condition yields

$$\begin{aligned} &\langle q_1, q_2, ...|iT^\dagger|p_1, p_2, ...\rangle - \langle q_1, q_2, ...|iT|p_1, p_2, ...\rangle \\ &\qquad = i\,(2\pi)^4\,\delta^{(4)}(p_i - q_f)\,\big(\mathcal{T}^*_{if}(q_1, q_2, ..., p_1, p_2, ...) - \mathcal{T}_{fi}(p_1, p_2, ..., q_1, q_2, ...)\big)\,. \end{aligned} \tag{2.13}$$

Inserting a complete set of intermediate states $|k_1, k_2, ...\rangle$ on the right-hand side of eq. (2.12) we find[#2]

$$\begin{aligned} \langle q_1, q_2, ...|T^\dagger T|p_1, p_2, ...\rangle = \sum\!\!\!\!\!\!\int_n &(2\pi)^4\,\delta^{(4)}(q_f - k_n)\,(2\pi)^4\,\delta^{(4)}(p_i - k_n) \\ &\times \mathcal{T}^*_{nf}(q_1, q_2, ..., k_1, k_2, ...)\,\mathcal{T}_{ni}(p_1, p_2, ..., k_1, k_2, ...)\,. \end{aligned} \tag{2.14}$$

[#2] By convention we choose the first equality $i(T^\dagger - T) = T^\dagger T$ in eq. (2.12), taking the second one $i(T^\dagger - T) = T\,T^\dagger$ would lead to a similar result.

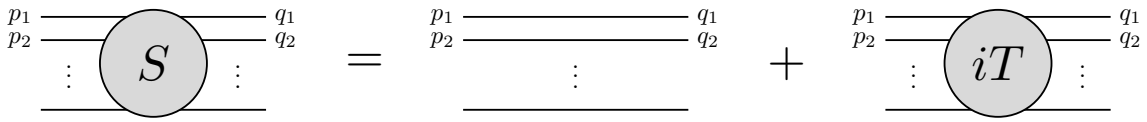

Fig. 2.1: Diagrammatic sketch of the relation between S-matrix and T-matrix elements as defined in eq. (2.10).

Using $\delta^{(4)}(q_f - k_n)\,\delta^{(4)}(p_i - k_n) = \delta^{(4)}(p_i - q_f)\,\delta^{(4)}(p_i - k_n)$ under the integral, both sides of the unitarity condition given in eqs. (2.13) and (2.14) contain one delta function enforcing overall four-momentum conservation in the initial to final state system. In the following these delta functions will be dropped, assuming four-momentum conservation in the initial to final state system implicitly. Hence, the unitarity condition for a generic scattering amplitude reads

$$\begin{aligned} &i\big(\mathcal{T}^*_{if}(q_1, q_2, ..., p_1, p_2, ...) - \mathcal{T}_{fi}(p_1, p_2, ..., q_1, q_2, ...)\big) \\ &\qquad = (2\pi)^4 \sum\!\!\!\!\!\!\int_n \delta^{(4)}(p_i - k_n)\,\mathcal{T}^*_{nf}(q_1, q_2, ..., k_1, k_2, ...)\,\mathcal{T}_{ni}(p_1, p_2, ..., k_1, k_2, ...)\,. \end{aligned} \tag{2.15}$$

2.1.2 Analyticity and singularities

In this section we want to discuss the consequences of *maximal analyticity* on the S-matrix. A general mathematical rigorous proof of analyticity is still pending, but progress has been made [107, 111–115] showing a close connection to *causality*. Therefore we will treat the statement of analyticity as an axiom of scattering theory [107].

On the level of T-matrix elements the statement of maximal analyticity implies that the scattering amplitude is holomorphic in all its continuous variables, *i.e.*, the four-momenta of the involved particles. Additionally, only two kinds of singularities are allowed, namely *branch cuts* and *poles*, which can be related to intermediate physical states of the scattering process. In order to study these singularities it is useful to define a new set of continuous variables. Since overall momentum conservation is implied, not all momenta in eq. (2.11) are allowed to be independent. Commonly, the square of the total energy s in the center-of-mass system (CMS) is chosen as one of these new variables. Further details on choosing an appropriate set of kinematical variables for the special case of $2 \to 2$ scattering will be discussed in sec. 2.2.1.

In accordance to the statement above, the scattering amplitude will be holomorphic in the variable s. Hence, s is treated to be complex from now on and the amplitude can be *analytically continued* into the complex plane. Still for physically allowed scattering processes, the variable s is bounded to be real and above the respective threshold of the transition. The domain in which all kinematical variables of the amplitude take physically allowed values is known as *physical region*. Since singularities arise from intermediate physical states, the scattering amplitude will be defined for all values of s in the complex plane except for the position of these singularities. Intermediate physical states can lead to two different kinds of singularities: branch cuts appear for multi-particle intermediate states while poles are connected to *bound states*, *virtual states*, or *resonances*.

In general multi-particle states, *i.e.*, states consisting of two or more individual particles, will form a continuum of s values where they are allowed to go *on-shell* starting at the respective threshold and extending to infinity.[#3] This continuum of singularities manifests as branch cut reaching from the corresponding threshold (*branch point*) to infinity. Consequently, the scattering amplitude has to be a multi-valued function in the complex s-plane. We will deal with this fact by introducing a RIEMANN surface on which the amplitude can be interpreted as a single-valued function again. The branch cut then determines where to cut the surface in different RIEMANN sheets.[#4] When s is real and above the threshold, the physical scattering region is reached by evaluating the amplitude on the *first* or *physical sheet* at $s + i\epsilon$ and approaching the real axis from above $\epsilon \to 0^+$. If a scattering process allows only for one multi-particle intermediate state, its amplitude possesses two *Riemann* sheets. Hence, the physical region can also be accessed from the *second* or *unphysical sheet* by approaching the real axis from below $s - i\epsilon$, again taking the limit $\epsilon \to 0^+$. Any further opening of a multi-particle channel gives rise to additional unphysical RIEMANN sheets.

Single-particle states associated with poles of the amplitude can be grouped into three categories [116, 117]: a bound state pole will appear below threshold on the real axis of the physical sheet at the value of s corresponding to its squared invariant mass. Similarly, a virtual state appears as a pole on the real axis on unphysical sheets again at the value of s corresponding to its squared invariant mass.[#5] In contrast to these two types the poles associated with a resonance will appear as a pole in the complex plane of an unphysical sheet.[#6] Its location determines the mass M_R and width Γ_R of the resonance according to

$$\sqrt{s_R} = M_R - \tfrac{i}{2}\Gamma_R\,, \tag{2.16}$$

where the square-root function is chosen such that $M_R > 0$. As a result of the SCHWARZ *reflection principle* (*cf.* sec. 3.1) these poles will always appear in complex conjugate pairs in the complex s-plane, *i.e.*, at s_R and s_R^*.

2.1.3 Crossing symmetry

Another useful property of the S-matrix resulting from analyticity is *crossing symmetry* [110, 118]. On the level of T-matrix elements it states the following: consider an arbitrary scattering process where one of the incoming particles is denoted by $\phi(p)$ with four-momentum p. The corresponding T-matrix element can be related to a similar process where the incoming particle is replaced by its respective outgoing antiparticle $\bar{\phi}(-p)$ of

[#3] Consider for simplicity a two-particle intermediate state: its squared center-of-mass energy will be given by $(\sqrt{p^2 + M_1^2} + \sqrt{p^2 + M_2^2}\,)^2$ where the M_i denote the masses of the particles and $p = |\mathbf{p}_i|$ the absolute value of the three momentum. Since all values $p \geq 0$ are allowed physically, s can take values from the threshold $(M_1 + M_2)^2$ up to infinity.

[#4] Mathematically speaking the path of the branch cut is arbitrary, only the branch point (threshold) is fixed. For convenience we will choose the branch cuts to run along the real axis.

[#5] As example consider proton-neutron scattering, which form an $I = \frac{1}{2}$ isospin doublet. In nature one bound state appears identified by the deuteron, an $I = 0$ isospin singlet state. The corresponding $I = 1$ isospin triplet state is not realized in nature, but can be interpreted as a virtual state.

[#6] A common example for such a state is the $\rho(770)$ resonance appearing in P-wave $\pi\pi \to \pi\pi$ scattering.

opposite four-momentum according to

$$\mathcal{T}(\phi(p) + ... \to ...) = \mathcal{T}(... \to ... + \bar{\phi}(-p)) \,. \tag{2.17}$$

Here the dots are meant to represent the remaining incoming and outgoing particles.

In a more formal way the property in eq. (2.17) can be summarized as: scattering amplitudes involving antiparticles are given by an analytic continuation in the respective four-momenta of the corresponding scattering amplitude containing the associate particles. Note that the energy of each particle p^0 is defined to be positive, hence the energy of the antiparticle is continued to $-p^0 < 0$. Therefore an antiparticle can be considered as a particle moving backwards in time.

2.2 The scattering amplitude for $2 \to 2$ processes

As discussed in sec. 2.1.1, the T-matrix element defines the transition amplitude for a generic scattering process. Now we want to study the properties of $2 \to 2$ scattering amplitudes in more detail. Obviously, similar considerations can be made as well for arbitrary other configurations [117].

Throughout this thesis two different kinds of $2 \to 2$ scattering processes will be investigated: transitions involving four pseudoscalar mesons according to the reaction

$$\varphi^a(p_1)\,\varphi^b(p_2) \to \varphi^c(p_3)\,\varphi^d(p_4)\,, \tag{2.18}$$

and processes involving three pseudoscalar mesons and one vector meson given by

$$V^a_\lambda(p_1)\,\varphi^b(p_2) \to \varphi^c(p_3)\,\varphi^d(p_4)\,. \tag{2.19}$$

In these reactions $\varphi^a(p_i)$ denotes an arbitrary pseudoscalar meson of species a that carries the four-momentum $p_i = (p_i^0, \mathbf{p}_i)^T$. Likewise, a vector meson with *helicity* λ is denoted by $V^a_\lambda(p_i)$.

The LORENTZ-invariant T-matrix element (2.11) for the former reaction (2.18) defines the $2 \to 2$ scattering amplitude according to

$$\langle \varphi^c(p_3)\,\varphi^d(p_4)|iT|\varphi^a(p_1)\,\varphi^b(p_2)\rangle = i(2\pi)^4\,\delta^{(4)}(p_1{+}p_2{-}p_3{-}p_4)\,\mathcal{T}^{cd,ab}(p_1,p_2,p_3,p_4)\,, \tag{2.20}$$

where the amplitude $\mathcal{T}^{cd,ab}$ will only depend on scalar products of the involved four-momenta. A sketch of the reaction in eq. (2.18) as well as two examples of possible contributions to the T-matrix element are depicted in figs. 2.2 and 2.3.

Similarly, the T-matrix element for the latter reaction (2.19) is defined by

$$\langle \varphi^c(p_3)\,\varphi^d(p_4)|iT|V^a_\lambda(p_1)\,\varphi^b(p_2)\rangle = i(2\pi)^4\,\delta^{(4)}(p_1{+}p_2{-}p_3{-}p_4)\,\mathcal{T}^{cd,ab}_\lambda(p_1,p_2,p_3,p_4)\,, \tag{2.21}$$

where $\mathcal{T}^{cd,ab}_\lambda$ is a so-called *helicity amplitude*. The scattering process $V\varphi \to \varphi\varphi$ contains an odd number of pseudoscalars, *i.e.* the process is of odd intrinsic parity. Therefore $\mathcal{T}^{cd,ab}_\lambda$ can be further decomposed into a kinematical prefactor containing the polarization

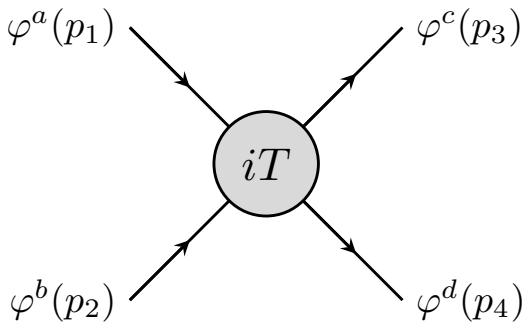

Fig. 2.2: Diagrammatic sketch of the T-matrix element for a generic $2 \to 2$ scattering process $\varphi^a(p_1)\,\varphi^b(p_2) \to \varphi^c(p_3)\,\varphi^d(p_4)$ as defined in eq. (2.20).

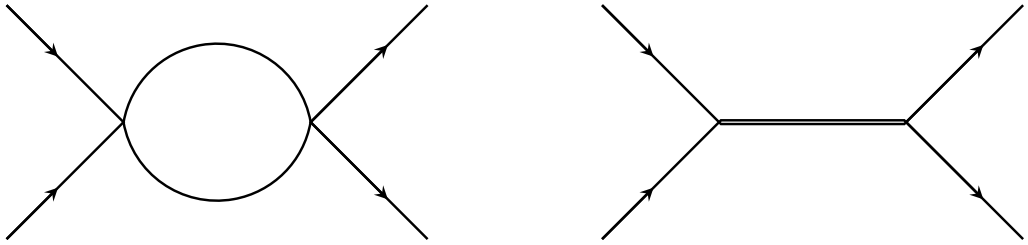

Fig. 2.3: Two FEYNMAN diagrams that may contribute to the T-matrix element in eq. (2.20): the two-particle intermediate loop (left) and a resonance exchange (right).

vector n_λ^μ of the vector meson and a *scalar amplitude* $\mathcal{F}^{cd,ab}$ accounting for the dynamical information of the scattering process [119–121]

$$\mathcal{T}_\lambda^{cd,ab}(p_1,p_2,p_3,p_4) = i\epsilon_{\mu\nu\alpha\beta}\, n_\lambda^\mu(p_1)\, p_2^\nu\, p_3^\alpha\, p_4^\beta\, \mathcal{F}^{cd,ab}(p_1,p_2,p_3,p_4)\,. \tag{2.22}$$

Like the amplitude $\mathcal{T}^{cd,ab}$ of $\varphi\varphi \to \varphi\varphi$ scattering defined in eq. (2.20), the scalar amplitude introduced in eq. (2.22) for $V\varphi \to \varphi\varphi$ scattering will only depend on scalar products of the involved four momenta. Consequently, the dependence of the T-matrix elements on the kinematical variables for both types of processes can be treated completely analogously.

2.2.1 Kinematics

The following discussion of kinematics for generic $2 \to 2$ scattering processes will be based on the example of the interaction of four pseudoscalar mesons as defined in eq. (2.18). We want to stress that the presented framework will also hold for $2 \to 2$ scattering amplitudes involving three pseudoscalar mesons and one vector meson as defined in eq. (2.19).

In general the four-momenta appearing in eq. (2.20) can be either timelike, lightlike, or spacelike, thus in MINKOWSKI space the scalar product $(p_i)^2$ can take arbitrary real values. Since each of the four particles will contribute one four-momentum, it seems the amplitude in eq. (2.20) contains 16 kinematical degrees of freedom. However, not all of them are independent: four degrees of freedom are fixed by the on-shell condition

$$p_i^0 = \sqrt{\mathbf{p}_i^2 + M_i^2}\,, \tag{2.23}$$

where M_i denotes the mass of the particle and the square root is chosen such that $p_i^0 \geq 0$ holds. Moreover, another four degrees of freedom can be eliminated by overall energy-momentum conservation of the process $p_1 + p_2 = p_3 + p_4$ fixing one of the four-momenta in terms of the others. Finally, switching to CMS reveals that further six degrees of freedom can be removed. In CMS the additional constraints (*e.g.* choose $\mathbf{p}_1 = -\mathbf{p}_2$ and $\mathbf{p}_3 = -\mathbf{p}_4$) for the three-momenta hold. We know already that one of these momenta (*e.g.* take $\mathbf{p}_4$) will be fixed by energy-momentum conservation. The constraints of the three-momenta in the CMS imply that they have to be located in a plane. Accordingly, the absolute value of one of the three vectors (*e.g.* $|\mathbf{p}_1|$ or $|\mathbf{p}_3|$) together with the angle between them $\angle(\mathbf{p}_1, \mathbf{p}_3)$ will be the only independent kinematical variables. The CMS is an inertial frame and thus connected to all other inertial frames by an appropriate LORENTZ transformation, thus the removal of these six degrees of freedom holds in all inertial frames.[#7] Hence, besides the masses of the respective particles any $2 \to 2$ scattering process will depend on two independent kinematical variables only.

Conveniently, instead of the four-momenta a set of three LORENTZ-invariant MANDELSTAM variables is defined

$$\begin{aligned} s &\equiv (p_1 + p_2)^2 = (p_3 + p_4)^2 \,, \\ t &\equiv (p_1 - p_3)^2 = (p_2 - p_4)^2 \,, \\ u &\equiv (p_1 - p_4)^2 = (p_2 - p_3)^2 \,. \end{aligned} \tag{2.24}$$

Due to energy-momentum conservation it immediately follows that

$$3r \equiv s + t + u = \sum_{i=1}^{4} M_i^2 \tag{2.25}$$

holds. As given by eq. (2.25) we note that only two MANDELSTAM variables defined in eq. (2.24) are allowed to be independent, which is in agreement with the findings of the previous paragraph. Hence, without any loss of generality the kinematical dependence of the scattering amplitude given in eq. (2.20) can also be given in terms of MANDELSTAM variables.

Especially when dealing with partial-wave amplitudes it turns out to be useful to define a set of one MANDELSTAM variable and one scattering angle instead of two MANDELSTAM variables to describe the kinematics. Since we have already seen that in the CMS the constraints on the kinematical variables take a simple form, we will choose the three-momenta to be $\mathbf{p}_1 = -\mathbf{p}_2$ and $\mathbf{p}_3 = -\mathbf{p}_4$. This allows us to rewrite eq. (2.24) in terms of the energies p_i^0, masses M_i, and three-momenta $\mathbf{p}_i$ of the involved particles as well as the scattering angle $z_s \equiv \cos\theta_s$:

$$\begin{aligned} s &= (p_1^0 + p_2^0)^2 = (p_3^0 + p_4^0)^2 \,, \\ t &= M_1^2 + M_3^2 - 2p_1^0\, p_3^0 + 2|\mathbf{p}_1|\,|\mathbf{p}_3|\, z_s = M_2^2 + M_4^2 - 2p_2^0\, p_4^0 + 2|\mathbf{p}_2|\,|\mathbf{p}_4|\, z_s \,, \\ u &= M_1^2 + M_4^2 - 2p_1^0\, p_4^0 - 2|\mathbf{p}_1|\,|\mathbf{p}_4|\, z_s = M_2^2 + M_3^2 - 2p_2^0\, p_3^0 - 2|\mathbf{p}_2|\,|\mathbf{p}_3|\, z_s \,, \end{aligned} \tag{2.26}$$

[#7] The same result can be obtained as a direct consequence of LORENTZ invariance, since the group of LORENTZ transformations is six-dimensional.

where we have chosen $\theta_s = \angle(\mathbf{p}_1, \mathbf{p}_3)$.[#8] Equation (2.26) allows us to identify $\sqrt{s}$ with the total energy in the CMS of the considered transition (2.18) and accordingly we will refer to it as the s-channel scattering process. Taking the on-shell constraint (2.23) into account, we find expressions for the absolute values of the three-momenta in terms of s and M_i given by

$$|\mathbf{p}_{1,2}|^2 = \frac{\lambda(s, M_1^2, M_2^2)}{4s}\,, \qquad |\mathbf{p}_{3,4}|^2 = \frac{\lambda(s, M_3^2, M_4^2)}{4s}\,. \tag{2.27}$$

Here we introduce the KÄLLÉN triangle function

$$\lambda(x,y,z) \equiv x^2+y^2+z^2-2(xy+xz+yz) = \left(\left(\sqrt{y}-\sqrt{z}\right)^2-x\right)\left(\left(\sqrt{y}+\sqrt{z}\right)^2-x\right), \tag{2.28}$$

which stays unchanged under permutation of its arguments. Inserting eq. (2.27) into eq. (2.23) yields for the energies

$$p_{1,2}^0 = \frac{s \pm \Delta_{12}}{2\sqrt{s}}\,, \qquad p_{3,4}^0 = \frac{s \pm \Delta_{34}}{2\sqrt{s}}\,, \tag{2.29}$$

with $\Delta_{ij} = M_i^2 - M_j^2$. Accordingly, the two remaining MANDELSTAM variables t and u can be expressed in terms of s and z_s as[#9]

$$\begin{aligned} t &= \frac{1}{2}\left(3r - s - \frac{\Delta_{12}\,\Delta_{34}}{s} + \frac{\sqrt{\lambda(s, M_1^2, M_2^2)\,\lambda(s, M_3^2, M_4^2)}}{s}\,z_s\right), \\ u &= \frac{1}{2}\left(3r - s + \frac{\Delta_{12}\,\Delta_{34}}{s} - \frac{\sqrt{\lambda(s, M_1^2, M_2^2)\,\lambda(s, M_3^2, M_4^2)}}{s}\,z_s\right), \end{aligned} \tag{2.30}$$

and consequently the scattering angle will satisfy

$$z_s = \frac{s\,(t-u) + \Delta_{12}\,\Delta_{34}}{\sqrt{\lambda(s, M_1^2, M_2^2)\,\lambda(s, M_3^2, M_4^2)}}\,. \tag{2.31}$$

Taking eqs. (2.26) and (2.30) into account it is straightforward to define the physically allowed values of the MANDELSTAM variables for the considered scattering process (2.18). Given that the particle energies (2.23) have to satisfy $p_i^0 \geq M_i$ we conclude

$$s \geq \max\!\left((M_1 + M_2)^2, (M_3 + M_4)^2\right), \tag{2.32}$$

thus the scattering process will be allowed as soon as s exceeds the respective production thresholds of the incoming $(M_1 + M_2)^2$ and outgoing pair of particles $(M_3 + M_4)^2$. Accordingly, we will refer to the right-hand side of eq. (2.32) as the s-channel *scattering*

[#8] The definition of θ_s is purely conventional, in general any possible pair of an incoming and an outgoing three-momentum leads to a valid description of the system. Only the sign of θ_s might differ when switching between conventions.

[#9] In this reduction the square root functions have to be treated with special care. Here and in the following expressions involving the square root are chosen such that $\sqrt{x} > 0$ for $x \in \mathbb{R}^+$ is fulfilled, which directly implies $\sqrt{x^2} = |x|$.

threshold. For any given s that fulfils eq. (2.32) the limits of the other two MANDELSTAM variables t and u can simply be found by imposing $-1 \leq z_s \leq 1$ on the scattering angle in eq. (2.30).

The amplitude reveals a simple symmetry: under simultaneous exchange of the momenta $p_1 \leftrightarrow p_2$ as well as the quantum numbers carried by the particle φ^a with their counterparts carried by particle φ^b the T-matrix elements have to satisfy

$$\mathcal{T}^{cd,ab}(s,t,u) = \mathcal{T}^{cd,ba}(s,u,t)\,. \tag{2.33}$$

Since a similar interchange is also possible for the outgoing particles φ^c and φ^d, we note that

$$\mathcal{T}^{cd,ab}(s,t,u) = \mathcal{T}^{dc,ba}(s,t,u)\,, \tag{2.34}$$

imposed by the definitions of the MANDELSTAM variables in eq. (2.24).

So far we considered the s-channel process (2.18) with the CMS energy given by $\sqrt{s}$. Crossing symmetry dictates that the reaction depicted in fig. 2.2 likewise describes the scattering processes

$$\varphi^a(p_1)\,\bar{\varphi}^c(-p_3) \to \bar{\varphi}^b(-p_2)\,\varphi^d(p_4)\,, \qquad \varphi^a(p_1)\,\bar{\varphi}^d(-p_4) \to \bar{\varphi}^b(-p_2)\,\varphi^c(p_3)\,, \tag{2.35}$$

in terms of the same T-matrix element as defined in eq. (2.20) when applying the correct analytic continuations in the four-momenta, *cf.* sec. 2.1.3. According to eq. (2.24) these continuations will yield $\sqrt{t}$ as CMS energy in the former process, thus we will refer to it as t-channel scattering. Since in the latter process of eq. (2.35) the CMS energy is given by $\sqrt{u}$, it will be referred as u-channel scattering. In accordance to the discussion in the previous paragraphs, we find for the t-channel MANDELSTAM variables

$$\begin{aligned} u &= \frac{1}{2}\left(3r - t + \frac{\Delta_{13}\,\Delta_{24}}{t} + \frac{\sqrt{\lambda(t,M_1^2,M_3^2)\,\lambda(t,M_2^2,M_4^2)}}{t}\,z_t\right), \\ s &= \frac{1}{2}\left(3r - t - \frac{\Delta_{13}\,\Delta_{24}}{t} - \frac{\sqrt{\lambda(t,M_1^2,M_3^2)\,\lambda(t,M_2^2,M_4^2)}}{t}\,z_t\right), \end{aligned} \tag{2.36}$$

by interchanging the four-momenta $p_2 \leftrightarrow -p_3$. Likewise the t-channel scattering angle will be defined by $\theta_t = \angle(\mathbf{p}_1, -\mathbf{p}_2)$ which yields

$$z_t = \frac{t\,(u-s) - \Delta_{13}\,\Delta_{24}}{\sqrt{\lambda(t,M_1^2,M_3^2)\,\lambda(t,M_2^2,M_4^2)}}\,. \tag{2.37}$$

By interchange of the four-momenta $p_2 \leftrightarrow -p_4$, the u-channel MANDELSTAM variables are given by

$$\begin{aligned} s &= \frac{1}{2}\left(3r - u - \frac{\Delta_{14}\,\Delta_{23}}{u} + \frac{\sqrt{\lambda(u,M_1^2,M_4^2)\,\lambda(u,M_2^2,M_3^2)}}{u}\,z_u\right), \\ t &= \frac{1}{2}\left(3r - u + \frac{\Delta_{14}\,\Delta_{23}}{u} - \frac{\sqrt{\lambda(u,M_1^2,M_4^2)\,\lambda(u,M_2^2,M_3^2)}}{u}\,z_u\right), \end{aligned} \tag{2.38}$$

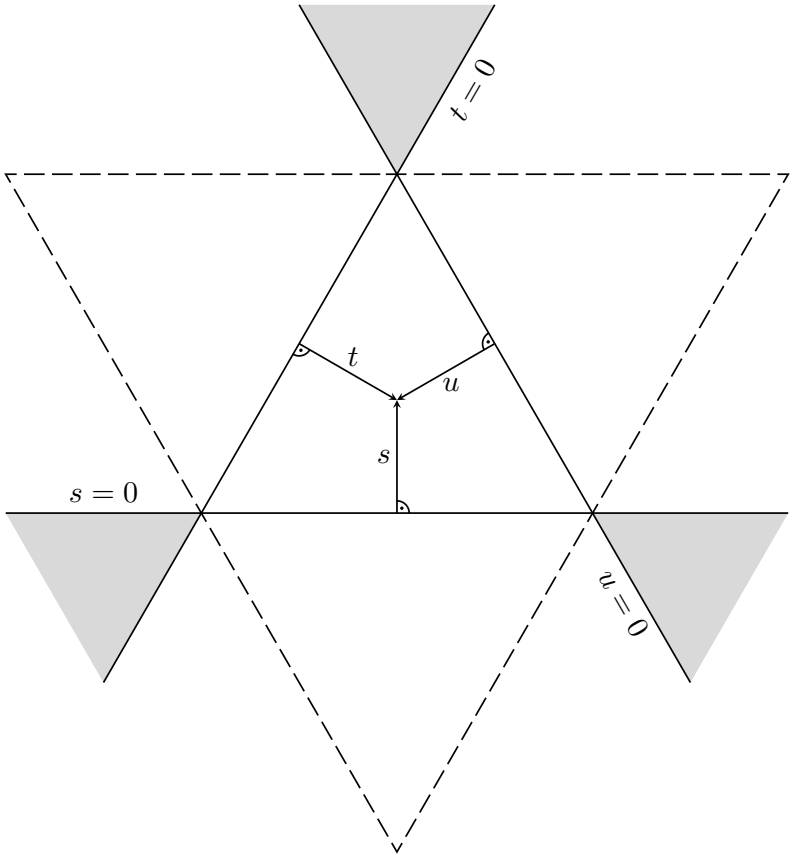

Fig. 2.4: MANDELSTAM diagram for a $2 \to 2$ scattering process of particles with equal mass M, revealing a $\frac{2\pi}{3}$ threefold rotational symmetry. The height of the equilateral triangle enclosed by the lines of $s = 0$, $t = 0$, and $u = 0$ is given by $3r = 4M^2$. The three vectors for the s-, t-, and u-axes are pointing to the triangle center at $s = t = u = r$. Note that the subthreshold triangle is represented by the dashed lines of $s = 4M^2$, $t = 4M^2$, and $u = 4M^2$. Starting at the top in clockwise direction, the physically allowed regions of s-, t-, and u-channel scattering are denoted by the grey areas.

and the corresponding u-channel scattering angle $\theta_u = \angle(\mathbf{p}_1, \mathbf{p}_3)$ defines

$$z_u = \frac{u\,(s-t) + \Delta_{14}\,\Delta_{23}}{\sqrt{\lambda(u, M_1^2, M_4^2)\,\lambda(u, M_2^2, M_3^2)}}\,. \tag{2.39}$$

In analogy to eq. (2.32) the physical regions of the t- and u-channel scattering processes are limited by the conditions

$$t \geq \max\big((M_1 + M_3)^2, (M_2 + M_4)^2\big)\,, \qquad u \geq \max\big((M_1 + M_4)^2, (M_2 + M_3)^2\big)\,, \tag{2.40}$$

for the respective CMS energies, together with the bound $-1 \leq z_{t,u} \leq 1$ on the scattering angles. Hence, eq. (2.40) defines the t- and u-channel scattering-thresholds, *i.e.*, t and u exceeding the respective production thresholds of the incoming and outgoing particles.

There is a simple way to represent the kinematics of a $2 \to 2$ scattering process in the s-t-u-plane graphically. We start by constructing an equilateral triangle of height $3r$,

where each side of this triangle will represent one of the lines $s = 0$, $t = 0$, or $u = 0$, *cf.* eq. (2.25). For any given point within the triangle the sum of perpendicular distances to each side of the triangle will be equal to its height, hence this represents the constraint in eq. (2.25). By equipping the perpendicular distance with negative sign to when pointing to the outside of the triangle, we can extend these findings to any given point in the plane. Hence, the three perpendicular vectors pointing towards the center of the triangle can be identified with the s-, t-, and u-axes. An example of such a MANDELSTAM diagram is depicted in fig. 2.4.

We are now prepared to consider the kinematics in the situation where one of the particles is heavy enough to exceed the production threshold of the other three particles. Choosing the configuration $M_1 > M_2 + M_3 + M_4$ the transition shown in fig. 2.2 will also allow for a description of the $1 \to 3$ decay process

$$\varphi^a(p_1) \to \bar{\varphi}^b(-p_2)\, \varphi^c(p_3)\, \varphi^d(p_4)\,. \tag{2.41}$$

As dictated by crossing symmetry the decay process will again be described by the T-matrix element defined in eq. (2.20) when applying the appropriate analytic continuations of the four-momenta. Clustering the reaction products into two-body subsystems will allow for a description of the $1 \to 3$ decay process (*three-body decay*) in terms of the s-, t-, and u-channel $2 \to 2$ scattering kinematics given by eqs. (2.30), (2.36), and (2.38). Hence, the physical region of the three-body decay in terms of the CMS energies in the two-body subsystems will be bounded by

$$\begin{aligned} (M_3 + M_4)^2 \leq s &\leq (M_1 - M_2)^2\,, \\ (M_2 + M_4)^2 \leq t &\leq (M_1 - M_3)^2\,, \\ (M_2 + M_3)^2 \leq u &\leq (M_1 - M_4)^2\,, \end{aligned} \tag{2.42}$$

and the according scattering angles $-1 \leq z_{s,t,u} \leq 1$. The thresholds on the CMS energies can be extracted from eq. (2.24) by transforming to the rest frames of the respective two-body subsystems. Accordingly, we will refer to the limits in eq. (2.42) as the s-, t-, and u-channel *decay-* (lower bound) and *pseudo-thresholds* (upper bound). Eq. (2.42) constrains all three MANDELSTAM variables to be positive within the physical decay region, thus in a MANDELSTAM diagram this region has to be located within the equilateral triangle given by the lines $s = 0$, $t = 0$, and $u = 0$, *cf.* fig. 2.4. Another useful representation of the decay region is provided in a DALITZ plot [122–124], *cf.* app. B.

2.2.2 Unitarity condition

Returning to the unitarity condition of a general T-matrix element derived in sec. 2.1.1, we are now equipped with the tools needed to further simplify eq. (2.15) for the special case of $2 \to 2$ scattering. As discussed in sec. 2.2.1 the T-matrix element for such a process is a function of the MANDELSTAM variables and obeys the principles of maximal analyticity, *cf.* sec. 2.1.2. Hence, in the s-channel above the scattering threshold the

following identities for the T-matrix elements will hold [125]:

$$\mathcal{T}_{fi}(p_1,p_2,p_3,p_4) \equiv \lim_{\epsilon\to 0^+} \mathcal{T}_{fi}(s+i\epsilon,t,u)\,, \qquad \mathcal{T}^*_{if}(p_3,p_4,p_1,p_2) \equiv \lim_{\epsilon\to 0^+} \mathcal{T}_{fi}(s-i\epsilon,t,u)\,, \tag{2.43}$$

where the amplitude for fixed initial and final state particle content is now holomorphic in all its continuous kinematical variables as required by analyticity. Equation (2.43) directly implies that the left-hand side of eq. (2.15) can be identified with the discontinuity of $\mathcal{T}_{fi}$ along the real s-axis above the scattering threshold

$$\begin{aligned}\mathcal{T}_{fi}(p_1,p_2,p_3,p_4) - \mathcal{T}^*_{if}(p_3,p_4,p_1,p_2)& \\ = \lim_{\epsilon\to 0^+} \big[\mathcal{T}_{fi}(s+i\epsilon,t,u) - \mathcal{T}_{fi}(s-i\epsilon,t,u)\big] &\equiv \operatorname{disc}_s \mathcal{T}_{fi}(s,t,u)\,.\end{aligned} \tag{2.44}$$

Accordingly, for a $2 \to 2$ scattering process eq. (2.15) simplifies to

$$\operatorname{disc}_s \mathcal{T}_{fi}(s,t,u) = i\,(2\pi)^4 \sum\!\!\!\!\!\!\int_n \delta^{(4)}(p_1+p_2-k_1-k_2)\,\mathcal{T}^*_{nf}(p_3,p_4,k_1,k_2)\,\mathcal{T}_{ni}(p_1,p_2,k_1,k_2)\,, \tag{2.45}$$

where the allowed intermediate states are already implicitly restricted to two-particle states.[#10] Thus, every two-particle intermediate state that is allowed to go on-shell will contribute with a discontinuity in $\mathcal{T}_{fi}$ along the real s-axis above its production threshold, *cf.* sec. 2.1.2. The branch cuts induced by eq. (2.45) are therefore referred to as *unitarity* or *right-hand cuts*.

Invariance under time reversal implies $\mathcal{T}_{fi} = \mathcal{T}_{if}$ for the T-matrix elements of $2 \to 2$ scattering and accordingly

$$\lim_{\epsilon\to 0^+} \mathcal{T}_{fi}(s+i\epsilon,t,u) = \lim_{\epsilon\to 0^+} \mathcal{T}^*_{fi}(s-i\epsilon,t,u) = \lim_{\epsilon\to 0^+} \mathcal{T}_{fi}((s-i\epsilon)^*,t,u)\,. \tag{2.46}$$

Hence, the amplitude obeys the Schwarz *reflection principle* (3.1) and the discontinuity is purely imaginary

$$\operatorname{disc}_s \mathcal{T}_{fi}(s,t,u) = 2i \lim_{\epsilon\to 0^+} \operatorname{Im} \mathcal{T}_{fi}(s+i\epsilon,t,u)\,, \tag{2.47}$$

leading to the unitarity condition along the s-channel right-hand cut

$$\begin{aligned}\lim_{\epsilon\to 0^+} \operatorname{Im} \mathcal{T}_{fi}(s+i\epsilon,t,u) = 8\pi^4 \sum\!\!\!\!\!\!\int_n \delta^{(4)}(p_1+p_2-k_1-k_2)& \\ \times \mathcal{T}^*_{nf}(q_1,q_2,k_1,k_2)\,\mathcal{T}_{ni}(p_1,p_2,k_1,k_2)\,.&\end{aligned} \tag{2.48}$$

In the following we will call a $2 \to 2$ scattering process *elastic* if the particle content in the initial-, intermediate-, and final-states coincides. Therefore, when speaking of *elastic unitarity* we will consider only one two-particle set in the sum over the intermediate states of the unitarity condition (2.48).

[#10] Of course the general unitarity condition for $2 \to 2$ scattering will allow for any multi-particle intermediate state in accordance with the considered underlying interaction. But throughout this thesis we will focus on two-particle intermediate states only.

We want to stress that that the whole derivation of eq. (2.48) relies on the assumption that the initial and final states can be represented as asymptotic states, in order to define the S-matrix elements properly, *cf.* sec. 2.1.1. Since an unstable particle decaying into three others cannot be treated as an asymptotic state,[#11] scattering processes that allow for the possibility of a $1 \to 3$ decay are by now explicitly excluded in the derivation of eq. (2.48). However, a solution to this problem exists by making use of analytic continuation: consider a world in which the unstable particle is too light to decay. The scattering amplitude involving this particle in such a world can be defined properly and eq. (2.48) will hold. Now we will treat the scattering amplitude to be also analytic in the particle's squared mass M^2, hence the amplitude can be analytically continued in M^2 to a physical world in which the decay is kinematically allowed. Due to the additional cut structure in M^2 opening at the three-particle production threshold, the analytically continued amplitude spoils the SCHWARZ reflection principle. Thus eq. (2.48) is no longer valid, however the unitarity condition in eq. (2.45) involving the discontinuity along the s-channel right-hand cut will hold [11, 126, 127].

2.3 Elastic $\pi\pi$ and $\pi\eta$ scattering processes

Final-state rescattering of $\pi\pi$ and $\pi\eta$ subsystems will play a key role in the description of the three-body decays studied throughout this thesis. Therefore, a detailed understanding of $\pi\pi \to \pi\pi$ and $\pi\eta \to \pi\eta$ scattering processes will be of major relevance in the later discussion. In this section we want to present a general treatment of elastic $\pi\pi$ and $\pi\eta$ scattering in the isospin limit[#12] and derive a decomposition of the respective amplitudes into partial waves of fixed isospin and angular momentum. According to the constraints of analyticity and unitarity (*cf.* sec. 2.2.2), along the upper rim of the right-hand cut these partial waves can be expressed in terms of the corresponding *scattering phase shifts* only. These real-valued functions encode the universal information on the $\pi\pi$ and $\pi\eta$ scattering processes of given isospin and angular momentum.

2.3.1 The $\pi\pi$ scattering amplitude

In sec. 1.2.2 we have deduced that the pions form a triplet of the third isospin component I_3 with total isospin of $I = 1$. Accordingly the three pion flavors of the physical basis can be represented uniquely as states of $|I, I_3\rangle$ given by

$$|\pi^+\rangle = |1, 1\rangle\,, \qquad |\pi^0\rangle = |1, 0\rangle\,, \qquad |\pi^-\rangle = |1, -1\rangle\,. \tag{2.49}$$

In the following it will be convenient to work with the pion state of the HERMITIAN basis. These states $|\pi^i\rangle$ can be related to the physical ones by

$$|\pi^+\rangle = -\frac{1}{\sqrt{2}}|\pi^1 + i\pi^2\rangle\,, \qquad |\pi^0\rangle = |\pi^3\rangle\,, \qquad |\pi^-\rangle = \frac{1}{\sqrt{2}}|\pi^1 - i\pi^2\rangle\,. \tag{2.50}$$

[#11] Note that in principle there is an exception to this statement, if the lifetime of the decaying particle is much larger than the timescale of the considered type of interaction [109].

[#12] We will treat the pion triplet as mass degenerated $M_\pi \equiv M^2_{\pi^+} = M^2_{\pi^0}$.

It follows directly that the states $|\pi^1\rangle$ and $|\pi^2\rangle$ of the HERMITIAN basis lack a defined third isospin component.

Out of the three physical one-pion states nine different two-pion states can be constructed. Their CLEBSCH-GORDAN decomposition [117] in terms of isospin states is given by[#13]

$$\begin{aligned}
|\pi^\pm\pi^\pm\rangle &= |2,\pm2\rangle\,, \qquad |\pi^\pm\pi^\mp\rangle = \frac{1}{\sqrt{6}}|2,0\rangle \pm \frac{1}{\sqrt{2}}|1,0\rangle + \frac{1}{\sqrt{3}}|0,0\rangle\,,\\
|\pi^\pm\pi^0\rangle &= \frac{1}{\sqrt{2}}\big(|2,\pm1\rangle \pm |1,\pm1\rangle\big)\,, \qquad |\pi^0\pi^\pm\rangle = \frac{1}{\sqrt{2}}\big(|2,\pm1\rangle \mp |1,\pm1\rangle\big)\,,\\
|\pi^0\pi^0\rangle &= \sqrt{\frac{2}{3}}|2,0\rangle - \frac{1}{\sqrt{3}}|0,0\rangle\,.
\end{aligned} \tag{2.51}$$

We note that only two of these states have a defined total isospin component. However all two-pion combinations are eigenstates of the third isospin component, using the fact that I_3 is an additive quantum number. Inverting eq. (2.51) leads to the decomposition in terms of definite isospin multiplets according to

$$\begin{aligned}
|2,\pm2\rangle &= |\pi^\pm\pi^\pm\rangle\,, \qquad |2,\pm1\rangle = \frac{1}{\sqrt{2}}|\pi^\pm\pi^0 + \pi^0\pi^\pm\rangle\,,\\
|2,0\rangle &= \frac{1}{\sqrt{6}}|\pi^+\pi^- + \pi^-\pi^+ + 2\pi^0\pi^0\rangle\,,\\
|1,\pm1\rangle &= \pm\frac{1}{\sqrt{2}}|\pi^\pm\pi^0 - \pi^0\pi^\pm\rangle, \qquad |1,0\rangle = \frac{1}{\sqrt{2}}|\pi^+\pi^- - \pi^-\pi^+\rangle\,,\\
|0,0\rangle &= \frac{1}{\sqrt{3}}|\pi^+\pi^- + \pi^-\pi^+ - \pi^0\pi^0\rangle\,,
\end{aligned} \tag{2.52}$$

and similarly we find by inserting eq. (2.50) into eq. (2.52) the decomposition in terms of the HERMITIAN states

$$\begin{aligned}
|2,\pm2\rangle &= \frac{1}{2}|\pi^1\pi^1 \pm i\pi^1\pi^2 \pm i\pi^2\pi^1 - \pi^2\pi^2\rangle\,,\ |2,\pm1\rangle = \mp\frac{1}{2}|\pi^1\pi^3 + \pi^3\pi^1 \pm i\pi^2\pi^3 \pm i\pi^3\pi^2\rangle\,,\\
|2,0\rangle &= -\frac{1}{\sqrt{6}}|\pi^1\pi^1 + \pi^2\pi^2 - 2\pi^3\pi^3\rangle\,,\\
|1,\pm1\rangle &= -\frac{1}{2}|\pi^1\pi^3 - \pi^3\pi^1 \pm i\pi^2\pi^3 \mp i\pi^3\pi^2\rangle, \qquad |1,0\rangle = \frac{i}{\sqrt{2}}|\pi^1\pi^2 - \pi^2\pi^1\rangle\,,\\
|0,0\rangle &= -\frac{1}{\sqrt{3}}|\pi^1\pi^1 + \pi^2\pi^2 + \pi^3\pi^3\rangle\,.
\end{aligned} \tag{2.53}$$

Thus a general two-pion system can form an $I = 0, 1, 2$ isospin state. Since the pions are BOSONS, they have to obey BOSE symmetry whereby the isospin wave function is

[#13] Here, the CONDON-SHORTLEY phase convention is applied [128].

required to be even (odd) under the exchange of the pions if the angular momentum quantum number ℓ is even (odd). It follows immediately that the $I = 0$ and $I = 2$ states require even ℓ, while the $I = 1$ states are connected to an odd value of ℓ. Additionally, we note that all two-pion isospin states $I = 0, 1, 2$ are even under G-parity (1.40).

We want to investigate the behaviour of the pion states under isospin symmetry a bit more formally: an arbitrary one-pion state transforms under the D^1 representation of the SU(2) isospin algebra according to

$$|\pi^i\rangle \mapsto R^i{}_j\,|\pi^j\rangle\,, \tag{2.54}$$

with $R \in \mathrm{SO}(3)$ being an orthogonal 3×3 matrix with unit determinant describing a proper rotation in the three-dimensional isospin space [129]. The two-pion state has to transform like a rank-two tensor under the $D^1 \otimes D^1$ representation of SU(2) given by

$$|\pi^i\pi^j\rangle \mapsto R^i{}_k\,R^j{}_l\,|\pi^k\pi^l\rangle\,. \tag{2.55}$$

Since the isospin rotation operation performed in eqs. (2.54) and (2.55) only changes the third isospin component without affecting the total isospin, the isospin states of fixed I have to transform among themselves, *cf.* eq. (2.53). Therefore, the space of two-pion states contains three subspaces that are closed under isospin rotations. From eq. (2.53) it follows directly that the $I = 0$ state forms a singlet, the $I = 1$ states a triplet, and the $I = 2$ states a quintet of isospin, which transform under SU(2) according to the $D^1 \otimes D^1 = D^0 \oplus D^1 \oplus D^2$ representations, respectively.

According to eq. (2.20) the T-matrix element for the scattering process $\pi^i(p_1)\,\pi^j(p_2) \to \pi^k(p_3)\,\pi^l(p_4)$ will be defined by

$$\langle\pi^k(p_3)\,\pi^l(p_4)|iT|\pi^i(p_1)\,\pi^j(p_2)\rangle = i\,(2\pi)^4\,\delta^{(4)}(p_1 + p_2 - p_3 - p_4)\,\mathcal{T}_{\pi\pi}^{kl,ij}(s,t,u)\,. \tag{2.56}$$

The Mandelstam variables in the s-channel of this scattering process will be given by

$$s = 4(p^2 + M_\pi^2)\,, \qquad t = -2p^2(1 - z_s)\,, \qquad u = -2p^2(1 + z_s)\,, \tag{2.57}$$

in the CMS as discussed in sec. 2.2.1, where $p = |\mathbf{p}_1|$ denotes the absolute value of the CMS three-momentum and $z_s = \cos\theta_s$ defines the s-channel scattering angle.

Since the function $\mathcal{T}_{\pi\pi}^{kl,ij}$ has to obey isospin symmetry, a further reduction in terms of one single scalar amplitude can be obtained [68, 130]. We note that $\mathcal{T}_{\pi\pi}^{kl,ij}$ has to stay invariant under SU(2) isospin transformations (2.54)

$$\mathcal{T}_{\pi\pi}^{kl,ij} = R^k{}_c\,R^l{}_d\,R^i{}_a\,R^j{}_b\,\mathcal{T}_{\pi\pi}^{cd,ab}\,. \tag{2.58}$$

Now we define row vectors of R according to $w_c = R^k{}_c$, $x_d = R^l{}_d$, $y_a = R^i{}_a$, and $z_b = R^j{}_b$ and define the function f in order to rewrite the right-hand side of eq. (2.58)

$$f(\mathbf{w},\mathbf{x},\mathbf{y},\mathbf{z}) = w_c\,x_d\,y_a\,z_b\,\mathcal{T}_{\pi\pi}^{cd,ab}\,. \tag{2.59}$$

Performing a second isospin rotation on f yields

$$\begin{aligned} f(\mathbf{w},\mathbf{x},\mathbf{y},\mathbf{z}) &= w_c\,x_d\,y_a\,z_b\,R^c{}_p\,R^d{}_q\,R^a{}_m\,R^b{}_n\,\mathcal{T}_{\pi\pi}^{pq,mn} \\ &= (R^T\,\mathbf{w})_p\,(R^T\,\mathbf{x})_q\,(R^T\,\mathbf{y})_m\,(R^T\,\mathbf{z})_n\,\mathcal{T}_{\pi\pi}^{pq,mn} \\ &= f(R^T\,\mathbf{w}, R^T\,\mathbf{x}, R^T\,\mathbf{y}, R^T\,\mathbf{z})\,, \end{aligned} \tag{2.60}$$

which imposes a rotation by R^T of the arguments in f. Again using the fact that f has to stay invariant under isospin rotations we can conclude: f is only allowed to depend on scalar products of the introduced vectors and each term has to contain all of them linearly. This leads to the decomposition

$$f(\mathbf{w},\mathbf{x},\mathbf{y},\mathbf{z}) = (\mathbf{w}\cdot\mathbf{x})(\mathbf{y}\cdot\mathbf{z})\,\mathcal{A}(s,t,u)+(\mathbf{w}\cdot\mathbf{y})(\mathbf{x}\cdot\mathbf{z})\,\mathcal{B}(s,t,u)+(\mathbf{w}\cdot\mathbf{z})(\mathbf{y}\cdot\mathbf{x})\,\mathcal{C}(s,t,u)\,, \quad (2.61)$$

where the functions $\mathcal{A}$, $\mathcal{B}$, and $\mathcal{C}$ can be interpreted as the s-, t-, and u-channel scattering amplitudes, respectively. Using the characteristic properties of the rotation matrices R, which simplifies the scalar products according to

$$(\mathbf{w}\cdot\mathbf{x})(\mathbf{y}\cdot\mathbf{z}) = \delta^{kl}\,\delta^{ij}\,, \qquad (\mathbf{w}\cdot\mathbf{y})(\mathbf{x}\cdot\mathbf{z}) = \delta^{jl}\,\delta^{ik}\,, \qquad (\mathbf{w}\cdot\mathbf{z})(\mathbf{y}\cdot\mathbf{x}) = \delta^{jk}\,\delta^{il}\,, \quad (2.62)$$

reduces the expression in eq. (2.61) to

$$\mathcal{T}_{\pi\pi}^{kl,ij}(s,t,u) = \delta^{kl}\,\delta^{ij}\,\mathcal{A}(s,t,u) + \delta^{jl}\,\delta^{ik}\,\mathcal{B}(s,t,u) + \delta^{jk}\,\delta^{il}\,\mathcal{C}(s,t,u)\,. \quad (2.63)$$

As the last step in the reduction of $\mathcal{T}_{\pi\pi}^{kl,ij}$ we want to show that the three functions $\mathcal{A}$, $\mathcal{B}$, and $\mathcal{C}$ can be related to each other using the invariance of the process under crossing symmetry, *cf.* sec. 2.1.3. The simultaneous exchange of $i \leftrightarrow j$ and $p_1 \leftrightarrow p_2$ (or $t \leftrightarrow u$) yields

$$\mathcal{A}(s,t,u) = \mathcal{A}(s,u,t)\,, \qquad \mathcal{B}(s,t,u) = \mathcal{C}(s,u,t)\,. \quad (2.64)$$

Similarly, we find

$$\mathcal{A}(s,t,u) = \mathcal{C}(u,t,s)\,, \qquad \mathcal{B}(s,t,u) = \mathcal{B}(u,t,s)\,, \quad (2.65)$$

for $i \leftrightarrow k$ and $p_1 \leftrightarrow -p_3$ (or $s \leftrightarrow u$) as well as

$$\mathcal{A}(s,t,u) = \mathcal{B}(t,s,u)\,, \qquad \mathcal{C}(s,t,u) = \mathcal{C}(t,s,u)\,, \quad (2.66)$$

when exchanging $i \leftrightarrow l$ and $p_1 \leftrightarrow -p_4$ (or $s \leftrightarrow t$). Hence, the symmetry in the arguments of the three functions obtained in eqs. (2.64), (2.65), and (2.66) allow us to rewrite eq. (2.61) in terms of one single function only:

$$\mathcal{T}_{\pi\pi}^{kl,ij}(s,t,u) = \delta^{kl}\,\delta^{ij}\,\mathcal{A}(s,t,u) + \delta^{jl}\,\delta^{ik}\,\mathcal{A}(t,u,s) + \delta^{jk}\,\delta^{il}\,\mathcal{A}(u,s,t)\,, \quad (2.67)$$

which by convention will be the s-channel scattering amplitude.

In eq. (2.53) we have seen that the two-pion states can be decomposed into the total isospin combinations of $I = 0, 1, 2$. By defining amplitudes of definite total isospin

$${}_J\langle\pi^k(p_3)\,\pi^l(p_4)|iT|\pi^i(p_1)\,\pi^j(p_2)\rangle_I = i\,(2\pi)^4\,\delta^{(4)}(p_1+p_2-p_3-p_4)\,\delta_{IJ}\,\mathcal{P}_I^{kl,ij}\,\mathcal{T}_I^{\pi\pi}(s,t,u)\,, \quad (2.68)$$

and corresponding isospin projection operators $\mathcal{P}_I^{kl,ij}$ we can decompose the scattering amplitude $\mathcal{T}_{\pi\pi}^{kl,ij}$ in terms of

$$\mathcal{T}_{\pi\pi}^{kl,ij}(s,t,u) = \mathcal{P}_0^{kl,ij}\,\mathcal{T}_0^{\pi\pi}(s,t,u) + \mathcal{P}_1^{kl,ij}\,\mathcal{T}_1^{\pi\pi}(s,t,u) + \mathcal{P}_2^{kl,ij}\,\mathcal{T}_2^{\pi\pi}(s,t,u)\,. \quad (2.69)$$

The isospin projection operators can be constructed exploiting the transformation properties of the two-pion states under isospin rotations (2.55). We know that the $I = 0$ singlet state has to transform like a scalar, thus the corresponding projector needs to be fully symmetric in the isospin indices. The $I = 1$ triplet states must transform antisymmetrically under isospin rotation, hence their projector needs to be odd under exchange of $i \leftrightarrow j$ or $k \leftrightarrow l$. On the other hand the $I = 2$ quintet states are again symmetric under the transformation, thus the projector has to be even under $i \leftrightarrow j$ or $k \leftrightarrow l$. Removing the scalar part from the $I = 2$ component and adjusting the normalizations properly, the isospin projection operators are given by

$$\mathcal{P}_0^{kl,ij} = \frac{1}{3}\delta^{kl}\,\delta^{ij}\,, \quad \mathcal{P}_1^{kl,ij} = \frac{1}{2}\big(\delta^{ik}\,\delta^{jl} - \delta^{il}\,\delta^{jk}\big)\,, \quad \mathcal{P}_2^{kl,ij} = \frac{1}{2}\big(\delta^{ik}\,\delta^{jl} + \delta^{il}\,\delta^{jk}\big) - \frac{1}{3}\delta^{kl}\,\delta^{ij}\,, \tag{2.70}$$

and obey the projector identities

$$\mathcal{P}_I^{kl,ab}\,\mathcal{P}_J^{ab,ij} = \delta_{IJ}\,\mathcal{P}_I^{kl,ij}\,, \qquad \mathcal{P}_I^{kl,ij} = \mathcal{P}_I^{ij,kl}\,, \qquad \sum_I \mathcal{P}_I^{kl,ij} = \delta^{ik}\,\delta^{jl}\,. \tag{2.71}$$

Comparing eqs. (2.67) and (2.69) we find

$$\begin{aligned}
\mathcal{T}_0^{\pi\pi}(s,t,u) &= 3\mathcal{A}(s,t,u) + \mathcal{A}(t,u,s) + \mathcal{A}(u,s,t)\,,\\
\mathcal{T}_1^{\pi\pi}(s,t,u) &= \mathcal{A}(t,u,s) - \mathcal{A}(u,s,t)\,,\\
\mathcal{T}_2^{\pi\pi}(s,t,u) &= \mathcal{A}(t,u,s) + \mathcal{A}(u,s,t)\,.
\end{aligned} \tag{2.72}$$

Now we want to make use of the unitarity condition of the scattering amplitude as discussed in sec. 2.2.2. We will treat the $\pi\pi$ scattering to be elastic, since the first physical allowed intermediate state[#14] contributing will be four pions. Thus strictly speaking the elastic approximation holds only for CMS energies $s < 16M_\pi^2$ below the four-pion threshold.[#15] In this low energy region the intermediate states are given by $|\pi^a(k_1)\,\pi^b(k_2)\rangle$ and the integral sum in eq. (2.48) can be replaced by

$$\sum\!\!\!\!\!\!\int_n \mapsto \frac{1}{2}\sum_{a,b}\int \frac{\mathrm{d}^3\mathbf{k}_1}{(2\pi)^3\,2k_1^0}\,\frac{\mathrm{d}^3\mathbf{k}_2}{(2\pi)^3\,2k_2^0}\,, \tag{2.73}$$

where the sum over the intermediate states a, b runs from 1 to 3 and the symmetry factor in front compensates for the double counting of identical states. Making use of isospin projection operators (2.70) the unitarity condition (2.48) can be given directly in terms of the definite isospin amplitudes by

$$\begin{aligned}
\operatorname{Im}\mathcal{T}_I^{\pi\pi}(s,z_s) = \frac{1}{16\pi^2}\int \frac{\mathrm{d}^3\mathbf{k}_1}{2k_1^0}\,\frac{\mathrm{d}^3\mathbf{k}_2}{2k_2^0}\,\delta^{(4)}(p_1+p_2-k_1-k_2)\\
\times\,\mathcal{T}_I^{\pi\pi}(p_1,p_2,k_1,k_2)\,(\mathcal{T}_I^{\pi\pi})^*(k_1,k_2,p_3,p_4)\,,
\end{aligned} \tag{2.74}$$

[#14] As long we restrict ourselves to G-parity conserving strong processes, only even multiplets of pions are allowed to contribute as intermediate states in $\pi\pi \to \pi\pi$, *cf.* ch. 1.

[#15] In practice it turns out that the four-pion-state contribution can be safely neglected even up to $s \gtrsim 1\,\mathrm{GeV}^2$ due to the soft opening of the four-particle phase space, *cf.* [120,131]. Actually, $K\bar{K}$ systems for energies above $s > 4M_K^2$ will be the dominant inelastic effects in $I = 0$ S-wave $\pi\pi \to \pi\pi$ scattering [132–134].

where the left-hand side is implicitly understood to be evaluated for $s + i\epsilon$ in the limit of $\epsilon \to 0^+$ along the right-hand cut. Choosing the CMS fixes the three-momenta $\mathbf{p}_1 = -\mathbf{p}_2$ and accordingly $\mathbf{p}_3 = -\mathbf{p}_4$ allows us to split the delta function into $\delta(\sqrt{s} - k_1^0 - k_2^0)\,\delta^{(3)}(\mathbf{k}_1 + \mathbf{k}_2)$. The evaluation of the first integration over $\mathbf{k}_2$ will fix the momenta $\mathbf{k}_1 = -\mathbf{k}_2$ and energies $k_1^0 = k_2^0$, thus we define $k \equiv |\mathbf{k}_1| = \sqrt{(k_1^0)^2 - M_\pi^2}$. Switching now to spherical coordinates in the remaining integral with $\mathrm{d}^3\mathbf{k}_1 = \mathrm{d}\Omega_s'\,\mathrm{d}k\,k^2 = \mathrm{d}\Omega_s'\,\mathrm{d}k_1^0\,k_1^0\,k$ the unitarity condition in eq. (2.74) simplifies to

$$\begin{aligned}\operatorname{Im}\mathcal{T}_I^{\pi\pi}(s,z_s) &= \frac{1}{64\pi^2}\int\frac{\mathrm{d}\Omega_s'\,\mathrm{d}k_1^0}{k_1^0}\sqrt{(k_1^0)^2 - M_\pi^2}\,\delta(\sqrt{s} - 2k_1^0)\,\mathcal{T}_I^{\pi\pi}(s,z_s')\,(\mathcal{T}_I^{\pi\pi})^*(s,z_s'') \\ &= \frac{1}{128\pi^2}\,\sigma_\pi(s)\int\mathrm{d}\Omega_s'\,\mathcal{T}_I^{\pi\pi}(s,z_s')\,(\mathcal{T}_I^{\pi\pi})^*(s,z_s'')\,,\end{aligned} \tag{2.75}$$

where $\sigma_\pi(s) \equiv \sqrt{1 - 4M_\pi^2/s}$ defines the two-pion phase-space function. The introduced scattering angles z_s, z_s', and z_s'' are defined in the initial-to-final $\angle(\mathbf{p}_1, \mathbf{p}_3)$, the initial-to-intermediate $\angle(\mathbf{p}_1, \mathbf{k}_1)$, and the intermediate-to-final $\angle(\mathbf{k}_1, \mathbf{p}_3)$ systems, respectively. Accordingly, the solid angle $\mathrm{d}\Omega_s'$ is defined in the initial to intermediate system. Expanding both sides of eq. (2.75) in terms of partial waves

$$\mathcal{T}_I^{\pi\pi}(s,z_s) = 32\pi\sum_{\ell=0}^{\infty}(2\ell+1)\,P_\ell(z_s)\,t_{I\ell}^{\pi\pi}(s)\,, \tag{2.76}$$

and using the properties of the Legendre polynomials P_ℓ (*cf.* app. A.2) we arrive at the unitarity condition of the ℓ-th partial-wave amplitude

$$\lim_{\epsilon\to0^+}\operatorname{Im}t_{I\ell}^{\pi\pi}(s+i\epsilon) = \lim_{\epsilon\to0^+}\sigma_\pi(s)\,|t_{I\ell}^{\pi\pi}(s+i\epsilon)|^2\,, \tag{2.77}$$

valid for real values of $s > 4M_\pi^2$. In other words, the partial-wave amplitude along the upper rim of the right-hand cut has to be of the form (*cf.* app. A.3)

$$\lim_{\epsilon\to0^+} t_{I\ell}^{\pi\pi}(s+i\epsilon) = \sigma_\pi^{-1}(s)\,\sin\delta_{I\ell}^{\pi\pi}(s)\,\exp\bigl[i\delta_{I\ell}^{\pi\pi}(s)\bigr]\,, \tag{2.78}$$

where the real-valued functions $\delta_{I\ell}^{\pi\pi}$ define the $\pi\pi$ scattering phase-shifts of isospin I and angular momentum ℓ. As already stated earlier, I and ℓ have to be both even or odd in order to fulfil the constraints of Bose symmetry on the T-matrix element. This property is now encoded in the behaviour of the isospin-projection operators and Legendre polynomials, which map the system under simultaneous interchange of the pion isospin indices $i \leftrightarrow j$ and momenta $p_1 \leftrightarrow p_2$ (or $z_s \mapsto -z_s$) to

$$\mathcal{P}_I^{kl,ij} \mapsto (-)^I\,\mathcal{P}^{kl,ij}\,, \qquad P_\ell(z_s) \mapsto (-)^\ell\,P_\ell(z_s)\,. \tag{2.79}$$

Truncating the sum in eq. (2.76) after S- and P-waves we obtain the isospin amplitudes of elastic $\pi\pi$ scattering in the isospin limit along the upper rim of the unitarity cut according to

$$\begin{aligned}\lim_{\epsilon\to0^+}\mathcal{T}_0^{\pi\pi}(s+i\epsilon,z_s) &= 32\pi\,\sigma_\pi^{-1}(s)\,\sin\delta_{00}^{\pi\pi}(s)\,\exp\bigl[i\delta_{00}^{\pi\pi}(s)\bigr]\,, \\ \lim_{\epsilon\to0^+}\mathcal{T}_1^{\pi\pi}(s+i\epsilon,z_s) &= 96\pi\,z_s\,\sigma_\pi^{-1}(s)\,\sin\delta_{11}^{\pi\pi}(s)\,\exp\bigl[i\delta_{11}^{\pi\pi}(s)\bigr]\,, \\ \lim_{\epsilon\to0^+}\mathcal{T}_2^{\pi\pi}(s+i\epsilon,z_s) &= 32\pi\,\sigma_\pi^{-1}(s)\,\sin\delta_{20}^{\pi\pi}(s)\,\exp\bigl[i\delta_{20}^{\pi\pi}(s)\bigr]\,.\end{aligned} \tag{2.80}$$

2.3.2 The $\pi\eta$ scattering amplitude

In an analogous fashion to sec. 2.3.1 we want to decompose the scattering amplitude for the $\pi\eta \to \pi\eta$ process. The η can be identified as the $I = 0$ isospin singlet counterpart of the pion $I = 1$ isospin triplet, *cf.* sec. 1.2.2. Hence, in terms of a $|I, I_3\rangle$ state it can be represented by

$$|\eta\rangle = |0, 0\rangle \,. \tag{2.81}$$

Accordingly, three different two-particle states of total isospin $I = 1$ can be formed out of a $\pi\eta$ pair

$$|\pi^+\eta\rangle = |1, 1\rangle \,, \qquad |\pi^0\eta\rangle = |1, 0\rangle \,, \qquad |\pi^-\eta\rangle = |1, -1\rangle \,, \tag{2.82}$$

which can be identified by their third isospin component I_3 uniquely. Considering the G-parity transformation properties (1.40) of the pions and the η, we note that the $|\pi\eta\rangle$ states will be odd under G.

The T-matrix element (2.20) for the $\pi^i(p_1)\,\eta(p_2) \to \pi^j(p_3)\,\eta(p_4)$ scattering process will be defined by

$$\langle \pi^j(p_3)\,\eta(p_4)|iT|\pi^i(p_1)\,\eta(p_2)\rangle = i(2\pi)^4\,\delta^{(4)}(p_1 + p_2 - p_3 - p_4)\,\mathcal{T}^{ij}_{\pi\eta}(t, z_t) \,, \tag{2.83}$$

where the MANDELSTAM variables are chosen according to

$$s = (p_1 - p_4)^2 \,, \qquad t = (p_1 + p_2)^2 \qquad u = (p_1 - p_3)^2 \,, \tag{2.84}$$

and z_t denotes the scattering angle in the t-channel, *cf.* sec. 2.2.1. Since the T-matrix element obeys isospin symmetry, we have to ensure identical pion-isospin indices for the considered initial and final states. Therefore, the scattering amplitude is given in terms of one single $I = 1$ isospin amplitude[#16]

$$\mathcal{T}^{ij}_{\pi\eta}(t, z_t) = \delta^{ij}\,\mathcal{T}^{\pi\eta}_1(t, z_t) \,. \tag{2.85}$$

Under the assumption of elastic scattering,[#17] only $|\pi^a(k_1)\,\eta(k_2)\rangle$ are allowed to contribute as intermediate states in the unitarity condition for the scattering amplitude, *cf.* sec. 2.2.2. Replacing the integral sum in eq. (2.48) by

$$\sum\!\!\!\!\!\!\int_n \;\mapsto\; \sum_a \int \frac{\mathrm{d}^3\mathbf{k}_1}{(2\pi)^3\,2k_1^0}\,\frac{\mathrm{d}^3\mathbf{k}_2}{(2\pi)^3\,2k_2^0} \,, \tag{2.86}$$

[#16] The t- and u-channel both equally define the $\pi\eta \to \pi\eta$ scattering amplitude while the s-channel amplitude can be identified with $\eta\eta \to \pi\pi$ scattering, which is not of interest here. Nevertheless we want to point out that the s-channel, where isospin conservation forces the $|\pi^i\pi^j\rangle$ state to be of total isospin $I = 0$, gives rise to inelastic contributions in the unitarity conditions of $\pi\pi \to \pi\pi$ and $\eta\eta \to \eta\eta$.

[#17] Under the assumption of isospin symmetry two-pion states are not allowed to contribute as intermediate states in this process. This can be seen easily considering the opposite transformation properties under G-parity of the respective two-particle systems. Hence, the first reasonable contribution in the $\pi\eta$ S-wave will come from $K\bar{K}$-systems for energies $t > 4M_K^2$ [135, 136]. For the higher partial waves the first inelastic contribution to $\pi\eta$ scattering will stem from three-pion states above the threshold $t > 9M_\pi^2$ [137–139]. It is worth to mention that this transition is of odd intrinsic parity and therefore governed by the chiral anomaly of QCD [140, 141].

where the sum over the isospin index a runs from 1 to 3, unitarity demands the isospin amplitude to fulfil

$$\begin{aligned}\operatorname{Im}\mathcal{T}_1^{\pi\eta}(t,z_t) = \frac{1}{8\pi^2}\int \frac{\mathrm{d}^3\mathbf{k}_1}{2k_1^0}\,\frac{\mathrm{d}^3\mathbf{k}_2}{2k_2^0}\,\delta^{(4)}(p_1+p_2-k_1-k_2)\\ \times\,\mathcal{T}_1^{\pi\eta}(p_1,p_2,k_1,k_2)\,(\mathcal{T}_1^{\pi\eta})^*(k_1,k_2,p_3,p_4)\,,\end{aligned} \tag{2.87}$$

where the left-hand side is implicitly understood to be evaluated for $t+i\epsilon$ in the limit of $\epsilon\to 0^+$ along the right-hand cut. The integrals over the intermediate-state momenta will be treated in a similar manner as discussed in sec. 2.3.1 for the $\pi\pi$ scattering amplitude. Choosing the center-of-mass frame $\mathbf{p}_1=-\mathbf{p}_2$ and $\mathbf{p}_3=-\mathbf{p}_4$ allows us to split the four-dimensional delta function. The three-dimensional part of the delta function will fix $\mathbf{k}_1=-\mathbf{k}_2$ when performing the first integral over $\mathbf{k}_2$. Accordingly, the leftover one-dimensional delta function demands that $k_1^0=\sqrt{k^2+M_\pi^2}$ and $k_2^0=\sqrt{k^2+M_\eta^2}$, where $k^2\equiv|\mathbf{k}_1|^2=\lambda(t,M_\pi^2,M_\eta^2)/(4t)$ as given in eq. (2.27) yields the correct $\pi\eta$ phase-space factor when integrating over $\mathrm{d}^3\mathbf{k}_1=\mathrm{d}\Omega_t'\,\mathrm{d}k\,k^2$. This simplifies eq. (2.87) to

$$\operatorname{Im}\mathcal{T}_1^{\pi\eta}(t,z_t) = \frac{1}{64\pi^2}\sqrt{\frac{\lambda(t,M_\pi^2,M_\eta^2)}{t^2}}\int \mathrm{d}\Omega_t'\,\mathcal{T}_1^{\pi\eta}(t,z_t')\,(\mathcal{T}_1^{\pi\eta})^*(t,z_t'')\,, \tag{2.88}$$

where the scattering angles z_t, z_t', and z_t'' are chosen in the initial to final $\angle(\mathbf{p}_1,\mathbf{p}_3)$, the initial-to-intermediate $\angle(\mathbf{p}_1,\mathbf{k}_1)$, and the intermediate-to-final state systems $\angle(\mathbf{k}_1,\mathbf{p}_3)$, respectively. The solid angle $\mathrm{d}\Omega_t'$ is defined analogously in the initial-to-intermediate system. We define the partial wave decomposition of the isospin amplitude according to

$$\mathcal{T}_1^{\pi\eta}(t,z_t) = 16\pi\sum_{\ell=0}^{\infty}(2\ell+1)\,P_\ell(z_t)\,t_{1\ell}^{\pi\eta}(t)\,, \tag{2.89}$$

and using the properties of the Legendre polynomials P_ℓ (*cf.* app. A.2) directly reduces eq. (2.88) to the unitarity condition for the partial-wave amplitudes given by

$$\lim_{\epsilon\to0^+}\operatorname{Im}t_{1\ell}^{\pi\eta}(t+i\epsilon) = \lim_{\epsilon\to0^+}\sqrt{\frac{\lambda(t,M_\pi^2,M_\eta^2)}{t^2}}\left|t_{1\ell}^{\pi\eta}(t+i\epsilon)\right|^2, \tag{2.90}$$

valid along the upper rim of the unitarity cut for real values of $t>(M_\pi+M_\eta)^2$. Hence, in terms of the real-valued $\pi\eta$ scattering phase-shifts $\delta_{1\ell}^{\pi\eta}$ elastic unitarity states (*cf.* app. A.3)

$$\lim_{\epsilon\to0^+}t_{1\ell}^{\pi\eta}(t+i\epsilon) = \sqrt{\frac{t^2}{\lambda(t,M_\pi^2,M_\eta^2)}}\,\sin\delta_{1\ell}^{\pi\eta}(t)\,\exp\bigl[i\delta_{1\ell}^{\pi\eta}(t)\bigr]\,. \tag{2.91}$$

Restricting ourselves to S- and P-wave contributions only, the isospin amplitude for elastic $\pi\eta$ scattering in the isospin limit along the upper rim of the unitarity cut can be decomposed into

$$\begin{aligned}\lim_{\epsilon\to0^+}\mathcal{T}_1^{\pi\eta}(t+i\epsilon,z_t) = 16\pi\sqrt{\frac{t^2}{\lambda(t,M_\pi^2,M_\eta^2)}}\,\Bigl(\sin\delta_{10}^{\pi\eta}(t)\,\exp\bigl[i\delta_{10}^{\pi\eta}(t)\bigr]\\ +\,3z_t\,\sin\delta_{11}^{\pi\eta}(t)\,\exp\bigl[i\delta_{11}^{\pi\eta}(t)\bigr]\Bigr)\,.\end{aligned} \tag{2.92}$$

Part II

Introduction to dispersion relations

Chapter 3

Dispersion relations for functions with one cut

As discussed in ch. 2, S-matrix elements share certain powerful analytic constraints on which dispersion theory is founded. Exploiting basic theorems of complex analysis, dispersion relations connect the discontinuity of a function along its branch cuts to the function itself via an integral equation, and therefore provide an analytic continuation into the entire complex plane. In this chapter we focus exclusively on these mathematical aspects of dispersion theory. We want to introduce these fundamental concepts on a couple of examples for complex-valued single-variable functions f possessing only a right-hand cut. An application of this framework to physical $2 \to 2$ scattering amplitudes will be discussed in ch. 4.

This chapter is structured as follows: the spectral representation of f is discussed in sec. 3.1. In sec. 3.2 we introduce the Omnès function Ω and the Omnès representation of f in terms of this function. A matching scheme for a change between the two representations is described in sec. 3.3. In sec. 3.4 the concept of basis functions is introduced. Finally, a comment on the possibility of allowing for polynomial shifts in the Omnès representation of f is given in sec. 3.5. For further details on general aspects of dispersion theory we suggest [44, 107, 108, 111, 142, 143]. A highly recommended comprehensive and mathematically rigorous formulation of the subjects of this chapter can be found in [144].

3.1 Spectral representation of dispersion relations

In order to introduce the mathematical concepts of dispersion relations we start with a basic example. Consider a complex-valued function $f(s)$ that fulfills the following properties:

- f is a holomorphic function in the cut complex plane $\mathbb{C} \setminus \mathbb{B}_+$ excluding a branch cut $\mathbb{B}_+ = [s_0, \infty)$ along the positive real axis starting at some value $s_0 > 0$;
- f takes real values for any $s \in \mathbb{R} \setminus \mathbb{B}_+$;
- $f(s) \asymp s^n$ with $n \in \mathbb{R}$, *i.e.*, f will not grow faster than some power n of s when taking the limit of $|s| \to \infty$.

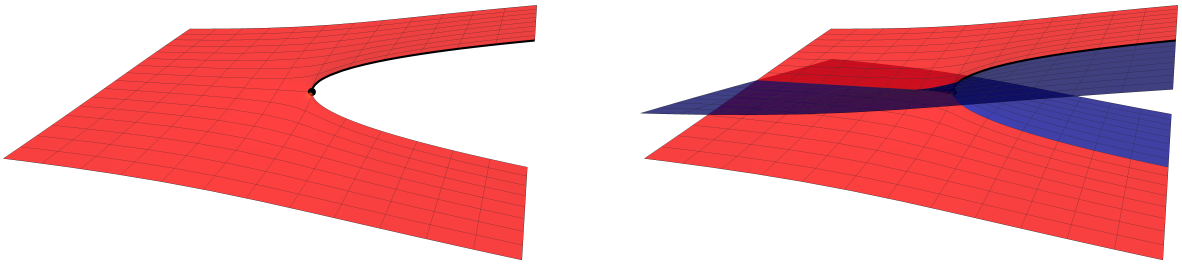

Fig. 3.1: Sketch of the imaginary part of $f(s) = -\sqrt{s_0 - s}$ in the complex s-plane in arbitrary units. The real and imaginary s-axes are pointing from the left to the right and from the front to the back, respectively. The branch point $s_0 > 0$ is marked by the black dot and the thick black line marks $s + i\epsilon$ for $s \in \mathbb{R}$ in the limit of $\epsilon \to 0^+$. Evaluating $\operatorname{Im} f(s)$ for complex values of s yield the function on the first (red) and second RIEMANN sheet (blue), which are smoothly connected along the branch cut.

A function that obeys these properties satisfies the SCHWARZ *reflection principle*

$$f^*(s) = f(s^*), \tag{3.1}$$

for any given $s \in \mathbb{C} \setminus \mathbb{B}_+$. This principle allows us directly to relate the discontinuity of f to its imaginary part

$$\operatorname{disc} f(s) = \lim_{\epsilon \to 0^+} \left[f(s + i\epsilon) - f(s - i\epsilon) \right] = 2i \lim_{\epsilon \to 0^+} \operatorname{Im} f(s + i\epsilon)\,, \tag{3.2}$$

since $f(s - i\epsilon) = f^*(s + i\epsilon)$ holds for $s \in \mathbb{R}$ according to eq. (3.1).

We want to give a simple example of a function fulfilling the properties discussed in the previous paragraph. Consider the equation $s = w^2$ which has two solutions $w = \pm\sqrt{s}$. Hence, the square root is a multivalued function yielding two distinct RIEMANN sheets representing the two solutions $\pm\sqrt{s}$. Since we have chosen $\sqrt{s} > 0$ for $s > 0$ in ch. 2, a valid example will be given by $f(s) = -\sqrt{s_0 - s}$. By definition f will represent the function f_I evaluated on the first RIEMANN sheet, while $f_{II}(s) = \sqrt{s_0 - s}$ will yield f on the second RIEMANN sheet. A sketch of this example function in the complex s-plane is given in fig. 3.1.

3.1.1 Unsubtracted spectral representation

According to CAUCHY's integral formula any given function f holomorphic in the complex s-plane enclosed by the contour $\mathcal{C}$ can be represented by

$$f(s) = \frac{1}{2\pi i} \oint_{\mathcal{C}} \mathrm{d}x\, \frac{f(x)}{x - s}\,, \tag{3.3}$$

where the integration path has to be taken in a counter-clockwise sense. Given that f possesses a right-hand cut as defined in sec. 3.1, a valid integration path that avoids this branch cut needs to be defined. Apart from this limitation the contour is allowed to be

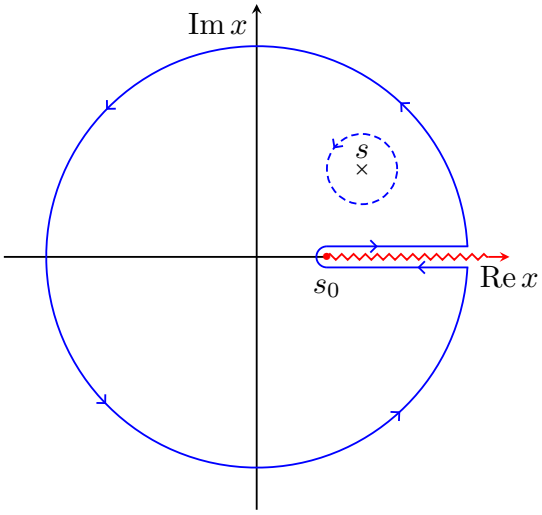

Fig. 3.2: Choices of the integration contour (blue) in the complex x-plane. The dashed path depicts a closed circular contour of CAUCHY's integral formula (3.3), while the solid path represents the enlarged contour enclosing the cut complex plane $\mathbb{C} \setminus \mathbb{B}_+$. Starting at $s_0 > 0$, the branch cut (red) extends to infinity along the positive real axis. The integration contour will avoid this cut by running along the upper and lower rims according to the prescription $x \pm i\epsilon$ in the limit $\epsilon \to 0^+$.

chosen freely as long as the point s is encircled, a proper choice of such a path is shown in fig. 3.2. This allows us to split eq. (3.3) into three contributions

$$\begin{aligned} f(s) &= \frac{1}{2\pi i} \lim_{\epsilon \to 0^+} \int_{s_0}^{\infty} \mathrm{d}x \, \frac{f(x+i\epsilon)}{x-s} - \frac{1}{2\pi i} \lim_{\epsilon \to 0^+} \int_{s_0}^{\infty} \mathrm{d}x \, \frac{f(x-i\epsilon)}{x-s} + \frac{1}{2\pi i} \int_{\gamma_\mathcal{A}} \mathrm{d}x \, \frac{f(x)}{x-s} \\ &= \frac{1}{\pi} \lim_{\epsilon \to 0^+} \int_{s_0}^{\infty} \mathrm{d}x \, \frac{\operatorname{Im} f(x+i\epsilon)}{x-s} + \frac{1}{2\pi i} \int_{\gamma_\mathcal{A}} \mathrm{d}x \, \frac{f(x)}{x-s} \,. \end{aligned} \tag{3.4}$$

According to eq. (3.2) the numerators of the former two integrals can be identified with the imaginary part of f evaluated on the upper rim of the cut. The latter part in eq. (3.4) contains the contribution of the integral along the complex arc parameterized by the path $\gamma_\mathcal{A}$ of radius Λ^2. In order to account for any given value of $s \in \mathbb{C} \setminus \mathbb{B}_+$ this radius Λ^2 needs to be sent to infinity.

We want to study the behavior of the second integral of eq. (3.4) in more detail. Along the complex arc the path $\gamma_\mathcal{A}$ can be parameterized by a circular segment

$$\gamma_\mathcal{A}(\phi) = c + \Lambda^2 \exp(i\phi) \tag{3.5}$$

of radius $\Lambda^2 > 0$ and origin $c \in \mathbb{C} \setminus \mathbb{B}_+$. The integral along the path γ_A is then given by

$$\int_{\gamma_\mathcal{A}} \mathrm{d}x \, h(x) = \int_{\phi(x+i\epsilon)}^{\phi(x-i\epsilon)} \mathrm{d}\phi \, h\big(\gamma_\mathcal{A}(\phi)\big) \, \gamma'_\mathcal{A}(\phi) = i \int_{\phi(x+i\epsilon)}^{\phi(x-i\epsilon)} \mathrm{d}\phi \, \Lambda^2 \, h\big(\gamma_\mathcal{A}(\phi)\big) \, \exp(i\phi) \,, \tag{3.6}$$

where we introduced the function $h(x) = f(x)/(x-s)$. Provided that h asymptotically falls off fast enough, *i.e.*, $h(s) \asymp x^{n-1}$ with $n < 0$ when taking the limit $|x| \to \infty$, the

contribution along an infinite arc will vanish:

$$\lim_{\Lambda^2\to\infty}\int_{\gamma_{\mathcal{A}}} \mathrm{d}x\, h(x) = 0\,. \tag{3.7}$$

Accordingly, the asymptotic behavior of $f(s) \asymp s^n$ needs to be restricted likewise. Since in such a case the integrand in the first term on the second line of eq. (3.4) vanishes asymptotically faster than s^{-1}, the integral along the branch cut will converge. This allows us directly to relate the function f with $n < 0$ for any $s \in \mathbb{C} \setminus \mathbb{B}_+$ to

$$f(s) = \frac{1}{\pi}\lim_{\epsilon\to 0^+}\int_{s_0}^{\infty}\mathrm{d}x\,\frac{\operatorname{Im} f(x+i\epsilon)}{x-s}\,, \tag{3.8}$$

which is a dispersion relation for f or, to be more precise, this special case is known as the *unsubtracted spectral representation* of f.[#1] Note that eq. (3.8) provides an analytic continuation of f into the complex plane determined entirely by the information on its imaginary part along the upper rim of the branch cut.

3.1.2 Subtracted spectral representation

We would like to allow for a less restrictive asymptotic behavior of the function f according to $f(s) \asymp s^n$ with $n \geq 0$ in the limit of $|s| \to \infty$. Therefore, we introduce a new function [145]

$$g(x) \equiv \frac{f(x)}{Q_m(x)\,(x-s)}\,, \tag{3.9}$$

where Q_m is a polynomial of degree $m = \lfloor n \rfloor + 1$ with real coefficients $s_j < s_0$ of the form

$$Q_m(x) = (x-s_1)\cdot(x-s_2)\cdot\ldots\cdot(x-s_m)\,. \tag{3.10}$$

Accordingly, the function g is meromorphic on $\mathbb{C} \setminus \mathbb{B}_+$, *i.e.*, it exhibits isolated poles at the zeros of the denominator in eq. (3.9). As a more generalized version of eq. (3.3) we consider the *residue theorem*

$$\sum_j \operatorname{res}(g,\zeta_j) = \frac{1}{2\pi i}\oint_{\mathcal{C}}\mathrm{d}x\,\frac{f(x)}{Q_m(x)(x-s)}\,, \tag{3.11}$$

where the *residue* of g at an isolated pole ζ_j of degree k is given by

$$\operatorname{res}(g,\zeta_j) = \frac{1}{(k-1)!}\lim_{x\to\zeta_j}\frac{\mathrm{d}^{k-1}}{\mathrm{d}x^{k-1}}\big[(x-\zeta_j)^k\, g(x)\big]\,. \tag{3.12}$$

The integration contour will be chosen as depicted in fig. 3.3, such that all singularities apart from the branch cut are enclosed by the path $\gamma_{\mathcal{C}}$.

[#1] Dispersion relations are commonly stated in the form of an integral over the imaginary part of f. However, we want to stress that the derivation will also hold for functions that do not obey the Schwarz reflection principle. In such a case the imaginary part of f in eq. (3.8) needs to be replaced by the discontinuity of f.

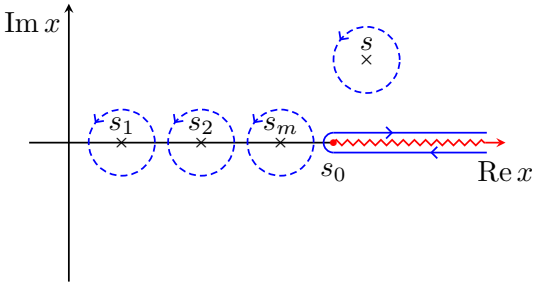

Fig. 3.3: Choices of the integration contour (blue) in the complex x-plane. The dashed paths depict closed circular contours around the isolated poles $s, s_1, s_2, ..., s_m$ in the residue theorem (eq. (3.11)), while the solid path represents the enlarged contour enclosing $\mathbb{C}\backslash\mathbb{B}_+$ running along the upper and lower rim of the cut according to the prescription $x \pm i\epsilon$ in the limit of $\epsilon \to 0^+$. Starting at $s_0 > 0$, the branch cut (red) extends to infinity along the positive real axis.

In order to solve the left-hand side of eq. (3.11) we assume that all poles are of degree one, *i.e.* the denominator of eq. (3.9) exhibits $m+1$ separated zeros at $s, s_1, ..., s_m$. Therefore we can apply eq. (3.12) with $k = 1$ on the left-hand side of eq. (3.11) resulting in

$$\begin{aligned}
\sum_j \operatorname{res}(g, \zeta_j) &= \frac{f(s)}{Q_m(s)} + \frac{f(s_1)}{(s_1 - s)\cdot(s_1 - s_2)\cdot ... \cdot (s_1 - s_m)} \\
&\qquad + \frac{f(s_2)}{(s_2 - s)\cdot(s_2 - s_1)\cdot ... \cdot (s_2 - s_m)} + ... \\
&= \frac{1}{Q_m(s)}\Big[(f(s) - \frac{(s - s_2)\cdot ... \cdot (s - s_m)}{(s_1 - s_2)\cdot ... \cdot (s_1 - s_m)} f(s_1) \\
&\qquad - \frac{(s - s_1)\cdot ... \cdot (s - s_m)}{(s_2 - s_1)\cdot ... \cdot (s_2 - s_m)} f(s_2) + ...\Big] \\
&= \frac{1}{Q_m(s)}\big[f(s) - P_{m-1}(s)\big]\,,
\end{aligned} \tag{3.13}$$

where P_{m-1} is a polynomial of degree $m-1$. We want to stress that this is only one possible choice on the location of $s_1, s_2, ..., s_m$. In fact any other arrangement of the zeros in Q_m will yield a similar result as given in eq. (3.13), although the coefficients of P_{m-1} might depend on the exact choice of $s_1, s_2, ..., s_m$.

In accordance with eq. (3.4) the right-hand side of eq. (3.11) can be rewritten as

$$\frac{1}{2\pi i}\oint_\gamma \mathrm{d}x\, \frac{f(x)}{Q_m(x)(x - s)} = \frac{1}{\pi}\lim_{\epsilon\to 0^+}\int_{s_0}^{\infty}\mathrm{d}x\, \frac{\operatorname{Im} f(x + i\epsilon)}{Q_m(x)\,(x - s)} + \frac{1}{2\pi i}\int\limits_{|x|=\Lambda^2}\mathrm{d}x\, \frac{f(x)}{Q_m(x)\,(x - s)}\,, \tag{3.14}$$

where we used the fact that Q_m a real-valued polynomial along the real axis and free of any cuts. Taking the limit $\Lambda^2 \to \infty$ we note that the integrand falls off fast enough such

that the former integral in eq. (3.14) along the branch cut will converge while the latter integral along the complex arc vanishes (3.7). Hence, for any $s \in \mathbb{C} \setminus \mathbb{B}_+$ the function f is given by the dispersion relation

$$f(s) = P_{m-1}(s) + \frac{Q_m(s)}{\pi} \lim_{\epsilon \to 0^+} \int_{s_0}^{\infty} \mathrm{d}x \, \frac{\operatorname{Im} f(x + i\epsilon)}{Q_m(x)\,(x - s)}\,, \tag{3.15}$$

which is the so-called *m-times subtracted spectral representation* of f.[#2] In contrast to eq. (3.8), f is not entirely determined by its imaginary part along the upper rim of the branch cut, since eq. (3.15) contains an additional *subtraction polynomial* P_{m-1} that needs to be fixed. The coefficients of P_{m-1} corresponding to the *subtraction points* s_j are called *subtraction constants*. As f obeys the SCHWARZ reflection principle it follows immediately that the subtraction constants have to be real, *cf.* eq. (3.13).

By comparing eqs. (3.8) and (3.15) we note that the minimal number of subtractions m needed in order to obtain convergence of the dispersive integral is given by

$$m = \begin{cases} \lfloor n \rfloor + 1\,, & \text{if } n \geq 0 \\ 0\,, & \text{if } n < 0 \end{cases}\,, \tag{3.16}$$

for any function f possessing a branch cut along $s \in \mathbb{B}_+$ that grows asymptotically like $f(s) \asymp s^n$ with $n \in \mathbb{R}$ as $|s| \to \infty$.[#3] Of course it is always possible to *over-subtract* the dispersion relation in eq. (3.15) with $m' > m$ according to

$$f(s) = P_{m'-1}(s) + \frac{s^k}{\pi} \lim_{\epsilon \to 0^+} \int_{s_0}^{\infty} \mathrm{d}x \, \frac{\operatorname{Im} f(x + i\epsilon)}{x^{m'}\,(x - s)}\,, \tag{3.17}$$

where for the sake of simplicity all subtraction points are set to zero. Accordingly, the asymptotic behavior of the polynomials P_{m-1} and $P_{m'-1}$ differs drastically, as they are of different degree in s. Since both eqs. (3.15) and (3.17) describe the same function there needs to be a relation between the subtraction polynomial and the dispersive integral.

In order to study this in more detail we choose $m' = m + 1$, thus the relation

$$\frac{s^m}{x^m\,(x - s)} = \frac{s^m}{x^{m+1}} + \frac{s^{m+1}}{x^{m+1}\,(x - s)} \tag{3.18}$$

allows us to rewrite the m-times subtracted spectral representation according to

$$\begin{aligned} f(s) &= P_{m-1}(s) + \frac{s^m}{\pi} \lim_{\epsilon \to 0^+} \int_{s_0}^{\infty} \mathrm{d}x \, \frac{\operatorname{Im} f(x + i\epsilon)}{x^m\,(x - s)} \\ &= P_{m-1}(s) + \frac{s^m}{\pi} \lim_{\epsilon \to 0^+} \int_{s_0}^{\infty} \mathrm{d}x \, \frac{\operatorname{Im} f(x + i\epsilon)}{x^{m+1}} + \frac{s^{m+1}}{\pi} \lim_{\epsilon \to 0^+} \int_{s_0}^{\infty} \mathrm{d}x \, \frac{\operatorname{Im} f(x + i\epsilon)}{x^{m+1}\,(x - s)}\,. \end{aligned} \tag{3.19}$$

[#2] Like for the unsubtracted case, the derivation of the dispersion relation in eq. (3.15) will also hold for a more general case where f does not fulfil the SCHWARZ reflection principle. In such a case the imaginary part in eq. (3.15) needs to be replaced by the discontinuity of f and the subtraction polynomial is allowed to contain complex-valued subtraction constants.

[#3] We want to stress that eq. (3.15) even applies to functions without a cut. In such a case the dispersion integral will be zero, thus f is an entire function given in terms of the subtraction polynomial of degree $n \in \mathbb{N}_0$.

A comparison of eqs. (3.17) and (3.19) yields

$$P_m(s) = P_{m-1}(s) + \frac{s^m}{\pi} \lim_{\epsilon \to 0^+} \int_{s_0}^{\infty} \mathrm{d}x \, \frac{\operatorname{Im} f(x + i\epsilon)}{x^{m+1}} \,, \tag{3.20}$$

where the remaining integral is independent of s. Thus it can be absorbed in the polynomial. By repeated use of eq. (3.18) we are able to generalize the relation in eq. (3.20) for $m' > m$ to

$$P_{m'-1}(s) = P_{m-1}(s) + \sum_{j=0}^{m'-m-1} \frac{s^{m+j}}{\pi} \lim_{\epsilon \to 0^+} \int_{s_0}^{\infty} \mathrm{d}x \, \frac{\operatorname{Im} f(x + i\epsilon)}{x^{m+j+1}} \,, \tag{3.21}$$

which is a so-called *sum rule*.

Hence, the interplay between the subtraction polynomial and the remainder of the dispersion integral is balanced in such a way that the asymptotic behavior of f remains unchanged if the number of subtractions is increased. More precisely, the additional subtraction constants that appear when raising the number of subtractions are directly fixed by eq. (3.21). Thus, an improvement of the convergence behavior of the dispersion integral (3.15) is only possible when violating the sum rule at the cost of introducing additional subtraction constants and a less restrictive asymptotic behavior of f.

3.2 The Omnès function

In addition to the functions considered so far (*cf.* sec. 3.1), it turns out to be useful to investigate the properties of a more special type of functions. This new type of complex-valued function Ω will obey the following additional requirements:

- $\log \Omega$ is a holomorphic function in the cut complex plane $\mathbb{C} \setminus \mathbb{B}_+$, *i.e.* Ω does not possess any zeros;
- Ω is normalized according to the condition $\Omega(0) = 1$;
- $\arg \Omega$ is bounded along the branch cut $\mathbb{B}_+$, thus

  $$\lim_{\epsilon \to 0^+} \arg \Omega(s + i\epsilon) \equiv \delta(s) \asymp k\pi \tag{3.22}$$

  with $k \in \mathbb{R}$ will hold when taking the limit $s \to +\infty$.[#4]

Since the logarithm of Ω can be expressed as

$$\log \Omega(s) = \log \big|\Omega(s)\big| + i \arg \Omega(s) \,, \tag{3.23}$$

we note that the discontinuity can be related to

$$\operatorname{disc} \big[\log \Omega(s) \big] = 2i \lim_{\epsilon \to 0^+} \operatorname{Im} \big[\log \Omega(s + i\epsilon) \big] = 2i \, \delta(s) \,. \tag{3.24}$$

[#4] Obviously, identifying $\arg \Omega(s+i\epsilon)$ with a real-valued function $\delta(s)$ along the right-hand cut does not happen without an ulterior motive. Its physical importance arises when setting it equal to a scattering phase shift, *cf.* sec. 2.3.

Accordingly, we are allowed cast eq. (3.24) into a once-subtracted spectral representation (3.15) given by

$$\log\Omega(s) = c + \frac{s}{\pi}\int_{s_0}^{\infty}\mathrm{d}x\,\frac{\delta(x)}{x\,(x-s)}\,, \tag{3.25}$$

where the subtraction polynomial reduces to a constant c and the subtraction point is chosen to be $s_1 = 0$. Given that the normalization condition $\Omega(0) = 1$ needs to be fulfilled, the subtraction constant c is fixed to zero. Thus Ω is represented by the dispersive integral

$$\Omega(s) = \exp\left[\frac{s}{\pi}\int_{s_0}^{\infty}\mathrm{d}x\,\frac{\delta(x)}{x\,(x-s)}\right]. \tag{3.26}$$

Any function Ω that meets these requirements is called Omnès *function* [146, 147]. We note that Ω is fixed as soon as its argument along the upper rim of the cut is known. In case that the discontinuity vanishes, *i.e.*, $\delta(x) = 0$ for all $x \in \mathbb{R}$, eq. (3.26) directly requires $\Omega(s) = 1$ for all $s \in \mathbb{C}$.

We already know the asymptotic behavior of $\arg\Omega$ along the cut. However, we should also investigate the behavior of Ω in the limit of $|s| \to \infty$. Given that the argument of Ω approaches a constant asymptotically, we introduce a cutoff Λ^2 above which we will assume $\delta(x) = k\pi$. Thus the integral in eq. (3.26) can be split into two parts:

$$\frac{s}{\pi}\int_{s_0}^{\infty}\mathrm{d}x\,\frac{\delta(x)}{x\,(x-s)} = -\frac{1}{\pi}\int_{s_0}^{\Lambda^2}\mathrm{d}x\,\frac{\delta(x)}{x} + s\,k\int_{\Lambda^2}^{\infty}\mathrm{d}x\,\frac{1}{x\,(x-s)}\,, \tag{3.27}$$

where we already imposed the limit $|s| \to \infty$ under the former integral. Accordingly, this part is independent of s and yields a constant only. The latter integral can be solved analytically resulting in

$$s\,k\int_{\Lambda^2}^{\infty}\mathrm{d}x\,\frac{1}{x\,(x-s)} = k\log\frac{\Lambda^2}{\Lambda^2 - s}\,. \tag{3.28}$$

Inserting eqs. (3.27) and (3.28) into eq. (3.26) we conclude that the Omnès function behaves asymptotically like

$$\Omega(s) \asymp s^{-k}\,, \tag{3.29}$$

taking the limit $|s| \to \infty$.

Next to the normalization condition $\Omega(0) = 1$, it might be also of interest to study the next coefficients of the Taylor expansion around $s = 0$ given by

$$\Omega(s) = 1 + \Omega'(0)\,s + \frac{1}{2}\Omega''(0)\,s^2 + \frac{1}{6}\Omega'''(0)\,s^3 + \mathcal{O}(s^4)\,. \tag{3.30}$$

Given that Ω possesses a branch cut this expansion will only be valid for $|s| < s_0$. The first three derivatives of the Omnès function at zero are given by

$$\Omega'(0) = \omega_1\,, \qquad \Omega''(0) = 2\omega_2 + \omega_1^2\,, \qquad \Omega'''(0) = 6(\omega_3 + \omega_2\,\omega_1) + \omega_1^3\,, \tag{3.31}$$

where we introduced the function

$$\omega_j = \frac{1}{\pi}\int_{s_0}^{\infty}\mathrm{d}x\,\frac{\delta(x)}{x^{j+1}}\,. \tag{3.32}$$

3.2.1 Homogeneous Omnès problem

Now that we have introduced the Omnès function Ω, we would like to return to a more general type of function f. Therefore we soften the constraints on f and demand the following properties:

- f is holomorphic on $\mathbb{C} \setminus \mathbb{B}_+$;
- f obeys the Schwarz reflection principle;
- $f(s) \asymp s^n$ with $n \in \mathbb{R}$ when taking the limit $|s| \to \infty$;
- $\arg f$ is bounded along the branch cut $\mathbb{B}_+$, accordingly

$$\lim_{\epsilon \to 0^+} \arg f(s + i\epsilon) \equiv \delta(s) \asymp k\pi \tag{3.33}$$

  with $k \in \mathbb{R}$ will hold when taking the limit $s \to +\infty$.

The problem of finding a general solution for the function f with the given requirements is known as the (*homogeneous*) Omnès *problem*.

However, it is possible to find a solution to this problem. Since f satisfies the Schwarz reflection principle, its discontinuity can be represented in the form (*cf.* app. A.3)

$$\begin{aligned} \operatorname{disc} f(s) &= 2i \lim_{\epsilon \to 0^+} \operatorname{Im} f(s + i\epsilon) \\ &= 2i \lim_{\epsilon \to 0^+} f(s + i\epsilon) \sin \delta(s) \exp\big[-i\delta(s) \big] . \end{aligned} \tag{3.34}$$

Casting eq. (3.34) into an m-times subtracted spectral representation (3.15) results in

$$f(s) = P_{m-1}(s) + \frac{Q_m(s)}{\pi} \lim_{\epsilon \to 0^+} \int_{s_0}^{\infty} \mathrm{d}x \, \frac{f(x + i\epsilon) \sin \delta(x) \exp\big[-i\delta(x) \big]}{Q_m(x)\,(x - s)} , \tag{3.35}$$

where the minimal number of subtractions m needed is given by eq. (3.16). The function f appears on both sides of eq. (3.35), thus the dispersive representation can be seen as integral equation that determines f.

In addition to eq. (3.35) an alternative way of solving the homogeneous Omnès problem exists. We consider the function

$$h(s) \equiv \frac{f(s)}{\Omega(s)} , \tag{3.36}$$

where we made use of the fact that there exists an Omnès function Ω for which

$$\lim_{\epsilon \to 0^+} \arg f(s + i\epsilon) = \lim_{\epsilon \to 0^+} \arg \Omega(s + i\epsilon) \tag{3.37}$$

holds along the branch cut, *cf.* sec. 3.2. Given that both f and Ω are holomorphic on $\mathbb{C}\setminus\mathbb{B}_+$ and Ω is free of any zeros, the function h introduced in eq. (3.36) will be holomorphic on

$\mathbb{C}\setminus\mathbb{B}_+$ as well. In addition both functions f and Ω fulfil the SCHWARZ reflection principle, accordingly the discontinuity of h will be given by

$$\begin{aligned}\operatorname{disc} h(s) &= 2i \lim_{\epsilon\to 0^+} \operatorname{Im} h(s+i\epsilon) = 2i \lim_{\epsilon\to 0^+} \operatorname{Im}\left[\frac{f(s+i\epsilon)}{\Omega(s+i\epsilon)}\right] \\ &= 2i \lim_{\epsilon\to 0^+} \operatorname{Im}\left[\frac{\big|f(s+i\epsilon)\big| \exp\big(i \arg f(s+i\epsilon)\big)}{\big|\Omega(s+i\epsilon)\big| \exp\big(i \arg \Omega(s+i\epsilon)\big)}\right] = 2i \lim_{\epsilon\to 0^+} \operatorname{Im}\left[\frac{\big|f(s+i\epsilon)\big|}{\big|\Omega(s+i\epsilon)\big|}\right] = 0\,.\end{aligned} \tag{3.38}$$

Thus h is free of any branch cuts, *i.e.* it must be an entire function. Since the asymptotic behavior of $f(s) \asymp s^n$ and $\Omega(s) \asymp s^{-k}$ is known, h has to be a polynomial of degree $\lfloor n+k \rfloor$ and the solution of the homogeneous OMNÈS problem given by

$$f(s) = P_{\lfloor n+k \rfloor}(s)\, \Omega(s)\,. \tag{3.39}$$

This solution is called OMNÈS *representation* of f. We note that the coefficients of the polynomial $P_{\lfloor n+k \rfloor}$ are required to be real, otherwise f would spoil the SCHWARZ reflection principle. In addition we want to stress that the polynomials appearing in eqs. (3.35) and (3.39) might differ, *cf.* sec. 3.3.

3.2.2 Inhomogeneous Omnès problem

Given the discontinuity of f in the homogeneous OMNÈS problem (3.34), we would like to relax the constraints on f to the *inhomogeneous* OMNÈS *problem*. Therefore we will consider a function f with the following requirements:

- f is holomorphic on $\mathbb{C} \setminus \mathbb{B}_+$;
- $f(s) \asymp s^n$ with $n \in \mathbb{R}$ when taking the limit $|s| \to \infty$;
- the discontinuity of f along the cut is given by

$$\operatorname{disc} f(s) = 2i \lim_{\epsilon\to 0^+} \big[f(s+i\epsilon) + \hat{f}(s)\big]\, \sin\delta(s)\, \exp\big[i\delta(s)\big]\,; \tag{3.40}$$

- the real-valued function δ is bounded on $\mathbb{B}_+$, *i.e.* $\delta(s) \asymp k\pi$ with $k \in \mathbb{R}$ for $s \to +\infty$;
- the *hat function* $\hat{f}$ might take complex values and the discontinuity equation of f implies $\hat{f}(s) \asymp s^n$ for $s \to +\infty$.

We note that neither $\arg f(s+i\epsilon) = \delta(s)$ in the limit of $\epsilon \to 0^+$ along the branch cut will hold, nor the SCHWARZ reflection principle needs to be satisfied. Casting eq. (3.40) into an m-times subtracted spectral representation (3.15) yields

$$f(s) = P_{m-1}(s) + \frac{Q_m(s)}{\pi} \lim_{\epsilon\to 0^+} \int_{s_0}^{\infty} \mathrm{d}x\, \frac{\big[f(x+i\epsilon) + \hat{f}(x)\big]\, \sin\delta(x)\, \exp\big[-i\delta(x)\big]}{Q_m(x)\,(x-s)}\,, \tag{3.41}$$

where the appropriate minimal number of subtractions m is given by eq. (3.16).

In accordance to sec. 3.2.1 we want to study the function h defined in eq. (3.36) again. Still h will be holomorphic on $\mathbb{C} \setminus \mathbb{B}_+$, as f and Ω are holomorphic on $\mathbb{C} \setminus \mathbb{B}_+$ and Ω does not possess any zeros. Its discontinuity along $\mathbb{B}_+$ is given by

$$\begin{aligned}
\operatorname{disc} h(s) &= \lim_{\epsilon \to 0^+} \left[\frac{f(s+i\epsilon)}{\Omega(s+i\epsilon)} - \frac{f(s-i\epsilon)}{\Omega(s-i\epsilon)} \right] = \lim_{\epsilon \to 0^+} \left[\frac{f(s+i\epsilon)}{\Omega(s+i\epsilon)} - \frac{f(s-i\epsilon)}{\Omega^*(s+i\epsilon)} \right] \\
&= \lim_{\epsilon \to 0^+} \left[\frac{f(s+i\epsilon)\, \exp\big[-i\delta(s)\big] - f(s-i\epsilon)\, \exp\big[i\delta(s)\big]}{\big|\Omega(s+i\epsilon)\big|} \right] \\
&= \lim_{\epsilon \to 0^+} \left[\frac{\big[f(s+i\epsilon) - f(s-i\epsilon)\big] \exp\big[i\delta(s)\big] - 2i\, f(s+i\epsilon)\, \sin\delta(s)}{\big|\Omega(s+i\epsilon)\big|} \right] \\
&= 2i \lim_{\epsilon \to 0^+} \frac{\hat{f}(s)\, \sin\delta(s)}{\big|\Omega(s+i\epsilon)\big|} \,,
\end{aligned} \tag{3.42}$$

where we employed the fact that Ω satisfies the Schwarz reflection principle, although it might be spoiled by f. Note that in the last equality we made use of eq. (3.40). Accordingly, the discontinuity of h (3.42) will only depend on $\hat{f}$ and δ, but not on f itself. Equipped with the asymptotic behavior of $h(s) \asymp s^{n+k}$, we are allowed to cast the discontinuity of h into an m-times subtracted spectral representation (3.15) given by

$$h(s) = P_{m-1}(s) + \frac{Q_m(s)}{\pi} \lim_{\epsilon \to 0^+} \int_{s_0}^{\infty} \mathrm{d}x\, \frac{\hat{f}(x)\, \sin\delta(x)}{\big|\Omega(x+i\epsilon)\big|\, Q_m(x)\, (x-s)} \,. \tag{3.43}$$

Again, the minimal number of subtractions m needed for convergence of the dispersion integral is given by eq. (3.16). Solving eq. (3.43) for f we find its Omnès representation

$$f(s) = \Omega(s) \left[P_{m-1}(s) + \frac{Q_m(s)}{\pi} \lim_{\epsilon \to 0^+} \int_{s_0}^{\infty} \mathrm{d}x\, \frac{\hat{f}(x)\, \sin\delta(x)}{\big|\Omega(x+i\epsilon)\big|\, Q_m(x)\, (x-s)} \right] . \tag{3.44}$$

In fact eq. (3.44) is the most general solution of the inhomogeneous Omnès problem. This can easily be proven by considering a function v being a solution to the homogeneous Omnès problem (3.39) with $v(s) \asymp s^n$ for $|s| \to \infty$ and $\arg v(s+i\epsilon) = \delta(s)$ along the cut. According to eqs. (3.34) and (3.40) the discontinuity of $f+v$ will be given by

$$\operatorname{disc}\big[f(s)+v(s)\big] = 2i \lim_{\epsilon \to 0^+} \big[f(s+i\epsilon) + v(s+i\epsilon) + \hat{f}(s)\big]\, \sin\delta(s)\, \exp\big[-i\delta(s)\big] \,. \tag{3.45}$$

It follows immediately that $f+v$ will be a solution of the inhomogeneous Omnès problem if f is one. The polynomials in eqs. (3.39) and (3.44) are both of degree $m-1 = \lfloor n+k \rfloor$, thus the sum of them will be of the same degree. Consequently, the representation given in eq. (3.44) is indeed the general solution of the inhomogeneous Omnès problem.

Since this representation will be of crucial importance in the following chapters, we want to study its properties in more detail. First of all, the minimal number of subtractions m needed to obtain convergence of the dispersion integral (3.44) will be given by

$$m = \begin{cases} \lfloor n+k \rfloor + 1 \,, & \text{if } n+k \geq 0 \\ 0 \,, & \text{if } n+k < 0 \end{cases} \,, \tag{3.46}$$

given that the asymptotic behavior on $\hat{f}$ and δ is assumed to be $\hat{f}(s) \asymp s^n$ and $\delta(s) \asymp k\pi$. A comparison of eqs. (3.39) and (3.44) reveals that the inhomogeneous solution reduces to the homogeneous solution if the hat function $\hat{f}$ is set to zero and $\arg f(s+i\epsilon)$ equals $\delta(s)$ along the cut. Moreover, if $\hat{f}$ is real-valued and the subtraction constants as well as the subtraction points are real, f will satisfy the SCHWARZ reflection principle. On the other hand, as soon as $\hat{f}$ develops a non-vanishing imaginary part, f immediately spoils the SCHWARZ reflection principle.

Equation (3.44) might lead to a misunderstanding in the special case of $k \in \mathbb{Z}$. In this scenario the asymptotic behavior of the function δ dictates $\delta(s) = k\pi$ for $s \gg \Lambda^2$. Accordingly the sine function in the discontinuity will vanish, which introduces a cutoff in dispersion integral at Λ^2. It might be tempting to reduce the number of subtractions in such a case, since the convergence behavior of the dispersive integral is now controlled by the cutoff. Nevertheless, an approach with less subtractions than required by the asymptotics will not yield a legitimate solution. Recalling the derivation of the spectral representation this becomes immediately clear, since the minimal number of subtractions are needed as well to get rid of the contributions from the complex arc, *cf.* sec. 3.1.2.

In accordance to the discussion in sec. 3.1.2, we are allowed to over-subtract the OMNÈS representation. Taking $m' > m$ subtractions yields the sum rule

$$P_{m'-1}(s) = P_{m-1}(s) + \sum_{j=0}^{m'-m-1} \frac{s^{m+j}}{\pi} \lim_{\epsilon\to 0^+} \int_{s_0}^{\infty} \mathrm{d}x \, \frac{\hat{f}(x)\, \sin\delta(x)}{\left|\Omega(x+i\epsilon)\right| \, x^{m+j+1}} \,, \tag{3.47}$$

where for the sake of simplicity all subtraction points are chosen to be zero. The derivation proceeds in the same way as discussed for eq. (3.21).

Finally when considering the OMNÈS representation (3.44) as an integral equation that fixes f, it turns out to be superior to the spectral representation (3.41). This becomes clear when studying the following example with $n \geq 0$ and $k \geq 0$: the OMNÈS representation needs a minimal number of $m = \lfloor n+k \rfloor + 1$ subtractions, thus the subtraction polynomial contains m subtraction constants as degrees of freedom. On the other hand, the spectral representation of the same function f needs $\lfloor n \rfloor + 1$ subtractions and therefore exhibits $\lfloor n \rfloor + 1$ subtraction constants as free parameters. Accordingly, in the case of $k < 1$ both representations yield an equal number of parameters. However, if *e.g.* $k = 1$ the OMNÈS representation will contain one parameter more than the spectral representation, *i.e.*, solving eq. (3.41) cannot be unique and it will allow for a one-parameter family of solutions. Given that the OMNÈS representation is the general solution of the inhomogeneous OMNÈS problem, the solution of eq. (3.44) has to be unique. Accordingly, eq. (3.44) will always be used when dealing with inhomogeneous OMNÈS problems [120, 121, 127, 148–156].

3.3 Matching of dispersive representations

In sec. 3.2.2 we discussed two different dispersive representations for the function f. The considered function will behave asymptotically like $f(s) \asymp s^n$ with $n > 0$. Accordingly,

the function in the spectral (3.41) and the OMNÈS representation (3.44) is given by

$$\begin{aligned} f(s) &= \sum_{j=0}^{m-1} \alpha_j \, s^j + \frac{s^m}{\pi} \lim_{\epsilon \to 0^+} \int_{s_0}^{\infty} \mathrm{d}x \, \frac{\left[f(x+i\epsilon) + \hat{f}(x) \right] \, \sin\delta(x) \, \exp\left[-i\delta(x) \right]}{x^m \, (x-s)} \\ &= \Omega(s) \left[\sum_{j=0}^{m'-1} \beta_j \, s^j + \frac{s^{m'}}{\pi} \lim_{\epsilon \to 0^+} \int_{s_0}^{\infty} \mathrm{d}x \, \frac{\hat{f}(x) \, \sin\delta(x)}{\left| \Omega(x+i\epsilon) \right| \, x^{m'} \, (x-s)} \right], \end{aligned} \tag{3.48}$$

where the minimal numbers of subtractions needed to achieve convergence of the dispersion integrals are given by $m = \lfloor n \rfloor + 1$ and $m' = \lfloor n + k \rfloor + 1$. The subtraction polynomials are given explicitly in terms of the subtraction constants α_j and β_j. For the sake of simplicity all subtraction points are equal to zero in both representations.

We want to relate the subtraction constants of the two different representations given in eq. (3.48). Considering the specific case of $k \geq 0$ with $m' \geq \lfloor n \rfloor + 1$ subtractions, the TAYLOR expansions of both representations will not yield any contribution from the dispersive integrals up to order $\lfloor n \rfloor$. Performing an expansion around $s = 0$, which will converge as long as $|s| < s_0$, allows us directly to match the first $\lfloor n \rfloor + 1$ subtraction constants of both representations. In the OMNÈS representation Ω is expanded according to eq. (3.30). As an example with fixed $n = 3$, we find

$$\begin{aligned} \alpha_0 &= \beta_0 \,, & \alpha_2 &= \beta_2 + 2\beta_1 \Omega'(0) + \beta_0 \, \Omega'(0) \,, \\ \alpha_1 &= \beta_1 + \beta_0 \, \Omega''(0) \,, & \alpha_3 &= \beta_3 + 3\beta_2 \, \Omega'(0) + 3\beta_1 \, \Omega''(0) + \beta_0 \, \Omega'''(0) \,. \end{aligned} \tag{3.49}$$

3.4 Basis functions

We want to consider the solution of the inhomogeneous OMNÈS problem in a more restricted system. Therefore the following requirements will hold:

- f_1, f_2 are solutions of the inhomogeneous OMNÈS problem;
- $\hat{f}$ will depend linearly on f, thus $\hat{f}(s) = \hat{f}[f](s)$ will satisfy

$$\hat{f}[\lambda_1 f_1 + \lambda_2 f_2](s) = \lambda_1 \, \hat{f}[f_1](s) + \lambda_2 \, \hat{f}[f_2](s) \,, \tag{3.50}$$

  where $\lambda_1, \lambda_2 \in \mathbb{C}$ denote some arbitrary constants.

To illustrate the impact of this additional constraint on the inhomogeneous OMNÈS problem we decompose f and $\hat{f}$ in the following form:

$$f(s) = \sum_j^{m-1} \lambda_j \, f_j(s) \,, \qquad \hat{f}[f](s) = \sum_j^{m-1} \lambda_j \, \hat{f}_j(s) \,, \tag{3.51}$$

where $\hat{f}_j$ will be a short hand notation for $\hat{f}[f_j]$ and m denotes the number of subtractions needed in the OMNÈS representation of f. It is always possible to find such a decomposition so that without loss of generality eq. (3.44) holds for the individual f_j, given that f is

a solution to the inhomogeneous Omnès problem. Choosing the coefficients λ_j identical to the subtraction constants in the Omnès representation of f reveals

$$f_j(s) = \Omega(s)\left[s^j + \frac{Q_m(s)}{\pi}\lim_{\epsilon\to 0^+}\int_{s_0}^{\infty}\mathrm{d}x\,\frac{\hat{f}_j(x)\,\sin\delta(x)}{\left|\Omega(x+i\epsilon)\right|\,Q_m(x)\,(x-s)}\right]. \tag{3.52}$$

In contrast to f, the *basis functions* f_j defined in this way will be independent of the subtraction constants [157,158]. Accordingly once the dependence $\hat{f}[f]$ is fixed, eq. (3.52) can be used as an integral equation determining the basis functions of f for any given δ.

The decomposition into the basis functions given in eq. (3.51) can also be used to generate the basis functions of the spectral representation. Using the matching constraints discussed in sec. 3.3 we can relate the basis functions of the Omnès representation directly to the ones of the spectral representation. For instance, consider the case $n = 1$ and $k \leq 1$ with all subtraction points set to zero, *cf.* eqs. (3.48) and (3.49):

$$\begin{aligned} f(s) &= \beta_0\, f_0(s) + \beta_1\, f_1(s) = \alpha_0\, f_0(s) + \left[\alpha_1 - \alpha_0\,\Omega'(0)\right] f_1(s) \\ &= \alpha_0\left[f_0(s) - \Omega'(0)\, f_1(s)\right] + \alpha_1\, f_1(s) = \alpha_0\, f_0^{\mathrm{SR}}(s) + \alpha_1\, f_1^{\mathrm{SR}}(s)\,, \end{aligned} \tag{3.53}$$

where $f_0^{\mathrm{SR}} \equiv f_0(s) - \Omega'(0)\, f_1(s)$ and $f_1^{\mathrm{SR}} \equiv f_1$ define the basis functions of the spectral representation.[#5] Using the linearity of the hat function $\hat{f}[f_0^{\mathrm{SR}}] = \hat{f}[f_0] - \Omega'(0)\,\hat{f}[f_1]$, the Omnès representation of f_0^{SR} will be given by

$$f_0^{\mathrm{SR}}(s) = \Omega(s)\left[1 - \Omega'(0)\, s + \frac{s^2}{\pi}\lim_{\epsilon\to 0^+}\int_{s_0}^{\infty}\mathrm{d}x\,\frac{\hat{f}_0^{\mathrm{SR}}(x)\,\sin\delta(x)}{\left|\Omega(x+i\epsilon)\right|\,x^2\,(x-s)}\right]. \tag{3.54}$$

Thus eq. (3.53) defines the change of basis from f_j in the Omnès representation to f_j^{SR} in the spectral representation, or accordingly the exchange of the subtraction constants β_j with α_j.

3.5 Polynomial shifts

In order to investigate the transformation properties of the dispersive representation for f under polynomial shifts, the function f is satisfies the following constraints:

- f is a solution of the inhomogeneous Omnès problem;
- Δf and $\Delta\hat{f}$ are polynomials whose degree is at most $\lfloor n \rfloor$, given that f behaves asymptotically like $f(s) \asymp s^n$ with $n > 0$;
- f and $\hat{f}$ transform under the polynomial shift according to

$$f(s) \mapsto F(s) \equiv f(s) + \Delta f(s)\,, \qquad \hat{f}(s) \mapsto \hat{F}(s) \equiv \hat{f}(s) + \Delta\hat{f}(s)\,, \tag{3.55}$$

  where F is a solution of the inhomogeneous Omnès problem with the corresponding hat function $\hat{F}$.

[#5] In the case at hand, the number of subtraction constants in the Omnès and spectral representations are equal, *i.e.*, there is no ambiguity present in the latter representation. Of course when constructing a case that is not unique in the spectral representation, the identification of basis functions encounters this ambiguity, too.

The idea of this investigation goes back to [159]. Note that Δf as defined above will neither alter the asymptotic behavior nor the analytic structure of the transformed function F. Since Δf is an entire function its discontinuity will vanish, thus the shifted discontinuity will be given by

$$\operatorname{disc} f(s) \mapsto \operatorname{disc} F(s) = \operatorname{disc} f(s)\,. \tag{3.56}$$

Equation (3.40) infers directly that $\hat{f}$ has to transform opposite to f under the polynomial shift

$$\hat{f}(s) \mapsto \hat{F}(s) = \hat{f}(s) - \Delta f(s)\,. \tag{3.57}$$

Accordingly, f and F both can be given in terms of a m-times subtracted spectral representation (3.41) with the only difference that the subtraction polynomial for F will be given by $P_{m-1}(s) + \Delta f(s)$, where P_{m-1} denotes the respective subtraction polynomial in the representation of f.

However, in the Omnès representation of f given in eq. (3.44) this transformation behavior is not immediately evident. We want to study this issue in more detail by considering the Omnès representation of the shifted function F given by

$$\begin{aligned} f(s) + \Delta f(s) = \Omega(s) \Bigg[& P_{m-1}(s) + \Delta P(s) \\ & + \frac{Q_m(s)}{\pi} \lim_{\epsilon \to 0^+} \int_{s_0}^{\infty} \mathrm{d}x \, \frac{\left[\hat{f}(x) - \Delta f(x)\right] \sin \delta(x)}{\left|\Omega(x + i\epsilon)\right| Q_m(x)\,(x - s)} \Bigg]\,, \end{aligned} \tag{3.58}$$

in terms of the same δ as for the representation of f. Thus we need to tackle the question whether ΔP, *i.e.*, the shift of the subtraction polynomial P_{m-1}, can be given as a polynomial of degree $m-1$ at most. Ignoring the contributions to f for now, a rearrangement of eq. (3.58) yields

$$\Delta P(s) = \frac{\Delta f(s)}{\Omega(s)} + \frac{Q_m(s)}{\pi} \lim_{\epsilon \to 0^+} \int_{s_0}^{\infty} \mathrm{d}x \, \frac{\Delta f(x) \sin \delta(x)}{\left|\Omega(x + i\epsilon)\right| Q_m(x)\,(x - s)}\,. \tag{3.59}$$

According to the requirements on Ω given in sec. 3.2 the inverse of the Omnès function will satisfy

$$\operatorname{disc} \frac{1}{\Omega(s)} = -2i \lim_{\epsilon \to 0^+} \frac{\sin \delta(s)}{\left|\Omega(s + i\epsilon)\right|}\,, \tag{3.60}$$

which allows for spectral representation with $m = \lfloor n + k \rfloor + 1 \geq \lfloor k \rfloor + 1$ subtractions

$$\frac{1}{\Omega(s)} = P^{\Omega}_{m-1}(s) - \frac{Q_m(s)}{\pi} \lim_{\epsilon \to 0^+} \int_{s_0}^{\infty} \mathrm{d}x \, \frac{\sin \delta(x)}{\left|\Omega(x + i\epsilon)\right| Q_m(x)\,(x - s)}\,. \tag{3.61}$$

Correspondingly, the subtraction polynomial denoted by P^{Ω}_{m-1} is of degree $m-1$. Therefore eq. (3.59) can be rewritten as

$$\Delta P(s) = P^{\Omega}_{m-1}(s)\, \Delta f(s) + \frac{Q_m(s)}{\pi} \lim_{\epsilon \to 0^+} \int_{s_0}^{\infty} \mathrm{d}x \, \frac{\left[\Delta f(x) - \Delta f(s)\right] \sin \delta(x)}{\left|\Omega(x + i\epsilon)\right| Q_m(x)\,(x - s)}\,. \tag{3.62}$$

Given that Δf is a polynomial of degree $\lfloor n \rfloor$ it can be represented by

$$\Delta f = \sum_{j=0}^{\lfloor n \rfloor} c_j \, s^j \,, \tag{3.63}$$

where $c_j \in \mathbb{C}$ denote the expansion coefficients. Inserting eq. (3.63) into eq. (3.62) and use the identity in eq. (A.24) yields

$$\Delta P(s) = P^{\Omega}_{m-1}(s) \sum_{j=0}^{\lfloor n \rfloor} c_j \, s^j + \frac{Q_m(s)}{\pi} \sum_{j=1}^{\lfloor n \rfloor} \sum_{l=0}^{j-1} c_j \, s^{j-l-1} \lim_{\epsilon \to 0^+} \int_{s_0}^{\infty} \mathrm{d}x \, \frac{x^l \, \sin \delta(x)}{\left| \Omega(x + i\epsilon) \right| \, Q_m(x)} \,. \tag{3.64}$$

Since the remaining dispersion integral collapsed to a constant, ΔP is indeed a polynomial. However, the right-hand side of eq. (3.64) seem to imply that ΔP is of degree $m + \lfloor n \rfloor - 1$ instead of $m - 1$, which would lead to a contradiction for $n \geq 1$. A closer look at eq. (3.61) reveals that this conclusion is wrong. Since the asymptotic behavior of $1/\Omega$ is given by $1/\Omega(s) \asymp s^k$, its spectral representation needs a minimal number of $m^{\Omega} = \lfloor k \rfloor + 1$ subtractions, *cf.* eq. (3.29). Thus with the chosen $m = \lfloor n + k \rfloor + 1$ subtractions the representation for $1/\Omega$ is over-subtracted, accordingly there has to be a sum rule dealing with the additional $\lfloor n \rfloor$ subtractions and renders ΔP to be of degree $m - 1$.

In order to prove this we choose all subtraction points equal to zero and $n \geq 1$. Thus the m-times subtracted spectral representation of $1/\Omega$ satisfies the sum rule (3.21)

$$P^{\Omega}_{m-1}(s) = P^{\Omega}_{m-\lfloor n \rfloor - 1}(s) - \sum_{j=0}^{\lfloor n \rfloor - 1} s^{m-\lfloor n \rfloor + j} \, \mu_{m-\lfloor n \rfloor + j + 1} \,, \tag{3.65}$$

where we introduced the short-hand notation for the remainder of the dispersive integral

$$\mu_j \equiv \lim_{\epsilon \to 0^+} \frac{1}{\pi} \int_{s_0}^{\infty} \mathrm{d}x \, \frac{\sin \delta(x)}{\left| \Omega(x + i\epsilon) \right| \, x^j} \,. \tag{3.66}$$

Accordingly, eq. (3.64) reads

$$\begin{aligned} \Delta P(s) = P^{\Omega}_{m-\lfloor n \rfloor - 1}(s) \sum_{j=0}^{\lfloor n \rfloor} c_j \, s^j - \sum_{j=0}^{\lfloor n \rfloor} \sum_{l=0}^{\lfloor n \rfloor - 1} c_j \, s^{m-\lfloor n \rfloor + j + l} \, \mu_{m-\lfloor n \rfloor + l + 1} \\ + \sum_{j=1}^{\lfloor n \rfloor} \sum_{l=0}^{j-1} c_j \, s^{m+j-l-1} \, \mu_{m-l} \,. \end{aligned} \tag{3.67}$$

Performing an index shift of $l \mapsto \lfloor n \rfloor - l - 1$ in the second term on the right-hand side, it can be split into

$$\sum_{j=0}^{\lfloor n \rfloor} \sum_{l=0}^{\lfloor n \rfloor - 1} c_j \, s^{m+j-l-1} \, \mu_{m-l} = \sum_{j=1}^{\lfloor n \rfloor} \sum_{l=0}^{j-1} c_j \, s^{m+j-l-1} \, \mu_{m-l} + \sum_{j=0}^{\lfloor n \rfloor} \sum_{l=j}^{\lfloor n \rfloor - 1} c_j \, s^{m+j-l-1} \, \mu_{m-l} \,. \tag{3.68}$$

Inserted back into eq. (3.67) yields

$$\Delta P(s) = P^{\Omega}_{m-\lfloor n \rfloor - 1}(s) \sum_{j=0}^{\lfloor n \rfloor} c_j \, s^j + \sum_{j=0}^{\lfloor n \rfloor} \sum_{l=j}^{\lfloor n \rfloor - 1} c_j \, s^{m+j-l-1} \, \mu_{m-l} \,, \tag{3.69}$$

where it is now explicitly shown that the highest power of s appearing on the right-hand side is given by $m - 1$ in the case of $j = l$.

Chapter 4

Dispersion relations for functions with two cuts

In this chapter, we broaden the discussion on the mathematical concepts of dispersion theory to describe T-matrix elements for arbitrary $2 \to 2$ scattering processes. The scattering amplitude for a process involving altogether four particles in the initial and final state will depend on the three MANDELSTAM variables variables s, t, and u, of which only two are independent, *cf.* ch. 2. Since the dispersive framework introduced in ch. 3 is developed for functions that depend on one complex variable only, it cannot be applied to $2 \to 2$ scattering amplitudes without further ado. In the following we will derive a more general dispersion-theoretical framework that allows for a description of $2 \to 2$ scattering amplitudes. Applications of this dispersive framework in the analysis of physical $1 \to 3$ decay processes, based on equations of the KHURI–TREIMAN type, are discussed in chs. 5, 6, and 7.

This chapter is organized as follows: in sec. 4.1 we introduce the fixed-t dispersive representation for the $2 \to 2$ scattering amplitude and discuss its analytical properties. Combining this dispersive formalism with the constraints on the discontinuities of the amplitude demanded by two-body unitarity, we derive its reconstruction theorem in sec. 4.2. For further details on fixed-t dispersion relations we suggest [142, 143, 160]. A highly recommended pedagogical discussion can also be found in [144].

4.1 Fixed-t dispersion relations

We denote the T-matrix element of an arbitrary $2 \to 2$ scattering process involving four particles of fixed species by $\mathcal{M}$.[#1] According to sec. 2.2.1, $\mathcal{M}$ can be expressed in terms of the MANDELSTAM variables

$$\mathcal{M}(s,t) \equiv \mathcal{M}(s,t,u) = \mathcal{M}(s,t,3r-s-t)\,, \tag{4.1}$$

[#1] In cases of $2 \to 2$ scattering amplitudes involving three pseudoscalar particles and one vector particle we are interested only in the analytic structure of the scalar amplitude $\mathcal{F}$ containing the dynamical information, accordingly in such a case $\mathcal{M}$ will refer to $\mathcal{F}$ instead of the full T-matrix element, *cf.* sec. 2.2.

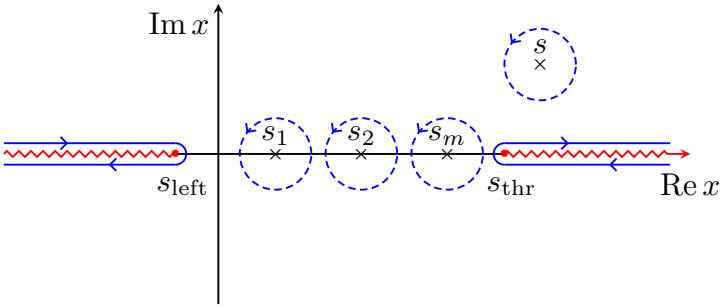

Fig. 4.1: Choices of the integration contour (blue) in the complex x-plane. The dashed paths depict closed circular contours around the isolated poles $s, s_1, s_2, ..., s_m$ in the residue theorem (3.11), while the solid path represents the enlarged contour enclosing $\mathbb{C}\backslash(\mathbb{B}_+ \cup \mathbb{B}_-)$ running along the upper and lower rim of the cuts according to the prescription $x \pm i\epsilon$ in the limit of $\epsilon \to 0^+$. Starting at $s_{\text{thr}} > 0$, the right-hand cut (red) extends to infinity along the positive real axis. The left-hand cut (red) starts at $s_{\text{left}} = 3r - t - u_{\text{thr}}$ and extends to minus infinity along the negative real axis.

where we made use of eq. (2.25), which states that only two of them are independent, *i.e.*, we have chosen s and t. Of course we assume that the squares of the involved four-momenta are known. Given that $\mathcal{M}(s,t)$ as a function of two variables would require a more sophisticated mathematical framework than discussed in ch. 3, we simplify the problem by fixing one of the MANDELSTAM variables. Accordingly, the amplitude is a function of the variable s only

$$\mathcal{M}(s) = \mathcal{M}(s,t)\,, \tag{4.2}$$

for t being fixed. The analytic structure of $\mathcal{M}(s)$ can now be studied by extending the concepts introduced in ch. 3.

We choose t to be real and below any t-channel production threshold $t < t_{\text{thr}}$. In the s-channel we allow for an intermediate multi-particle state to go on-shell for $s \geq s_{\text{thr}}$, leading to a right-hand cut $\mathbb{B}_+ = [s_{\text{thr}}, \infty)$. Moreover, there might also be an intermediate multi-particle state contributing in the u-channel above the threshold $u \geq u_{\text{thr}}$. Using eq. (2.25) we can relate the unitarity cut in the u-channel to a *left-hand cut* in the complex s-plane given by $\mathbb{B}_- = (-\infty, s_{\text{left}}]$ with

$$s \leq 3r - t - u_{\text{thr}} \equiv s_{\text{left}}\,. \tag{4.3}$$

For the following discussion to apply we need to require $s_{\text{left}} < s_{\text{thr}}$, *i.e.*, the branch cuts are not allowed to overlap. Accordingly, the lower bound on t is given by

$$t > 3r - s_{\text{thr}} - u_{\text{thr}}\,. \tag{4.4}$$

In the MANDELSTAM plane a valid line of fixed t needs to be parallel to $t = 0$ and is demanded to cross the subthreshold diagram twice, *cf.* fig. 2.4.

Given these constraints, the considered amplitude $\mathcal{M}$ is a holomorphic function in s on $\mathbb{C} \setminus (\mathbb{B}_+ \cup \mathbb{B}_-)$. Assuming an asymptotic behaviour of $\mathcal{M} \asymp s^n$ with $n \in \mathbb{R}$, the amplitude can be treated in a similar manner to eq. (3.11) when choosing the integration contour as

depicted in fig. 4.1. In accordance to the derivation of the spectral representation we find the *fixed-t dispersion relation* for $\mathcal{M}$ given by

$$\mathcal{M}(s) = P_{m-1}(s) + \frac{Q_m(s)}{2\pi i}\int_{s_{\text{thr}}}^{\infty}\mathrm{d}x\,\frac{\operatorname{disc}\mathcal{M}(x)}{Q_m(x)\,(x-s)} + \frac{Q_m(s)}{2\pi i}\int_{-\infty}^{s_{\text{left}}}\mathrm{d}x\,\frac{\operatorname{disc}\mathcal{M}(x)}{Q_m(x)\,(x-s)}\,, \quad (4.5)$$

where the subtraction points s_j in the polynomials Q_m need to lie between the two cuts $s_j \in \mathbb{R}\setminus(\mathbb{B}_+\cup\mathbb{B}_-)$. The adequate minimal number of subtractions m will be given by eq. (3.16) as derived for the spectral representation in eq. (3.15). It turns out to be useful to define

$$\begin{aligned}\operatorname{disc}_x\mathcal{M}(x,t,3r-t-x) \equiv \lim_{\epsilon\to 0^+}\big[&\mathcal{M}(x+i\epsilon,t,3r-t-x-i\epsilon)\\ &-\mathcal{M}(x-i\epsilon,t,3r-t-x+i\epsilon)\big]\,,\end{aligned} \quad (4.6)$$

for t kept fixed. Since the discontinuity, s_{left}, and the subtraction polynomial P_{m-1} depend on the choice of t, the dispersion relation given in eq. (4.5) changes for different t. In order to allow for a variation in t within its given bounds, we write

$$\begin{aligned}\mathcal{M}(s,t,3r-s-t) = P^t_{m-1}(s) &+ \frac{Q_m(s)}{2\pi i}\int_{s_{\text{thr}}}^{\infty}\mathrm{d}x\,\frac{\operatorname{disc}_x\mathcal{M}(x,t,3r-t-x)}{Q_m(x)\,(x-s)}\\ &+ \frac{Q_m(s)}{2\pi i}\int_{-\infty}^{s_{\text{left}}(t)}\mathrm{d}x\,\frac{\operatorname{disc}_x\mathcal{M}(x,t,3r-t-x)}{Q_m(x)\,(x-s)}\,.\end{aligned} \quad (4.7)$$

Still the subtraction polynomial P^t_{m-1} is of order $m-1$ in s, but its coefficients c_j might depend on t, *i.e.*

$$P^t_{m-1}(s) = \sum_{j=0}^{m-1} c_j(t)\,s^j\,. \quad (4.8)$$

Note that this dependence of the coefficients on t is not required to be of polynomial form.

We want to comment on the analytic structure of the fixed-t dispersion relation for $\mathcal{M}$ given in eq. (4.7): according to the statement of maximal analyticity, the amplitude $\mathcal{M}$ is holomorphic in both s and t, *cf.* sec. 2.1.2. In the dispersion relation at hand, these two variables are treated on an unequal footing. By construction the right-hand side of eq. (4.7) will be holomorphic in s on $\mathbb{C}\setminus(\mathbb{B}_+\cup\mathbb{B}_-)$. However, this does not apply for t, given that t is constrained to take real values bounded by $t \le t_{\text{thr}}$ and eq. (4.4). But within the values under consideration the right-hand side will be a smooth function in t (*i.e.* a C^∞ function), since the left-hand side is holomorphic in t and therefore C^∞ in t.

We want to draw the attention to the second dispersion integral along the left-hand cut in eq. (4.7). Performing a change of variables

$$\begin{gathered}y = 3r-t-x\,,\qquad \mathrm{d}x = -\mathrm{d}y\,,\qquad x-s = u-y\,,\\ y(s_{\text{left}}) = u_{\text{thr}}\,,\qquad y(-\infty)=\infty\,,\end{gathered} \quad (4.9)$$

and using eq. (4.6) to derive

$$\begin{aligned}\operatorname{disc}_x\mathcal{M}(x,t,3r-t-x) &= \lim_{\epsilon\to 0^+}\big[\mathcal{M}(3r-t-y+i\epsilon,t,y-i\epsilon)\\ &\qquad -\mathcal{M}(3r-t-y-i\epsilon,t,y+i\epsilon)\big] \qquad (4.10)\\ &\equiv -\operatorname{disc}_y\mathcal{M}(3r-t-y,t,y)\,,\end{aligned}$$

we find

$$\begin{aligned}\frac{Q_m(s)}{2\pi i}\int_{-\infty}^{s_{\text{left}}(t)}\mathrm{d}x\,\frac{\operatorname{disc}_x\mathcal{M}(x,t,3r-x-t)}{Q_m(x)\,(x-s)}\\ =\frac{Q_m(3r-t-u)}{2\pi i}\int_{u_{\text{thr}}}^{\infty}\mathrm{d}y\,\frac{\operatorname{disc}_y\mathcal{M}(3r-t-y,t,y)}{Q_m(3r-t-y)\,(y-u)}\,.\end{aligned}\tag{4.11}$$

According to eq. (A.26) the polynomials Q_m fulfil the relation

$$\frac{Q_m(3r-t-u)}{Q_m(3r-t-y)}=\frac{Q_m(u)}{Q_m(y)}+(y-u)\,q_{m-1}^{y}(u)\,,\tag{4.12}$$

with q_{m-1}^{y} being another polynomial in u of degree $m-1$ whose coefficients depend on y. Combining eqs. (4.11) and (4.12) yields

$$\begin{aligned}&\frac{Q_m(s)}{2\pi i}\int_{-\infty}^{s_{\text{left}}(t)}\mathrm{d}x\,\frac{\operatorname{disc}_x\mathcal{M}(x,t,3r-x-t)}{Q_m(x)\,(x-s)}\\ &\qquad=\frac{Q_m(u)}{2\pi i}\int_{u_{\text{thr}}}^{\infty}\mathrm{d}y\,\frac{\operatorname{disc}_y\mathcal{M}(3r-t-y,t,y)}{Q_m(y)\,(y-u)}\\ &\qquad\quad+\frac{1}{2\pi i}\int_{u_{\text{thr}}}^{\infty}\mathrm{d}y\,q_{m-1}^{y}(u)\operatorname{disc}_y\mathcal{M}(3r-t-y,t,y)\,.\end{aligned}\tag{4.13}$$

Since the coefficients of q_{m-1}^{y} are of order $\mathcal{O}(y^{-m-1})$, the second integral converges and reduces to a polynomial in u of degree $m-1$. The polynomial in u is absorbed into the subtraction polynomial by a redefinition of P_{m-1}^{t} when eq. (4.13) is inserted into eq. (4.7), which yields

$$\begin{aligned}\mathcal{M}(s,t,3r-s-t)=P_{m-1}^{t}(s)+\frac{Q_m(s)}{2\pi i}\int_{s_{\text{thr}}}^{\infty}\mathrm{d}x\,\frac{\operatorname{disc}_x\mathcal{M}(x,t,3r-x-t)}{Q_m(x)\,(x-s)}\\ +\frac{Q_m(u)}{2\pi i}\int_{u_{\text{thr}}}^{\infty}\mathrm{d}x\,\frac{\operatorname{disc}_x\mathcal{M}(3r-t-x,t,x)}{Q_m(x)\,(x-u)}\,.\end{aligned}\tag{4.14}$$

Comparing eqs. (4.7) with (4.14) we note that the dispersion integral along the left-hand cut can be rewritten as a dispersion integral along the right-hand cut of the crossed channel. This is an important feature of the fixed-t dispersion relation, since the constraints of unitarity yield a direct access to the hight-hand cuts of the amplitude, *cf.* sec. 2.2.2. In general this does not apply for left-hand cuts.

In practice the information on the discontinuities of a scattering amplitude $\mathcal{M}$ along the right-hand cuts is limited and not available to infinite energies. Since the fixed-t dispersive representation requires knowledge of the discontinuities up to infinity, we have to make assumptions on their high-energy behaviour or introduce a cutoff in the integration. Moreover, the maximal number of needed subtractions m is restricted by the Froissart–Martin bound, stating that the scattering amplitude behaves asymptotically like $\mathcal{M}\asymp s\log^2 s$. However, a formal proof of this statement is only available for

$2 \to 2$ scattering processes involving four scalar particles [161, 162]. Thus in general the Froissart–Martin bound will serve as an additional constraint that can be imposed on the amplitude. Nevertheless, in some cases it might be wise to oversubtract the dispersive representation to suppress the contributions of the high-energy region, *i.e.*, the scattering amplitude will grow asymptotically faster than required by the Froissart–Martin. The additional subtraction constants arising in this way can be understood to parameterize the lack of knowledge on the discontinuity at high energies. Therefore, they are very similar to the LECs introduced in effective field theories, *cf.* sec. 1.3.

4.1.1 Symmetric fixed-t dispersion relation

We want to investigate the behaviour of eq. (4.14) for a special type of amplitudes. Consider an amplitude which is symmetric under exchange of $s \leftrightarrow u$, *i.e.*

$$\mathcal{M}(s,t,3r-s-t) = \mathcal{M}(3r-s-t,t,s)\,, \tag{4.15}$$

and $s_{\text{thr}} = u_{\text{thr}}$. Thus, for the discontinuities in eq. (4.14)

$$\text{disc}_x\, \mathcal{M}(x,t,3r-t-x) = \text{disc}_x\, \mathcal{M}(3r-t-x,t,x) \tag{4.16}$$

will hold.[#2] The symmetric fixed-t dispersion relation for $\mathcal{M}$ reads

$$\begin{aligned}\mathcal{M}(s,t,3r-s-t) = P^t_{m-1}(s) &+ \frac{Q_m(s)}{2\pi i}\int_{s_{\text{thr}}}^{\infty}\mathrm{d}x\,\frac{\text{disc}_x\,\mathcal{M}(x,t,3r-x-t)}{Q_m(x)\,(x-s)} \\ &+ \frac{Q_m(u)}{2\pi i}\int_{u_{\text{thr}}}^{\infty}\mathrm{d}x\,\frac{\text{disc}_x\,\mathcal{M}(x,t,3r-t-x)}{Q_m(x)\,(x-u)}\,.\end{aligned} \tag{4.17}$$

In order to maintain the symmetry given in eq. (4.15), the right-hand side of eq. (4.14) must be symmetric under interchange of $s \leftrightarrow u$ for t fixed. Since the two dispersion integrals are invariant under this symmetry, it is clear that the subtraction polynomial has to P^t_{m-1} has to obey

$$P^t_{m-1}(s) = P^t_{m-1}(3r-s-t)\,. \tag{4.18}$$

Inserting eq. (4.8) into the symmetry constraint yields

$$0 = (2s+t-3r)\sum_{j=1}^{m-1} c_j(t)\sum_{l=0}^{j-1} s^{j-l-1}\,(3r-s-t)^l\,, \tag{4.19}$$

where we applied eq. (A.24). Given that eq. (4.19) has to hold for all $s \in \mathbb{C}\setminus\mathbb{B}_+\cup\mathbb{B}_-$, it can be used to constrain the coefficients c_j of the subtraction polynomial, *e.g.* $m=2$ results in $c_1(t)=0$. Thus for $m=1$ and $m=2$ the polynomial is independent of s and

[#2] Note that eq. (4.16) is not in contradiction with eq. (4.10). The former equation relates s- and u-channel discontinuities along the right-hand cuts, while the latter one links the s-channel discontinuity along the left-hand cut to the u-channel discontinuity along the right-hand cut.

fully determined by $c_0(t)$. However, for $m > 2$ the symmetry condition relates c_1 to all other c_j with $j > 1$ and P^t_{m-1} in general depends on s, *e.g.* $m = 3$ yields

$$0 = c_1(t) + (3r - t)\, c_2(t)\,. \tag{4.20}$$

Thus, $P_2(t)$ will be given by

$$P_2(t) = c_0(t) + c_2(t)\, s\, (s + t - 3r) = c_0(t) - c_2(t)\, s\, u\,, \tag{4.21}$$

where eq. (2.25) is used.

4.1.2 Antisymmetric fixed-*t* dispersion relation

In analogy to consideration of a symmetric amplitude (4.15), we want to study an amplitude that is antisymmetric under interchange of $s \leftrightarrow u$, *i.e.*

$$\mathcal{M}(s, t, 3r - s - t) = -\mathcal{M}(3r - s - t, t, s)\,, \tag{4.22}$$

and $s_{\text{thr}} = u_{\text{thr}}$. Inserting the discontinuity relation for eq. (4.22) given by

$$\text{disc}_x\, \mathcal{M}(x, t, 3r - t - x) = -\text{disc}_x\, \mathcal{M}(3r - t - x, t, x) \tag{4.23}$$

into the general fixed-t dispersion relation (4.14) results in

$$\begin{aligned} \mathcal{M}(s, t, 3r - s - t) = P^t_{m-1}(s) &+ \frac{Q_m(s)}{2\pi i} \int_{s_{\text{thr}}}^{\infty} \mathrm{d}x\, \frac{\text{disc}_x\, \mathcal{M}(x, t, 3r - x - t)}{Q_m(x)\,(x - s)} \\ &- \frac{Q_m(u)}{2\pi i} \int_{u_{\text{thr}}}^{\infty} \mathrm{d}x\, \frac{\text{disc}_x\, \mathcal{M}(x, t, 3r - t - x)}{Q_m(x)\,(x - u)}\,. \end{aligned} \tag{4.24}$$

Accordingly, eq. (4.24) fulfils the antisymmetry relation defined in eq. (4.22), if the subtraction polynomial P^t_{m-1} is antisymmetric under interchange of $s \leftrightarrow u$, *i.e.*

$$P^t_{m-1}(s) = -P^t_{m-1}(3r - s - t)\,. \tag{4.25}$$

Casting the general form of P^t_{m-1} given in eq. (4.8) into eq. (4.25) yields

$$0 = \sum_{j=0}^{m-1} c_j(t) \left[s^j + (3r - s - t)^j \right], \tag{4.26}$$

relating the coefficients c_j. In the special case of $m = 1$ eq. (4.26) results in $c_0(t) = 0$, thus $P_0(t)$ has to vanish. For any given $m > 1$ the antisymmetry condition allows us to relate c_0 to all other coefficients c_j with $j > 0$, *e.g.* $m = 3$ yields

$$0 = 2c_0(t) + c_1(t)\,(3r - t) + c_2(t) \left[s^2 + (3r - s - t)^2 \right]. \tag{4.27}$$

Hence, using eq. (2.25) the subtraction polynomial P^t_2 is given by

$$P^t_2(s) = \frac{(2s + t - 3r)}{2} \left[c_1(t) + c_2(t)\,(3r - t) \right] = \frac{(s - u)}{2} \left[c_1(t) + c_2(t)\,(3r - t) \right]. \tag{4.28}$$

4.2 The reconstruction theorem

To proceed with the dispersive treatment of $2 \to 2$ scattering processes we want to recall the analytic properties of the fixed-t dispersion relation given in eq. (4.14). The right-hand side of this equation is holomorphic in s apart from the branch cuts starting at the production thresholds s_{thr} and u_{thr}, but the derivation of the fixed-t dispersion relation relies on real values of t. Therefore the right-hand side of the equation is only a smooth function in t. However, maximal analyticity states that the left-hand side is holomorphic in both s and t up to the branch cuts of the different channels, *cf.* sec. 2.1.2.

In the following we want to derive a dispersive representation for $\mathcal{M}$ satisfying the constraints of analyticity such that the amplitude is a holomorphic function in both s and t up to the branch cuts. In order to achieve this we expand the amplitude into partial waves inside the fixed-t dispersion relation to find explicit expressions for the discontinuities. However, several kinematical requirements have to be satisfied. First, for eq. (4.14) to hold, t is constrained by eq. (4.4) and $t < t_{\text{thr}}$. Second, the partial-wave expansion is defined in the scattering region, *e.g.*, $s \geq s_{\text{thr}}$ in the s-channel expansion. If we consider processes for which none of the particle masses exceed the production threshold of the other three particles (*i.e.*, we exclude the possibility of $1 \to 3$ decays), we can find kinematical regions where both requirements are met.

This so-called *reconstruction theorem* states that a given $2 \to 2$ scattering amplitude $\mathcal{M}$ can be reconstructed just from the information on the discontinuities of the partial waves under consideration and some polynomial contributions obeying the exact same symmetries as $\mathcal{M}$. It was first derived for the $\pi\pi$ scattering amplitude [163, 164] and later generalized to arbitrary $2 \to 2$ scattering processes of spin-zero particles [165, 166]. Since this dispersive representation relies on the partial-wave expansion of the considered amplitude, we begin the discussion by restricting ourselves to amplitudes involving four pseudoscalar particles. An extension to amplitudes containing one vector particle will be considered at the end of this section.

In the specific case of $2 \to 2$ scattering processes involving only spin-zero pseudoscalar particles, the amplitude $\mathcal{M}$ can be expanded in terms of ordinary LEGENDRE polynomials. The s-channel (2.30) partial-wave expansion of $\mathcal{M}$ reads

$$\mathcal{M}(s, z_s) = \sum_{\ell=0}^{\infty} \left[\lambda(s, M_1^2, M_2^2)\, \lambda(s, M_3^2, M_4^2)\right]^{\ell/2} P_\ell(z_s)\, f_\ell(s)\,. \tag{4.29}$$

where f_ℓ defines the ℓ-th partial-wave amplitude.[#3] Note that the factor in the square bracket is purely conventional and only introduced to avoid possible kinematical singularities arising from eq. (2.31). Similar expressions can be obtained for the t- (2.36) and u-channels (2.38), where we will denote the partial-wave amplitudes of these channels by g_ℓ and h_ℓ, respectively.

In the following we will truncate the expansion of the discontinuities after S- and P-waves, thus we assume that contribution of D- and higher partial waves to the discon-

[#3] For the sake of simplicity possible contributions of different isospin combinations to the same angular momentum ℓ are subsumed in the partial-wave amplitudes f_ℓ.

tinuities can be neglected, *i.e.*,

$$\operatorname{disc}_s \mathcal{M}(s,z_s) = \operatorname{disc} f_0(s) + z_s \sqrt{\lambda(s,M_1^2,M_2^2)\,\lambda(s,M_3^2,M_4^2)}\operatorname{disc} f_1(s)\,, \tag{4.30}$$

for the s-channel and similarly for the t- and u-channels. Accordingly, the fixed-t dispersion relation reads

$$\begin{aligned}\mathcal{M}(s,t,3r-s-t) = {}& P^t_{m-1}(s)\\ &+ \frac{Q_m(s)}{2\pi i}\int_{s_{\text{thr}}}^{\infty}\mathrm{d}x\,\frac{\operatorname{disc} f_0(x) + \big[x\,(t-y)+\Delta_{12}\,\Delta_{34}\big]\operatorname{disc} f_1(x)}{Q_m(x)\,(x-s)}\\ &+ \frac{Q_m(u)}{2\pi i}\int_{u_{\text{thr}}}^{\infty}\mathrm{d}x\,\frac{\operatorname{disc} h_0(x) + \big[x\,(y-t)+\Delta_{14}\,\Delta_{23}\big]\operatorname{disc} h_1(x)}{Q_m(x)\,(x-u)}\,,\end{aligned} \tag{4.31}$$

with $y = 3r - t - x = s + u - x$ in the integrals for the P-wave contributions. The s-channel P-wave dispersion integral can be further simplified to

$$\begin{aligned}&\frac{Q_m(s)}{2\pi i}\int_{s_{\text{thr}}}^{\infty}\mathrm{d}x\,\frac{\big[x\,(x-s+t-u)+\Delta_{12}\,\Delta_{34}\big]\operatorname{disc} f_1(x)}{Q_m(x)\,(x-s)}\\ &\qquad = \big[s\,(t-u)+\Delta_{12}\,\Delta_{34}\big]\,\frac{Q_{m-2}(s)}{2\pi i}\int_{s_{\text{thr}}}^{\infty}\mathrm{d}x\,\frac{\operatorname{disc} f_1(x)}{Q_{m-2}(x)\,(x-s)} + \dots\,,\end{aligned} \tag{4.32}$$

where the dots represent polynomial contributions in s of degree $m-1$ that can be absorbed into the subtraction polynomial P^t_{m-1}. Note that we reduced the number of subtractions by two in the remaining dispersion integral, *cf.* eq. (3.21). This dispersion integral will still converge, since $f_1(s) \asymp s^{n-2}$ as defined in eq. (4.29), if behaves asymptotically like $\mathcal{M}(s,z_s) \asymp s^n$. A similar decomposition can be found for the u-channel P-wave contribution. Inserting these findings into the fixed-t dispersion relation yields

$$\begin{aligned}\mathcal{M}(s,t,3r-s-t) = {}& P^t_{m-1}(s)\\ &+ \frac{Q_m(s)}{2\pi i}\int_{s_{\text{thr}}}^{\infty}\mathrm{d}x\,\frac{\operatorname{disc} f_0(x)}{Q_m(x)\,(x-s)} + \frac{Q_m(u)}{2\pi i}\int_{u_{\text{thr}}}^{\infty}\mathrm{d}x\,\frac{\operatorname{disc} h_0(x)}{Q_m(x)\,(x-u)}\\ &+ \big[s\,(t-u)+\Delta_{12}\,\Delta_{34}\big]\,\frac{Q_{m-2}(s)}{2\pi i}\int_{s_{\text{thr}}}^{\infty}\mathrm{d}x\,\frac{\operatorname{disc} f_1(x)}{Q_{m-2}(x)\,(x-s)}\\ &+ \big[u\,(s-t)+\Delta_{14}\,\Delta_{23}\big]\,\frac{Q_{m-2}(u)}{2\pi i}\int_{u_{\text{thr}}}^{\infty}\mathrm{d}x\,\frac{\operatorname{disc} h_1(x)}{Q_{m-2}(x)\,(x-u)}\,.\end{aligned} \tag{4.33}$$

Thus an expansion of the discontinuities into partial waves renders the dispersion integrals free of any t dependence.

Analogously to the derivation of the fixed-t dispersion relation it is also possible to write down a fixed-u or fixed-s dispersion relation of $\mathcal{M}$. Following the steps of the

derivation described in sec. 4.1 with keeping u fixed, we find

$$\begin{aligned}\mathcal{M}(3r-t-u,t,u) = P^u_{m-1}(t)\\ &+\frac{Q_m(s)}{2\pi i}\int_{s_{\text{thr}}}^{\infty}\mathrm{d}x\,\frac{\operatorname{disc} f_0(x)}{Q_m(x)\,(x-s)}+\frac{Q_m(t)}{2\pi i}\int_{t_{\text{thr}}}^{\infty}\mathrm{d}x\,\frac{\operatorname{disc} g_0(x)}{Q_m(x)\,(x-t)}\\ &+\big[s\,(t-u)+\Delta_{12}\,\Delta_{34}\big]\,\frac{Q_{m-2}(s)}{2\pi i}\int_{s_{\text{thr}}}^{\infty}\mathrm{d}x\,\frac{\operatorname{disc} f_1(x)}{Q_{m-2}(x)\,(x-s)}\\ &+\big[t\,(u-s)-\Delta_{13}\,\Delta_{24}\big]\,\frac{Q_{m-2}(t)}{2\pi i}\int_{t_{\text{thr}}}^{\infty}\mathrm{d}x\,\frac{\operatorname{disc} g_1(x)}{Q_{m-2}(x)\,(x-t)}\,.\end{aligned} \tag{4.34}$$

The dispersion integrals for the s-channel contribution are the same as in eq. (4.33), but the integrals for the u-channel are replaced by integrals for the t-channel. Moreover, the P^u_{m-1} is now a polynomial in t of degree $m-1$ whose coefficients depend on u. Similarly, the fixed-s dispersive representation will be given by

$$\begin{aligned}\mathcal{M}(s,3r-s-u,u) = P^s_{m-1}(u)\\ &+\frac{Q_m(t)}{2\pi i}\int_{t_{\text{thr}}}^{\infty}\mathrm{d}x\,\frac{\operatorname{disc} g_0(x)}{Q_m(x)\,(x-t)}+\frac{Q_m(u)}{2\pi i}\int_{u_{\text{thr}}}^{\infty}\mathrm{d}x\,\frac{\operatorname{disc} h_0(x)}{Q_m(x)\,(x-u)}\\ &+\big[t\,(u-s)-\Delta_{13}\,\Delta_{24}\big]\,\frac{Q_{m-2}(t)}{2\pi i}\int_{t_{\text{thr}}}^{\infty}\mathrm{d}x\,\frac{\operatorname{disc} g_1(x)}{Q_{m-2}(x)\,(x-t)}\\ &+\big[u\,(s-t)+\Delta_{14}\,\Delta_{23}\big]\,\frac{Q_{m-2}(u)}{2\pi i}\int_{u_{\text{thr}}}^{\infty}\mathrm{d}x\,\frac{\operatorname{disc} h_1(x)}{Q_{m-2}(x)\,(x-u)}\,,\end{aligned} \tag{4.35}$$

containing the same dispersion integrals for the t- and u-channels as given in eqs. (4.33) and (4.34), while the coefficients of P^s_{m-1} will depend on s.

Therefore we combine eqs. (4.33), (4.34), and (4.35) to

$$\begin{aligned}\mathcal{M}(s,t,u) = P_{m-1}(s,t,u)+\frac{Q_m(s)}{2\pi i}\int_{s_{\text{thr}}}^{\infty}\mathrm{d}x\,\frac{\operatorname{disc} f_0(x)}{Q_m(x)\,(x-s)}\\ &+\frac{Q_m(t)}{2\pi i}\int_{t_{\text{thr}}}^{\infty}\mathrm{d}x\,\frac{\operatorname{disc} g_0(x)}{Q_m(x)\,(x-t)}+\frac{Q_m(u)}{2\pi i}\int_{u_{\text{thr}}}^{\infty}\mathrm{d}x\,\frac{\operatorname{disc} h_0(x)}{Q_m(x)\,(x-u)}\\ &+\big[s\,(t-u)+\Delta_{12}\,\Delta_{34}\big]\,\frac{Q_{m-2}(s)}{2\pi i}\int_{s_{\text{thr}}}^{\infty}\mathrm{d}x\,\frac{\operatorname{disc} f_1(x)}{Q_{m-2}(x)\,(x-s)}\\ &+\big[t\,(u-s)-\Delta_{13}\,\Delta_{24}\big]\,\frac{Q_{m-2}(t)}{2\pi i}\int_{t_{\text{thr}}}^{\infty}\mathrm{d}x\,\frac{\operatorname{disc} g_1(x)}{Q_{m-2}(x)\,(x-t)}\\ &+\big[u\,(s-t)+\Delta_{14}\,\Delta_{23}\big]\,\frac{Q_{m-2}(u)}{2\pi i}\int_{u_{\text{thr}}}^{\infty}\mathrm{d}x\,\frac{\operatorname{disc} h_1(x)}{Q_{m-2}(x)\,(x-u)}\,,\end{aligned} \tag{4.36}$$

where P_{m-1} is now a polynomial in all three MANDELSTAM variables. Since the non-polynomial parts of the dispersion relation depend on one MANDELSTAM variable only,

we introduce a set of *single-variable amplitudes*. In the s-channel these amplitudes will be given by

$$\begin{aligned}\mathcal{F}_0(s) &= P^0_{m-1}(s) + \frac{Q_m(s)}{2\pi i}\int_{s_{\text{thr}}}^{\infty}\mathrm{d}x\,\frac{\operatorname{disc} f_0(x)}{Q_m(x)\,(x-s)}\,,\\ \mathcal{F}_1(s) &= P^1_{m-3}(s) + \frac{Q_{m-2}(s)}{2\pi i}\int_{s_{\text{thr}}}^{\infty}\mathrm{d}x\,\frac{\operatorname{disc} f_1(x)}{Q_{m-2}(x)\,(x-s)}\,.\end{aligned} \tag{4.37}$$

Likewise, we define single variable amplitudes for the t- and u-channel denoted by $\mathcal{G}_\ell$ and $\mathcal{H}_\ell$. Assuming that the contributions of the subtraction polynomial P_{m-1} in eq. (4.36) can be fully absorbed in the polynomials defined along with the single-variable amplitudes, we arrive at the decomposition

$$\begin{aligned}\mathcal{M}(s,t,u) = \mathcal{F}_0(s) + \mathcal{G}_0(t) + \mathcal{H}_0(u) + \big[s\,(t-u) + \Delta_{12}\,\Delta_{34}\big]\,\mathcal{F}_1(s)\\ + \big[t\,(u-s) - \Delta_{13}\,\Delta_{24}\big]\,\mathcal{G}_1(t) + \big[u\,(s-t) + \Delta_{14}\,\Delta_{23}\big]\,\mathcal{H}_1(u)\,,\end{aligned} \tag{4.38}$$

which is the reconstruction theorem for $\mathcal{M}$.

4.2.1 Symmetric and antisymmetric decompositions

Following the discussion of the symmetry behaviour of the fixed-t dispersion relation (*cf.* sec. 4.1.1) we want to investigate these symmetries within the reconstruction theorem. We start by considering an amplitude that is symmetric under interchange of $t \leftrightarrow u$, *i.e.*

$$\mathcal{M}(s,t,u) = \mathcal{M}(s,u,t)\,, \tag{4.39}$$

and $t_{\text{thr}} = u_{\text{thr}}$. Thus two of the involved particles must have equal masses, *e.g.* we choose $M_3 = M_4$. According to the symmetry properties of the partial wave decomposition given in eq. (4.29) and the scattering angle z_s (2.31), the discontinuity of the s-channel (4.30) is only allowed to contain even partial waves, *i.e.*

$$\operatorname{disc}_s \mathcal{M}(s,z_s) = \operatorname{disc} f_0(s)\,. \tag{4.40}$$

Similar considerations for the scattering angles z_t (2.37) and z_u (2.39) yield the discontinuity of the t-channel

$$\operatorname{disc}_t \mathcal{M}(t,z_t) = \operatorname{disc} h_0(t) - z_t\,\sqrt{\lambda(t,M_1^2,M_3^2)\,\lambda(t,M_2^2,M_3^2)}\operatorname{disc} h_1(t)\,, \tag{4.41}$$

in terms of the u-channel partial-wave amplitudes. Repeating the steps performed in the derivation of eq. (4.38) we find the reconstruction theorem

$$\begin{aligned}\mathcal{M}(s,t,u) = \mathcal{F}_0(s) + \mathcal{H}_0(t) + \mathcal{H}_0(u) + \big[t\,(s-u) + \Delta_{13}\,\Delta_{23}\big]\,\mathcal{H}_1(t)\\ + \big[u\,(s-t) + \Delta_{13}\,\Delta_{23}\big]\,\mathcal{H}_1(u)\,,\end{aligned} \tag{4.42}$$

which respects the symmetry behaviour defined in eq. (4.39).

Analogously to the discussion started in sec. 4.1.2 on the antisymmetric fixed-t dispersion relation, we want to study an amplitude that is antisymmetric under interchange of $t \leftrightarrow u$, *i.e.*

$$\mathcal{M}(s,t,u) = -\mathcal{M}(s,u,t)\,, \tag{4.43}$$

and $t_{\text{thr}} = u_{\text{thr}}$. Again we will fix the particle masses $M_3 = M_4$. In contrast to the previous case, an antisymmetric behaviour as given in eq. (4.43) demands

$$\text{disc}_s\,\mathcal{M}(s,z_s) = z_s\,\sqrt{\lambda(s,M_1^2,M_2^2)\,\lambda(s,M_3^2,M_3^2)}\,\text{disc}\,f_1(s)\,, \tag{4.44}$$

for the discontinuity of $\mathcal{M}$ in the s-channel. The S-wave amplitude has to vanish, since only odd s-channel partial-wave amplitudes obey the correct transformation behaviour under $t \leftrightarrow u$ (2.30). Likewise the t-channel discontinuity has to satisfy

$$\text{disc}_t\,\mathcal{M}(t,z_t) = -\text{disc}\,h_0(t) + z_t\,\sqrt{\lambda(t,M_1^2,M_3^2)\,\lambda(t,M_2^2,M_3^2)}\,\text{disc}\,h_1(t)\,, \tag{4.45}$$

i.e., it can be expressed in terms of the u-channel partial-wave amplitudes. Restricting to these discontinuities in the derivation of the reconstruction theorem (4.38) yields

$$\begin{aligned}\mathcal{M}(s,t,u) = \mathcal{H}_0(u) - \mathcal{H}_0(t) + (t-u)\,\mathcal{F}_1(s) - \big[t\,(s-u) + \Delta_{13}\,\Delta_{23}\big]\,\mathcal{H}_1(t) \\ + \big[u\,(s-t) + \Delta_{13}\,\Delta_{23}\big]\,\mathcal{H}_1(u)\,,\end{aligned} \tag{4.46}$$

which obeys the antisymmetry behaviour demanded in eq. (4.43). Note that in eq. (4.46) we absorbed a factor of s into $\mathcal{F}_1$ by redefinition of eq. (4.37).

Finally, consider an amplitude that is antisymmetric under pairwise interchange of all Mandelstam variables, *i.e.*

$$\mathcal{M}(s,t,u) = -\mathcal{M}(s,u,t) = \mathcal{M}(t,u,s) = -\mathcal{M}(t,s,u) = \mathcal{M}(u,s,t) = -\mathcal{M}(u,t,s)\,. \tag{4.47}$$

Accordingly, the thresholds obey $s_{\text{thr}} = t_{\text{thr}} = u_{\text{thr}}$ and three of the particles have equal masses, *e.g.* we choose $M_2 = M_3 = M_4$. Given the transformation properties of the scattering angles z_s, z_t, and z_u defined in eqs. (2.31), (2.37), and (2.39), we conclude for the fully antisymmetric discontinuities depending solely on the s-channel P-wave amplitude given by

$$\text{disc}_x\,\mathcal{M}(x,z_x) = z_x\,\sqrt{\lambda(x,M_1^2,M_2^2)\,\lambda(x,M_2^2,M_2^2)}\,\text{disc}\,f_1(x)\,, \tag{4.48}$$

with $x \in \{s,t,u\}$. Therefore the reconstruction theorem yields

$$\mathcal{M}(s,t,u) = (t-u)\,\mathcal{F}_1(s) + (u-s)\,\mathcal{F}_1(t) + (s-t)\,\mathcal{F}_1(u)\,, \tag{4.49}$$

which is indeed fully antisymmetric under pairwise interchange of the Mandelstam variables.

4.2.2 Analytic properties of the decomposition

Although the derivation of the reconstruction theorem for $\mathcal{M}$ relies on "fixed-t" dispersion relations in the three channels, eq. (4.38) will apply also if the MANDELSTAM variables are complex. Moreover, the single-variable amplitudes introduced in eq. (4.37) posses right-hand cuts only. They are holomorphic on $\mathbb{C}$ except for a branch cut along the positive real axis starting at the respective threshold s_{thr}, t_{thr}, or u_{thr}, and therefore allow for a continuation of $\mathcal{M}$ to complex values in all three MANDELSTAM variables. Note that the cuts in the single-variable amplitudes result in the correct cut structure for $\mathcal{M}$ required by analyticity. Accordingly, the right-hand side of eq. (4.38) is holomorphic in all MANDELSTAM variables up to the cuts. On the other hand the dynamical information included in the reconstruction theorem is limited by the number of partial-wave amplitudes considered in the expansion of the discontinuities. Hence, the reconstruction theorem provides only a valid description of the scattering process in the region where the contributions of higher partial waves to the discontinuities can be safely neglected.

The reconstruction theorem provides a drastic simplification of the dispersive representation for $\mathcal{M}$. It reduces the investigation of $\mathcal{M}$, which depends on two independent MANDELSTAM variables and possesses several cuts, to the single-variable functions of simpler analytic structure. However, it is important to realise that in general the absorption of the subtraction polynomial P_{m-1} in eq. (4.36) into the single-variable amplitudes is not unique. Due to eq. (2.25) it is possible to find polynomial shifts given by

$$\mathcal{F}_\ell(s) \mapsto \mathcal{F}_\ell(s) + \Delta\mathcal{F}_\ell(s) \tag{4.50}$$

for the s-channel single-variable amplitudes (similarly for $\mathcal{G}_\ell$ and $\mathcal{H}_\ell$), which leave $\mathcal{M}$ unchanged. As an example, consider the reconstruction theorem given in eq. (4.42), the most general polynomial shifts meeting the requirement

$$\begin{aligned} 0 = \Delta\mathcal{F}_0(s) + \Delta\mathcal{H}_0(t) + \Delta\mathcal{H}_0(u) + \left[t\,(s-u) + \Delta_{13}\,\Delta_{23}\right]\Delta\mathcal{H}_1(t) \\ + \left[u\,(s-t) + \Delta_{13}\,\Delta_{23}\right]\Delta\mathcal{H}_1(u) \end{aligned} \tag{4.51}$$

are given by

$$\begin{aligned} \Delta\mathcal{F}_0(s) &= 2a + b\,(r-s) + c\left[2s^2 + 9r\,(r-s)\right] + d\left[2s^3 + 27r^2\,(r-s)\right], \\ \Delta\mathcal{H}_0(t) &= -a + b\,(r-t) - c\,(t^2 + \Delta_{13}\,\Delta_{23}) - d\left[t^3 + 3\Delta_{13}\,\Delta_{23}\,(3r-t)\right], \\ \Delta\mathcal{H}_1(t) &= c + 3d\,(3r-t)\,. \end{aligned} \tag{4.52}$$

Accordingly, eq. (4.42) reveals a four-parameter ambiguity with $a, b, c, d \in \mathbb{C}$.[#4]

By definition the single-variable amplitudes (4.37) share the same discontinuity as the partial-wave amplitudes along the right-hand cuts. However, the partial-wave amplitudes possess left-hand cuts as well. Thus a single-variable function and its respective partial-wave amplitude do not coincide in general. We want to investigate the partial-wave

[#4] If the considered amplitude $\mathcal{M}$ is required to fulfil the SCHWARZ reflection principle, the ambiguity parameters need to be real.

amplitude in more detail. Using the orthogonality relation of the LEGENDRE polynomials (A.12) we can project eq. (4.29) onto distinct partial-wave amplitudes in the s-channel by

$$f_\ell(s) = \frac{2\ell+1}{2} \left[\lambda(s, M_1^2, M_2^2)\, \lambda(s, M_3^2, M_4^2)\right]^{-\ell/2} \int_{-1}^{1} \mathrm{d}z_s\, P_\ell(z_s)\, \mathcal{M}(s, z_s)\,. \tag{4.53}$$

Separating the contributions of $\mathcal{F}_\ell$ as given in eq. (4.38) defines the hat functions $\hat{\mathcal{F}}_\ell$ according to

$$\begin{aligned} \hat{\mathcal{F}}_0(s) &= \frac{1}{2} \int_{-1}^{1} \mathrm{d}z_s \left[\mathcal{M}(s, z_s) - \mathcal{F}_0(s)\right], \\ \hat{\mathcal{F}}_1(s) &= \frac{3}{2} \int_{-1}^{1} \mathrm{d}z_s\, z_s \frac{\mathcal{M}(s, z_s) - \left[s\,(t-u) + \Delta_{12}\,\Delta_{34}\right] \mathcal{F}_1(s)}{\sqrt{\lambda(s, M_1^2, M_2^2)\, \lambda(s, M_3^2, M_4^2)}}\,. \end{aligned} \tag{4.54}$$

Thus the partial-wave amplitudes are given by

$$f_\ell = \mathcal{F}_\ell(s) + \hat{\mathcal{F}}_\ell(s)\,. \tag{4.55}$$

Analogous expressions can be found for the t- and u-channel partial-wave projections. Since $\mathcal{F}_\ell$ contains the complete information of f_ℓ along the right-hand cut, $\hat{\mathcal{F}}_\ell$ is demanded to possess the left-hand cut of f_ℓ. In particular $\hat{\mathcal{F}}_\ell$ is free of any right-hand cuts. Moreover, by definition eq. (4.53) is independent of the polynomial shifts (4.50), thus the hat functions need to obey

$$\hat{\mathcal{F}}_\ell(s) \mapsto \hat{\mathcal{F}}_\ell(s) - \Delta\mathcal{F}_\ell(s)\,. \tag{4.56}$$

Note that the partial waves given in eq. (4.55) will contain contributions to the right-hand cuts only for S- and P-waves, since in the derivation of eq. (4.38) we truncated the expansion of the discontinuities for D- and higher partial waves. However, note that this only accounts for the right-hand cuts. In general the right-hand side of eq. (4.53) will not vanish for $\ell \geq 2$.

4.2.3 Extension to amplitudes involving a spin-one particle

We want to extend the reconstruction theorem to amplitudes involving three spin-zero pseudoscalar particles and a spin-one vector particle. In the following we will work on the level of the scalar amplitude defined in eq. (2.22) after the separation of the kinematical prefactor, which is a polynomial in the momenta and therefore does not contribute to the discontinuity of the amplitude. Thus $\mathcal{M}$ will refer to this scalar amplitude. Due to the spin structure of this scattering process, the expansion is performed in terms of derivatives of the LEGENDRE polynomials [120, 167]. Thus the s-channel (2.30) partial-wave expansion is given by

$$\mathcal{M}(s, z_s) = \sum_{\ell=1}^{\infty} \left[\lambda(s, M_1^2, M_2^2)\, \lambda(s, M_3^2, M_4^2)\right]^{(\ell-1)/2} P_\ell'(z_s)\, f_\ell(s)\,, \tag{4.57}$$

where the ℓ-th partial wave is denoted by f_ℓ. Similarly, the t- and u-channel partial waves will be denoted by g_ℓ and h_ℓ. As in the spin-zero case, the factor in the square bracket is purely conventional to absorb possible kinematical singularities arising from eq. (2.31). Note that the expansion in this case starts at P-waves, since the spin structure of the considered process does not allow for S-wave contributions.

We truncate the expansion of the discontinuities after P- and D-waves, *i.e.*, contributions of F- and higher partial waves will be neglected. Thus the expansion in the s-channel reads

$$\operatorname{disc}_s\mathcal{M}(s,z_s) = \operatorname{disc} f_1(s) + 3z_s\sqrt{\lambda(s,M_1^2,M_2^2)\,\lambda(s,M_3^2,M_4^2)}\operatorname{disc} f_2(s)\,, \tag{4.58}$$

and analogously for the t- and u-channels. Casting these discontinuities into fixed-t, fixed-u, and fixed-s dispersion relations and following the steps in the derivation of eq. (4.36) we arrive at

$$\begin{aligned}\mathcal{M}(s,t,u) = P_{m-1}(s,t,u) &+ \frac{Q_m(s)}{2\pi i}\int_{s_\text{thr}}^\infty \mathrm{d}x\,\frac{\operatorname{disc} f_1(x)}{Q_m(x)\,(x-s)}\\ &+ \frac{Q_m(t)}{2\pi i}\int_{t_\text{thr}}^\infty \mathrm{d}x\,\frac{\operatorname{disc} g_1(x)}{Q_m(x)\,(x-t)} + \frac{Q_m(u)}{2\pi i}\int_{u_\text{thr}}^\infty \mathrm{d}x\,\frac{\operatorname{disc} h_1(x)}{Q_m(x)\,(x-u)}\\ &+ \big[s\,(t-u)+\Delta_{12}\,\Delta_{34}\big]\,\frac{3Q_{m-2}(s)}{2\pi i}\int_{s_\text{thr}}^\infty \mathrm{d}x\,\frac{\operatorname{disc} f_2(x)}{Q_{m-2}(x)\,(x-s)}\\ &+ \big[t\,(u-s)-\Delta_{13}\,\Delta_{24}\big]\,\frac{3Q_{m-2}(t)}{2\pi i}\int_{t_\text{thr}}^\infty \mathrm{d}x\,\frac{\operatorname{disc} g_2(x)}{Q_{m-2}(x)\,(x-t)}\\ &+ \big[u\,(s-t)+\Delta_{14}\,\Delta_{23}\big]\,\frac{3Q_{m-2}(u)}{2\pi i}\int_{u_\text{thr}}^\infty \mathrm{d}x\,\frac{\operatorname{disc} h_2(x)}{Q_{m-2}(x)\,(x-u)}\,.\end{aligned} \tag{4.59}$$

The non-polynomial contributions are now given explicitly in terms of the dispersion integrals, while P_{m-1} is a polynomial in all three MANDELSTAM variables. Since the dispersion integrals depend on one MANDELSTAM variable only, we define single variable functions

$$\begin{aligned}\mathcal{F}_1(s) &= P^1_{m-1}(s) + \frac{Q_m(s)}{2\pi i}\int_{s_\text{thr}}^\infty \mathrm{d}x\,\frac{\operatorname{disc} f_1(x)}{Q_m(x)\,(x-s)}\,,\\ \mathcal{F}_2(s) &= P^2_{m-3}(s) + \frac{3Q_{m-2}(s)}{2\pi i}\int_{s_\text{thr}}^\infty \mathrm{d}x\,\frac{\operatorname{disc} f_2(x)}{Q_{m-2}(x)\,(x-s)}\end{aligned} \tag{4.60}$$

for the s-channel and similarly for the t- and u-channels, which will be denoted by $\mathcal{G}_\ell$ and $\mathcal{H}_\ell$. Under the assumption that P_{m-1} can be fully absorbed into the subtraction polynomials given in eq. (4.60), we find

$$\begin{aligned}\mathcal{M}(s,t,u) = \mathcal{F}_1(s) + \mathcal{G}_1(t) + \mathcal{H}_1(u) &+ \big[s\,(t-u)+\Delta_{12}\,\Delta_{34}\big]\,\mathcal{F}_2(s)\\ &+ \big[t\,(u-s)-\Delta_{13}\,\Delta_{24}\big]\,\mathcal{G}_2(t) + \big[u\,(s-t)+\Delta_{14}\,\Delta_{23}\big]\,\mathcal{H}_2(u)\,.\end{aligned} \tag{4.61}$$

This is the reconstruction theorem of the scalar amplitude $\mathcal{M}$ taking P- and D-wave contributions to the discontinuities into account. It fulfils the analytic properties discussed in sec. 4.2.2.

As in the spin-zero case, we can use the orthogonality relation of the derivatives of the LEGENDRE polynomials (A.18) to project onto the ℓ-th partial-wave amplitude in the s-channel

$$f_\ell(s) = \frac{1}{2}\big[\lambda(s,M_1^2,M_2^2)\,\lambda(s,M_3^2,M_4^2)\big]^{(1-\ell)/2}\int_{-1}^{1}\mathrm{d}z_s\,\big[P_{\ell-1}(z_s)+P_{\ell+1}(z_s)\big]\,\mathcal{M}(s,z_s)\,. \tag{4.62}$$

Accordingly, the hat functions $\hat{\mathcal{F}}_\ell$ can be found by separating the contribution of $\mathcal{F}_\ell$ yielding

$$\begin{aligned}\hat{\mathcal{F}}_1(s) &= \frac{3}{4}\int_{-1}^{1}\mathrm{d}z_s\,(1-z_s^2)\,\big[\mathcal{M}(s,z_s)-\mathcal{F}_1(s)\big]\,,\\ \hat{\mathcal{F}}_2(s) &= \frac{15}{4}\int_{-1}^{1}\mathrm{d}z_s\,z_s\,(z_s^2-1)\,\frac{\mathcal{M}(s,z_s)-\big[s\,(t-u)+\Delta_{12}\,\Delta_{34}\big]\,\mathcal{F}_2(s)}{\sqrt{\lambda(s,M_1^2,M_2^2)\,\lambda(s,M_3^2,M_4^2)}}\,,\end{aligned} \tag{4.63}$$

and the partial-wave amplitudes are given by

$$f_1(s) = \mathcal{F}_1(s)+\hat{\mathcal{F}}_1(s)\,,\qquad f_2(s) = \frac{1}{3}\big[\mathcal{F}_2(s)+\hat{\mathcal{F}}_2(s)\big]\,. \tag{4.64}$$

Again, similar expressions can be found for the t- and u-channels.

Continuing the discussion on symmetry and antisymmetry behaviour of $\mathcal{M}$ under interchange of the MANDELSTAM variables (*cf.* sec. 4.2.1), we want to consider a scalar function completely symmetric under pairwise interchange of the MANDELSTAM variables

$$\mathcal{M}(s,t,u) = \mathcal{M}(s,u,t) = \mathcal{M}(t,u,s) = \mathcal{M}(t,s,u) = \mathcal{M}(u,s,t) = \mathcal{M}(u,t,s)\,. \tag{4.65}$$

The thresholds have to be identical $s_{\mathrm{thr}} = t_{\mathrm{thr}} = u_{\mathrm{thr}}$, which forces three of the particle masses to be equal, *e.g.* we choose $M_2 = M_3 = M_4$. According to the transformation properties of the scattering angles given in eqs. (2.31), (2.37), and (2.39) only odd partial waves are allowed to contribute to the discontinuities in such a system, thus forcing the D-waves to vanish. The discontinuities in all three channels will be given by

$$\mathrm{disc}_x\,\mathcal{M}(x,z_x) = \mathrm{disc}\,f_1(x)\,, \tag{4.66}$$

where $x \in \{s,t,u\}$. Hence, the reconstruction theorem of a fully symmetric scalar function will be given by

$$\mathcal{M}(s,t,u) = \mathcal{F}_1(s)+\mathcal{F}_1(t)+\mathcal{F}_1(u)\,. \tag{4.67}$$

Furthermore, we want to consider a scalar amplitude $\mathcal{M}$ antisymmetric under interchange of $t \leftrightarrow u$, *i.e.*

$$\mathcal{M}(s,t,u) = -\mathcal{M}(s,u,t)\,, \tag{4.68}$$

and $t_{\mathrm{thr}} = u_{\mathrm{thr}}$. Accordingly, two of the particle masses need to be identical, *e.g.* we choose $M_3 = M_4$. Since the scattering angle z_s is odd under exchange of $t \leftrightarrow u$, we find for the s-channel discontinuity

$$\mathrm{disc}_s\,\mathcal{M}(s,z_s) = 3z_s\sqrt{\lambda(s,M_1^2,M_2^2)\,\lambda(s,M_3^2,M_3^2)}\,\mathrm{disc}\,f_2(s)\,. \tag{4.69}$$

For the t-channel discontinuity the antisymmetry behaviour of $\mathcal{M}$ yields

$$\operatorname{disc}_t \mathcal{M}(t, z_t) = -\operatorname{disc} h_1(t) + 3 z_t \sqrt{\lambda(t, M_1^2, M_3^2)\, \lambda(t, M_2^2, M_3^2)}\, \operatorname{disc} g_2(t)\,, \tag{4.70}$$

in terms of the u-channel partial-wave amplitudes. Therefore the reconstruction theorem for $\mathcal{M}$ is given by

$$\begin{aligned} \mathcal{M}(s,t,u) = \mathcal{H}_1(u) - \mathcal{H}_1(t) + (t-u)\,\mathcal{F}_2(s) - \big[t\,(s-u) + \Delta_{13}\,\Delta_{23}\big]\,\mathcal{H}_2(t) \\ + \big[u\,(s-t) + \Delta_{13}\,\Delta_{23}\big]\,\mathcal{H}_2(u)\,. \end{aligned} \tag{4.71}$$

Note that a factor of s is absorbed in the definition of $\mathcal{F}_2$.

Part III

Hadronic η and η' decays

Chapter 5

Dispersion relations for $\eta' \to \pi\pi\eta$[#1]

The decay $\eta' \to \pi\pi\eta$ has received considerable interest in past years for several reasons. Due to the $\mathrm{U}(1)_A$ anomaly the η' is not a NAMBU–GOLDSTONE BOSON and therefore "standard" ChPT based on the spontaneous breaking of $\mathrm{SU}(3)_L \times \mathrm{SU}(3)_R$ chiral symmetry fails to adequately describe processes involving the η', *cf.* ch. 1. In the limit of the number of colors N_C becoming large ("large-N_C limit") the axial anomaly vanishes, which leads to a $\mathrm{U}(3)_L \times \mathrm{U}(3)_R$ symmetry, so that a simultaneous expansion in small momenta, small quark masses, and large N_C gives rise to a power counting scheme that in principle allows one to describe interactions of the pseudoscalar nonet (π, K, η, η'). However, the question whether this framework dubbed large-N_C ChPT [168, 169] is actually well-established remains under discussion, mainly due to the large η' mass. This is an issue that can in principle be addressed by a study of $\eta' \to \pi\pi\eta$. So far there are indications that a large-N_C ChPT treatment alone is not sufficient to describe the decay, as final-state interactions play a rather important role, *cf.* refs. [169, 170].

Furthermore, the $\eta' \to \pi\pi\eta$ decay channel could be used to constrain $\pi\eta$ scattering: the η' mass is sufficiently small so that the channel is not polluted by nonvirtual intermediate states other than the rather well-constrained $\pi\pi$ scattering. In the past claims were made that the mechanism via the intermediate scalar resonance $a_0(980) \to \pi\eta$ even dominates the decay [171–173]. These claims are based on effective LAGRANGIAN models with the explicit inclusion of a scalar nonet incorporating the $a_0(980)$, $f_0(980)$, and $\sigma/f_0(500)$ resonances. They were further supported by refs. [174, 175]: a chiral unitary approach shows large corrections in the $\pi\eta$ channel and there is a dominant low-energy constant in the U(3) ChPT calculation that is saturated mostly by the $a_0(980)$. The $\pi\eta$ P-wave, however, was found to be strongly suppressed [176–178].

The $\eta' \to \pi^0\pi^0\eta$ decay channel is expected to show a *cusp effect* at the charged-pion threshold [178] that in principle can be used to obtain information on $\pi\pi$ scattering lengths. So far this phenomenon has not been observed: the most recent measurement with the GAMS-4π spectrometer did not have sufficient statistics to resolve this subtle effect [179].

The extraction of $\pi\eta$ scattering parameters such as the scattering length and the effective range parameter is a more complicated subject compared to $\pi\pi$ scattering. There

[#1] The contents of this chapter have been published in [154].

is no one-loop cusp effect as in the $\pi\pi$ channel, since the $\pi\eta$ threshold sits on the border of the physical region and not inside. The hope of extracting scattering parameters from a two-loop cusp is shattered likewise: there is a rather subtle cancellation of this effect at threshold (*cf.* refs. [180, 181] for an elaborate discussion).

Measurements of the DALITZ plot of the charged channel have been performed by the VES [182] and BESIII [183] collaborations, while earlier measurements at rather low statistics have been reported in refs. [184, 185]. The more recent measurements seem to disagree considerably with regard to the values of the DALITZ-plot parameters, and also in comparison with the GAMS-4π measurement [179] the picture remains inconsistent.

In this chapter we present the dispersion-theoretical analysis of $\eta' \to \pi\pi\eta$ decays by employing integral equations of the KHURI–TREIMAN type [11]. The discussion is structured as follows: we will start by defining the necessary kinematical variables as well as describing the resulting analytic structure of the $\eta' \to \pi\pi\eta$ matrix element in sec. 5.1, before deriving and analyzing dispersion relations of KHURI–TREIMAN type for the decay amplitude in sec. 5.2. The results of the fits to data will be discussed in sec. 5.3. Predictions for higher order DALITZ-plot parameters, the occurrence of ADLER zeros close to the soft-pion points, and the decay into the neutral final state $\eta' \to \pi^0\pi^0\eta$ are discussed in sec. 5.4. Finally, we perform a matching of the free parameters to U(3) extensions of ChPT in sec. 5.5. Some technical details are relegated to the appendices.

5.1 Kinematics and the matrix element

We define transition amplitude and kinematic variables of the $\eta' \to \eta\pi\pi$ decay in the usual fashion (*cf.* sec. 2.2),

$$\langle \pi^i(p_2)\, \pi^j(p_3)\, \eta(p_4)|iT|\eta'(p_1)\rangle = i\,(2\pi)^4 \delta^{(4)}(p_1 - p_2 - p_3 - p_4)\, \delta^{ij} \mathcal{M}(s,t,u)\,, \tag{5.1}$$

where i, j refer to the pion isospin indices.[#2] We define the MANDELSTAM variables for the three-particle decay processes according to

$$s = (p_2 + p_3)^2\,, \quad t = (p_2 + p_4)^2\,, \quad u = (p_3 + p_4)^2\,, \tag{5.2}$$

which fulfill the relation

$$3r \equiv s + t + u = M_{\eta'}^2 + M_\eta^2 + 2M_\pi^2\,. \tag{5.3}$$

The process is invariant under exchange of the pions, *i.e.*, under $t \leftrightarrow u$ the amplitude obeys the symmetry property

$$\mathcal{M}(s,t,u) = \mathcal{M}(s,u,t)\,. \tag{5.4}$$

In the CMS of the two pions, one has

$$t(s, z_s) = u(s, -z_s) = \frac{1}{2}\big(3r - s + \kappa_{\pi\pi}(s)\, z_s\big)\,, \tag{5.5}$$

[#2] In the following, we will consider both the charged decay channel $\eta' \to \pi^+\pi^-\eta$ and the neutral channel $\eta' \to \pi^0\pi^0\eta$. They differ only by isospin-breaking effects.

where $z_s = \cos\theta_s$ refers to the s-channel scattering angle,

$$z_s = \frac{t-u}{\kappa_{\pi\pi}(s)}\,, \quad \kappa_{\pi\pi}(s) = \frac{\sqrt{\lambda(M_\pi^2, M_\pi^2, s)\,\lambda(M_\eta^2, M_{\eta'}^2, s)}}{s}\,. \tag{5.6}$$

Similarly, in the CMS of the t-channel, one finds

$$s(t,z_t) = \frac{1}{2}\Big(3r - t - \frac{\Delta}{t} - \kappa_{\pi\eta}(t)\,z_t\Big)\,, \qquad u(t,z_t) = \frac{1}{2}\Big(3r - t + \frac{\Delta}{t} + \kappa_{\pi\eta}(t)\,z_t\Big)\,, \tag{5.7}$$

with $\Delta \equiv (M_{\eta'}^2 - M_\pi^2)(M_\eta^2 - M_\pi^2)$ and

$$z_t = \frac{t\,(u-s) - \Delta}{t\,\kappa_{\pi\eta}(t)}\,, \qquad \kappa_{\pi\eta}(t) = \frac{\sqrt{\lambda(M_\pi^2, M_\eta^2, t)\,\lambda(M_\pi^2, M_{\eta'}^2, t)}}{t}\,. \tag{5.8}$$

Due to crossing symmetry, the u-channel relations follow directly from $t \leftrightarrow u$, $z_t \leftrightarrow -z_u$. The physical thresholds in the three channels are given by

$$s_{\rm thr} = 4M_\pi^2\,, \quad t_{\rm thr} = u_{\rm thr} = (M_\pi + M_\eta)^2. \tag{5.9}$$

5.2 Khuri–Treiman equations for $\eta' \to \pi\pi\eta$

In this section, we set up dispersion relations of Khuri–Treiman type for the decay process $\eta' \to \pi\pi\eta$, in analogy to previous work on different decays into three pions [11, 120, 127, 186]. The idea is to derive a set of integral equations for the scattering processes $\eta\eta' \to \pi\pi$ and $\pi\eta' \to \pi\eta$ with hypothetical mass assignments that make these (quasi-) elastic: in such a kinematic regime the derivation is straightforward. The dispersion relation for the decay channel is then obtained by analytic continuation of the scattering processes to the decay region.

5.2.1 Reconstruction theorem and Omnès representation

We will begin our discussion by decomposing the amplitude according to the reconstruction theorem in terms of functions of one Mandelstam variable only, *cf.* sec. 4.2. This form will prove very convenient in the derivation of the integral equations and their numerical solution at a later stage. Given the smallness of the available phase space, the partial-wave expansion is truncated after S- and P-waves. Furthermore, a P-wave contribution to $\pi\pi$ s-channel rescattering is forbidden by charge conjugation symmetry. Thus the s- and t-channel discontinuities read[#3]

$$\mathrm{disc}_s\,\mathcal{M}(s,t,u) = \mathrm{disc}\,f_0^0(s)\,, \qquad \mathrm{disc}_t\,\mathcal{M}(s,t,u) = \mathrm{disc}\,g_0^1(t) - z_t\,t\,\kappa_{\pi\eta}(t)\,\mathrm{disc}\,g_1^1(t)\,, \tag{5.10}$$

[#3]Here and in the following, relations that involve the discontinuity are always thought to contain an implicit θ-function that denotes the opening of the respective threshold, *i.e.* $\theta(s - s_{\rm thr})$ for the $\pi\pi$ channel and $\theta(t - t_{\rm thr})$ for the $\pi\eta$ channel.

where f_ℓ^I and g_ℓ^I refer to the partial-wave amplitudes of angular momentum ℓ and isospin I: isospin conservation of the decay constrains the total isospin of the final-state pion pair to $I = 0$, while the $\pi\eta$ system always has $I = 1$. Since $\mathcal{M}$ obeys the symmetry property given in eq. (5.4), the u-channel discontinuity follows directly from $t \leftrightarrow u$, $z_t \leftrightarrow -z_u$. In analogy to the derivation of eq. (4.42) we find the reconstruction theorem for $\mathcal{M}$ to be given by

$$\mathcal{M}(s,t,u) = \mathcal{F}_0^0(s) + \mathcal{G}_0^1(t) + \mathcal{G}_0^1(u) + \big[t\,(s-u) + \Delta\big]\mathcal{G}_1^1(t) + \big[u\,(s-t) + \Delta\big]\mathcal{G}_1^1(u)\,, \tag{5.11}$$

where $\mathcal{F}_\ell^I$ and $\mathcal{G}_\ell^I$ are functions of one variable that only possess a right-hand cut. We stress that the truncation of higher partial-wave amplitudes in the derivation of eq. (5.11) only neglects the discontinuities or rescattering phases in partial waves of angular momentum $\ell \geq 2$: projecting $\mathcal{M}$ on the $\pi\pi$ D-wave (in the s-channel) yields a non-vanishing result, however, this D-wave is bound to be real apart from three-particle-cut contributions.

We will briefly discuss the final-state scattering amplitudes that are involved in the $\eta' \to \pi\pi\eta$ decay, namely $\pi\pi \to \pi\pi$ and $\pi\eta \to \pi\eta$, *cf.* sec. 2.3. Given again the maximum energies accessible in the decay, both rescattering channels are treated in the elastic approximation, such that the corresponding partial waves can be parametrized in terms of a phase shift only, without any inelasticity effects. The $\pi\pi$ scattering amplitude (confined to $I = 0$) is approximated as

$$\mathcal{T}_0^{\pi\pi}(s, z_s) = 32\pi\,\sigma_\pi^{-1}(s)\sin\delta_0^0(s)\,\exp\big[i\delta_0^0(s)\big]\,, \tag{5.12}$$

with δ_0^0 denoting the S-wave phase shift. Analogously, the $\pi\eta$ scattering amplitude can be represented, neglecting D- and higher waves, according to

$$\mathcal{T}^1(t, z_t) = 16\pi\sqrt{\frac{t^2}{\lambda(M_\pi^2, M_\eta^2, t)}}\,\Big(\sin\delta_0^1(t)\,\exp\big[i\delta_0^1(t)\big] + 3z_t\,\sin\delta_1^1(t)\,\exp\big[i\delta_1^1(t)\big]\Big)\,, \tag{5.13}$$

where δ_ℓ^1 is the $\pi\eta$ phase shift of angular momentum ℓ.

The unitarity condition for the decay of the η' to a generic three-body final state n can be written as

$$\operatorname{disc}\mathcal{M}_n = i\,(2\pi)^4 \sum\!\!\!\!\!\!\int_m \delta^{(4)}(p_n - p_m)\mathcal{T}_{m,n}^*\mathcal{M}_m\,, \tag{5.14}$$

where $\mathcal{M}_m$ denotes the $\eta' \to m$ decay amplitude and $\mathcal{T}_{m,n}$ describes the $m \to n$ transition, while the sum runs over all possible intermediate states m, *cf.* sec. 2.2.2. The integration over the intermediate-state momenta is implied in this short-hand notation. Limiting the sum to $\pi\pi$ and $\pi\eta$ rescattering, carrying out the phase-space integration, and inserting the partial-wave expansion for the $\pi\pi$ and $\pi\eta$ amplitudes eqs. (5.12) and (5.13), we find

$$\begin{aligned}
\operatorname{disc}_s\mathcal{M}(s,t,u) &= \frac{i}{2\pi}\int \mathrm{d}\Omega_s'\,\sin\delta_0^0(s)\,\exp\big[-i\delta_0^0(s)\big]\,\mathcal{M}(s,t',u')\,,\\
\operatorname{disc}_t\mathcal{M}(s,t,u) &= \frac{i}{2\pi}\int \mathrm{d}\Omega_t'\,\Big(\sin\delta_0^1(t)\,\exp\big[-i\delta_0^1(t)\big]\\
&\qquad + 3z_t''\sin\delta_1^1(t)\,\exp\big[-i\delta_1^1(t)\big]\Big)\,\mathcal{M}(s',t,u')\,,
\end{aligned} \tag{5.15}$$

and similarly for the u-channel. Here, $\mathrm{d}\Omega'_{s,t}$ denotes the angular integration between the initial and intermediate state of the respective s- or t-channel subsystem, while $z''_{s,t}$ refers to the CMS scattering angles between the intermediate and final state. Finally, we can insert the expansion (5.10) on the left- and the reconstruction theorem of the decay amplitude (5.11) on the right-hand side of eq. (5.15) and find the unitarity relations for the single-variable functions $\mathcal{F}_\ell^I$ and $\mathcal{G}_\ell^I$:

$$\begin{aligned} \operatorname{disc}\mathcal{F}_0^0(s) &= 2i\big[\mathcal{F}_0^0(s) + \hat{\mathcal{F}}_0^0(s)\big]\sin\delta_0^0(s)\,\exp\big[-i\delta_0^0(s)\big]\,, \\ \operatorname{disc}\mathcal{G}_\ell^1(t) &= 2i\big[\mathcal{G}_\ell^1(t) + \hat{\mathcal{G}}_\ell^1(t)\big]\sin\delta_\ell^1(t)\exp\big[-i\delta_\ell^1(t)\big]\,, \end{aligned} \tag{5.16}$$

where we used the fact that the inhomogeneities $\hat{\mathcal{F}}_\ell^I$ and $\hat{\mathcal{G}}_\ell^I$ given by

$$\begin{aligned} \hat{\mathcal{F}}_0^0(s) &= 2\langle\mathcal{G}_0^1\rangle + \left[\frac{3}{2}(s-r)(3r-s) + 2\Delta\right]\langle\mathcal{G}_1^1\rangle + s\,\kappa_{\pi\pi}\,\langle z_s\,\mathcal{G}_1^1\rangle + \frac{\kappa_{\pi\pi}^2}{2}\,\langle z_s^2\,\mathcal{G}_1^1\rangle\,, \\ \hat{\mathcal{G}}_0^1(t) &= \langle\mathcal{F}_0^0\rangle^- + \langle\mathcal{G}_0^1\rangle^+ + \frac{1}{4}\left[3(r-t)(3r-t) + \Delta\left(2 - \frac{\Delta}{t^2}\right)\right]\langle\mathcal{G}_1^1\rangle^+ \\ &\quad - \frac{\kappa_{\pi\eta}}{2}\left[t + \frac{\Delta}{t}\right]\langle z_t\,\mathcal{G}_1^1\rangle^+ - \frac{\kappa_{\pi\eta}^2}{4}\,\langle z_t^2\,\mathcal{G}_1^1\rangle^+\,, \\ \hat{\mathcal{G}}_1^1(t) &= \frac{3}{t\,\kappa_{\pi\eta}}\left\{\langle z_t\,\mathcal{F}_0^0\rangle^- - \langle z_t\,\mathcal{G}_0^1\rangle^+ - \frac{1}{4}\left[3(r-t)(3r-t) + \Delta\left(2 - \frac{\Delta}{t^2}\right)\right]\langle z_t\,\mathcal{G}_1^1\rangle^+\right. \\ &\quad \left. + \frac{\kappa_{\pi\eta}}{2}\left[t + \frac{\Delta}{t}\right]\langle z_t^2\,\mathcal{G}_1^1\rangle^+ - \frac{\kappa_{\pi\eta}^2}{4}\,\langle z_t^3\,\mathcal{G}_1^1\rangle^+\right\}, \end{aligned} \tag{5.17}$$

are free of right-hand cuts. Here we used the short-hand notation

$$\begin{aligned} \langle z^n\,\mathcal{B}_\ell^I\rangle &:= \frac{1}{2}\int_{-1}^{1}\mathrm{d}z\,z^n\,\mathcal{B}_\ell^I\left(\frac{3r - s + z\kappa_{\pi\pi}(s)}{2}\right), \\ \langle z^n\,\mathcal{B}_\ell^I\rangle^\pm &:= \frac{1}{2}\int_{-1}^{1}\mathrm{d}z\,z^n\,\mathcal{B}_\ell^I\left(\frac{3r - t + z\kappa_{\pi\eta}(t) \pm \Delta/t}{2}\right). \end{aligned} \tag{5.18}$$

Note that the analytic continuation of eqs. (5.17) and (5.18) both in the MANDELSTAM variables and the decay mass $M_{\eta'}$ involves several subtleties. This is discussed in detail in refs. [127, 157, 186–188] for $\eta^{(\prime)} \to 3\pi$, as well as in ref. [120] for $\omega/\phi \to 3\pi$ and in ref. [158] specifically for $\eta' \to \eta\pi\pi$. One important consequence is the generation of three-particle-cut contributions in the decay kinematics considered here.

The unitarity relations given in eq. (5.16) are an inhomogeneous OMNÈS problem for the single-variable amplitudes $\mathcal{F}_\ell^I$ and $\mathcal{G}_\ell^I$ with inhomogeneities $\hat{\mathcal{F}}_\ell^I$ and $\hat{\mathcal{G}}_\ell^I$, *cf.* sec. 3.2.2. Accordingly, the solution can be written as

$$\begin{aligned} \mathcal{F}_0^0(s) &= \Omega_0^0(s)\left\{P_0^0(s) + \frac{s^n}{\pi}\int_{s_\mathrm{thr}}^{\infty}\frac{\mathrm{d}x}{x^n}\,\frac{\hat{\mathcal{F}}_0^0(x)\sin\delta_0^0(x)}{|\Omega_0^0(x)|\,(x-s)}\right\}, \\ \mathcal{G}_\ell^1(t) &= \Omega_\ell^1(t)\left\{P_\ell^1(t) + \frac{t^n}{\pi}\int_{t_\mathrm{thr}}^{\infty}\frac{\mathrm{d}x}{x^n}\,\frac{\hat{\mathcal{G}}_\ell^1(x)\sin\delta_\ell^1(x)}{|\Omega_\ell^1(x)|\,(x-t)}\right\}. \end{aligned} \tag{5.19}$$

The order n of the subtraction polynomials in the dispersion relations is determined such that the dispersion integrals are convergent. However, we can always oversubtract the dispersion integral at the expense of having to fix the additional subtraction constants and possible ramifications for the high-energy behavior of our amplitude, *cf.* sec. 3.1.2.[#4] To study the convergence behavior of the integrand we have to make assumptions about the asymptotic behavior of the phase shifts. We assume

$$\delta_0^0(s) \to \pi\,, \quad \delta_0^1(t) \to \pi\,, \quad \delta_1^1(t) \to 0\,, \tag{5.20}$$

as $s, t \to \infty$. Note that an asymptotic behavior of $\delta(s) \to k\pi$ implies that the corresponding Omnès function behaves like s^{-k} in the same limit, *cf.* sec. 3.2.

Finally, we assume an asymptotic behavior of the amplitude inspired by the Froissart–Martin bound [161, 162],

$$\mathcal{M}_0^0(s) = \mathcal{O}(s)\,, \quad \mathcal{M}_0^1(t) = \mathcal{O}(t)\,, \quad \mathcal{M}_1^1(t) = \mathcal{O}(t^{-1})\,, \tag{5.21}$$

which allows the following choice for the subtraction polynomials:

$$P_0^0(s) = \alpha_0 + \beta_0 \frac{s}{M_{\eta'}^2} + \gamma_0 \frac{s^2}{M_{\eta'}^4}\,, \qquad P_0^1(t) = \alpha_1 + \beta_1 \frac{t}{M_{\eta'}^2} + \gamma_1 \frac{t^2}{M_{\eta'}^4}\,, \qquad P_1^1(t) = 0\,. \tag{5.22}$$

The subtraction constants thus defined are correlated since the decomposition eq. (5.11) is not unique. By virtue of eq. (5.3), there exists a four-parameter polynomial transformation of the single-variable amplitudes $\mathcal{F}_\ell^I$ and $\mathcal{G}_\ell^I$ that leaves $\mathcal{M}$ invariant, *cf.* eq. (4.52). Restricting the asymptotic behavior to eq. (5.21) reduces it to the following two-parameter transformation:

$$\mathcal{F}_0^0(s) \mapsto \mathcal{F}_0^0(s) + 2c_1 + c_2\,\frac{s-r}{M_{\eta'}^2}\,, \qquad \mathcal{G}_0^1(t) \mapsto \mathcal{G}_0^1(t) - c_1 + c_2\,\frac{t-r}{M_{\eta'}^2}\,, \tag{5.23}$$

which can be used to set the first two coefficients in the Taylor expansion of $\mathcal{G}_0^1(t)$ around $t = 0$ to zero. Since the transformation polynomial is a trivial solution of the dispersion relation (with vanishing discontinuity), the transformed representation still can be cast in the form of eq. (5.19). Relabeling the transformed subtraction constants and inhomogeneities to the original names, we obtain the following form of the integral equations:

$$\begin{aligned}
\mathcal{F}_0^0(s) &= \Omega_0^0(s)\left\{\alpha_0 + \beta_0\,\frac{s}{M_{\eta'}^2} + \gamma_0\,\frac{s^2}{M_{\eta'}^4} + \frac{s^3}{\pi}\int_{s_\text{thr}}^\infty \frac{\mathrm{d}x}{x^3}, \frac{\hat{\mathcal{F}}_0^0(x)\sin\delta_0^0(x)}{|\Omega_0^0(x)|\,(x-s)}\right\},\\
\mathcal{G}_0^1(t) &= \Omega_0^1(t)\left\{\gamma_1\,\frac{t^2}{M_{\eta'}^4} + \frac{t^3}{\pi}\int_{t_\text{thr}}^\infty \frac{\mathrm{d}x}{x^3}\,\frac{\hat{\mathcal{G}}_0^1(x)\sin\delta_0^1(x)}{|\Omega_0^1(x)|\,(x-t)}\right\},\\
\mathcal{G}_1^1(t) &= \frac{\Omega_1^1(t)}{\pi}\int_{t_\text{thr}}^\infty \mathrm{d}x\,\frac{\hat{\mathcal{G}}_1^1(x)\sin\delta_1^1(x)}{|\Omega_1^1(x)|(x-t)}\,.
\end{aligned} \tag{5.24}$$

[#4] Each additional subtraction constant contributes an additional power of s to the asymptotic behavior of the amplitude if the corresponding sum rule for the subtraction constant is not fulfilled exactly. This can lead to a violation of the Froissart–Martin bound.

In the following, we will neglect the P-wave in $\pi\eta$ scattering as it is strongly suppressed with respect to the S-wave of $\pi\pi$ and $\pi\eta$ scattering, *cf. e.g.* ref. [178, 189]. In fact, the P-wave in $\pi\eta$ scattering has exotic quantum numbers, such that the phase shift is expected to be very small at low energies. In ChPT, this phase (or the corresponding discontinuity) only starts at $\mathcal{O}(p^8)$ (three loops) and is therefore, in this respect, as suppressed as all higher partial waves.

The decomposition of the amplitude in this case simply reads

$$\mathcal{M}(s,t,u) = \mathcal{F}_0^0(s) + \mathcal{G}_0^1(t) + \mathcal{G}_0^1(u)\,. \tag{5.25}$$

We will call the dispersive representation as outlined above "DR_4", as it depends on four subtraction constants. In our numerical analysis, we compare it to a representation where we further reduce the number of free parameters by assuming a more restrictive asymptotic behavior of the amplitude: $\mathcal{M}(s,t,u) = \mathcal{O}(s^0, t^0, u^0)$ for large values of s, t, u, respectively. In this case, the symmetrization procedure in the reconstruction theorem is possible for S-waves only and the single-variable functions fulfill the integral equations

$$\begin{aligned}
\mathcal{F}_0^0(s) &= \Omega_0^0(s)\left\{\alpha + \beta\,\frac{s}{M_{\eta'}^2} + \frac{s^2}{\pi}\int_{s_\mathrm{thr}}^\infty \frac{\mathrm{d}x}{x^2}\,\frac{\hat{\mathcal{F}}_0^0(x)\sin\delta_0^0(x)}{|\Omega_0^0(x)|\,(x-s)}\right\},\\
\mathcal{G}_0^1(t) &= \Omega_0^1(t)\left\{\gamma\,\frac{t}{M_{\eta'}^2} + \frac{t^2}{\pi}\int_{t_\mathrm{thr}}^\infty \frac{\mathrm{d}x}{x^2}\,\frac{\hat{\mathcal{G}}_0^1(x)\sin\delta_0^1(x)}{|\Omega_0^1(x)|\,(x-t)}\right\}.
\end{aligned} \tag{5.26}$$

Note that the transformation (5.23) still allows us to set the first subtraction constant in $\mathcal{G}_0^1$ to zero. The second subtraction constant cannot be removed without changing the asymptotic behavior. As there are three subtraction constants α, β, and γ, we refer to this setup as "DR_3".

The representation DR_4 (5.24) with $\delta_1^1(t) = 0$ is equivalent to DR_3 (5.26), provided that the subtraction constants γ_0 and γ_1 fulfill a certain sum rule in order to guarantee the constraint of the asymptotic behavior. Explicitly, the relation between the DR_4 and DR_3 subtraction constants is given by

$$\begin{aligned}
\alpha_0 &= \alpha + \gamma\,\frac{3r}{M_{\eta'}^2}\,, & \beta_0 &= \beta - \gamma\left(1 + 3r\,\omega_0^0\right),\\
\gamma_0 &= \mathcal{I}_0^0 + \gamma\,M_{\eta'}^2\left(\omega_0^0 - \frac{3r}{2}\,\tilde{\omega}_0^0\right), & \gamma_1 &= \mathcal{I}_0^1 + \gamma\,M_{\eta'}^2\,\omega_0^1\,,
\end{aligned} \tag{5.27}$$

where $\omega_\ell^I \equiv \Omega_\ell^{I\prime}(0)$, $\tilde{\omega}_\ell^I \equiv \Omega_\ell^{I\prime\prime}(0) - 2(\Omega_\ell^{I\prime}(0))^2$, and the sum rule is encoded by the integrals

$$\mathcal{I}_0^0 = \frac{M_{\eta'}^4}{\pi}\int_{s_\mathrm{thr}}^\infty \frac{\mathrm{d}x}{x^3}\,\frac{\hat{\mathcal{F}}_0^0(x)\sin\delta_0^0(x)}{|\Omega_0^0(x)|}\,, \qquad \mathcal{I}_0^1 = \frac{M_{\eta'}^4}{\pi}\int_{t_\mathrm{thr}}^\infty \frac{\mathrm{d}x}{x^3}\,\frac{\hat{\mathcal{G}}_0^1(x)\sin\delta_0^1(x)}{|\Omega_0^1(x)|}\,. \tag{5.28}$$

Since the Froissart–Martin bound is strictly valid only for elastic scattering, a pragmatic approach concerning the number of subtractions is advisable. On the one hand, we try to work with the minimal number of subtractions allowing for a good fit of the data. On the other hand, additional subtractions help to reduce the dependence on

the high-energy behavior of the phase shifts. Therefore, in our analysis we compare both representations DR_3 and DR_4.

As we will show, the representation DR_3 of eqs. (5.25) and (5.26) indeed allows for a perfect fit of the data from the VES [182] and BESIII [183] experiments. With data of even higher statistics, it might become possible to include the P-wave in the fit. In this case, one needs to determine the four subtraction constants of the DR_4 representation in eq. (5.24). A fifth subtraction constant would be introduced if we assumed a different high-energy behavior of δ_1^1: if a resonance with exotic quantum numbers $I^G(J^{PC}) = 1^-(1^{-+})$ coupling to $\pi\eta$ exists (the search for which seems inconclusive so far [190, 191]) and we assume the P-wave phase to approach π instead of 0 asymptotically, the P-wave would allow for a non-vanishing (constant) subtraction polynomial in eq. (5.19), which cannot be removed by the transformation (5.23).

The inclusion of a D-wave contribution in $\pi\pi$ rescattering, which has been suggested in ref. [169] (in the form of the $f_2(1270)$ resonance) would require even higher-order subtraction polynomials, *cf.* also ref. [192].

5.2.2 Numerical solution of the dispersion relations

The numerical treatment of the integral equations (5.24) or (5.26) is a rather nontrivial matter, and specific care has to be taken in calculating the Omnès functions, the inhomogeneities with their complicated structure, as well as the dispersion integrals over singular integrands. All the details can be found in [119, 157, 158, 187, 188].

The solution of the integral equations is obtained by an iteration procedure: we start with arbitrary functions $\mathcal{F}_0^0$ and $\mathcal{G}_0^1$, which we choose to be the respective Omnès functions Ω_0^0 and Ω_0^1; the final result is of course independent of the particular choice of these starting points. Then we calculate the inhomogeneities $\hat{\mathcal{F}}_0^0$ and $\hat{\mathcal{G}}_0^1$ according to eq. (5.17), and insert them back into the dispersion integrals (5.24) or (5.26). This procedure is repeated until sufficient convergence with respect to the input functions is reached. The iteration is observed to converge rather quickly after only a few steps.

The integral equations have a remarkable property that greatly reduces the numerical cost of the calculations: they are linear in the subtraction constants, *cf.* sec. 3.4. Thus we can write (for the DR_3 representation)

$$\mathcal{M}(s,t,u) = \alpha\,\mathcal{M}_\alpha(s,t,u) + \beta\,\mathcal{M}_\beta(s,t,u) + \gamma\,\mathcal{M}_\gamma(s,t,u)\,, \tag{5.29}$$

where we have defined

$$\mathcal{M}_\alpha(s,t,u) \equiv \mathcal{M}(s,t,u)\big|_{\alpha=1,\,\beta=\gamma=0}\,, \tag{5.30}$$

and analogously for the remaining *basis amplitudes*. Each basis amplitude fulfills the decomposition (5.25), and we denote the corresponding single-variable amplitudes by $\mathcal{F}_\alpha^0(s)$, $\mathcal{G}_\alpha^1(t)$, etc., *i.e.*

$$\mathcal{M}_\alpha(s,t,u) = \mathcal{F}_\alpha^0(s) + \mathcal{G}_\alpha^1(t) + \mathcal{G}_\alpha^1(u)\,. \tag{5.31}$$

We can perform the iteration procedure separately for each of these while fixing the subtraction constants after the iteration.

5.2.3 Phase-shift input

The crucial input in the dispersion relation consists of the $\pi\pi$ and $\pi\eta$ S-wave phase shifts δ_0^0 and δ_0^1. Below the threshold of inelastic channels, the dispersion relation correctly describes rescattering effects according to WATSON's final-state theorem with phases δ_0^0 and δ_0^1 that are equal to the phase shifts of elastic scattering. In principle, a coupled-channel analysis could be used to describe the process above the opening of inelastic channels, *e.g.* the explicit inclusion of $K\bar{K}$ intermediate states would provide a fully consistent description in the region of the $f_0(980)$ and $a_0(980)$ resonances; such a coupled-channel generalization of the KHURI–TREIMAN equations has recently been investigated for $\eta \to 3\pi$ [151]. Alternatively, the single-channel equations (5.19) remain valid if we promote δ_0^0 and δ_0^1 to *effective* phase shifts for this decay. As a full coupled-channel analysis is beyond the goal of this work, we construct effective phase shifts and quantify the uncertainties above the inelastic threshold. In such an effective one-channel problem, there are two extreme scenarios of the phase motion of δ_0^0 at the $f_0(980)$ resonance, depending on how strongly the system couples to strangeness [193,194]: large strangeness production manifests itself as a peak at the position of the $f_0(980)$ in the corresponding OMNÈS function, and thus the phase shift is increased by about π while running through the resonance (this scenario is also realized in the elastic $\pi\pi$ scattering phase shift). If the coupling to the channel with strangeness is weak, the corresponding OMNÈS function has a dip at the resonance position and the corresponding phase shift decreases (this is realized in the phase of the nonstrange scalar form factor of the pion). Scenarios in between these two extremes are conceivable.

For the input on the elastic $\pi\pi$ phase shift, we use the results of very sophisticated analyses of the ROY (and similar) equations [133, 134]. As both analyses agree rather well, we only take one of these parametrizations [133] into account. In fig. 5.1, we show our phase $\delta_0^0(s)$, which agrees with the ROY solution [133] below the inelastic threshold. The uncertainty due to the variation of the parameters in the ROY solution is shown as a red band labeled "low-energy uncertainty."

Now, the continuation into the inelastic region is modeled as follows. We calculate the S-waves for $\eta\eta' \to \pi\pi$ and $\eta\eta' \to K\bar{K}$ in large-N_C ChPT at next-to-leading order (tree level) and unitarize this coupled-channel system with an OMNÈS matrix taken from ref. [195]. The large-N_C ChPT representation depends on the LECs L_2 and L_3. We take their values from the most recent dispersive analysis of $K_{\ell 4}$ decays [196],

$$L_2^r = 0.63(13) \times 10^{-3}\,, \quad L_3^r = -2.63(46) \times 10^{-3}\,, \tag{5.32}$$

and vary each of them within its uncertainty. Adding the variations of the phase shift in quadrature generates the broad blue band labeled "high-energy uncertainty" in fig. 5.1. This treatment correctly generates a smooth phase drop by π with respect to the elastic $\pi\pi$ scattering phase, and the uncertainty band covers a broad energy range for the position of this decrease. Still, the phase drops at sufficiently high energies such that the corresponding OMNÈS function, shown in fig. 5.2, exhibits a peak at the position of the $f_0(980)$ resonance. Asymptotically, we smoothly drive δ_0^0 to a value of π. We wish to emphasize that the role of the large-N_C input is not essential and only that of an auxiliary tool, which allows for a smooth construction that obeys the two desired features:

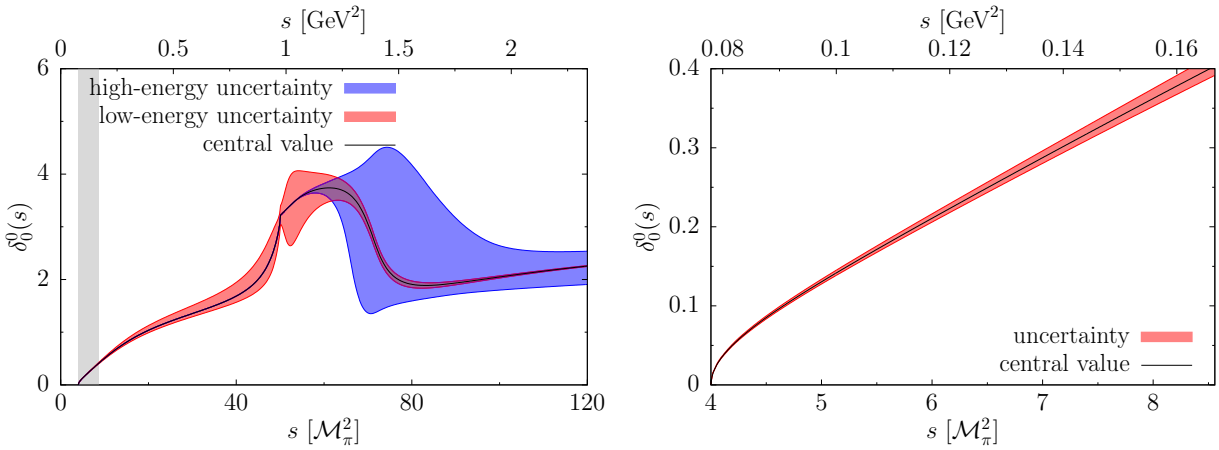

Fig. 5.1: The isospin-zero $\pi\pi$ S-wave effective phase shift δ_0^0, constructed with input from [133]. In the left panel, the physical region of the decay $\eta' \to \pi\pi\eta$ between the thresholds $s = 4M_\pi^2$ and $s = (M_{\eta'} - M_\eta)^2$ is indicated by the gray area. The right panel shows a magnification of the physical decay region.

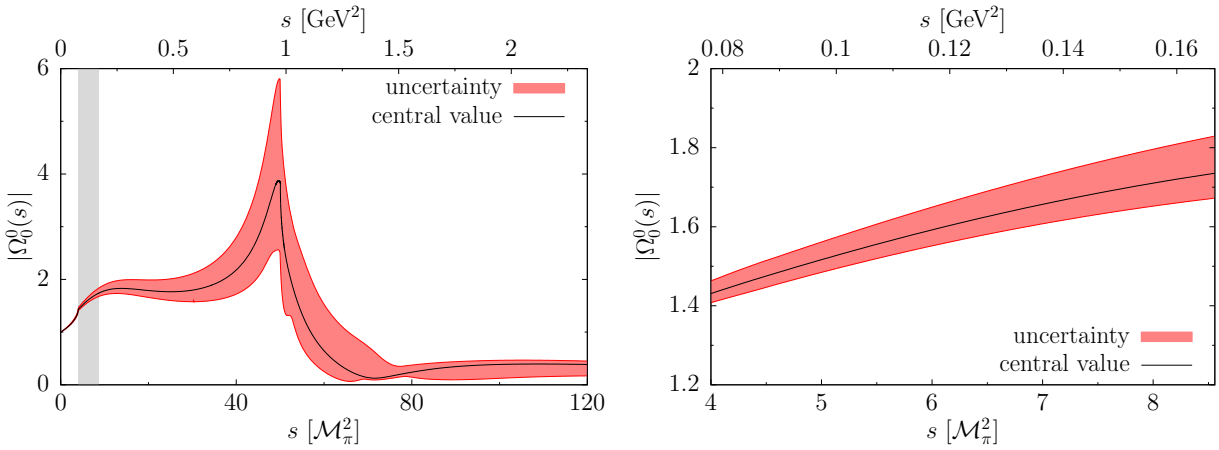

Fig. 5.2: The absolute value of the Omnès function $|\Omega_0^0|$, calculated from the $\pi\pi$ S-wave effective phase shift δ_0^0. The uncertainty band includes both uncertainties in the phase, combined in quadrature.

the occurrence of an $f_0(980)$ peak in accordance with expectations from scalar-resonance models (*cf. e.g.*, sec. 5.5.1), and an asymptotic phase of π (as opposed to 2π, say). The large high-energy uncertainty in fig. 5.1 should safely cover a large variety of phases obeying these constraints. Note, finally, that in the physical region of the decay $\eta' \to \pi\pi\eta$, the uncertainties of the phase and the Omnès function are small.

In the same spirit of an effective one-channel treatment, we consider isospin-breaking effects. In the isospin limit, our formalism applies identically to both the charged and the neutral processes $\eta' \to \pi^+\pi^-\eta$ and $\eta' \to \pi^0\pi^0\eta$. In order to account for the most important isospin-breaking effects, we construct effective phase shifts for the neutral decay mode that have the correct thresholds and reproduce the expected nonanalytic cusp behavior, as we explain in detail in app. C.1.

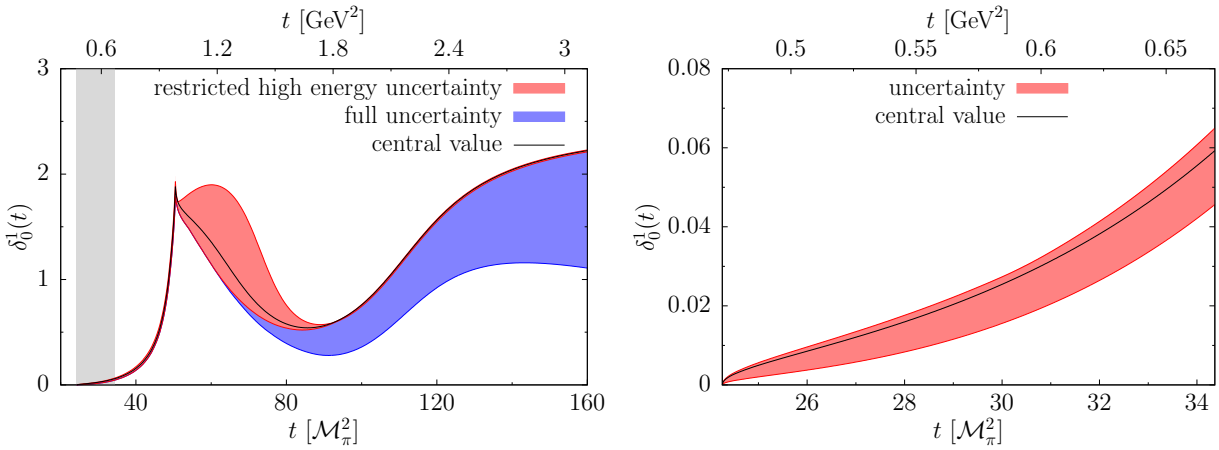

Fig. 5.3: The $\pi\eta$ S-wave effective phase shift δ_0^1 [135]. In the left panel, the physical region of the decay $\eta' \to \pi\pi\eta$ between the thresholds $t = (M_\eta + M_\pi)^2$ and $t = (M_{\eta'} - M_\pi)^2$ is indicated by the gray area. The right panel magnifies the physical decay region. The restricted high-energy uncertainty band is generated by varying the parameter in the range $105^\circ \leq \delta_{12} \leq 125^\circ$, while the full uncertainty band is obtained from the parameter range $90^\circ \leq \delta_{12} \leq 125^\circ$.

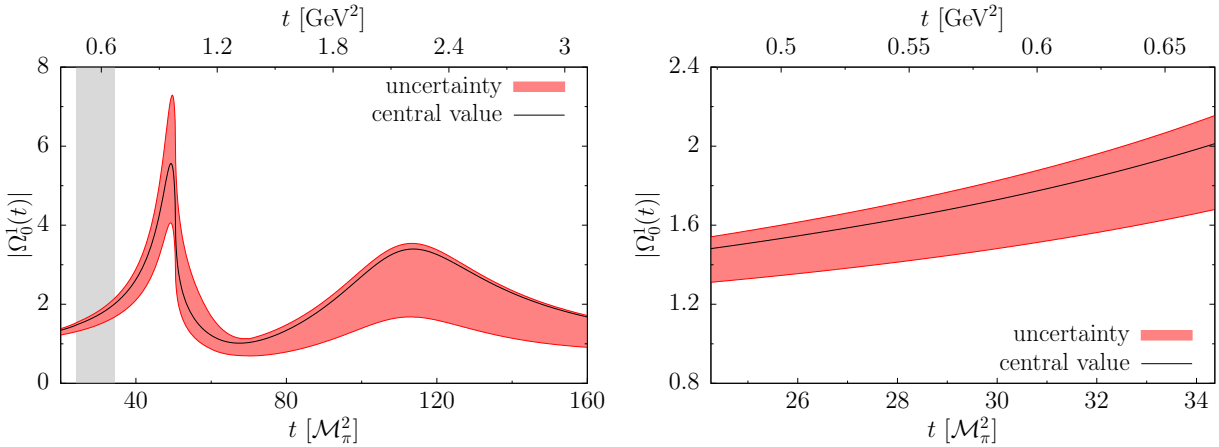

Fig. 5.4: The absolute value of the Omnès function $|\Omega_0^1|$, calculated from the $\pi\eta$ S-wave effective phase shift δ_0^1. The uncertainty band corresponds to the full parameter variation, $90^\circ \leq \delta_{12} \leq 125^\circ$.

For the $\pi\eta$ phase shift δ_0^1, we take the phase of the scalar form factor $F_S^{\pi\eta}$ of ref. [135] as input, shown in fig. 5.3. In that reference, a $\pi\eta$–$K\bar{K}$ S-wave coupled-channel T-matrix has been constructed, to which chiral constraints [73] have been imposed as well as experimental information on the $a_0(980)$ and $a_0(1450)$ resonances. The remaining model uncertainty has been subsumed in the dependence on one single phase δ_{12}. The "central" solution corresponds to a parameter value of $\delta_{12} = 107.5^\circ$, while the uncertainty band is generated as an envelope of the solutions obtained by varying the parameter in the restricted range $90^\circ \leq \delta_{12} \leq 125^\circ$ that is compatible with chiral predictions for the scalar radius. The largest part of the high-energy uncertainty is generated by values of the

parameter in the range $90^\circ \leq \delta_{12} \leq 105^\circ$, as shown in fig. 5.3: while for all $\delta_{12} \geq 105^\circ$, the phase approaches its asymptotic value of π very quickly above the $a_0(1450)$ resonance, this convergence becomes very slow and is extended over a vast energy range for $\delta_{12} < 105^\circ$. As this high-energy behavior turns out to affect the uncertainties in some (but not all) quantities extracted from data fits rather strongly, we will occasionally also refer to the reduced uncertainty, induced by the more restricted range $105^\circ \leq \delta_{12} \leq 125^\circ$. The Omnès function with an uncertainty band generated by the full variation $90^\circ \leq \delta_{12} \leq 125^\circ$ is shown in fig. 5.4. In particular, we observe a pronounced peak at the position of the $a_0(980)$ resonance for all parameter values.

5.3 Determination of the subtraction constants

After having solved the integral equations numerically, we have to determine the free parameters in the dispersion relation, *i.e.* the subtraction constants α, β, and γ in the case of the DR_3 representation, or α_0, β_0, γ_0, and γ_1 in the case of DR_4. We summarize the experimental situation on $\eta' \to \pi\pi\eta$ Dalitz plots in sec. 5.3.1. In sec. 5.3.2, we discuss the results of fitting the subtraction constants to the most recent data sets.

5.3.1 Sampling of experimental Dalitz plots

In experimental analyses of the $\eta' \to \pi\pi\eta$ Dalitz plot, one defines symmetrized coordinates x and y according to

$$x = \frac{\sqrt{3}}{2M_{\eta'}\,Q_{\eta'}}\,(t-u)\,, \qquad y = (M_\eta + 2M_\pi)\,\frac{(M_{\eta'}-M_\eta)^2 - s}{2M_\pi\,M_{\eta'}\,Q_{\eta'}} - 1\,, \tag{5.33}$$

where $Q_{\eta'} \equiv M_{\eta'} - M_\eta - 2M_\pi$, *cf.* app. B. The squared amplitude of the decay is then expanded in terms of these variables,

$$|\mathcal{M}_{\mathrm{exp}}(x,y)|^2 = |\mathcal{N}_{\mathrm{exp}}|^2\big(1 + a\,y + b\,y^2 + c\,x + d\,x^2 + ...\big)\,, \tag{5.34}$$

and the parameters a, b, c, d are fitted to experimental data. Note that a nonzero value for the parameter c (in $\eta' \to \pi^+\pi^-\eta$) would indicate violation of charge conjugation symmetry; there is no indication of a nonzero c up to this point, *cf.* ch. 6. In the following we consider two recent measurements of the charged final state $\eta' \to \pi^+\pi^-\eta$. These determinations of the Dalitz-plot parameters by the BESIII [183] and the VES [182] collaborations currently feature the highest statistics. In tab. 5.1 we have summarized some details and results of the two experiments.

For our analysis, we have generated pseudodata samples from the Dalitz-plot distributions as measured by the two groups [198]; the resulting Dalitz-plot distributions are shown in fig. 5.5. To check our results we have refitted the parametrization (5.34) to the synthesized data sets, and find agreement with the fit parameters of tab. 5.1 within statistical uncertainties, as well as with the correlation matrix quoted in ref. [183]. We note that the two data sets disagree on the parameter a at the 2σ level; of course, it would be desirable that this experimental disagreement be resolved by future measurements.

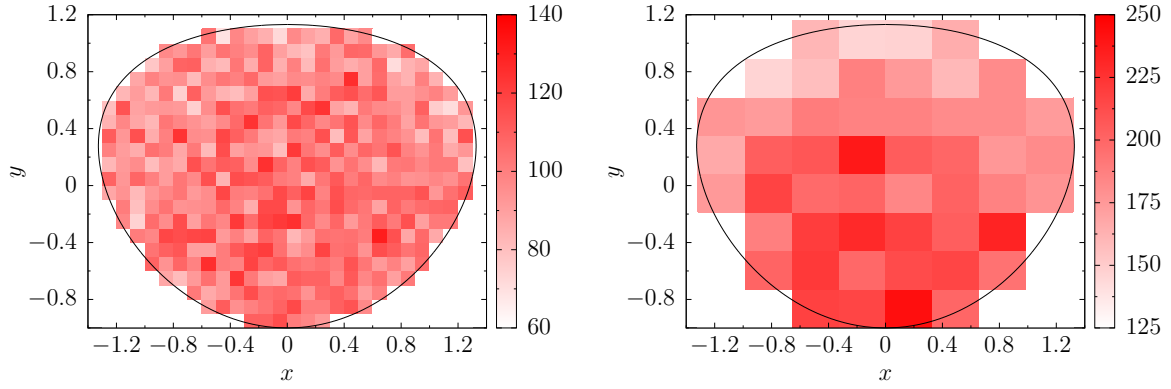

Fig. 5.5: Dalitz-plot samples for $\eta' \to \pi^+\pi^-\eta$ from the experimental Dalitz-plot distribution in tab. 5.1 for the BESIII (left panel) and the VES (right panel) experiment. BESIII uses a 26×22 grid with 438 bins in total and VES uses a 8×8 grid with 50 bins in total.

5.3.2 Fitting experimental data

We proceed by fitting the subtraction constants, which are the free parameters in our dispersive representation of the amplitude, to the following data.

- Dalitz-plot distribution for the charged channel from BESIII [183] and VES [182] experiments.
- The partial decay width $\Gamma(\eta' \to \pi^+\pi^-\eta)$ [197].

Note that we use *real* fit parameters: in principle the subtraction constants can have imaginary parts due to the complex discontinuity (5.16). However, since the imaginary parts of the subtraction constants are proportional to three-particle-cut contributions, and the available decay phase space of $\eta' \to \pi\pi\eta$ is small, the imaginary parts are so tiny that—given the precision of the data sets—their effect is entirely negligible (this is not the case for processes involving the decay of heavier mesons, compare *e.g.* refs. [120, 155]).

	a	b	c	d	# events
BESIII [183]	−47(11)(3)	−69(19)(9)	+19(11)(3)	−73(12)(3)	43 826(211)
VES [182]	−127(16)(8)	−106(28)(14)	+15(11)(14)	−82(17)(8)	$\simeq$ 8623

Tab. 5.1: Dalitz-plot parameter measurements by the BESIII and VES collaborations in units of 10^{-3}. The first error on the Dalitz-plot parameters is always statistical, the second systematic. We have estimated the number of $\eta' \to \pi^+\pi^-\eta$ events for the VES collaboration from the total number of selected η' events and the branching ratio $\mathrm{BR}(\eta' \to \pi^+\pi^-\eta) = (42.9 \pm 0.7)\%$ [197].

In the following, we set up a scheme that allows us to fit both the experimental Dalitz-plot distribution and the partial decay width simultaneously and avoids some strong correlations between the fitting parameters.[#5]

First, we perform the following transformation of the fit parameters:

$$\alpha = \bar{\mathcal{N}}\,\bar{\alpha}\,, \qquad \beta = \bar{\mathcal{N}}\,\bar{\beta}\,, \qquad \gamma = \bar{\mathcal{N}}\,\bar{\gamma}\,. \tag{5.35}$$

Hence, we write the squared amplitude as

$$|\mathcal{M}(s,t,u)|^2 = |\bar{\mathcal{N}}|^2\,|\bar{\mathcal{M}}(s,t,u)|^2\,, \qquad \int \mathrm{d}x\,\mathrm{d}y\,|\bar{\mathcal{M}}(x,y)|^2 = 1\,, \tag{5.36}$$

where

$$\bar{\mathcal{M}}(s,t,u) = \bar{\alpha}\,\mathcal{M}_\alpha(s,t,u) + \bar{\beta}\,\mathcal{M}_\beta(s,t,u) + \bar{\gamma}\,\mathcal{M}_\gamma(s,t,u)\,. \tag{5.37}$$

The normalization condition of $\bar{\mathcal{M}}$ defined in eq. (5.36) results in a quadratic equation for the rescaled subtraction constants $\bar{\alpha}$, $\bar{\beta}$, and $\bar{\gamma}$. We choose to express $\bar{\gamma}$ in terms of $\bar{\alpha}$ and $\bar{\beta}$. The experimental partial decay width now directly determines the normalization $\bar{\mathcal{N}}$ and has no influence on the parameters $\bar{\alpha}$ and $\bar{\beta}$.

On the other hand, the experimental Dalitz-plot distribution (5.34) has again an arbitrary normalization. Hence, we have to fit the Dalitz-plot data according to

$$|\mathcal{M}_{\mathrm{exp}}|^2 = |\mathcal{N}_{\mathrm{exp}}|^2\,\frac{|\bar{\mathcal{M}}|^2}{|\bar{\mathcal{M}}(x=y=0)|^2} \equiv |\mathcal{N}|^2\,|\bar{\mathcal{M}}|^2\,. \tag{5.38}$$

The Dalitz-plot distribution therefore determines the fitting parameters $\bar{\alpha}$, $\bar{\beta}$, and the irrelevant normalization $\mathcal{N}_{\mathrm{exp}}$ or $\mathcal{N}$.

Note that the experimental Dalitz-plot distribution is effectively described by three Dalitz-plot parameters a, b, and d. In the representation DR_3, the shape of the Dalitz-plot distribution depends only on the two fitting parameters $\bar{\alpha}$ and $\bar{\beta}$. Therefore, the parametrization DR_3 has predictive power. The representation DR_4 describes the shape of the Dalitz-plot distribution again in terms of three parameters.

The result of the fit to data provides us with a representation of the amplitude that fulfills the strong constraints of analyticity and unitarity. This will be an essential input for a forthcoming dispersive analysis of $\eta' \to 3\pi$ [199].[#6]

The experimental partial decay width [197]

$$\begin{aligned}\Gamma(\eta' \to \pi^+\pi^-\eta) &= \frac{1}{256\pi^3\,M_{\eta'}^3}\int \mathrm{d}s\,\mathrm{d}t|\mathcal{M}(s,t,u)|^2 \\ &= \frac{M_\pi\,Q_{\eta'}^2}{128\sqrt{3}\pi^3\,M_{\eta'}\,(M_\eta + 2M_\pi)}\int \mathrm{d}x\,\mathrm{d}y\,|\mathcal{M}(x,y)|^2 = 84.5(4.1)\times 10^{-6}\,\mathrm{GeV}\end{aligned} \tag{5.39}$$

[#5] We write down formulae for the DR_3 representation with subtraction constants α, β, and γ. The fitting procedure for the DR_4 representation is completely analogous.

[#6] Notice that the decay $\eta' \to 3\pi$ can proceed via $\eta' \to \pi\pi\eta$ and isospin-breaking rescattering $\pi\eta \to \pi\pi$ (which can be extracted from analytic continuation of the dispersive amplitude $\eta \to 3\pi$ [200]) and direct isospin breaking $\eta' \to 3\pi$.

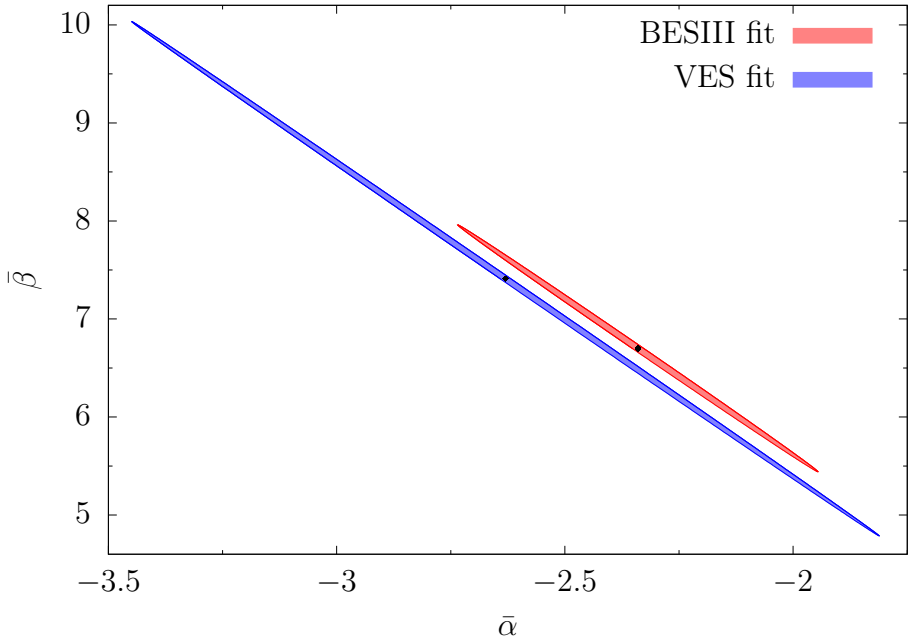

Fig. 5.6: Error ellipses for the DR_3 fits to BESIII and VES in the plane of the rescaled subtraction constants $(\bar{\alpha}, \bar{\beta})$, corresponding to 68.27% confidence regions.

fixes the normalization to

$$\bar{\mathcal{N}} = 13.88(34)\,. \tag{5.40}$$

For the rescaled subtraction constants in the DR_3 representation, the fit of the dispersive representation with central values of the phase input to the BESIII data sample [183] leads to

$$\begin{array}{l|cc} \bar{\alpha} = -2.34(26) & 1.00 & -1.00 \\ \bar{\beta} = 6.70(83) & & 1.00 \end{array}\,, \qquad \bar{\gamma}\big(\bar{\alpha}, \bar{\beta}\big) = 1.12(14)\,, \tag{5.41}$$

while the fit to the VES data [182] gives

$$\begin{array}{l|cc} \bar{\alpha} = -2.63(54) & 1.00 & -1.00 \\ \bar{\beta} = 7.41(1.73) & & 1.00 \end{array}\,, \qquad \bar{\gamma}\big(\bar{\alpha}, \bar{\beta}\big) = 1.29(29)\,. \tag{5.42}$$

	$-\alpha$	β	γ	χ^2/ndof
$\mathrm{DR}_3^{\mathrm{BESIII}}$	$33(4)(1)\,^{+5}_{-42}$	$93(12)(3)\,^{-15}_{+127}$	$16(2)(1)\,^{-3}_{+32}$	$459/435 \approx 1.06$
$\mathrm{DR}_3^{\mathrm{VES}}$	$36(7)(1)\,^{+6}_{-56}$	$103(24)(5)\,^{-19}_{+168}$	$18(4)(0)\,^{-4}_{+41}$	$43.1/47 \approx 0.92$

Tab. 5.2: Fit results for the DR_3 subtraction constants for the BESIII and VES data samples. The first error gives the combined uncertainty of the Dalitz-plot data and the partial decay width of $\eta' \to \pi^+\pi^-\eta$, while the second (asymmetric third) error gives the uncertainty due to the $\pi\pi$ $(\pi\eta)$ phase input.

The uncertainties and correlations are the statistical ones due to the fitted data. We observe a strong anti-correlation between $\bar{\alpha}$ and $\bar{\beta}$. Note that choosing one or the other of the two solutions of the quadratic constraint on $\bar{\gamma}$ just results in an irrelevant overall sign change of the amplitude.

Similarly, the fit of the dispersive representation DR_4 to BESIII results in

$$\begin{array}{r|rrr} \bar{\alpha}_0 = -0.84(8) & 1.00 & -0.86 & 0.28 \\ \bar{\beta}_0 = 2.01(46) & & 1.00 & -0.73 \\ \bar{\gamma}_0 = 1.79(1.25) & & & 1.00 \end{array}, \qquad \bar{\gamma}_1\big(\bar{\alpha}_0, \bar{\beta}_0, \bar{\gamma}_0\big) = 0.38(5)\,, \tag{5.43}$$

while the DR_4 fit to the VES data gives

$$\begin{array}{r|rrr} \bar{\alpha}_0 = -0.79(16) & 1.00 & -0.85 & 0.19 \\ \bar{\beta}_0 = 1.03(86) & & 1.00 & -0.67 \\ \bar{\gamma}_0 = 5.02(2.34) & & & 1.00 \end{array}, \qquad \bar{\gamma}_1\big(\bar{\alpha}_0, \bar{\beta}_0, \bar{\gamma}_0\big) = 0.40(10)\,. \tag{5.44}$$

Table 5.2 shows the χ^2/ndof and the absolute subtraction constants obtained from the DR_3 fits to the sampled BESIII and the VES data sets. The first error is the statistical fit uncertainty. It is dominated by the experimental uncertainty in the Dalitz-plot distribution, while the uncertainty due to the partial decay width is small. The second error is the systematic uncertainty due to the $\pi\pi$ phase input. The very asymmetric third error is due to the $\pi\eta$ phase input with a parameter variation in the range $90^\circ \leq \delta_{12} \leq 125^\circ$. The upper error corresponds to $\delta_{12} \geq 107.5^\circ$, while the lower error corresponds to $\delta_{12} \leq 107.5^\circ$. If the $\pi\eta$ phase variation is restricted to a parameter range of $105^\circ \leq \delta_{12} \leq 125^\circ$, the large lower error is much reduced and the uncertainty is covered by a symmetric error with the magnitude of the upper error.

The variation of the $\pi\eta$ phase input for $\delta_{12} \leq 105^\circ$ has some small effect on the χ^2: for BESIII, the variation is $\chi^2 \in [1.05, 1.09]$, for VES we find $\chi^2 \in [0.90, 0.93]$. One might be tempted to minimize the χ^2 with respect to δ_{12} and try to extract information on the parameter in the $\pi\eta$ phase shift. However, such an attempt is futile. Figure 5.3 shows that the variation of the phase mostly affects the high-energy region above 1 GeV.

	$-\alpha_0$	β_0	γ_0	γ_1	χ^2/ndof
$\mathrm{DR}_3^{\mathrm{BESIII}}$	$11.2(1.0)(4)\,^{+0.7}_{-1.1}$	$24(3)(1)\,^{+2}_{-13}$	$36(5)(5)\,^{-6}_{+40}$	$5.1(7)(2)\,^{-0.8}_{+0.9}$	$459/435 \approx 1.06$
$\mathrm{DR}_4^{\mathrm{BESIII}}$	$11.6(1.1)(1)\,^{+0.9}_{-2.5}$	$28(6)(3)\,^{-3}_{+9}$	$25(17)(6)\,^{-1}_{+2}$	$5.3(7)(1)\,^{-0.9}_{+3.2}$	$459/434 \approx 1.06$
$\mathrm{DR}_3^{\mathrm{VES}}$	$11.9(2.0)(2)\,^{+1.0}_{-1.0}$	$24(6)(1)\,^{+2}_{-14}$	$42(10)(7)\,^{-7}_{+54}$	$6.0(1.4)(1)\,^{-1.1}_{+1.5}$	$43.1/47 \approx 0.92$
$\mathrm{DR}_4^{\mathrm{VES}}$	$11.0(2.2)(1)\,^{+1.1}_{-2.7}$	$14(12)(4)\,^{-4}_{+10}$	$70(33)(7)\,^{-1}_{+2}$	$5.5(1.5)(1)\,^{-1.1}_{+3.3}$	$42.4/46 \approx 0.92$

Tab. 5.3: Fit results for the DR_4 subtraction constants for the BESIII and VES data samples, obtained from the three-parameter fits via the sum rule (5.27) and directly from the four-parameter fits. The first error is the fit uncertainty, the second (third) error is the systematic uncertainty due to the $\pi\pi$ ($\pi\eta$) phase input.

The variation in the parameter region $90^\circ \leq \delta_{12} \leq 105^\circ$ mainly controls how fast the phase reaches π in the "asymptotic" region. It would certainly be illusionary to extract information on the phase at such high energies from $\eta' \to \pi\pi\eta$ DALITZ-plot data. Hence, the variation of the phase parameter δ_{12} simply has to be treated as a source of systematic uncertainty.

The χ^2/ndof is close to 1 in both fits, even though compared to the phenomenological DALITZ-plot parametrization, the dispersive representation DR_3 needs one parameter less to describe the experimental data (disregarding the C-parity violating parameter c). At first sight, the obtained values for the subtraction constants in the DR_3 scheme seem to be compatible between the fits to the two experimental samples. In fact, there is a rather strong tension between the fits to the two experiments, disguised by the strong anti-correlation between $\bar{\alpha}$ and $\bar{\beta}$. The error ellipses in the $(\bar{\alpha}, \bar{\beta})$-plane reveal that the two fit results are not compatible with each other, *cf.* fig. 5.6.

Table 5.3 shows the χ^2/ndof and a comparison of the absolute subtraction constants in the DR_4 scheme, obtained directly from the DR_4 fits as well as extracted from the DR_3 fits via the sum rule (5.27). Due to correlations, the large systematic uncertainty from the $\pi\eta$ phase variation, which is visible in all DR_3 subtraction constants α, β, and γ, prominently shows up in the transformed constant γ_0, while we observe a cancellation of this systematic uncertainty in the other constants, especially in α_0 and γ_1. The main conclusion is, however, that tab. 5.3 demonstrates the full consistency of the two subtraction schemes with each other already within the statistical (fit) uncertainties alone.

	$\mathrm{DR}_3^{\mathrm{BESIII}}$	$\mathrm{DR}_4^{\mathrm{BESIII}}$	$\mathrm{DR}_3^{\mathrm{VES}}$	$\mathrm{DR}_4^{\mathrm{VES}}$
$-a$	$41(9)(1)\,^{-0}_{+1}$	$42(10)(1)(0)$	$148(18)(1)\,^{-1}_{+3}$	$145(18)(1)(0)$
$-b$	$88(7)(10)\,^{+5}_{-37}$	$76(18)(0)(0)$	$82(14)(12)\,^{+7}_{-51}$	$110(34)(0)(0)$
$-d$	$68(11)(2)\,^{-0}_{+17}$	$69(11)(0)(0)$	$86(22)(1)\,^{-1}_{+13}$	$85(22)(0)(1)$
$\kappa_{03}[y^3]$	$8(1)(2)\,^{-1}_{+4}$	$7(2)(1)(0)$	$16(3)(3)\,^{-1}_{+8}$	$20(5)(2)(0)$
$-\kappa_{21}[y\,x^2]$	$12(2)(0)(1)$	$11(2)(0)(1)$	$9(2)(0)\,^{+0}_{-1}$	$10(2)(0)(1)$
$\kappa_{04}[y^4]$	$3(1)(1)\,^{-0}_{+1}$	$3(1)(0)(0)$	$2(1)(1)\,^{-0}_{+1}$	$5(2)(0)(0)$
$\kappa_{22}[y^2\,x^2]$	$3(1)(0)\,^{-0}_{+1}$	$2(1)(0)(0)$	$5(2)(1)\,^{-0}_{+2}$	$6(2)(0)(0)$
$\kappa_{40}[x^4]$	$0(1)(0)(0)$	$0(1)(0)(0)$	$0(1)(0)(0)$	$0(1)(0)(0)$

Tab. 5.4: DALITZ-plot parameters obtained from a TAYLOR expansion of the dispersive amplitude according to eq. (5.34), using the best fitting values of the subtraction constants for the BESIII and VES data samples as input. All values are given in units of 10^{-3}. The values shown here are to be compared with tab. 5.1. The first error is the fit uncertainty, the second (third) error is the systematic uncertainty due to the $\pi\pi$ ($\pi\eta$) phase input.

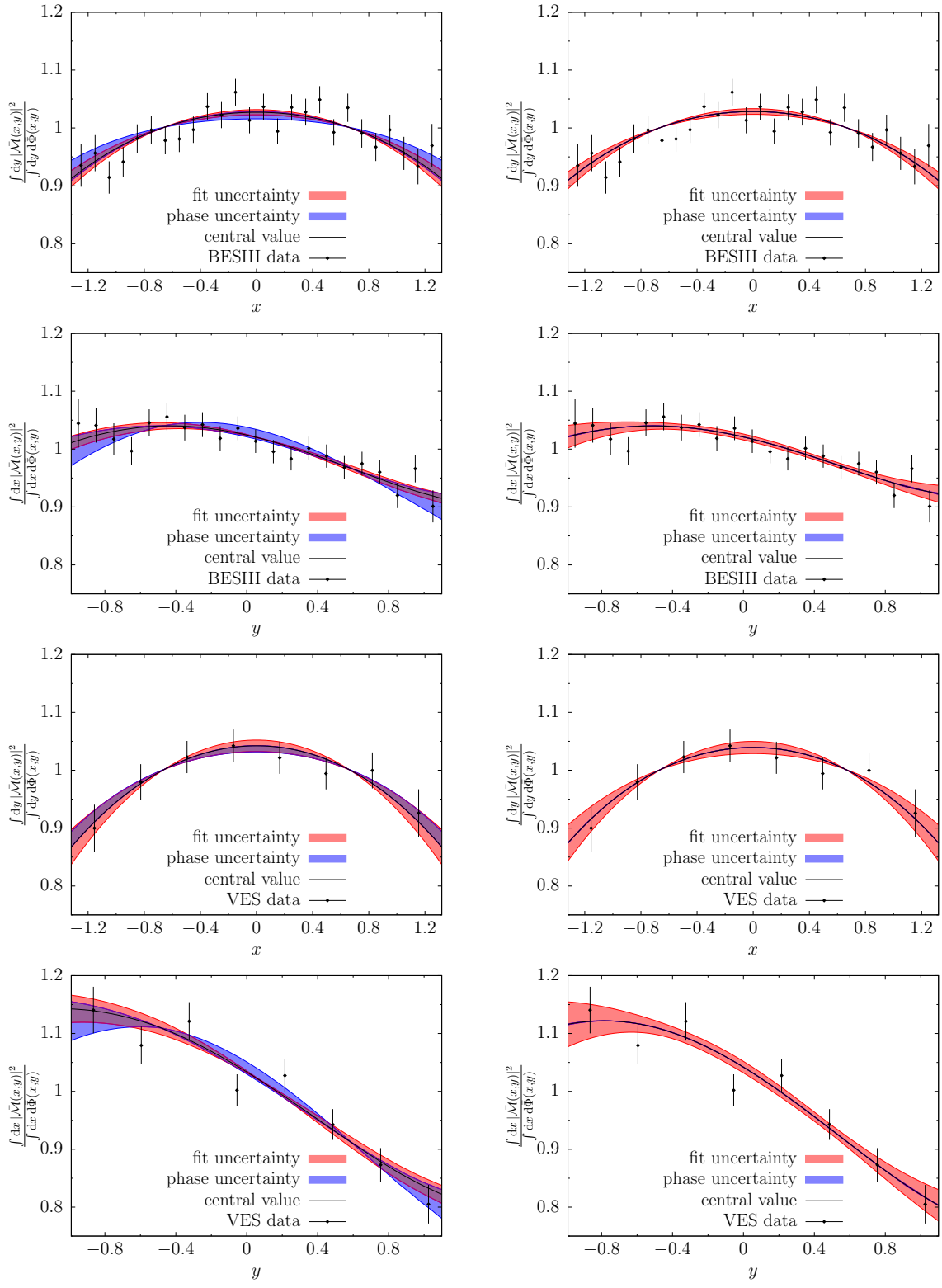

Fig. 5.7: Decay spectra for $\eta' \to \pi^+\pi^-\eta$ integrated over the variable y and divided by the integral over the normalized phase space $\mathrm{d}\bar{\Phi}(x,y)$ (first and third rows) and for $x \leftrightarrow y$ (second and fourth rows). We show the sampled data sets for the BESIII [183] (first and second rows) and the VES [182] experiments (third and fourth rows). The DR_3 (left column) and DR_4 fits (right column) are shown.

In fig. 5.7, we display the decay spectrum integrated over the DALITZ-plot variables x or y, respectively. The results of the two subtraction schemes DR_3 and DR_4 are very similar. The DR_4 scheme leads to a much smaller systematic uncertainty due to the phase input at the expense of a larger statistical fit uncertainty.

By expanding the fitted dispersive representations around the center of the DALITZ plot, we extract the DALITZ-plot parameters a, b, and d listed in tab. 5.4. The values of the polynomial fit to the DALITZ plot of tab. 5.1 are well reproduced within the uncertainties. Note that this is a nontrivial observation, as the dispersive amplitude obviously is no polynomial in the MANDELSTAM variables.

By comparing the two subtraction schemes DR_3 and DR_4, we see that the additional parameter in DR_4 has basically no influence on the χ^2 of the fits. From the point of view of the goodness of fit, the additional parameter in DR_4 is unnecessary. In other words, the subtraction constants extracted in the DR_4 fit are compatible within errors with the more restrictive high-energy behavior imposed on the DR_3 amplitude, and fulfill the corresponding sum rule (5.27), as can be seen in tab. 5.3.[#7] However, by comparing the systematic uncertainties, we see that the DR_3 representation is rather strongly affected by the uncertainties of the $\pi\eta$ phase shift in the high-energy region, especially the extracted DALITZ-plot parameters. The additional subtraction in DR_4 suppresses the influence of the high-energy phase uncertainty significantly. The price to pay is a larger (statistical) fit uncertainty due to the additional fit parameter. Forthcoming data of even higher statistics could reduce this fit uncertainty.

5.4 Predictions of the dispersive representation

With the subtraction constants of the dispersive representation fitted to experimental data on $\eta' \to \pi^+\pi^-\eta$, we are in the position to make certain additional predictions. In sec. 5.4.1, we quantify the nontrivial constraint between the leading DALITZ-plot parameters a, b, and d that exists in the three-parameter scheme DR_3. In sec. 5.4.2, we discuss higher terms in the polynomial expansion of the DALITZ-plot distribution. We study the issue of ADLER zeros of the dispersive amplitude in sec. 5.4.3. Finally, in view of upcoming high-precision measurements of the neutral decay channel, we specify predictions for the same in sec. 5.4.4, taking into account the dominant effects of isospin breaking.

5.4.1 The a-b-d constraint

Provided that the dispersive representation DR_3 with a more restrictive high-energy behavior and fewer subtractions than DR_4 allows a good fit to data, it is possible to formulate a relation between the three parameters a, b, and d, since in this scheme the DALITZ-plot distribution only depends on two parameters. Although this relation is nonlinear and cannot be easily given in closed form, we provide an approximate form of the constraint between a, b, and d valid in the vicinity of the BESIII DR_3 fit values in tab. 5.4. Defining

[#7] If the DR_4 subtraction constants are extracted from the DR_3 fit, the integral (5.28) leads to a tiny imaginary part in γ_0 and γ_1 that we neglect.

$$\Delta a \equiv a - a_{\text{BESIII}}\,, \qquad \Delta b \equiv b - b_{\text{BESIII}}\,, \qquad \Delta d \equiv d - d_{\text{BESIII}}\,, \tag{5.45}$$

we write the *a*-*b*-*d* constraint expanded to second order as

$$\Delta d = C_{10}\,\Delta a + C_{01}\,\Delta b + C_{20}\,\Delta a^2 + C_{11}\,\Delta a\,\Delta b + C_{02}\,\Delta b^2 \tag{5.46}$$

and find the following results for the coefficients C_{ij}:

$$\begin{array}{rr|ccccc} C_{10} = & 0.21\,^{+0.03}_{-0.09} & 1.00 & \begin{smallmatrix}0.91\\0.98\end{smallmatrix} & \begin{smallmatrix}-0.91\\-0.98\end{smallmatrix} & \begin{smallmatrix}0.92\\0.70\end{smallmatrix} & \begin{smallmatrix}0.88\\-0.41\end{smallmatrix} \\ C_{01} = & 1.71\,^{+0.43}_{-0.97} & & 1.00 & \begin{smallmatrix}-1.00\\-1.00\end{smallmatrix} & \begin{smallmatrix}0.99\\0.80\end{smallmatrix} & \begin{smallmatrix}0.97\\-0.27\end{smallmatrix} \\ C_{20} = & -0.43\,^{-0.11}_{+0.24} & & & 1.00 & \begin{smallmatrix}-0.99\\-0.80\end{smallmatrix} & \begin{smallmatrix}-0.97\\0.27\end{smallmatrix} \\ C_{11} = & -0.00\,^{-0.00}_{+0.00} & & & & 1.00 & \begin{smallmatrix}0.99\\0.35\end{smallmatrix} \\ C_{02} = & -0.02\,^{-0.01}_{+0.01} & & & & & 1.00 \end{array}\,, \tag{5.47}$$

where the uncertainties and correlations are due to the variation of the phase shifts, calculated from covariance matrices based on finite differences and an asymmetry due to the $\pi\eta$ phase variation.

Inserting the differences Δa and Δb between the VES and BESIII fits from tab. 5.4 into the *a*-*b*-*d* constraint (5.46) and propagating the uncertainties from eq. (5.47) leads to

$$\Delta d = -\left(18\,^{+2}_{-7}\right) \times 10^{-3}\,, \tag{5.48}$$

in agreement with the actual difference Δd. The systematic uncertainty of the difference Δd is reduced compared to the uncertainties of the two determinations of the parameter d, since these variations are correlated. Restricting the variation of the $\pi\eta$ phase to $105^\circ \leq \delta_{12} \leq 125^\circ$ further reduces the lower asymmetric error to a value smaller in magnitude than the upper error.

The relation (5.46) could be used in forthcoming experiments to perform a phenomenological fit of the Dalitz-plot distribution, where the number of free parameters is reduced by one. Alternatively, the consistency with this constraint may be checked *a posteriori*. We emphasize, though, that the relation is based on parameters extracted from fits using the dispersive representation, which has a more physical energy dependence than just a polynomial; as the example of the VES data demonstrates, it is not guaranteed that a direct polynomial fit leads to identical results (*cf.* again tabs. 5.1 and 5.4). In the case of the neutral decay channel $\eta' \to \pi^0\pi^0\eta$, the Dalitz-plot parametrization might differ by an isospin-breaking effect, which should be corrected for before the constraint is applied; *cf.* sec. 5.4.4.

5.4.2 Higher order Dalitz-plot parameters

From the result of the dispersion relation fitted to data, we can extract not only the Dalitz-plot parameters a, b, and d, but also the coefficients of higher terms in the expansion around the center of the Dalitz plot. We define these coefficients as follows:

$$|\mathcal{M}_{\text{exp}}|^2 = |\mathcal{N}_{\text{exp}}|^2 \sum_{i,j=0}^{\infty} \kappa_{ij}\, x^i\, y^j\,, \tag{5.49}$$

where $\kappa_{00} = 1$, $\kappa_{01} = a$, $\kappa_{02} = b$, and $\kappa_{20} = d$. C-parity implies $\kappa_{ij} = 0$ for odd i. The values for the parameters κ_{ij} with $i + j \leq 4$ are listed in tab. 5.4 for the fits of the dispersion relation to the BESIII and VES data sets. We observe a clear hierarchy

$$a, b, d > \kappa_{ij}\big|_{i+j=3} > \kappa_{ij}\big|_{i+j=4}\,, \tag{5.50}$$

with $\kappa_{ij}|_{i+j=4}$ an order of magnitude smaller than the parameters a, b, and d. The results extracted from the DR_3 and DR_4 schemes are compatible with each other. In the case of DR_3, the systematic uncertainties from the variation of the $\pi\eta$ phase shift dominate, while in the case of DR_4, the main uncertainties are the statistical fit errors and the systematic uncertainties are suppressed. There are, however, some deviations between the fits to the two different experimental data sets, mainly in κ_{03}, which are a consequence of the observed tension in the leading Dalitz-plot parameters.

If forthcoming experiments reach significantly higher statistics, it might become possible to extract these parameters directly in a phenomenological polynomial fit to data and compare with our predictions.

5.4.3 Adler zeros

In the limit of one of the pion momenta going to zero, $p_1 \to 0$ or $p_2 \to 0$, current algebra predicts two Adler *zeros* of the amplitude [66, 67, 170]. These *soft-pion theorems* are protected by $\mathrm{SU}(2)_L \times \mathrm{SU}(2)_R$ symmetry, hence they only receive corrections of $\mathcal{O}(M_\pi^2)$, *cf.* sec. 1.3. While the off-shell continuation of the amplitude cannot be defined unambiguously, the Adler theorem implies that the on-shell amplitude is of $\mathcal{O}(M_\pi^2)$ at the two soft-pion points

$$\begin{aligned} s_1 &= 2M_\pi^2\,, \qquad t_1 = M_{\eta'}^2\,, \qquad u_1 = M_\eta^2\,, \\ s_2 &= 2M_\pi^2\,, \qquad t_2 = M_\eta^2\,, \qquad u_2 = M_{\eta'}^2\,. \end{aligned} \tag{5.51}$$

In the past, claims have been made that the $a_0(980)$ resonance removes the Adler zeros based on the explicit inclusion of a scalar resonance propagator [171]. Let us study this issue within our dispersive framework.

In fig. 5.8, we show the result for the dispersive amplitude fitted to data, evaluated along a line of fixed $s = 2M_\pi^2$. Both subtraction schemes DR_3 and DR_4 lead to very similar results. We encounter zeros in both the real and imaginary part of the amplitude at positions close to the soft-pion points, but for slightly smaller values of $|t - u|$. At the resonance positions

$$|t - u| \approx 2M_{a_0}^2 - M_{\eta'}^2 - M_\eta^2\,, \tag{5.52}$$

which are also close but outside the soft-pion points, we observe a large peak in the imaginary part and another zero in the real part. We conclude that the dispersive representation refutes the resonance argument of ref. [171] that for $\eta' \to \pi\pi\eta$ the low-energy theorem does not result in an Adler zero of the amplitude. Although the corrections at the soft-pion points are of $\mathcal{O}(M_\pi^2/(M_{\eta'}^2 - M_{a_0}^2))$, which is not a small quantity, the zeros of the amplitude survive and are just shifted to smaller values of $|t - u|$.

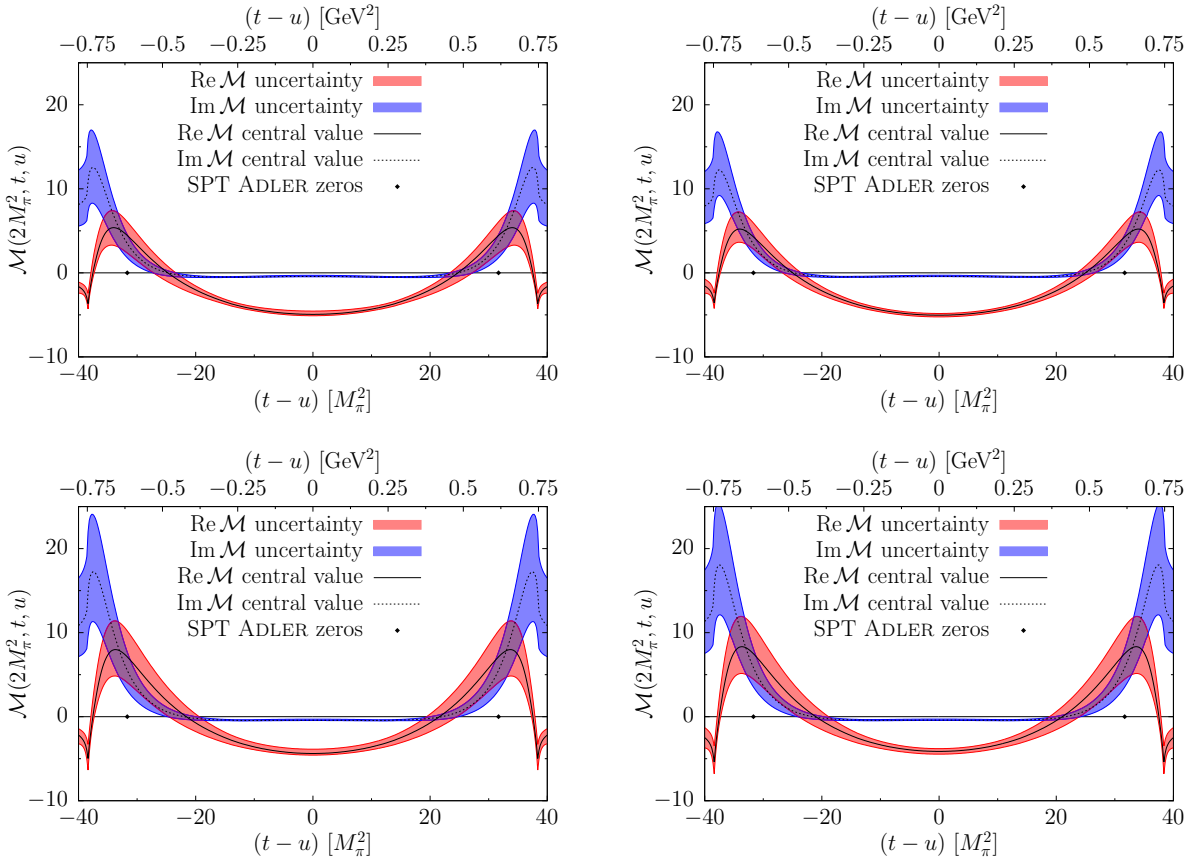

Fig. 5.8: Real and imaginary part of the amplitude along a line of fixed $s = 2M_\pi^2$. The upper two panels give the fit of the dispersive representation to the BESIII, the lower two panels to the VES data set. The DR_3 (left column) and DR_4 fits (right column) are shown.

5.4.4 Neutral channel

So far, we have analyzed experimental Dalitz-plot data sets for $\eta' \to \pi^+\pi^-\eta$. To deduce a comparably precise prediction for the neutral final state $\eta' \to \pi^0\pi^0\eta$, we have to consider potentially enhanced sources of isospin-symmetry violation. The consideration of isospin breaking, in particular due to the pion mass difference, in Dalitz-plot studies is a rather subtle affair, which has recently received some attention in the context of $\eta \to 3\pi$ decay studies [150, 201, 202]. While a correction for phase space alone is straightforward, it is often less so to construct an amplitude that accordingly has all the thresholds in the right places. This is particularly true in the context of dispersive analyses, as the ubiquitous phase shifts are typically derived from a formalism (the Roy equations) that incorporates isospin symmetry in an essential manner. Isospin-breaking effects are bound to affect neutral-pion final states more strongly, as the isospin-symmetric phase shifts use the *charged* pion mass as their reference scale. Furthermore, the pion mass difference induces a cusp in $\pi^0\pi^0$ invariant mass spectra at the $\pi^+\pi^-$ threshold [203, 204], a nonanalyticity

that cannot be approximated by a polynomial DALITZ-plot distribution. Such a cusp is known to appear more strongly in $\eta' \to \pi^0\pi^0\eta$ [178] than, *e.g.*, in $\eta \to 3\pi^0$ [205].[#8]

As we want to avoid the complications to solve KHURI–TREIMAN equations with coupled channels [151, 206], we once more follow the strategy proposed in sec. 5.2.3 and construct effective single-channel phase shifts, to be used as input for the corresponding Omnès functions, from the phases of certain scalar form factors. We observe that the cusp structure of the decay amplitude for $\eta' \to \pi^0\pi^0\eta$ is very similar to that of the neutral-pion scalar form factor

$$F_S^0(s) = \langle \pi^0(p_1)\, \pi^0(p_2) | \hat{m}\, (\bar{u}u + \bar{d}d) | 0 \rangle \,, \qquad s = (p_1 + p_2)^2 \,, \tag{5.53}$$

in particular given that crossed-channel effects in $\eta' \to \pi^0\pi^0\eta$ have a negligible influence on its strength [178]. We will therefore employ $\arg F_S^0$ as the input $\pi^0\pi^0$ S-wave phase shift.

The precise construction of the effective $\pi^0\pi^0$ phase shift from the corresponding scalar form factor is discussed in C.1. It takes into account the analytic structure near the two-pion thresholds, where isospin breaking is enhanced due to the proximity of (S-wave) threshold cusps, and scales effectively like $\sqrt{M_\pi^2 - M_{\pi^0}^2}$, where we denote by M_π the charged and by M_{π^0} the neutral pion mass. Regular, polynomial isospin-breaking effects of order $M_\pi^2 - M_{\pi^0}^2$ are still neglected and assumed to be very small. Similarly, we show there how a simple rescaling can be used to adapt the $\pi^\pm\eta$ phase shift to $\pi^0\eta$ in such a way as to put all thresholds into the right places.

Our prediction for the decay $\eta' \to \pi^0\pi^0\eta$ is therefore based on the subtraction constants as extracted from $\eta' \to \pi^+\pi^-\eta$, but with $\pi^0\pi^0$ and $\pi^0\eta$ phase shifts adapted as compared to the $\pi^+\pi^-$ and $\pi^\pm\eta$ ones; in this way, the dominant effects of isospin violation due to the charged-to-neutral pion mass difference are taken into account. The resulting decay spectrum projected on the y direction is shown in fig. 5.9, where the nonanalytic structure of the $\pi^+\pi^-$ cusp is clearly visible.

Another rather strong isospin-breaking effect appears in the change of coordinates from the MANDELSTAM variables to the DALITZ-plot variables x and y if the neutral pion mass is used in eq. (5.33) for the parametrization of the neutral DALITZ plot, *cf.* app. B. As such this effect has nothing to do with the decay amplitude itself but it affects the DALITZ-plot expansion parameters. We introduce the isospin-breaking parameter

$$\epsilon_{\text{iso}} \equiv \frac{(M_\eta + 2M_\pi)\, M_{\pi^0}\, Q_{\eta'}^0}{(M_\eta + 2M_{\pi^0})\, M_\pi\, Q_{\eta'}} - 1 \approx 4.7\% \,, \tag{5.54}$$

where $Q_{\eta'}^0 := M_{\eta'} - M_\eta - 2M_{\pi^0}$. Given the phenomenological observation that $1 \gg a, b, d > \kappa_{ij}$ for $i + j \geq 3$, we neglect terms of $\mathcal{O}(\epsilon_{\text{iso}}\, a^2, \epsilon_{\text{iso}}\, a\, b, \epsilon_{\text{iso}}\, a\, d, \epsilon_{\text{iso}}\, \kappa_{ij})$ and of second order in isospin breaking and find the following relation between the DALITZ-plot parameters in the charged (no superscript) and the neutral system (superscript "0"):

$$a^0 = a + \epsilon_{\text{iso}}\, (a + 2b) \,, \qquad b^0 = b\, (1 + 2\epsilon_{\text{iso}}) \,, \qquad d^0 = d \left(\frac{Q_{\eta'}^0}{Q_{\eta'}} \right)^2 . \tag{5.55}$$

[#8] At two-loop order, the lower $\pi^0\pi^0$ mass induces an anomalous threshold in the $\eta' \to \pi^+\pi^-\eta$ amplitude. We have checked, though, that this does not lead to any enhanced isospin-breaking effect, using the representation of ref. [178]. We thank M. Mikhasenko for suggesting this check.

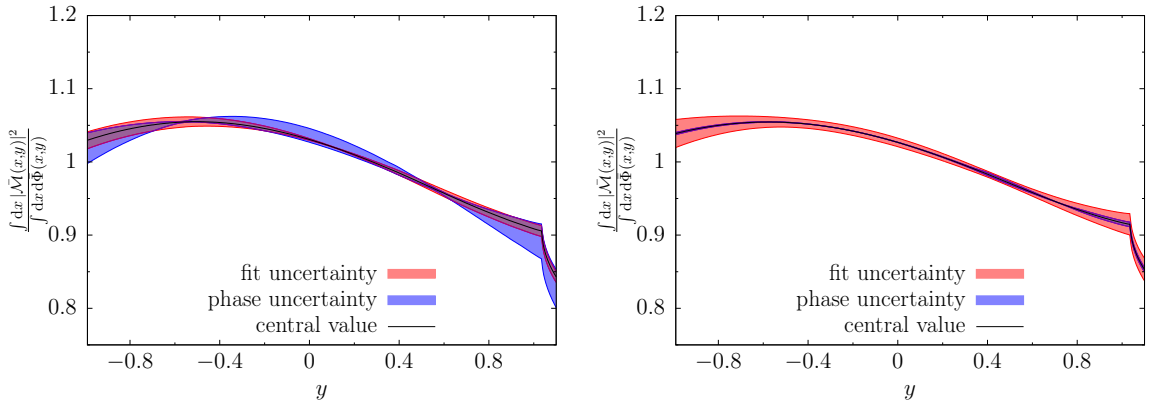

Fig. 5.9: Decay spectrum for $\eta' \to \pi^0\pi^0\eta$ integrated over the variable x and divided by the integral over the normalized phase space $\mathrm{d}\bar{\Phi}(x,y)$, where both are individually normalized as given in eq. (5.36). The prediction is based on the BESIII fit result for subtraction constants of the charged decay, *cf.* tabs. 5.2 and 5.3. The DR_3 (upper panel) and DR_4 fit results (lower panel) are shown. The two error bands in each figure give the uncertainties resulting from the fit to data and originating from the variation of the phase input, respectively.

For parameters comparable to the BESIII fit results, this amounts to a sizeable correction: we find $a^0 \approx 1.25\,a$, $b^0 \approx 1.09\,b$, $d^0 \approx 1.15\,d$.

In particular, this correction has to be taken into account if the *a*-*b*-*d* constraint (5.46) formulated in the charged system is employed for neutral Dalitz-plot parameters. For convenience, below we provide the explicit form of the *a*-*b*-*d* constraint for the neutral system. We apply the isospin correction to the BESIII fit values to define the reference point in the neutral system:

$$\Delta a^0 \equiv a^0 - a^0_{\mathrm{BESIII}}\,, \qquad \Delta b^0 \equiv b^0 - b^0_{\mathrm{BESIII}}\,, \qquad \Delta d^0 \equiv d^0 - d^0_{\mathrm{BESIII}}\,, \tag{5.56}$$

where

$$a^0_{\mathrm{BESIII}} = -51 \times 10^{-3}\,, \qquad b^0_{\mathrm{BESIII}} = -96 \times 10^{-3}\,, \qquad d^0_{\mathrm{BESIII}} = -78 \times 10^{-3}\,. \tag{5.57}$$

Then the *a*-*b*-*d* constraint reads again

$$\Delta d^0 = C^0_{10}\,\Delta a^0 + C^0_{01}\,\Delta b^0 + C^0_{20}\,(\Delta a^0)^2 + C^0_{11}\,\Delta a^0\,\Delta b^0 + C^0_{02}\,(\Delta b^0)^2\,, \tag{5.58}$$

where the neutral coefficients are given by

$$\begin{aligned}
C^0_{10} &= \left(\frac{Q^0_{\eta'}}{Q_{\eta'}}\right)^2 (1-\epsilon_{\mathrm{iso}})\,C_{10}\,, & C^0_{01} &= \left(\frac{Q^0_{\eta'}}{Q_{\eta'}}\right)^2 \big(C_{01} - 2\epsilon_{\mathrm{iso}}\,(C_{01}+C_{10})\big)\,,\\
C^0_{20} &= \left(\frac{Q^0_{\eta'}}{Q_{\eta'}}\right)^2 (1-2\epsilon_{\mathrm{iso}})\,C_{20}\,, & C^0_{11} &= \left(\frac{Q^0_{\eta'}}{Q_{\eta'}}\right)^2 \big(C_{11} - \epsilon_{\mathrm{iso}}\,(3C_{11}+4C_{20})\big)\,,\\
C^0_{02} &= \left(\frac{Q^0_{\eta'}}{Q_{\eta'}}\right)^2 \big(C_{02} - 2\epsilon_{\mathrm{iso}}\,(2C_{02}+C_{11})\big)\,.
\end{aligned} \tag{5.59}$$

With the values for the charged coefficients C_{ij} given in eq. (5.47), this results in

$$\begin{array}{rl|ccccc} C_{10}^0 = & 0.23\,^{+0.03}_{-0.09} & 1.00 & \begin{smallmatrix}0.91\\0.98\end{smallmatrix} & \begin{smallmatrix}-0.91\\-0.98\end{smallmatrix} & \begin{smallmatrix}0.91\\0.97\end{smallmatrix} & \begin{smallmatrix}0.87\\-0.45\end{smallmatrix} \\ C_{01}^0 = & 1.75\,^{+0.44}_{-0.99} & & 1.00 & \begin{smallmatrix}-1.00\\-1.00\end{smallmatrix} & \begin{smallmatrix}1.00\\1.00\end{smallmatrix} & \begin{smallmatrix}0.96\\-0.32\end{smallmatrix} \\ C_{20}^0 = & -0.44\,^{-0.11}_{+0.25} & & & 1.00 & \begin{smallmatrix}-1.00\\-1.00\end{smallmatrix} & \begin{smallmatrix}-0.96\\0.32\end{smallmatrix} \\ C_{11}^0 = & 0.09\,^{+0.03}_{-0.06} & & & & 1.00 & \begin{smallmatrix}0.97\\-0.27\end{smallmatrix} \\ C_{02}^0 = & -0.02\,^{-0.01}_{+0.01} & & & & & 1.00 \end{array} , \tag{5.60}$$

5.5 Comparison to chiral approaches

As we have seen in sec. 5.3, our dispersive amplitude allows a good fit to both Dalitz-plot data and the partial decay width. In a next step, we compare the dispersive amplitude with predictions from extensions of ChPT (*cf.* sec. 1.3); we choose next-to-leading order large-N_C ChPT and *resonance chiral theory* (RChT) for that purpose. The results for the amplitudes in both frameworks, taken from the analysis described in ref. [169], are discussed in sec. 5.5.1. We decompose these amplitudes into forms amenable to a comparison to the dispersion relations and perform the matching in sec. 5.5.2. This allows us to obtain chiral predictions for the subtraction constants and to compare them with the fits to data.

5.5.1 Amplitudes from large-N_C ChPT and RChT

Large-N_C chiral perturbation theory allows the explicit inclusion of the η' meson in an effective-Lagrangian framework. It is founded on the notion that as $N_C \to \infty$, the $\mathrm{U}(1)_A$ anomaly and thus the chiral-limit mass of the η' vanishes: the η' becomes a Nambu–Goldstone Boson as the $\mathrm{U}(3)_L \times \mathrm{U}(3)_R$ symmetry is spontaneously broken to $\mathrm{U}(3)_V$ [73, 168]. At leading order (LO) the $\eta' \to \pi\pi\eta$ amplitude is given as [169, 172, 207–212]

$$\mathcal{M}_{\mathrm{LO}}^{\mathrm{ChPT}}(s,t,u) = \frac{M_\pi^2}{6F_\pi^2}\left[2\sqrt{2}\cos(2\theta_P) - \sin(2\theta_P)\right], \tag{5.61}$$

where θ_P is the $\eta\eta'$ mixing angle that relates the flavor octet and singlet states to the physical states η and η' at leading order, and F_π is the pion decay constant. At next-to-leading order (NLO) loop contributions are still suppressed in the large-N_C counting scheme, and the full amplitude can be derived from the NLO Lagrangian [169],

$$\begin{aligned}\mathcal{M}_{\mathrm{NLO}}^{\mathrm{ChPT}}(s,t,u) = c_{qq}\Bigg[&\frac{M_\pi^2}{2} + \frac{2\,(3L_2+L_3)}{F_\pi^2}\left(s^2+t^2+u^2 - M_{\eta'}^4 - M_\eta^4 - 2M_\pi^4\right) \\ &- \frac{2L_5}{F_\pi^2}\left(M_{\eta'}^2 + M_\eta^2 + 2M_\pi^2\right)M_\pi^2 + \frac{24L_8}{F_\pi^2}M_\pi^4 + \frac{2}{3}\Lambda_2\,M_\pi^2\Bigg] \\ &+ c_{sq}\,\frac{\sqrt{2}}{3}\Lambda_2\,M_\pi^2\,,\end{aligned} \tag{5.62}$$

where c_{qq} and c_{sq} are functions of the octet and singlet decay constants $F_{8/0}$, as well as of the *two* mixing angles $\theta_{8/0}$ required in the $\eta\eta'$ mixing scheme at NLO [213, 214]:

$$c_{qq} = \frac{F_0^2\, S_0 - 2F_8^2\, S_8 + 2\sqrt{2} F_8\, F_0\, C_{08}}{3F_8^2\, F_0^2\, \cos^2(\theta_8 - \theta_0)}\,, \qquad c_{sq} = -\frac{\sqrt{2}F_0^2\, S_0 + \sqrt{2}F_8^2\, S_8 + F_0\, F_8\, C_{08}}{3F_8^2\, F_0^2\, \cos^2(\theta_8 - \theta_0)}\,, \tag{5.63}$$

where we defined $S_0 = \sin 2\theta_0$, $S_8 = \sin 2\theta_8$, and $C_{08} = \cos(\theta_0 + \theta_8)$. Numerically, we use $c_{qq} = 97.6(7.1)\,\text{GeV}^{-2}$ and $c_{sq} = 4.4(2.9)\,\text{GeV}^{-2}$ [169, 215] (*cf.* also ref. [216]).

For the low-energy constants L_2 and L_3, we use again the values from ref. [196], given in eq. (5.32), while for L_5 and L_8, we use the results of the global BE14 fit [217]:

$$L_5 = 1.01(06) \times 10^{-3}\,, \qquad L_8 = 0.47(10) \times 10^{-3}\,, \tag{5.64}$$

and finally $\Lambda_2 = 0.3$ [169].

The second chiral approach that we consider is resonance chiral theory, which describes the interactions between Nambu–Goldstone Bosons and resonances explicitly [218, 219]. RChT finds its most prominent application in the estimate of low-energy constants by means of resonance saturation. It can, however, also be used to directly derive the $\eta' \to \pi\pi\eta$ decay amplitude from the RChT Lagrangian [169]. To properly match it to the dispersive amplitude, it is useful to write it in the form

$$\begin{aligned}\mathcal{M}^{\text{RChT}}(s,t,u) = c_{qq}\Bigg[&\frac{M_S^2}{M_S^2 - s}\left(\rho - \frac{c_d^2\,\Delta}{F_\pi^2\, M_S^2} - \rho\,\frac{s}{M_S^2}\right) \\ &+ \left(\frac{M_S^2}{M_S^2 - s} + \frac{M_S^2}{M_S^2 - t} + \frac{M_S^2}{M_S^2 - u}\right)\left(\frac{\xi}{M_S^4} + \frac{\psi}{M_S^2} + c_d^2\right)\frac{M_S^2}{F_\pi^2}\Bigg]\,,\end{aligned} \tag{5.65}$$

where

$$\begin{aligned}\xi &= \left(M_{\eta'}^2 + M_\pi^2\right)\left(M_\eta^2 + M_\pi^2\right) c_d^2 - 6M_\pi^2\, r\, c_d\, c_m + 4M_\pi^4\, c_m^2\,, \\ \psi &= -3r\, c_d^2 + 4M_\pi^2\, c_m\, c_d\,, \qquad \rho = \frac{M_\pi^2}{2} - 3\,\frac{\psi + c_d^2\,(M_S^2 + r)}{F_\pi^2}\,.\end{aligned} \tag{5.66}$$

Here c_d and c_m describe the coupling between the scalar resonances and the Nambu–Goldstone Bosons, and $M_S = 980\,\text{MeV}$ is the mass of the scalar multiplet. We will use $c_d = 0.026(9)\,\text{GeV}$ and $c_m = 0.080(21)\,\text{GeV}$, which fulfill the theoretical constraint $4c_d\, c_m = F_\pi^2$ rather well [169].

In the limit of large scalar masses, that is s, t, u, M_π^2, M_η^2, $M_{\eta'}^2 \ll M_S^2$, the low-energy expansion of the amplitude (5.65) agrees with eq. (5.62) for [218]

$$3L_2 + L_3 = \frac{c_d^2}{2M_S^2}\,, \qquad L_5 = \frac{c_d\, c_m}{M_S^2}\,, \quad L_8 = \frac{c_m^2}{2M_S^2}\,, \qquad \Lambda_2 = 0\,. \tag{5.67}$$

We note that these relations are not at all well fulfilled for the values of the constants we employ, as cited above: in contrast to vector or axial-vector quantities, resonance saturation of low-energy constants by narrow scalars is problematic at best.

5.5.2 Matching chiral approaches with the dispersion relation

We perform the matching to the dispersion relations as follows: we decompose the chiral amplitudes into single-variable amplitudes and require that the TAYLOR coefficients of the latter agree between chiral and dispersive representations. This allows us to extract chiral predictions for the subtraction constants. The derivation of the explicit matching equations can be found in app. C.2.

In the case of large-N_C ChPT, it is not possible to match directly to the three-parameter representation (5.26), because the asymptotic behavior of the amplitude violates the condition that was used to fix the ambiguity of the decomposition. Therefore, one has to match the chiral amplitude to the four-parameter representation (5.24). In the case of RChT, the situation is different, because the asymptotic behavior allows a matching to the three-parameter representation DR_3. Hence, we have two possibilities: either we perform the matching with the DR_3 representation and require that the constant and linear terms of the TAYLOR expansion agree between RChT and dispersive representation, or we can also perform the matching with the DR_4 representation and match constant, linear, and quadratic terms in the expansion.

The results of the matching are shown in tab. 5.5 and should be compared to tabs. 5.2 and 5.3. In order to compare the chiral predictions with the fits to data, we define the quantity

$$\Delta^2_{\mathrm{exp}} \equiv \sum_{i,j} (t_i \mp t_i^{\mathrm{exp}})(C^{-1})_{ij}(t_j \mp t_j^{\mathrm{exp}})\,, \tag{5.68}$$

where t_i stands generically for the TAYLOR coefficients used in the matching equations and C_{ij} is the covariance matrix of $t_i \mp t_i^{\mathrm{exp}}$, including both statistical and systematic errors. We choose the sign that leads to the smaller value of Δ^2_{exp} (the minus sign for RChT and the plus sign for large-N_C ChPT)—we stress again that the dispersive fits to data determine the amplitude only up to an overall sign. In eq. (5.68), we choose to compare the TAYLOR coefficients instead of the subtraction constants, because their chiral prediction only depends on the model input and is not entangled with OMNÈS expansion parameters.

	$\alpha_{(0)}$	$\beta_{(0)}$	$\gamma_{(0)}$	γ_1	$\Delta^2_{\mathrm{BESIII}}$	Δ^2_{VES}
$\mathrm{DR}_3^{\mathrm{RChT}}$	$-7(4)$	$16(10)$	$0.8(4)$	-	18	17
$\mathrm{DR}_4^{\mathrm{RChT}}$	$-6(4)$	$12(9)$	$24(17)$	$0.8(4)$	145	116
$\mathrm{DR}_4^{\mathrm{ChPT}}$	$17(13)$	$-42(32)$	$-73(57)$	$-14(12)$	451	343

Tab. 5.5: Results of the matching between the dispersive amplitude and the large-N_C ChPT and RChT representations. In the case of RChT, the uncertainties are due to c_{qq}, c_d, and c_m, while for large-N_C ChPT, the errors are due to c_{qq}, c_{sq}, L_2, L_3, L_5, and L_8. The quantity Δ^2_{exp} is defined in eq. (5.68).

The analogous quantity for the DR_3 fits to BESIII and VES is

$$\Delta^2_{\mathrm{BESIII,VES}} = 22\,, \tag{5.69}$$

which quantifies again the tension between the two experiments. The values listed in tab. 5.5 show that for both chiral approaches the four-parameter matching involving the quadratic Taylor coefficients does not work at all. The fact that the DR_3 matching to RChT gives smaller values for Δ^2_{exp} is explained rather by the larger systematic uncertainties in this setup than a better agreement of the central values.

Given the tension between the two experiments, it is difficult to draw a conclusion concerning the two chiral approaches. We observe mainly two problems in the matching.

1. The overall normalization is not well reproduced.

2. While the matching in both DR_3 and DR_4 schemes leads to reasonable relative values of β/α or β_0/α_0, the predictions for the relative values of the terms γ/α or $\gamma_{0,1}/\alpha_0$ do not work at all.

In the case of large-N_C ChPT, the amplitude scales with $(3L_2{+}L_3)$, up to terms suppressed by M_π^2. On the one hand, the direct insertion of the phenomenological SU(3) LECs (5.32) could be problematic: *e.g.* we have not taken into account additional uncertainties due to the scale dependence of the SU(3) LECs, which does not appear at NLO in large-N_C ChPT. On the other hand, we cannot exclude that higher-order effects in the chiral and large-N_C expansion (*i.e.* effects only entering at one loop) produce large corrections.

5.6 Summary and conclusion

In this chapter we have presented a dispersive analysis of the decay $\eta' \to \pi\pi\eta$. We have derived a set of integral equations on the grounds of unitarity for the corresponding scattering process and performed an analytic continuation to the physical region of the three-particle decay. The integral equations depend on $\pi\pi$ and $\pi\eta$ scattering phase shifts as well as on a set of subtraction constants. The phase shift of $\pi\pi$ scattering is strongly constrained by chiral symmetry and Roy equations [133]. For the $\pi\eta$ phase shift, the phase of the scalar form factor $F_S^{\eta\pi}$ of ref. [135] is used as input.

Within two different subtraction schemes, the free constants have been fitted to data sets of the Dalitz-plot distribution, sampled from the experimentally measured polynomial Dalitz-plot parametrizations of the VES [182] and BESIII [183] experiments, as well as the partial decay width [197]. The fits to data require a smaller number of free parameters than a polynomial Dalitz-plot parametrization and still exhibit a good χ^2. Therefore, we have been able to derive a constraint between the Dalitz-plot parameters a, b, and d from one of the two dispersive representations. Furthermore, we have made predictions for higher-order polynomial parameters that have not been measured experimentally so far. By taking into account the leading isospin-breaking effects, we have also provided predictions for the neutral decay channel. We have further observed that the amplitude exhibits Adler zeros despite the presence of the nearby $a_0(980)$ resonance,

which only shifts the position of these zeros somewhat compared to the prediction of the soft-pion theorem.

Matching to large-N_C ChPT we find large deviations for the subtraction constants, rendering this approach unfit to be used in an attempt to extract information on $\pi\eta$ scattering. When matching to RChT, the deviations are a bit smaller. However, the matching in the three-parameter scheme shows less tension mainly because of the larger systematic uncertainties. Furthermore, the RChT framework does not easily allow for systematic improvements. Therefore, the theoretical prediction of the subtraction constants with chiral models as opposed to fitting them to data currently does not seem to be a viable option.

In the minimally subtracted dispersive amplitude representation, we have observed a rather significant dependence of the subtraction constants on the assumed high-energy behavior of the $\pi\eta$ phase shift input. More precise experimental data than the one available to us in this study is required to come to definite conclusions about the sensitivity of the $\eta' \to \pi\pi\eta$ decay to low-energy $\pi\eta$ scattering.

The derived amplitudes, compatible with the fundamental principles of analyticity and unitarity, provide ideal tools to analyze forthcoming high-precision Dalitz-plot data, in particular also for the neutral channel, by the A2 and BESIII collaborations [220, 221]; *cf.* also ref. [222] for a possible measurement at CB-ELSA. As a further theoretical development, the fitted dispersive parametrization will be used as an input in a forthcoming analysis of inelasticity effects in $\eta' \to 3\pi$ [199].

Chapter 6

C-violation and Dalitz-plot mirror symmetry breaking in $\eta \to \pi^+\pi^-\pi^0$

Since the flavorless isoscalar η meson and the isovector pions have opposite G-parity, the decay process of $\eta \to 3\pi$ is flavor-diagonal and only allowed to occur when isospin I- and/or charge-conjugation C-symmetry are broken, *cf.* ch. 1. Moreover, parity P is always conserved in $\eta \to 3\pi$, since the η as well as the pions are pseudoscalar particles. This directly implies CP-violation if C is broken in $\eta \to 3\pi$. Bose symmetry demands the three-pion system of total isospin I to be an eigenstate of $C = (-1)^{I+1}$ [223]. Consequently $\eta \to 3\pi$ in general can be mediated by three different operators: if C is conserved the process can only happen through an isovector $\Delta I = 1$ transition. When we allow for C-violation two further decay mechanisms are possible, via isoscalar $\Delta I = 0$ or isotensor $\Delta I = 2$ operators [223–226]. As a further consequence of Bose symmetry, the C-violating operators can only contribute to $\eta \to \pi^+\pi^-\pi^0$ but not to $\eta \to 3\pi^0$.

In general the Standard Model (SM) allows for transitions mediated by a C-conserving isospin-breaking $\Delta I = 1$ operator of either electromagnetic or strong origin, while flavor-diagonal C-violating $\Delta I = 0, 2$ operators are forbidden.[#1] According to Sutherland's theorem, a statement of current algebra, electromagnetic contributions in $\eta \to 3\pi$ are negligible [229, 230]. Thus the process has to be driven by the strong $\Delta I = 1$ operator generated by the difference of the up- and down-quark masses [88, 231, 232]. Indeed, as confirmed by ChPT calculations, the strong interaction provides the dominant contribution to $\eta \to 3\pi$ [233–235], while electromagnetic effects are found to add only tiny corrections [201, 236]. Therefore modern dispersion-theoretical studies of $\eta \to 3\pi$ focus on a consistent description of the final-state interactions driven by the SM strong $\Delta I = 1$ operator in order to extract the light-quark mass double ratio $Q^2 \equiv (\hat{m}^2 - m_s^2)/(m_u^2 - m_d^2)$ precisely [127, 148–152].

However, beyond the Standard Model (BSM) we are allowed to add the two C-violating $\Delta I = 0, 2$ operators that, besides the SM strong $\Delta I = 1$ operator, can contribute to $\eta \to \pi^+\pi^-\pi^0$. These additional contributions will become visible as breaking of mirror

[#1] Since only flavor-changing elements of the Cabibbo–Kobayashi–Maskawa matrix [227, 228] contain the non-zero phase that leads to C- and CP-violation, the contribution of SM weak interactions to C- and CP-violating $\eta \to \pi^+\pi^-\pi^0$ transitions invariably associated with strongly suppressed loop effects.

symmetry of $\pi^+ \leftrightarrow \pi^-$ in the DALITZ-plot distribution, which are generated by interference of the $\Delta I = 0, 2$ BSM operators with the $\Delta I = 1$ SM operator. In contrast to other C-violating BSM processes, like the $\eta \to 3\gamma$ decay, the breaking of mirror symmetry in $\eta \to \pi^+\pi^-\pi^0$ is linear in the BSM operators. For a detailed review on C- and CP-violating processes in the η and η' sector we suggest ref. [237]. Already in the 1960s it was claimed that $\eta \to \pi^+\pi^-\pi^0$ is far more sensitive to $\Delta I = 2$ than to $\Delta I = 0$ transitions, since the latter is suppressed by a large angular momentum barrier [224]. Effective BSM operators $X_I^{\not C}$ for $\eta \to \pi^+\pi^-\pi^0$ are given by

$$\begin{aligned} X_0^{\not C} &\sim \epsilon_{ijk}\,(\partial_\mu\partial_\nu\partial_\lambda\pi^i)(\partial^\mu\partial^\nu\pi^j)(\partial^\lambda\pi^k)\,\eta\,, \\ X_2^{\not C} &\sim \epsilon_{ij3}\,\pi^i\,(\partial_\mu\pi^j)(\partial^\mu\pi^3)\,\eta\,, \end{aligned} \tag{6.1}$$

involving at least six derivatives for a $\Delta I = 0$ transition, while for $\Delta I = 2$ only two derivatives are required. This implies a strong kinematic suppression of the $\Delta I = 0$ transition compared to $\Delta I = 2$ across the DALITZ plot given the small available phase space in $\eta \to \pi^+\pi^-\pi^0$, as long as the respective coupling strength of both operators is of similar size.

Studying the charge asymmetry of the $\eta \to \pi^+\pi^-\pi^0$ DALITZ-plot distribution offers an ideal stage in the search for BSM physics. The simplest observable that can be probed experimentally is the left-right asymmetry A_{LR} that compares the two halves of the DALITZ-plot distribution divided along the $\pi^+ \leftrightarrow \pi^-$ line of reflection [238]. It is also possible to construct more sophisticated quadrant and sextant asymmetry parameters A_Q and A_S that allow us to disentangle the contributions of the BSM $\Delta I = 0, 2$ operators, respectively [223, 225, 238]. The KLOE and KLOE-2 collaborations report all three asymmetry parameters to be consistent with zero [239, 240]. Alternatively, C-violation in the phenomenological expansion of the DALITZ-plot distribution can be studied by allowing for both C-conserving and C-violating terms, *cf.* app. B. Until now the KLOE-2 collaboration has probed the first four C-violating terms of this parameterization, which again are all consistent with zero [240]. Thus, experimentally there is no evidence found for C-violation in $\eta \to \pi^+\pi^-\pi^0$.

After the discovery of CP-violating $K_L^0 \to \pi\pi$ decays in the 1960s [241,242], theoretical studies of C-violation in $\eta \to \pi^+\pi^-\pi^0$ first came to prominence [223, 225, 238]. Since then C-violation in this decay has been neglected by theory until recently a new theoretical formalism was proposed in ref. [243]. In this framework the decay amplitude is decomposed into three contributions that can be associated with the $\Delta I = 0, 1, 2$ operators. The additional BSM amplitudes involve two complex-valued normalizations that fix the individual strengths of the $\Delta I = 0, 2$ transitions, respectively. Physically this approach is more meaningful compared to the simple phenomenological parameterization, as it allows for a direct extraction of the coupling strengths to the underlying BSM operators. However, the construction of the BSM amplitudes in ref. [243] is inconsistent at a certain level, since the description of crossed-channel final-state interactions is missing. Ref. [243] finds the BSM normalization of the $\Delta I = 0$ amplitude to be between two and four orders of magnitude larger than the $\Delta I = 2$ one, lifting the predicted kinematic suppression of the $\Delta I = 0$ transition [224], but again there is no hint for C-violation in $\eta \to \pi^+\pi^-\pi^0$ as both BSM normalizations are consistent with zero.

In this chapter we generalize the dispersion-theoretical analysis of C-conserving SM $\eta \to 3\pi$ decays to additional C-violating BSM contributions. Accordingly, the presented dispersive representation of $\eta \to 3\pi$ accounts for a consistent description of the final-state interactions among the pions in the $\Delta I = 0, 1, 2$ transitions, *cf.* chs. 4 and 5. The discussion is organized as follows: we start with the definition of the T-matrix element and the general kinematics of this process in sec. 6.1. In sec. 6.2 we discuss the dispersive representation of the C-conserving and C-violating parts of the amplitude. The determination of the subtraction constants, *i.e.*, the free parameters of our dispersive representation, by a χ^2-fit to data is described in sec. 6.3. Afterwards we compare our representation of the $\eta \to 3\pi$ amplitude to measurements of the DALITZ-plot distribution and theoretical constraints in sec. 6.4. We conclude with a short summary in sec. 6.5.

6.1 Kinematics and the matrix element

The T-matrix element of the $\eta(p_1) \to \pi^i(p_2)\,\pi^j(p_3)\,\pi^k(p_4)$ decay will be defined by

$$\big\langle \pi^i(p_2)\,\pi^j(p_3)\,\pi^k(p_4)\big|iT\big|\eta(p_1)\big\rangle = i\,(2\pi)^4\,\delta^{(4)}(p_1 - p_2 - p_3 - p_4)\,\mathcal{T}^{ijk}(s,t,u)\,, \tag{6.2}$$

where π^i denotes a pion state in the HERMITIAN basis (2.50). In general the amplitude $\mathcal{T}^{ijk}$ will contain contributions generated by either C-conserving $\Delta I = 1$ SM or C-violating $\Delta I = 0, 2$ BSM operators, which we split according to

$$\mathcal{T}^{ijk}(s,t,u) = \frac{\hat{M}^2_{K^+} - \hat{M}^2_{K^0}}{3\sqrt{3}F_\pi^2}\,\mathcal{T}_C^{ijk}(s,t,u) + \mathcal{T}_{\not C}^{ijk}(s,t,u)\,. \tag{6.3}$$

Conventionally the SM strong isospin-breaking normalization in terms of the QCD kaon mass splitting (1.56) is factored out from the C-conserving part of the amplitude [150,152]. In the following we refer to this normalization factor as ξ.

We treat the pion triplet as mass degenerated, *i.e.*, $M_\pi \equiv M_{\pi^\pm} = M_{\pi^0}$, accordingly the MANDELSTAM variables (*cf.* sec. 2.2.1) will be given by

$$s = (p_2 + p_3)^2\,, \qquad t = (p_2 + p_4)^2\,, \qquad u = (p_3 + p_4)^2\,, \tag{6.4}$$

and obey the identity

$$M_\eta^2 + 3M_\pi^2 = s + t + u \equiv 3r\,. \tag{6.5}$$

In the s-channel (2.30) we will make use of

$$t(s, z_s) = u(s, -z_s) = \frac{1}{2}\big(3r - s + \kappa(s)\,z_s\big)\,, \tag{6.6}$$

where $z_s \equiv \cos\theta_s$ defines the s-channel scattering angle (2.31)

$$z_s = \frac{t-u}{\kappa(s)}\,, \qquad \kappa(s) = \frac{\sqrt{\lambda(s, M_\pi^2, M_\pi^2)\,\lambda(s, M_\pi^2, M_\eta^2)}}{s}\,. \tag{6.7}$$

Analogous relations hold for the t- (2.36) and u-channels (2.38).

Next we want to discuss the isospin structure of the pions in $\mathcal{T}^{ijk}$. For the C-conserving SM part $\mathcal{T}_C^{ijk}$ the decomposition[#2]

$$\mathcal{T}_C^{ijk}(s,t,u) = \delta^{ij}\,\delta^{k3}\,\mathcal{M}_1^C(s,t,u) + \delta^{ik}\,\delta^{j3}\,\mathcal{M}_1^C(t,u,s) + \delta^{i3}\,\delta^{jk}\,\mathcal{M}_1^C(u,s,t) \tag{6.8}$$

holds, where we introduced the isovector amplitude $\mathcal{M}_1^C$ that fulfils the symmetry property

$$\mathcal{M}_1^C(s,t,u) = \mathcal{M}_1^C(s,u,t)\,. \tag{6.9}$$

On the other hand the isospin structure of the pions in the C-violating BSM part $\mathcal{T}_{\not C}^{ijk}$ can be separated according to

$$\mathcal{T}_{\not C}^{ijk}(s,t,u) = \epsilon^{ijk}\big[\mathcal{M}_0^{\not C}(s,t,u) + \delta^{k3}\,\mathcal{M}_2^{\not C}(s,t,u) + \delta^{j3}\,\mathcal{M}_2^{\not C}(t,u,s) + \delta^{i3}\,\mathcal{M}_2^{\not C}(u,s,t)\big]\,, \tag{6.10}$$

governed by the totally antisymmetric Levi-Civita tensor, *cf.* eq. (6.1). Under pairwise interchange of the Mandelstam variables the isoscalar amplitude $\mathcal{M}_0^{\not C}$ is totally antisymmetric

$$\begin{aligned}\mathcal{M}_0^{\not C}(s,t,u) &= \mathcal{M}_0^{\not C}(t,u,s) = \mathcal{M}_0^{\not C}(u,s,t)\\ &= -\mathcal{M}_0^{\not C}(s,u,t) = -\mathcal{M}_0^{\not C}(t,s,u) = -\mathcal{M}_0^{\not C}(u,t,s)\,,\end{aligned} \tag{6.11}$$

while the isotensor amplitude $\mathcal{M}_2^{\not C}$ obeys the antisymmetry property

$$\mathcal{M}_2^{\not C}(s,t,u) = -\mathcal{M}_2^{\not C}(s,u,t)\,. \tag{6.12}$$

In nature two versions of the $\eta \to 3\pi$ decay are realized: a charged $\eta \to \pi^+\pi^-\pi^0$ and a neutral $\eta \to 3\pi^0$ decay mode. We will describe these two modes by the amplitudes $\mathcal{M}_c$ and $\mathcal{M}_n$. According to the decomposition of $\mathcal{T}^{ijk}$ given in eqs. (6.8) and (6.10) these amplitudes are given by

$$\begin{aligned}\mathcal{M}_c(s,t,u) &= \mathcal{M}_1^C(s,t,u) + \xi^{-1}\left[\mathcal{M}_0^{\not C}(s,t,u) + \mathcal{M}_2^{\not C}(s,t,u)\right],\\ \mathcal{M}_n(s,t,u) &= \mathcal{M}_1^C(s,t,u) + \mathcal{M}_1^C(t,u,s) + \mathcal{M}_1^C(u,s,t)\,.\end{aligned} \tag{6.13}$$

6.2 Dispersion relations for $\eta \to 3\pi$

Following the steps described in ch. 4, we briefly want to discuss the dispersive framework for $\mathcal{M}_1^C$, $\mathcal{M}_0^{\not C}$, and $\mathcal{M}_2^{\not C}$ based on Khuri–Treiman equations, *cf.* also sec. 5.2. According to analyticity the three amplitudes are holomorphic in the Mandelstam plane up to branch cuts starting at the two-pion production threshold in all channels

$$s_{\text{thr}} = t_{\text{thr}} = u_{\text{thr}} = 4M_\pi^2\,. \tag{6.14}$$

[#2] The derivation of this decomposition follows the same ideas as already discussed for the $\pi\pi$ scattering amplitude in sec. 2.3.1 with keeping $l = 3$ fixed.

We relate these branch cuts in $\mathcal{M}_1^C$, $\mathcal{M}_0^{\not C}$, and $\mathcal{M}_2^{\not C}$ to the discontinuities of the partial-wave amplitudes b_ℓ^I in each channel, respectively. Here and in the following ℓ and I refer to the angular momentum and isospin quantum numbers of the two-body subsystems in the s-, t-, and u-channel expansions. Since the available phase space of $\eta \to 3\pi$ is small, we can safely neglect D- and higher partial-waves in these expansions, *i.e.*, only discontinuities of S- and P-waves will be considered. Accordingly, the reconstruction theorem allows us to decompose $\mathcal{M}_1^C$, $\mathcal{M}_0^{\not C}$, and $\mathcal{M}_2^{\not C}$ in terms of single-variable amplitudes $\mathcal{B}_\ell^I$ containing the information on the discontinuity of b_ℓ^I along the right-hand cut, *cf.* sec. 4.2. Contributions to the left-hand cuts of b_ℓ^I reside entirely in the crossed-channel projections $\hat{\mathcal{B}}_\ell^I$. Thus the partial-wave amplitudes will be given by

$$b_\ell^I(s) = \mathcal{B}_\ell^I(s) + \hat{\mathcal{B}}_\ell^I(s)\,. \tag{6.15}$$

6.2.1 Reconstruction theorems for $\mathcal{M}_1^C$, $\mathcal{M}_0^{\not C}$, and $\mathcal{M}_2^{\not C}$

We define the expansion of the isovector amplitude $\mathcal{M}_1^C$ into partial-wave amplitudes f_ℓ^I in analogy to eq. (4.29). Since $\mathcal{M}_1^C$ has to obey the symmetry relation given in eq. (6.9), the s-channel expansion allows only for contributions of even partial-wave amplitudes to the discontinuity[#3]

$$\operatorname{disc}_s \mathcal{M}_1^C(s,z_s) = \operatorname{disc} f_0^0(s) - \frac{2}{3}\operatorname{disc} f_0^2(s)\,. \tag{6.16}$$

Similarly, the t- and u-channel discontinuities read

$$\begin{aligned} \operatorname{disc}_t \mathcal{M}_1^C(t,z_t) &= \operatorname{disc} f_0^2(t) - z_t\,\kappa(t)\operatorname{disc} f_1^1(t)\,,\\ \operatorname{disc}_u \mathcal{M}_1^C(u,z_u) &= \operatorname{disc} f_0^2(u) + z_u\,\kappa(u)\operatorname{disc} f_1^1(u)\,. \end{aligned} \tag{6.17}$$

The numerical prefactors of the allowed two-body isospin combinations in these expansions can be extracted from the Clebsch–Gordon decomposition [14].

Following the steps in derivation of eq. (4.42) by using the discontinuities of eqs. (6.16) and (6.17) the reconstruction theorem for the isovector amplitude yields

$$\mathcal{M}_1^C(s,t,u) = \mathcal{F}_0^0(s) + (s-u)\,\mathcal{F}_1^1(t) + (s-t)\,\mathcal{F}_1^1(u) + \mathcal{F}_0^2(t) + \mathcal{F}_0^2(u) - \frac{2}{3}\,\mathcal{F}_0^2(s)\,, \tag{6.18}$$

where $\mathcal{F}_\ell^I$ denotes the single-variable amplitude. In accordance with eq. (6.9) this decomposition of $\mathcal{M}_1^C$ is symmetric under interchange of $t \leftrightarrow u$. Moreover, the decomposition is unaffected by a polynomial shift of the single-variable amplitudes $\mathcal{F}_\ell^I \mapsto \mathcal{F}_\ell^I + \Delta\mathcal{F}_\ell^I$ given by

$$\begin{aligned} \Delta\mathcal{F}_0^0(s) &= -4a + b\,(5s-9r) - 3c\,(s-r) - 27d\,r\,(s-r)\\ &\qquad + 4d\,s^2 - 162e\,r^2\,(s-r) - 4e\,s^2\,(s-9r)\,,\\ \Delta\mathcal{F}_1^1(s) &= c + 3d\,s + 9e\,s^2\,,\\ \Delta\mathcal{F}_0^2(s) &= 3a + 3b\,s - 3d\,s^2 + 3e\,s^2\,(s-9r)\,, \end{aligned} \tag{6.19}$$

[#3] Here and in the following relations that involve the discontinuity are always meant to be valid along the right-hand cut only, which starts at the two-pion threshold in the respective channel.

revealing a five-parameter ambiguity. Performing a partial-wave projection (4.53) of the decomposition given in eq. (6.18) we find

$$\begin{aligned}
\hat{\mathcal{F}}_0^0(s) &= \frac{2}{9}\big[3\langle\mathcal{F}_0^0\rangle + 9(s-r)\,\langle\mathcal{F}_1^1\rangle + 3\kappa(s)\,\langle z_s\,\mathcal{F}_1^1\rangle + 10\langle\mathcal{F}_0^2\rangle\big]\,,\\
\hat{\mathcal{F}}_1^1(s) &= \frac{1}{2\kappa(s)}\big[6\langle z_s\,\mathcal{F}_0^0\rangle + 9(s-r)\,\langle z_s\mathcal{F}_1^1\rangle + 3\kappa(s)\,\langle z_s^2\,\mathcal{F}_1^1\rangle - 10\langle z_s\,\mathcal{F}_0^2\rangle\big]\,,\\
\hat{\mathcal{F}}_0^2(s) &= \frac{1}{6}\big[6\langle\mathcal{F}_0^0\rangle - 9(s-r)\,\langle\mathcal{F}_1^1\rangle - 3\kappa(s)\,\langle z_s\,\mathcal{F}_1^1\rangle + 2\langle\mathcal{F}_0^2\rangle\big]\,,
\end{aligned} \tag{6.20}$$

where we used the short-hand notation for the angular integrals

$$\langle z_s^n\,\mathcal{F}_\ell^I\rangle = \frac{1}{2}\int_{-1}^{1}\mathrm{d}z_s\,z_s^n\,\mathcal{F}_\ell^I\big(t(s,z_s)\big)\,. \tag{6.21}$$

In accordance with eq. (6.11) the expansion the isoscalar amplitude $\mathcal{M}_0^{\not C}$ into partial waves allows only for terms that are antisymmetric under any pairwise interchange of MANDELSTAM variables. Hence, only odd partial-wave amplitudes g_ℓ^I will contribute to the discontinuity in all three channels $x \in \{s,t,u\}$ with

$$\mathrm{disc}_x\,\mathcal{M}_0^{\not C}(x,z_x) = z_x\,\kappa(x)\,\mathrm{disc}\,g_1^1(x)\,. \tag{6.22}$$

Repeating the steps in deriving eq. (4.49) with these discontinuities the reconstruction theorem for the isoscalar amplitude reads

$$\mathcal{M}_0^{\not C}(s,t,u) = (t-u)\,\mathcal{G}_1^1(s) + (u-s)\,\mathcal{G}_1^1(t) + (s-t)\,\mathcal{G}_1^1(u)\,, \tag{6.23}$$

which indeed is fully antisymmetric under pairwise interchange of the MANDELSTAM variables. Likewise to eq. (6.19) the decomposition into the single-variable amplitude $\mathcal{G}_\ell^I$ is not unambiguous, in fact eq. (6.23) stays invariant under a three-parameter polynomial shift $\mathcal{G}_\ell^I \mapsto \mathcal{G}_\ell^I + \Delta\mathcal{G}_\ell^I$ given by

$$\Delta\mathcal{G}_1^1(s) = a + b\,s + c\,s^2\,(3r - s)\,. \tag{6.24}$$

A partial-wave projection (4.53) of the decomposition given in eq. (6.23) reveals

$$\hat{\mathcal{G}}_1^1(s) = -\frac{3}{\kappa(s)}\big[3(s-r)\,\langle z_s\,\mathcal{G}_1^1\rangle + \kappa(s)\,\langle z_s^2\,\mathcal{G}_1^1\rangle\big]\,, \tag{6.25}$$

where the angular integrals contained in the projection $\hat{\mathcal{G}}_\ell^I$ are defined in analogy to eq. (6.21).

Since the isotensor amplitude $\mathcal{M}_2^{\not C}$ has to fulfil the antisymmetry property derived in eq. (6.12), a s-channel expansion of $\mathcal{M}_2^{\not C}$ is not allowed to contain even partial-wave amplitudes h_ℓ^I. Accordingly, the s-channel discontinuity of $\mathcal{M}_2^{\not C}$ reads

$$\mathrm{disc}_s\,\mathcal{M}_2^{\not C}(s,z_s) = 2z_s\,\kappa(s)\,\mathrm{disc}\,h_1^1(s)\,, \tag{6.26}$$

while for the t- and u-channel discontinuities we find

$$\begin{aligned} \text{disc}_t\, \mathcal{M}_2^{\not C}(t, z_t) &= \text{disc}\, h_0^2(t) - z_t\, \kappa(t)\, \text{disc}\, h_1^1(t)\,, \\ \text{disc}_u\, \mathcal{M}_2^{\not C}(u, z_u) &= -\text{disc}\, h_0^2(u) - z_u\, \kappa(u)\, \text{disc}\, h_1^1(u)\,. \end{aligned} \tag{6.27}$$

In analogy to eqs. (6.16) and (6.17) the Clebsch–Gordon decomposition [14] of the allowed two-body isospin combinations in these expansions determine the numerical prefactors.

Recapitulating the steps in deriving eq. (4.46) by using the discontinuities given in eqs. (6.26) and (6.27) the reconstruction theorem for the isotensor amplitude in terms of the single-variable amplitudes $\mathcal{H}_\ell^I$ yields

$$\mathcal{M}_2^{\not C}(s,t,u) = 2(t-u)\,\mathcal{H}_1^1(s) + (t-s)\,\mathcal{H}_1^1(u) + (s-u)\,\mathcal{H}_1^1(t) + \mathcal{H}_0^2(t) - \mathcal{H}_0^2(u)\,. \tag{6.28}$$

As required this decomposition of $\mathcal{M}_2^{\not C}$ is antisymmetric under interchange of $t \leftrightarrow u$. Moreover, we note that the decomposition into the single-variable functions reveals a four-parameter ambiguity that allows for a polynomial shift $\mathcal{H}_\ell^I \mapsto \mathcal{H}_\ell^I + \Delta\mathcal{H}_\ell^I$ according to

$$\begin{aligned} \Delta\mathcal{H}_1^1(s) &= a + b\,s + c\,s^2\,, \\ \Delta\mathcal{H}_0^2(s) &= d - 3a\,s + 3b\,s\,(s-3r) + 9c\,r\,s\,(s-2r) - c\,s^3\,. \end{aligned} \tag{6.29}$$

Performing a partial-wave projection (4.53) of eq. (6.28) we find

$$\begin{aligned} \hat{\mathcal{H}}_1^1(s) &= \frac{3}{2\kappa(s)}\big[3(s-r)\,\langle z_s\,\mathcal{H}_1^1\rangle + \kappa(s)\,\langle z_s^2\,\mathcal{H}_1^1\rangle + 2\langle z_s\,\mathcal{H}_0^2\rangle\big]\,, \\ \hat{\mathcal{H}}_0^2(s) &= \frac{1}{2}\big[9(s-r)\,\langle\mathcal{H}_1^1\rangle + 3\kappa(s)\,\langle z_s\,\mathcal{H}_1^1\rangle - 2\langle\mathcal{H}_0^2\rangle\big] \end{aligned} \tag{6.30}$$

in terms of the angular integrals (6.21).

Finally, we would like to address the leading corrections of the reconstruction theorems for $\mathcal{M}_1^C$, $\mathcal{M}_0^{\not C}$, and $\mathcal{M}_2^{\not C}$ stated in eqs. (6.18), (6.23), and (6.28). The next partial-wave amplitudes that will contribute to the discontinuities are coming from D- (I is even) and F-waves (I is odd). Since the symmetry structure of the isoscalar amplitude does not allow for even partial waves, it is obvious that eq. (6.23) actually holds up to corrections of F- and higher partial-waves. Moreover, possible D-wave contributions to the discontinuity of the isotensor amplitude (6.27) are only allowed to stem from $I = 2$. Apart from these effects, which should be tiny compared to a $I = 0$ D-wave channel that will appear in eq. (6.16), the isotensor amplitude is also free of D-wave contributions to the discontinuity. In contrast to the C-conserving amplitude $\mathcal{M}_1^C$ we conclude that the reconstruction theorems for the C-violating amplitudes $\mathcal{M}_0^{\not C}$ and $\mathcal{M}_2^{\not C}$ will not receive any (important) corrections from D-wave discontinuities of the partial-wave amplitudes.

6.2.2 Unitarity condition and the Omnès representation

It has been shown in many dispersion-theoretical analyses of SM $\eta \to 3\pi$ decays that the dominant contributions to the branch cuts of the partial-wave amplitudes $b_\ell^I \in \{f_\ell^I, g_\ell^I, h_\ell^I\}$

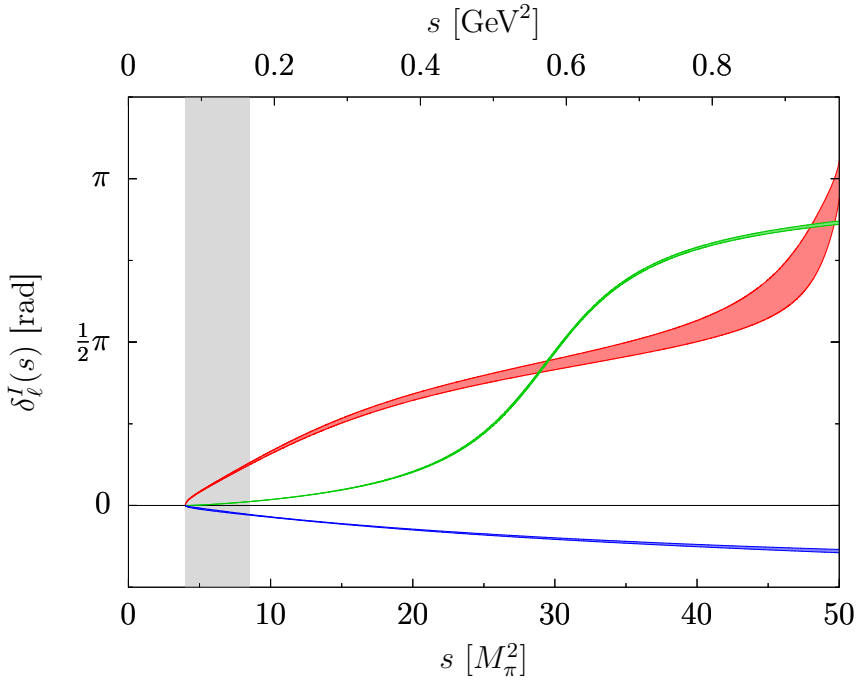

Fig. 6.1: The S- and P-wave $\pi\pi$ scattering phase shifts δ_ℓ^I at low energies as determined by ROY equation analysis [132, 133]: δ_0^0 (red), δ_1^1 (green), and δ_0^2 (blue). The gray region marks the phase-space boundaries of the $\eta \to 3\pi$ decay.

stem from elastic $\pi\pi$ final-state rescattering [127, 148–152].[#4] According to the elastic approximation the unitarity condition of b_ℓ^I along the right-hand cut reads [127, 244]

$$\operatorname{disc} b_\ell^I(s) = 2i\, b_\ell^I(s)\, \sin\delta_\ell^I(s)\, \exp\big[-i\delta_\ell^I(s)\big]\,, \tag{6.31}$$

determined by the information on the $\pi\pi$ scattering phase shifts δ_ℓ^I solely, *cf.* sec. 2.3.1. Since $\operatorname{disc} b_\ell^I = \operatorname{disc} \mathcal{B}_\ell^I$ along the right-hand cut 6.15, we notice that eq. (6.31) results in an inhomogeneous OMNÈS problem for the single-variable amplitude $\mathcal{B}_\ell^I$ with the inhomogeneity $\hat{\mathcal{B}}_\ell^I$, *cf.* sec. 3.2.2.

In order to assure convergence of the OMNÈS representation (3.44) for the single-variable amplitudes $\mathcal{B}_\ell^I$ we need to fix the subtraction scheme. To that end we have to make some assumptions on the high-energy behaviour of $\mathcal{B}_\ell^I$ and the $\pi\pi$ scattering phase shifts δ_ℓ^I. We force the amplitudes $\mathcal{M}_1^C$, $\mathcal{M}_0^{\not C}$, and $\mathcal{M}_2^{\not C}$ to scale asymptotically like constants, *i.e.*, we are even more restrictive than demanded by the FROISSART–MARTIN bound [161, 162], to keep the number of unknown subtraction constants as low as possible. In accordance with the reconstruction theorems derived in eqs. (6.18), (6.23), and (6.28) the single-variable amplitudes will behave like

$$\mathcal{B}_0^0(s) \asymp 1\,, \qquad \mathcal{B}_1^1 \asymp s^{-1}\,, \qquad \mathcal{B}_0^2 \asymp 1 \tag{6.32}$$

in the asymptotic limit $s \to \infty$. For the $\pi\pi$ scattering phase shifts δ_ℓ^I we rely on a representation using a ROY equation analysis [132, 133], which determines the behaviour

[#4] We want to mention that a more elaborate formalism accounting for $\pi\eta$ initial-state rescattering as well as coupled channel $K\bar{K}$ contributions has been investigated in [151].

of δ_ℓ^I at low energies very precisely, *cf.* fig. 6.1. However, at high energies these equations do not impose strong bounds on the behaviour of δ_ℓ^I. Therefore we continue the phase shifts by demanding

$$\delta_0^0(s) \to \pi\,, \qquad \delta_1^1(s) \to \pi\,, \qquad \delta_0^2(s) \to 0, \tag{6.33}$$

when approaching the asymptotic limit $s \to \infty$.

With these considerations made we will use a twice-subtracted Omnès representation for $\mathcal{B}_0^0$, while $\mathcal{B}_1^1$ and $\mathcal{B}_0^2$ are given by once-subtracted Omnès representations. Thus the single-variable amplitudes $\mathcal{F}_\ell^I$ appearing in the decomposition of the isovector amplitude $\mathcal{M}_1^C$ are given by

$$\begin{aligned}
\mathcal{F}_0^0(s) &= \Omega_0^0(s)\left[\alpha + \beta\, s + \frac{s^2}{\pi}\int_{4M_\pi^2}^\infty \frac{\mathrm{d}x}{x^2}\,\frac{\hat{\mathcal{F}}_0^0(x)\,\sin\delta_0^0(x)}{|\Omega_0^0(x)|\,(x-s)}\right],\\
\mathcal{F}_1^1(s) &= \Omega_1^1(s)\left[\gamma + \frac{s}{\pi}\int_{4M_\pi^2}^\infty \frac{\mathrm{d}x}{x}\,\frac{\hat{\mathcal{F}}_1^1(x)\,\sin\delta_1^1(x)}{|\Omega_1^1(x)|\,(x-s)}\right],\\
\mathcal{F}_0^2(s) &= \Omega_0^2(s)\left[\frac{s}{\pi}\int_{4M_\pi^2}^\infty \frac{\mathrm{d}x}{x}\,\frac{\hat{\mathcal{F}}_0^2(x)\,\sin\delta_0^2(x)}{|\Omega_0^2(x)|\,(x-s)}\right],
\end{aligned} \tag{6.34}$$

where we used eq. (6.19) and the result of sec. 3.5 to eliminate the subtraction constant in $\mathcal{F}_0^2$.

Similarly, the single-variable amplitude $\mathcal{G}_1^1$ contained in the decomposition of the isoscalar amplitude $\mathcal{M}_0^\phi$ reads

$$\mathcal{G}_1^1(s) = \Omega_1^1(s)\left[\varepsilon + \frac{s}{\pi}\int_{4M_\pi^2}^\infty \frac{\mathrm{d}x}{x}\,\frac{\hat{\mathcal{G}}_1^1(x)\,\sin\delta_1^1(x)}{|\Omega_1^1(x)|\,(x-s)}\right]. \tag{6.35}$$

According to the ambiguity shift defined in eq. (6.24) the representation for $\mathcal{G}_1^1$ is special: without spoiling the constraint on the high-energy behaviour of $\mathcal{M}_0^\phi$ we are allowed to write down twice- or even three-times subtracted Omnès representations for $\mathcal{G}_1^1$, which still depend on one subtraction constant only. Since the subtraction constants of these three representations are connected by a sum rule (3.21), the isoscalar amplitude $\mathcal{M}_0^\phi$ remains unchanged.

Finally, the single-variable amplitudes $\mathcal{H}_\ell^I$ appearing in the decomposition of the isotensor amplitude $\mathcal{M}_2^\phi$ satisfy

$$\begin{aligned}
\mathcal{H}_1^1(s) &= \Omega_1^1(s)\left[\vartheta + \frac{s}{\pi}\int_{4M_\pi^2}^\infty \frac{\mathrm{d}x}{x}\,\frac{\hat{\mathcal{H}}_1^1(x)\,\sin\delta_1^1(x)}{|\Omega_1^1(x)|\,(x-s)}\right],\\
\mathcal{H}_0^2(s) &= \Omega_0^2(s)\left[\frac{s}{\pi}\int_{4M_\pi^2}^\infty \frac{\mathrm{d}x}{x}\,\frac{\hat{\mathcal{H}}_0^2(x)\,\sin\delta_0^2(x)}{|\Omega_0^2(x)|\,(x-s)}\right],
\end{aligned} \tag{6.36}$$

where we made use of eq. (6.29) to eliminate the subtraction constant in $\mathcal{H}_0^2$.

We want to draw the attention to a powerful property of the integral equations derived so far: the OMNÈS representations of the single-variable amplitudes $\mathcal{B}_\ell^I$ and the angular projections $\hat{\mathcal{B}}_\ell^I$ are linear in the subtraction constants. Accordingly, as discussed in sec. 3.4 we can solve for *basis amplitudes* of $\mathcal{M}_1^C$, $\mathcal{M}_0^{\not C}$, and $\mathcal{M}_2^{\not C}$ that are independent of the subtraction constants by construction. It becomes immediately clear that the two subtraction constants ε and ϑ introduced in eqs. (6.35) and (6.36) will serve as overall normalizations of isoscalar and isotensor amplitudes, while their energy dependence (or the DALITZ-plot distribution) is a theoretical prediction solely determined by the $\pi\pi$ final-state dynamics. We want to emphasize that the two BSM amplitudes $\mathcal{M}_0^{\not C}$ and $\mathcal{M}_2^{\not C}$ contain only one subtraction constant each. On the other hand the representation of the SM isovector amplitude given in eq. (6.34) involves three subtraction constants α, β, and γ, which contain the normalization as well as information on the energy dependence of $\mathcal{M}_1^C$. In general all five subtraction constants α, β, γ, ε, and ϑ are allowed to be complex-valued.

6.2.3 Taylor invariants

As discussed in sec. 6.2.1 the decomposition of the amplitudes $\mathcal{M}_1^C$, $\mathcal{M}_0^{\not C}$, and $\mathcal{M}_2^{\not C}$ given in eqs. (6.18), (6.23), and (6.28) in terms of the single-variable amplitudes $\mathcal{B}_\ell^I \in \{\mathcal{F}_\ell^I, \mathcal{G}_\ell^I, \mathcal{H}_\ell^I\}$ are not unique as they remain invariant under the polynomial shifts of eqs. (6.20), (6.24), and (6.29), respectively. Hence, the free parameters of the dispersive framework (the subtraction constants) are not unique, as they depend on the chosen ambiguity shifts. Additionally the subtraction scheme, *i.e.*, the introduced number of subtractions to the dispersive relations, adjusts when changing the high-energy behaviour of the amplitudes. For this reason the subtraction constants defined in eqs. (6.34), (6.35), and (6.36) themselves do not form a suitable set of parameters that can be compared to *e.g.* chiral effective theories directly. However, it is possible to construct linear combinations of the subtraction constants that are invariant under the respective ambiguity shifts. These TAYLOR *invariants* are built upon a series expansion of the single-variable amplitudes $\mathcal{B}_\ell^I$ in the unphysical region at $s = 0$ given by

$$\mathcal{B}_\ell^I(s) = A_\ell^I + B_\ell^I\, s + C_\ell^I\, s^2 + D_\ell^I\, s^3 + \dots\,, \tag{6.37}$$

where the convergence behaviour of chiral effective theories should be best.

The idea of introducing TAYLOR invariants goes back to the dispersive analysis of $\mathcal{M}_1^C$ in refs. [150, 152]. According to eq. (6.20) the terms up to chiral order p^6 in the expansion of $\mathcal{F}_\ell^I$ as defined in eq. (6.37) are not unambiguous. Inserting this expansion into eq. (6.18) reveals

$$\begin{aligned}\mathcal{M}_1^C(s,t,u) = {} & F_0 + F_1\,(2s - t - u) + F_2\, s^2 + F_3\big[s\,(t+u) - 2t\,u\big] + F_4\, s^3 \\ & + F_5\left[\frac{1}{3}(2s^3 - t^3 - u^3) + s^2\,(t+u) + s\,(t^2+u^2) - 2t\,u\,(t+u)\right] + \mathcal{O}(p^8)\,,\end{aligned} \tag{6.38}$$

where we find a set of six TAYLOR invariants F_i defined by[#5]

$$F_0 = A_0^0 + r\,B_0^0 + \frac{4}{3}\big(A_0^2 + r\,B_0^2\big)\,, \qquad F_1 = \frac{1}{3}B_0^0 + A_1^1 - 3r^2\,C_1^1 - \frac{5}{9}B_0^2 - 3r\,C_0^2\,,$$
$$F_2 = C_0^0 + \frac{4}{3}C_0^2\,, \qquad F_3 = B_1^1 + C_0^2 + 9r\,D_0^2\,, \qquad F_4 = D_0^0 + \frac{4}{3}D_0^2\,, \qquad F_5 = C_1^1 - 3D_0^2\,. \tag{6.39}$$

Note that the coefficient F_0 contains only contributions up to p^2 in the chiral expansion, while F_2 is fully determined by contributions of chiral order p^4. Commonly, terms involving D_0^0, C_1^1, and D_0^2 are dropped as they are beyond the reach of one-loop ChPT [152]. Thus a reduced set of only four TAYLOR invariants F_0, F_1, F_2, and F_3 remains, while F_4 and F_5 vanish completely.[#6]

In a similar fashion we want to introduce TAYLOR invariants for the isoscalar and isotensor amplitudes. Since the reconstruction theorem for $\mathcal{M}_0^{\not C}$ defined in eq. (6.23) allows for an ambiguity shift (6.24) of chiral order p^8, we find

$$\mathcal{M}_0^{\not C}(s,t,u) = -G_0\,(s-t)(u-s)(t-u) + \mathcal{O}(p^{10}) \tag{6.40}$$

depending on a single TAYLOR invariant

$$G_0 = C_1^1 + 3r\,D_1^1 \tag{6.41}$$

fixed by the expansion of $\mathcal{G}_1^1$ according to eq. (6.37). Likewise, the ambiguity shifts (6.29) for the reconstruction theorem of isotensor amplitude $\mathcal{M}_2^{\not C}$ (6.28) demand

$$\mathcal{M}_2^{\not C}(s,t,u) = (t-u)\big[H_0 + H_1\,(2s-t-u) + H_2\,(t^2+u^2+t\,u)\big] + \mathcal{O}(p^8)\,, \tag{6.42}$$

when inserting the expansion of $\mathcal{H}_\ell^I$ given in eq. (6.37) up to chiral order p^6. The corresponding TAYLOR invariants of this expansion are given by

$$H_0 = 3A_1^1 + 3r\,B_1^1 + B_0^2 + 2r\,C_0^2\,, \qquad H_1 = B_1^1 + 3r\,C_1^1 - \frac{1}{3}C_0^2\,, \qquad H_2 = C_1^1 + D_0^2\,. \tag{6.43}$$

Note that H_0 contains only contributions up to p^4 in the chiral expansion.

6.3 Determination of the subtraction constants

In the previous section we derived dispersive representations for the $\mathcal{M}_1^C$, $\mathcal{M}_0^{\not C}$, and $\mathcal{M}_2^{\not C}$ components of the $\eta \to 3\pi$ amplitude that obey the fundamental properties of analyticity and unitarity. However, the five subtraction constants α, β, γ, ε, and ϑ appearing in eqs. (6.34), (6.35), and (6.36) are not fixed by unitarity. In order to determine these

[#5] Since eq. (6.20) allows only for shifts up to chiral order p^6 all higher terms in eq. (6.37) will not be affected by the ambiguity. Without further treatment these terms can be considered as TAYLOR invariants directly.

[#6] Obviously, this reduced set of TAYLOR invariants allows only for ambiguity shifts of eq. (6.20) where terms of chiral order p^6 are dropped.

free parameters we have to resort to external information on the $\eta \to 3\pi$ amplitude. We choose to take three different sources of input into account: binned DALITZ-plot distributions stemming from high-statistics measurements of the charged and neutral decay modes provided by the KLOE-2 (4.7×10^6 selected events of $\eta \to \pi^+\pi^-\pi^0$) [240] and A2 collaborations (7×10^6 selected events of $\eta \to 3\pi^0$) [245] as well as ChPT constraints on the TAYLOR invariants estimated from the C-conserving one-loop $\eta \to 3\pi$ amplitude [150, 152, 233]. We want to emphasize that in principle each of the three different sources of input allow us to determine the C-conserving subtraction constants α, β, and γ, but only the KLOE-2 data contains information on the C-violating effects needed to constrain ε and ϑ.[#7]

6.3.1 Total number of free parameters

At one loop ChPT predicts the numerical values of the C-conserving TAYLOR invariants as defined in eq. (6.39) (contributions above chiral order p^4 are dropped) to be

$$F_0 = 1.176(53)\,, \quad f_1 = 4.52(29)\,\mathrm{GeV}^{-2}\,, \quad f_2 = 16.4(4.9)\,\mathrm{GeV}^{-4}\,, \quad f_3 = 6.3(2.0)\,\mathrm{GeV}^{-4}\,, \tag{6.44}$$

where the invariant F_0 will be used to parameterize the normalization of the C-conserving amplitude $\mathcal{M}_1^C$ while the reduced invariants $f_i \equiv F_i/F_0$ determine its energy dependence. Note that in accordance with the definitions in sec. 6.1 the estimations given in eq. (6.44) are valid in the isospin limit. Furthermore, we want to stress that all invariants at one loop are real-valued.

A TAYLOR expansion of the OMNÈS representation for $\mathcal{M}_1^C$ (6.34) performed in accordance with the prescription given in eq. (6.37) reveals that the contributions from the OMNÈS functions are real, but the dispersion integrals will render the coefficients complex. Thus, the linear relations between the TAYLOR invariants and the subtraction constants α, β, and γ involve complex coefficients. Since the dispersion integrals arise from the crossed-channel discontinuities and we evaluate their TAYLOR coefficients at $s = 0$ below the two-pion threshold, the contributions of the dispersion integrals are small. Thus the TAYLOR invariants will only pick up tiny imaginary parts if we assume α, β, and γ to be real-valued.[#8] Accordingly, the number of independent parameters needed to fix $\mathcal{M}_1^C$ is halved from six to three.

Since we are yet missing any chiral effective theory approach that allows for an analogous extraction of C-violating TAYLOR invariants (6.41) and (6.43), there is no known restriction from theory, which states that the normalizations of the C-violating amplitudes $\mathcal{M}_0^{\not C}$ and $\mathcal{M}_2^{\not C}$ should be real-valued. Thus, the subtraction constants ε and ϑ will be treated as complex-valued increasing the total number of free parameters needed to be fixed by four.

[#7] Since the provided experimental DALITZ-plot distributions are arbitrarily normalized, it is only possible to fix the relative sizes of the subtraction constants. Furthermore the DALITZ-plot distributions are proportional to the squared modulus of the $\eta \to 3\pi$ amplitude, which means that using the experimental data alone we also loose the information of an overall phase.

[#8] Note that first contributions to the imaginary parts of the TAYLOR invariants will appear at two loops in the chiral expansion [152, 235].

6.3.2 Electromagnetic corrections to $\eta \to 3\pi$

Up to now we have assumed the pion triplet to be mass degenerate, *i.e.*, the amplitude given in eq. (6.13) relies on kinematical variables in the isospin limit. However, in the physical world the degeneracy is lifted by the electromagnetic contributions to the self-energy of the charged pions, *cf.* sec. 1.3.3. Since the physical phase space of $\eta \to 3\pi$ is small, the pion mass difference yields a relevant impact on the size of the physical region and of course the correct position of the respective two-pion thresholds, which must be accounted for. Similarly to the identity (6.5) fulfilled by s, t, and u in the isospin limit, the MANDELSTAM variables s_c, t_c, and u_c for the charged as well as s_n, t_n, and u_n for the neutral decay mode obey the relations

$$M_\eta^2 + 2M_{\pi^\pm}^2 + M_{\pi^0}^2 = s_c + t_c + u_c \equiv 3r_c\,, \qquad M_\eta^2 + 3M_{\pi^0}^2 = s_n + t_n + u_n \equiv 3r_n\,. \tag{6.45}$$

Accordingly, any comparison of our amplitude in the isospin symmetric world with experiment requires the application of an appropriate *kinematic map* relating the MANDELSTAM variables of the physical world to the ones in the isospin limit.

In general, the construction of such a kinematic map for $\eta \to 3\pi$ is all but unique. However, the difficulty is to find an acceptable choice for this map, which on the one hand yields a meaningful prescription of the complete DALITZ plot within its phase space boundary and on the other hand is easy to handle. Therefore, we will adopt the choice proposed in ref. [152] that bares the following properties: the mapping is *boundary preserving*, *i.e.*, the DALITZ-plot boundary of the physical phase space is mapped onto the boundary of the isospin symmetric phase space, and the identity $3r = s + t + u$ remains conserved (6.5). Furthermore, the map is chosen in such a way that it does not generate any fictitious singularity structure within the DALITZ plot. We find this kinematic map for $s_{c,n} \mapsto s$, $t_{c,n} \mapsto t$, and $u_{c,n} \mapsto u$ to be given by the prescriptions

$$\begin{aligned} s &= \sigma_{c,n}[s_{c,n}]\,, \qquad (t-u) = (t_{c,n} - u_{c,n})\,\tau_{c,n}[s_{c,n}]\,, \\ t &= \frac{1}{2}\big(3r - \sigma_{c,n}[s_{c,n}] + (t_{c,n} - u_{c,n})\,\tau_{c,n}[s_{c,n}]\big)\,, \\ u &= \frac{1}{2}\big(3r - \sigma_{c,n}[s_{c,n}] - (t_{c,n} - u_{c,n})\,\tau_{c,n}[s_{c,n}]\big)\,. \end{aligned} \tag{6.46}$$

Since we require the mapping to be boundary preserving, the conditions

$$\begin{aligned} \tau_c[s_c] &= \frac{\kappa(\sigma_c[s_c])}{\kappa_c(s_c)}\,, \qquad \kappa_c(s_c) = \frac{\sqrt{\lambda(s_c, M_{\pi^\pm}^2, M_{\pi^\pm}^2)\,\lambda(s_c, M_{\pi^0}^2, M_\eta^2)}}{s_c}\,, \\ \tau_n[s_n] &= \frac{\kappa(\sigma_n[s_n])}{\kappa_n(s_n)}\,, \qquad \kappa_n(s_n) = \frac{\sqrt{\lambda(s_n, M_{\pi^0}^2, M_{\pi^0}^2)\,\lambda(s_n, M_{\pi^0}^2, M_\eta^2)}}{s_n}\,, \end{aligned} \tag{6.47}$$

will hold, which fix the functions $\sigma_{c,n}$ and $\tau_{c,n}$ in terms of each other. The kinematical function κ defined in the isospin limit is given in eq. (6.7). Except for the boundary

conditions on $\sigma_{c,n}$ imposing

$$\begin{aligned} 4M_\pi^2 &= \sigma_c[4M_{\pi^\pm}^2]\,, & (M_\eta - M_\pi)^2 &= \sigma_c[(M_\eta - M_{\pi^0})^2]\,, \\ 4M_\pi^2 &= \sigma_n[4M_{\pi^0}^2]\,, & (M_\eta - M_\pi)^2 &= \sigma_n[(M_\eta - M_{\pi^0})^2]\,, \end{aligned} \tag{6.48}$$

the functions $\sigma_{c,n}$ can be chosen freely. Adding a fixed DALITZ-plot center as further constraint ($x_{c,n} = y_{c,n} = 0 \mapsto x = y = 0$) the functions $\sigma_{c,n}$ can be parameterized by parabolas going through these three points, respectively.[#9] The explicit expressions of $\sigma_{c,n}$ can be found in ref. [152]. Obviously, the deformation of the decay region imposed by the kinematical map is strongly energy dependent. However, throughout the entire DALITZ-plot the deformation is small, at maximum we find a deviation of 3.3% for the charged and 5.8% for the neutral mode in the respective sets of MANDELSTAM variables.

So far we discussed the purely kinematic deformation of the physical DALITZ plot arising from the electromagnetic pion mass difference. This deformation affects the C-conserving and C-violating contributions of the amplitude $\mathcal{M}_1^C$, $\mathcal{M}_0^{\not C}$, and $\mathcal{M}_2^{\not C}$ in the same manner and will be compensated by the kinematic map specified in eq. (6.46). However, the C-conserving part $\mathcal{M}_1^C$ is affected by a second, qualitatively different contribution, stemming from electromagnetic $\eta \to 3\pi$ transitions. In order to correct for this effect we will again make use of the approach proposed in ref. [152].

ChPT allows us to study the electromagnetic corrections in $\eta \to 3\pi$ systematically by comparing the one-loop representation of GASSER and LEUTWYLER (GL) [233] worked out in the isospin limit with the one of DITSCHE, KUBIS and MEISSNER (DKM) [201] that accounts for electromagnetic effects including contributions of order $e^2\,(m_u - m_d)$. Based on the assumption that the electromagnetic effects in $\eta \to 3\pi$ approximately factorize we form the ratios[#10]

$$\mathcal{K}_{c,n}(s_{c,n}, t_{c,n}, u_{c,n}) \equiv \frac{\mathcal{M}_{c,n}^{\mathrm{DKM}}(s_{c,n}, t_{c,n}, u_{c,n})}{\mathcal{M}_{c,n}^{\mathrm{GL}}(s_{c,n}, t_{c,n}, u_{c,n})}\,, \tag{6.49}$$

which will serve as correction factors for $\mathcal{M}_1^C$ appearing in the amplitudes for the charged and neutral decay modes (6.13). Within the entire physical region these correction factors vary in the tight ranges $1.031 < |\mathcal{K}_c|^2 < 1.078$ and $0.972 < |\mathcal{K}_n|^2 < 0.978$. Accordingly, they affect the energy dependence of DALITZ-plot distributions only little. However, these corrections have an important effect on the decay rates (and therefore on the rate $\mathrm{BR}(\eta \to 3\pi^0)/\mathrm{BR}(\eta \to \pi^+\pi^-\pi^0)$ of the branching ratios), as $|\mathcal{K}_c|^2$ will increase the amplitude modulus square of the charged mode $|\mathcal{M}_c|^2$ on average by 7.2%, whereas $|\mathcal{K}_n|^2$ reduces the amplitude modulus square of the neutral mode $|\mathcal{M}_n|^2$ on average by 2.6%.

[#9] Note that the straightforward application of the kinematical map (6.46) for the neutral $\eta \to 3\pi^0$ decay mode meets a technical problem: since s, t, and u are treated on an unequal footage, the map does not respect BOSE symmetry. However, this shortcoming is easily cured by applying three crossed versions of the mapping according to

$$\begin{aligned} \mathcal{M}_n(s_n, t_n, u_n) = \tfrac{1}{3}\big\{&\mathcal{M}_n\big(\sigma_n[s_n], (t_n - u_n)\,\tau_n[s_n]\big) + \mathcal{M}_n\big(\sigma_n[t_n], (u_n - s_n)\,\tau_n[t_n]\big) \\ &+ \mathcal{M}_n\big(\sigma_n[u_n], (s_n - t_n)\,\tau_n[u_n]\big)\big\}\,. \end{aligned}$$

[#10] Note that the COULOMB pole is subtracted from the representation of $\mathcal{M}_c^{\mathrm{DKM}}$, thus the ratio (6.49) is finite across the entire DALITZ plot, *cf.* ref. [152].

6.3.3 Fit setup

In the next step we want to determine the free parameters of our dispersive representation of $\eta \to 3\pi$ by a χ^2-fit to the three sets of available data: the experimental measurements of the $\eta \to \pi^+\pi^-\pi^0$ and $\eta \to 3\pi^0$ DALITZ-plot distributions as well as the theory constraints on the TAYLOR invariants of $\mathcal{M}_1^C$ in the isospin limit. As discussed in sec. 6.3.1 the amplitudes $\mathcal{M}_1^C$, $\mathcal{M}_0^{\not C}$, and $\mathcal{M}_2^{\not C}$ together contain seven real-valued subtraction constants α, β, γ, $\mathrm{Re}\,\varepsilon$, $\mathrm{Im}\,\varepsilon$, $\mathrm{Re}\,\vartheta$, and $\mathrm{Im}\,\vartheta$ we have to fix in the following.

First of all we recognize that the reduced TAYLOR invariants of $\mathcal{M}_1^C$ (6.44) as well as the experimental measurements of the DALITZ-plot distributions do not constrain the physical normalization of the amplitude. Accordingly, the normalization of the C-conserving amplitude $\mathcal{M}_1^C$ is solely fixed by the information on $\mathrm{Re}\,F_0$, which links α, β, and γ in a linear relation, *cf.* eq. (6.39). Note that this condition imposed on α, β, and γ fixes the strength of the C-violating parts of the amplitude $\mathcal{M}_0^{\not C}$, and $\mathcal{M}_2^{\not C}$ determined by $\mathrm{Re}\,\varepsilon$, $\mathrm{Im}\,\varepsilon$, $\mathrm{Re}\,\vartheta$, and $\mathrm{Im}\,\vartheta$ relative to the C-conserving normalization of $\mathcal{M}_1^C$. It also becomes immediately clear that the number of independent parameters needed to describe the reduced TAYLOR invariants and DALITZ-plot distributions is effectively reduced to six.

The experimental measurements of the DALITZ-plot distributions provided by the KLOE-2 and A2 collaborations [240, 245] are given in terms of the dimensionless DALITZ-plot coordinates

$$x_{c,n} = \frac{\sqrt{3}}{2M_\eta\, Q_{c,n}}\,(t_{c,n} - u_{c,n})\,, \qquad y_{c,n} = \frac{3}{2M_\eta\, Q_{c,n}}\big[(M_\eta - M_{\pi^0})^2 - s_{c,n}\big] - 1\,, \tag{6.50}$$

where $Q_c = M_\eta - 2M_{\pi^\pm} - M_{\pi^0}$ and $Q_n = M_\eta - 3M_{\pi^0}$ are the available kinetic energies, *cf.* app. B. KLOE-2 split the phase space of $\eta \to \pi^+\pi^-\pi^0$ into a total of 371 rectangular bins (bins overlapping with the phase space boundary were disregarded), whereas A2 provides altogether 441 rectangular bins for one DALITZ-plot sextant exploiting the symmetry behaviour of $\eta \to 3\pi^0$ (bins overlapping with the phase space boundary were accepted). We label the i-th bin with the coordinates $x_{c,n}^i, y_{c,n}^i$ at its center and use $\mathcal{D}_{c,n}^{\mathrm{exp}}, \Delta\mathcal{D}_{c,n}^{\mathrm{exp}}$ for the bin content and its uncertainty. These values will now be compared to the DALITZ-plot distributions $\mathcal{D}_{c,n}^{\mathrm{DR}}$ obtained by an integration of our dispersive amplitudes $\mathcal{M}_{c,n}$ (6.13) over the respective bin

$$\mathcal{D}_{c,n}^{\mathrm{DR}}(x_{c,n}^i, y_{c,n}^i) = \int_{\mathrm{bin}\,\#i} \mathrm{d}x_{c,n}\,\mathrm{d}y_{c,n}\,|\mathcal{M}_{c,n}(x_{c,n}, y_{c,n})|^2\,. \tag{6.51}$$

Since the experimental distributions involve arbitrary normalizations, we have to introduce two additional parameters $\mathcal{N}_{c,n}$ that need to be fixed. The discrepancy functions are then defined by

$$\chi^2_{c,n} = \sum_i \left(\frac{\mathcal{D}_{c,n}^{\mathrm{exp}}(x_{c,n}^i, y_{c,n}^i) - \mathcal{N}_{c,n}\,\mathcal{D}_{c,n}^{\mathrm{DR}}(x_{c,n}^i, y_{c,n}^i)}{\Delta\mathcal{D}_{c,n}^{\mathrm{exp}}(x_{c,n}^i, y_{c,n}^i)} \right)^2, \tag{6.52}$$

where the sum extends over the 371 bins for the KLOE-2 and 441 bins for the A2 data sets, respectively.

For the ChPT constraints on the C-conserving reduced TAYLOR invariants we will use the discrepancy function

$$\chi_0^2 = \sum_i \left(\frac{f_i^{\mathrm{ChPT}} - \mathrm{Re}\, f_i^{\mathrm{DR}}}{\Delta f_i^{\mathrm{ChPT}}} \right)^2 , \tag{6.53}$$

where the summation index i runs from 1 to 3, f_i^{ChPT} denote the central values given in eq. (6.44), and $\Delta f_i^{\mathrm{ChPT}}$ their respective uncertainties. The invariants $\mathrm{Re}\, f_i^{\mathrm{DR}}$ are obtained from eq. (6.39) by a TAYLOR expansion of the OMNÈS representation for $\mathcal{M}_1^C$ (6.34). Accordingly, the subtraction constants of our dispersive representation and the additional normalizations $\mathcal{N}_{c,n}$ are determined by the minimum of the total discrepancy function

$$\chi^2_{\mathrm{tot}} = \chi_0^2 + \chi_c^2 + \chi_n^2 \,. \tag{6.54}$$

6.4 Comparison with experimental measurements and theoretical constraints

In the following we want to present the results of our dispersion theoretical analysis of $\eta \to 3\pi$. We consider four different scenarios for the χ^2-fit described in sec. 6.3.3: two exclusive fits to the charged DALITZ-plot distribution from KLOE-2 as well as two combined fits to all three sets of data. For both cases we perform individual fits taking only the C-conserving part of the amplitude $\mathcal{M}_c$ into account ($\mathcal{M}_0^{\not C}$ and $\mathcal{M}_2^{\not C}$ are tuned to zero) as well as the explicit consideration of C-violating effects in $\mathcal{M}_c$ (contributions from $\mathcal{M}_1^C$, $\mathcal{M}_0^{\not C}$, and $\mathcal{M}_2^{\not C}$ are allowed), *cf.* eq. (6.13). We label the different fit scenarios by: FIT1 (exclusive, C-conserving), FIT2 (exclusive, C-violating), FIT3 (combined, C-conserving), FIT2 (combined, C-violating). A summary of the individual χ^2 contributions to the four scenarios is given in tab. 6.1.

We find for all considered fit scenarios a good agreement of our dispersive amplitude with data. Overall the individual parts of the discrepancy function χ_0^2, χ_c^2, and χ_n^2 in the

	χ_0^2	χ_c^2	χ_n^2	dof	χ^2_{tot}/dof	p-value
FIT1	(1.222)	387.8	(509.5)	368	1.054	22.9%
FIT2	(1.222)	381.7	(509.5)	364	1.049	25.1%
FIT3	1.247	387.9	509.3	811	1.108	1.7%
FIT4	1.247	381.8	509.3	807	1.106	1.9%

Tab. 6.1: Summary of the four considered fit scenarios: FIT1 (exclusive, C-conserving), FIT2 (exclusive, C-violating), FIT3 (combined, C-conserving), FIT2 (combined, C-violating). For fits obtained by dropping the contributions of χ_0^2 and χ_n^2 to the total discrepancy function χ^2_{tot}, their values are put in brackets.

four different scenarios are almost identical. In fact the dispersive representation is already perfectly fixed by the KLOE-2 data on $\eta \to \pi^+\pi^-\pi^0$ alone with the $\eta \to 3\pi^0$ DALITZ-plot distribution and the TAYLOR invariants for $\mathcal{M}_1^C$ being a prediction in excellent agreement with data. Accordingly, the differences between the results for the exclusive and combined fits are marginal, *i.e.*, comparing FIT1 vs. FIT3 and FIT2 vs. FIT4. Taking the C-violating contributions into account, we find a slight improvement of χ_c^2 by 6.1 units whereas χ_0^2 and χ_n^2 do not change at all, *i.e.*, comparing FIT1 vs. FIT2 and FIT3 vs. FIT4. Consequently, adding the contributions of $\mathcal{M}_0^{\not C}$ and $\mathcal{M}_2^{\not C}$ to our dispersive representation for $\mathcal{M}_c$ has no visible effect on the determination of $\mathcal{M}_1^C$. Furthermore, comparing the resulting discrepancy functions of the KLOE-2 and A2 data sets, we notice a slightly worse description of the DALITZ-plot distribution for the neutral $\eta \to 3\pi^0$ mode. This small tension of the dispersive representation for $\mathcal{M}_n$ and the experimental measurement from A2 has also been observed in ref. [152]. Nevertheless, the experimental data of both the charged and neutral mode together are well described by our dispersive representation.

Based on the findings discussed in the previous paragraph, the results presented below will be taken exclusively from FIT4. Moreover, the quoted total uncertainties of the investigated observables draw from the following sources: the experimental errors from the KLOE-2 and A2 DALITZ-plot distributions,[#11] the uncertainty originating from ChPT constraints including the TAYLOR invariants for $\mathcal{M}_1^C$ (6.44) and the electromagnetic correction factors $\mathcal{K}_{c,n}$ (6.49), and the uncertainty resulting from the variation of the phase shift input in the low- and high-energy region, *cf.* fig. 6.1. We will treat all these sources of error as symmetric and GAUSSIAN distributed. Accordingly, the combined total uncertainties are found by adding the individual contributions in quadrature and the presented correlation matrices are calculated from the respective total covariance matrices of the investigated observables.

6.4.1 Dalitz-plot distributions of $\mathcal{M}_c$ and $\mathcal{M}_n$

Considering the tiny influence on the discrepancy function when allowing for the effects of the C-violating amplitudes $\mathcal{M}_0^{\not C}$ and $\mathcal{M}_2^{\not C}$ we already note that their contributions to the $\eta \to \pi^+\pi^-\pi^0$ DALITZ-plot distribution is marginal, *cf.* tab. 6.1. A comparison of the dispersive DALITZ-plot distributions of the full amplitude $\mathcal{M}_c$ and the C-conserving part only $\mathcal{M}_1^C$ with the experimental measurement from KLOE-2 is depicted in fig. 6.2.

According to the definition of $\mathcal{M}_c$ given in eq. (6.13) we can decompose its DALITZ-plot distribution into

$$\begin{aligned}\left|\mathcal{M}_c(x_c,y_c)\right|^2 = \left|\mathcal{M}_1^C\right|^2 + 2\mathrm{Re}\left[\mathcal{M}_1^C\,(\xi^{-1}\mathcal{M}_0^{\not C})^*\right] + 2\mathrm{Re}\left[\mathcal{M}_1^C\,(\xi^{-1}\mathcal{M}_2^{\not C})^*\right] \\ + \left|\xi^{-1}\mathcal{M}_0^{\not C}\right|^2 + \left|\xi^{-1}\mathcal{M}_2^{\not C}\right|^2 + 2\mathrm{Re}\left[\xi^{-1}\mathcal{M}_0^{\not C}\,(\xi^{-1}\mathcal{M}_2^{\not C})^*\right],\end{aligned} \tag{6.55}$$

where for the sake of simplicity dependencies on x_c and y_c are dropped on the right-hand side. Note that the terms are ordered according to their powers in the C-violating effects

[#11] The A2 collaboration provided us with three independent sets of their data, so we gained control on the statistical and systematical uncertainties of their analysis. In case of the KLOE-2 data set we will consider only the statistical errors.

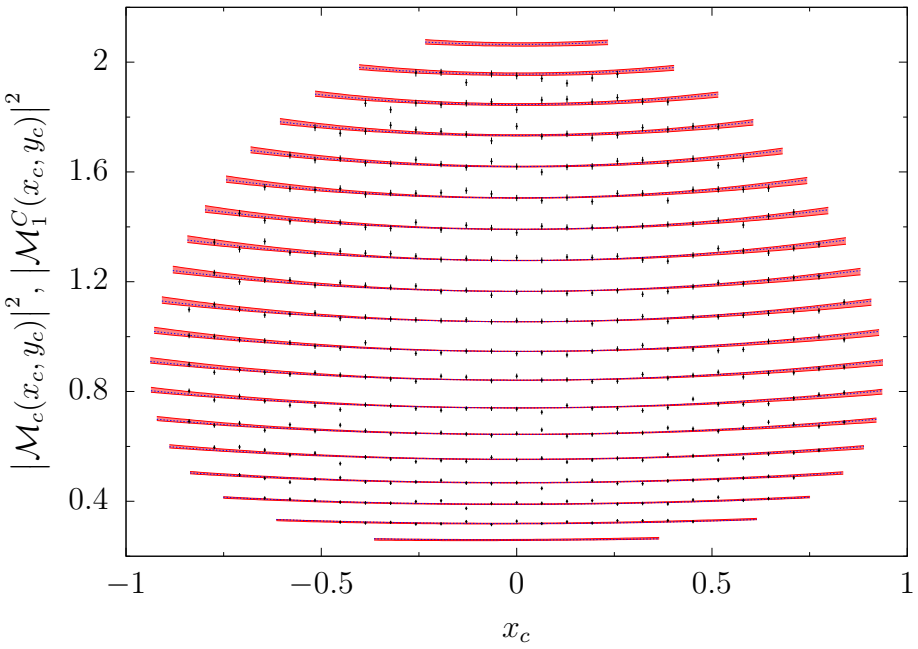

Fig. 6.2: Comparison of the dispersive DALITZ-plot distribution for $\eta \to \pi^+\pi^-\pi^0$ to experimental data. The distributions are normalized to one at the DALITZ-plot center $x_c = y_c = 0$. From the top to the bottom we depict slices through the DALITZ plot given for $y_c^{\min} = -0.95$ to $y_c^{\max} = 0.85$ at distances of $\Delta y_c = 0.1$. We show the modulus square of the full amplitude $|\mathcal{M}_c|^2$ with its uncertainty band covering the statistical and systematical errors added in quadrature (red) as well as the central solution for the C-conserving part $|\mathcal{M}_1^C|^2$ (blue). The 371 data points with error bars (black) were provided by the KLOE-2 collaboration [240].

$\mathcal{M}_0^{\not C}$ and $\mathcal{M}_2^{\not C}$. Since we have full control on the amplitudes $\mathcal{M}_1^C$, $\mathcal{M}_0^{\not C}$, and $\mathcal{M}_2^{\not C}$ appearing in eq. (6.55), we can study their disentangled contributions to the DALITZ-plot distribution individually, *cf.* fig. 6.3. We observe a clear hierarchy of these contributions: obviously, the C-conserving SM part determined by $\mathcal{M}_1^C$ is dominating. The two terms linear in the C-violating amplitudes $\mathcal{M}_0^{\not C}$ and $\mathcal{M}_2^{\not C}$ are suppressed by three orders of magnitude, while all remaining terms quadratic in C-violation are suppressed by five to six orders of magnitude. We want to emphasize that only the two contributions linear in the C-violating effects determine the size of the mirror symmetry breaking of the DALITZ-plot distribution under $t \leftrightarrow u$. Furthermore, we find both contributions to be of similar size, *i.e.*, the interference effect of $\mathcal{M}_1^C$ with $\mathcal{M}_0^{\not C}$ compared to the interference $\mathcal{M}_1^C$ with $\mathcal{M}_2^{\not C}$. Accordingly, $\mathcal{M}_0^{\not C}$ and $\mathcal{M}_2^{\not C}$ are of the same order of magnitude. Like the SM contribution $|\mathcal{M}_1^C|^2$, all effects quadratic in C-violation are symmetric under $t \leftrightarrow u$ and will therefore not contribute to the mirror symmetry breaking. As these effects are suppressed by five to six orders of magnitude compared to $|\mathcal{M}_1^C|^2$, we can safely neglect them from now on.

The DALITZ-plot distribution of $\mathcal{M}_c$ is conveniently parameterized in terms of a polynomial expansion at the DALITZ-plot center $x_c = y_c = 0$, *cf.* app. B. By now the first

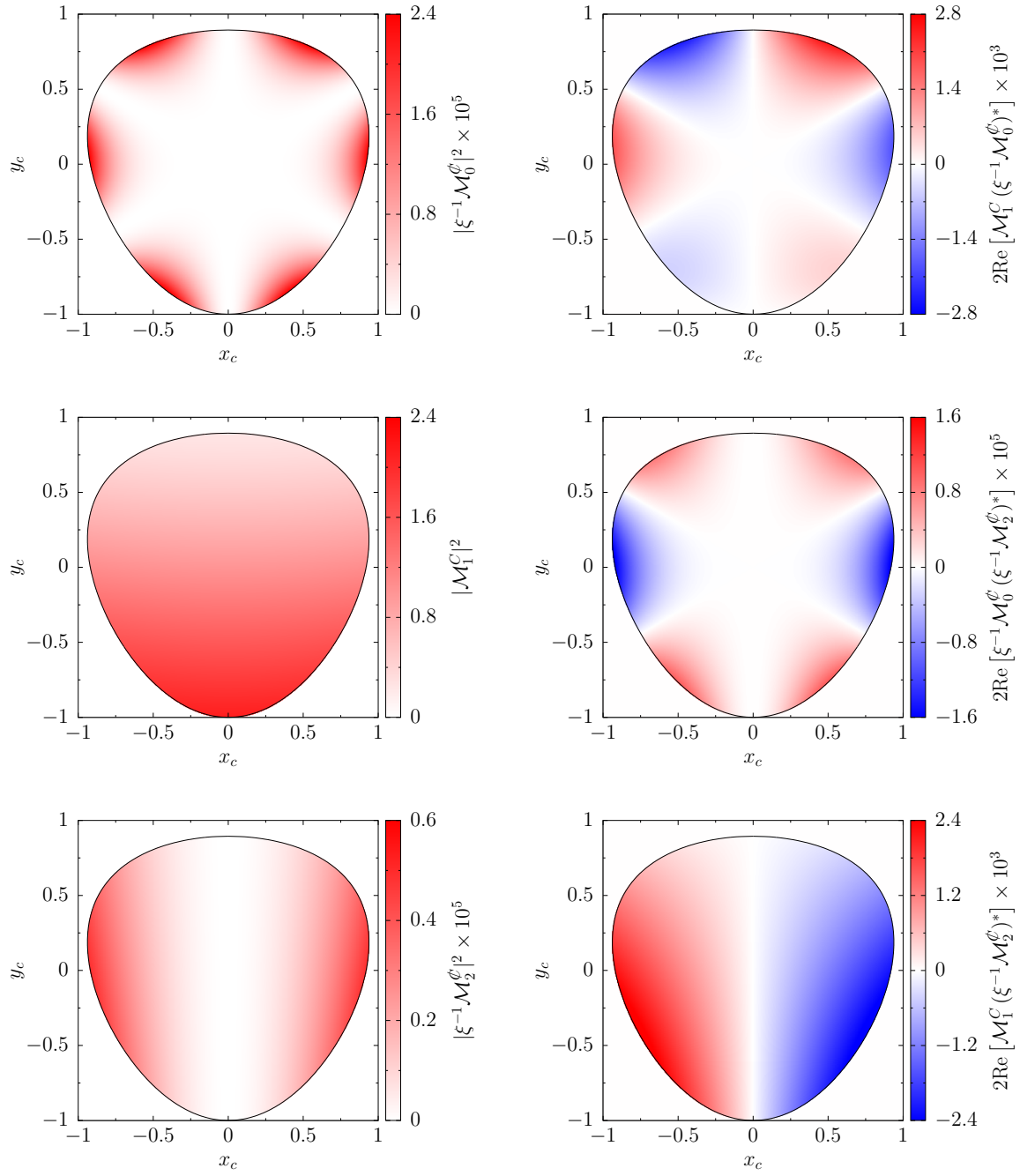

Fig. 6.3: Decomposition of the DALITZ-plot distributions contributing to $|\mathcal{M}_c|^2$ as given in eq. (6.55). The normalization of $|\mathcal{M}_c|^2$ is fixed to one at the DALITZ-plot center. All panels show the central solution of our dispersive representation. The by far dominant contribution stemming from the C-conserving part $|\mathcal{M}_1^C|^2$ is depicted in the center left panel. Interference terms of $\mathcal{M}_1^C$ with $\mathcal{M}_0^{\not C}$ and $\mathcal{M}_2^{\not C}$ giving rise to the breaking of mirror symmetry in the DALITZ-plot are displayed in the top and bottom right panels. Note that the scales of the individual contributions differ by several orders of magnitude.

seven coefficients of this phenomenological parameterization

$$|\mathcal{M}_c(x_c, y_c)|^2 \sim 1 + a\, y_c + b\, y_c^2 + c\, x_c + d\, x_c^2 + e\, x_c\, y_c + f\, y_c^3 + g\, x_c^2\, y_c + h\, x_c\, y_c^2 + l\, x_c^3 + \dots\,, \tag{6.56}$$

valid up to third order in x_c and y_c, have been studied by the KLOE-2 collaboration [240]. Note that non-vanishing values of the coefficients c, e, h, and l odd in x_c would directly implicate that C-conjugation symmetry is violated in $\eta \to \pi^+\pi^-\pi^0$ decays. We perform a two-dimensional Taylor expansion of our dispersive amplitude $\mathcal{M}_c$ and determine the C-conserving Dalitz-plot parameters generated exclusively by $\mathcal{M}_1^C$ to be

$$\begin{array}{rr|rrrrr} a = & -1.0819(14) & 1.00 & -0.06 & 0.39 & -0.47 & -0.37 \\ b = & 0.1487(34) & & 1.00 & 0.57 & -0.66 & -0.60 \\ d = & 0.088(13) & & & 1.00 & -0.92 & -0.99 \\ f = & 0.1131(47) & & & & 1.00 & 0.90 \\ g = & -0.068(15) & & & & & 1.00 \end{array} \,. \tag{6.57}$$

The uncertainties of the parameters b, d, and g are completely driven by the variation of the phase shift input, while the uncertainties of a and f gain sizeable contributions from all sources of error.

Similarly, for the C-violating Dalitz-plot parameters generated by the interference effects of $\mathcal{M}_1^C$ with $\mathcal{M}_0^{\not C}$ and $\mathcal{M}_2^{\not C}$ we find

$$\begin{array}{rr|rrrr} c = & -0.0021(13) & 1.00 & -0.25 & -0.20 & -0.08 \\ e = & 0.0034(34) & & 1.00 & -0.44 & 0.22 \\ h = & 0.0053(69) & & & 1.00 & -0.75 \\ l = & -0.0028(21) & & & & 1.00 \end{array} \,. \tag{6.58}$$

The uncertainties of these four parameters are dominated by the statistical error of the KLOE-2 data, while all other sources of uncertainty do not yield any significant contribution to the error budget.[#12] Accordingly, we can confirm that all C-violating parameters vanish within 1.6σ at most. Furthermore, the C-violating parameters turn out to be one order of magnitude smaller than d and g, which are the smallest coefficients of the C-conserving part of the parameterization (6.57). Separating the individual contributions to the central values of c, e, h, and l originating from the interference effect of $\mathcal{M}_1^C$ with $\mathcal{M}_0^{\not C}$ we find

$$c = +0.0002\,, \qquad e = +0.0011\,, \qquad h = +0.0055\,, \qquad l = -0.0027\,, \tag{6.59}$$

whereas the interference of $\mathcal{M}_1^C$ with $\mathcal{M}_2^{\not C}$ yields

$$c = -0.0023\,, \qquad e = +0.0023\,, \qquad h = -0.0002\,, \qquad l = -0.0001\,. \tag{6.60}$$

A comparison of the extracted Dalitz-plot parameters with the results from KLOE-2 as well as the two most recent dispersive analyses on C-conserving $\eta \to 3\pi$ decays [151, 152] are summarized in tab. 6.2.

[#12] Note that the estimated correlations between the C-conserving and C-violating parameters given in eqs. (6.57) and (6.58) are below 1%.

For completeness we also want to consider the DALITZ-plot distribution of the neutral $\eta \to 3\pi^0$ mode. In accordance with the discussion in app. B the phenomenological parameterization in terms of the coordinates z_n and ϕ_n is given by

$$|\mathcal{M}_n(z_n, \phi_n)|^2 \sim 1 + 2\alpha\, z_n + 2\beta\, z_n^{3/2} \sin 3\phi_n + 2\gamma\, z_n^2 + \dots\,, \tag{6.61}$$

accounting for terms up to fourth order in x_n and y_n. Again, we perform a two-dimensional TAYLOR expansion of our dispersive representation yielding

$$\begin{array}{r|lll} \alpha = -0.0293(31) & 1.00 & -0.77 & 0.87 \\ \beta = -0.0043(8) & & 1.00 & -0.95 \\ \gamma = 0.0033(7) & & & 1.00 \end{array}\,. \tag{6.62}$$

Our determination of the slope parameter α agrees well with the PDG world average [14]. Similarly, our value of β is compatible with the extraction of the A2 collaboration [245] and the dispersive analysis of ref. [152]. For our value of γ we find some tension when comparing to other determinations, *e.g.* $\gamma = 0.0019(3)$ taken from ref. [152]. However, the extraction of this parameter is already far beyond the scope of the present analysis.

Finally, we briefly want to discuss the ratio $\mathrm{BR}(\eta \to 3\pi^0)/\mathrm{BR}(\eta \to \pi^+\pi^-\pi^0)$ that is used as an internal consistency check for the electromagnetic corrections described in sec. 6.3.2. The partial decay widths $\Gamma_{c,n}$ of the $\eta \to 3\pi$ process are defined by

$$\Gamma_{c,n}(\eta \to 3\pi) = \frac{Q_{c,n}^2\, \xi^2}{384\sqrt{3}\pi^3 M_\eta}\, \frac{\mathcal{D}_{c,n}}{S_{c,n}}\,, \qquad \mathcal{D}_{c,n} = \int_{\mathrm{DP}} \mathrm{d}x_{c,n}\, \mathrm{d}y_{c,n}\, |\mathcal{M}_{c,n}(x_{c,n}, y_{c,n})|^2\,, \tag{6.63}$$

where $S_c = 1$ and $S_n = 6$ denoting the symmetry factors and $\mathcal{D}_{c,n}$ the integrals of the DALITZ-plot distributions over the full phase space. Since contributions antisymmetric under $t \leftrightarrow u$ cancel, $\mathcal{D}_c$ is determined entirely by $|\mathcal{M}_1^C|^2$. We extract

$$\frac{\mathrm{BR}(\eta \to 3\pi^0)}{\mathrm{BR}(\eta \to \pi^+\pi^-\pi^0)} = 1.423(48) \tag{6.64}$$

in perfect agreement with the PDG world average [14]. Note that the uncertainty quoted in eq. (6.64) is totally dominated by the errors on $\mathcal{K}_{c,n}$ (6.49).

	$-a$	b	$-c$	d	e	f	$-g$	h	l
KLOE-2	1.095(3)	0.145(3)	0.004(3)	0.081(3)	0.003(3)	0.141(7)	0.044(9)	0.011(9)	0.001(7)
DR Orsay	1.142	0.172	-	0.097	-	0.122	0.089	-	-
DR Bern	1.081(2)	0.144(4)	-	0.081(3)	-	0.118(4)	0.069(4)	-	-
this work	1.082(1)	0.149(3)	0.002(1)	0.088(13)	0.003(3)	0.113(5)	0.068(15)	0.005(7)	−0.003(2)

Tab. 6.2: Comparison of the DALITZ-plot parameters obtained in different analysis of the KLOE-2 data [240]. The values given in the first row are obtained by a direct fit of (6.56) to data. The dispersive analyses from the Orsay [151] and Bern groups [152] consider the C-conserving amplitude $\mathcal{M}_1^C$ only.

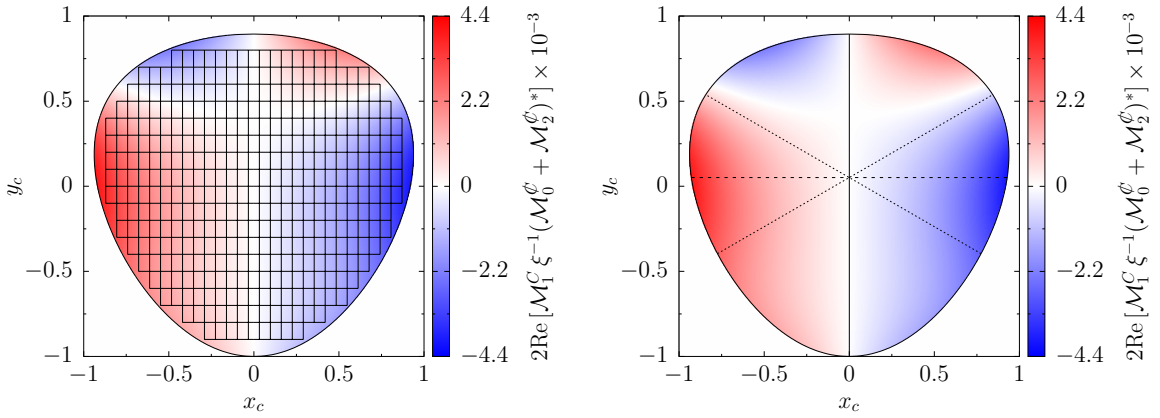

Fig. 6.4: Left panel: the illustration of the two-dimensional x_c-y_c grid used by the KLOE-2 collaboration for the binned Dalitz-plot distribution. In total this grid contains 371 bins. Note that KLOE-2 disregarded all bins that overlap with the phase-space boundary. Right panel: the Dalitz-plot geometry split into the sectors needed to probe its asymmetry parameters. The left-right asymmetry A_{LR} compares the population of the left and right halves divided by the line of $t_c = u_c$ (solid vertical line), A_Q the quadrants divided by $t_c = u_c$ and $s_c = r_c$ (solid vertical and dashed horizontal lines), and A_S the sextants divided by $t_c = u_c$, $s_c = t_c$, and $s_c = u_c$ (solid vertical and dashed diagonal lines). In both panels we depict the C-violating interference effects of $\mathcal{M}_1^C$ with $\mathcal{M}_0^{\not C}$ and $\mathcal{M}_2^{\not C}$.

6.4.2 Asymmetries and coupling strengths of $\mathcal{M}_0^{\not C}$ and $\mathcal{M}_2^{\not C}$

So far we studied the C-violating effects in the Dalitz-plot distribution by extracting the x_c-odd coefficients c, e, h, and l of the phenomenological parameterization (6.56). Besides these coefficients, we can also investigate three asymmetry parameters to quantify C-violating effects in the $\eta \to \pi^+\pi^-\pi^0$ Dalitz-plot distribution: the left-right A_{LR}, the quadrant A_Q, and sextant A_S asymmetry parameters [223, 225, 238]. These asymmetries compare the population of the Dalitz-plot distribution in the different sectors defined by the Dalitz-plot geometry, *cf.* fig. 6.4. For our dispersive representation of $\mathcal{M}_c$ we obtain

$$\left.\begin{aligned} A_{LR} &= -7.6(4.7) \\ A_Q &= 4.1(4.3) \\ A_S &= 3.7(4.3) \end{aligned}\right| \begin{array}{ccc} 1.00 & -0.44 & 0.35 \\ & 1.00 & -0.43 \\ & & 1.00 \end{array} , \tag{6.65}$$

where all three asymmetry parameters are given in units of 10^{-4}. We find A_{LR}, A_Q, and A_S in good agreement with the results reported by the KLOE-2 collaboration [240]. Again, there is no hint for C-violation as all three asymmetries are compatible with zero in not more than 1.6σ. Note that the error budget in eq. (6.65) is completely dominated by the statistical uncertainties of the KLOE-2 data.[#13]

[#13] In fact KLOE-2 reports that the systematic uncertainty of A_{LR} dominates the statistical one. Like the results for A_Q and A_S, A_{LR} is therefore compatible with zero in less than one-σ if systematic effects are taken into account.

In contrast to experimental studies of C-violating effects in the $\eta \to \pi^+\pi^-\pi^0$ DALITZ-plot distribution, which are limited to the investigation of x_c-odd coefficients of the phenomenological parameterization (6.56) or the probe of the DALITZ-plot asymmetries, our dispersion theoretical analysis provides us with the tools to disentangle the individual contributions of $\mathcal{M}_0^{\not C}$ and $\mathcal{M}_2^{\not C}$. Furthermore, we are in the position to extract coupling strengths of the underlying isoscalar and isotensor BSM operators. A matching of eq. (6.1) to the expansions (6.40) and (6.42) allows us to relate these operators to

$$X_0^{\not C} = -G_0\,(s-t)(u-s)(t-u)\,, \qquad X_2^{\not C} = H_0\,(t-u)\,, \tag{6.66}$$

where the TAYLOR invariants G_0 and H_0 determined by $\mathcal{M}_0^{\not C}$ and $\mathcal{M}_2^{\not C}$ can be identified with the respective BSM coupling strengths. For our dispersive representation we obtain

$$\begin{array}{l|llll} \xi^{-1}\,\mathrm{Re}\,G_0/\mathrm{GeV}^{-6} = \quad 23.3(25.6) & 1.00 & -0.93 & 0.72 & -0.72 \\ \xi^{-1}\,\mathrm{Im}\,G_0/\mathrm{GeV}^{-6} = -47.7(89.8) & & 1.00 & -0.74 & 0.74 \\ \xi^{-1}\,\mathrm{Re}\,H_0/\mathrm{GeV}^{-2} = \quad 6.9(109.8)\times 10^{-3} & & & 1.00 & -0.99 \\ \xi^{-1}\,\mathrm{Im}\,H_0/\mathrm{GeV}^{-2} = \quad 47.5(298.7)\times 10^{-3} & & & & 1.00 \end{array}\,. \tag{6.67}$$

Note that for the central values we find a ratio of $|G_0/H_0| \approx 10^3\,\mathrm{GeV}^{-4}$. Since the operator $X_0^{\not C}$ is kinematically suppressed compared to $X_2^{\not C}$ at small energies, we conclude that the magnitudes of G_0 and H_0 are tuned such that the kinematical suppression is overcome, *cf.* fig. 6.3 and eq. (6.66). This behavior of the amplitudes $\mathcal{M}_0^{\not C}$ and $\mathcal{M}_2^{\not C}$ has also been observed in ref. [243].

Carrying out the phase space integrals individually for contributions involving interference effects of $\mathcal{M}_0^{\not C}$ or $\mathcal{M}_2^{\not C}$ in the DALITZ-plot distribution, we can relate the asymmetry parameters (6.65) given in units of 10^{-4} to the coupling strengths of the isoscalar and isotensor BSM operators (6.66) according to

$$\begin{aligned} A_{LR} &= \xi^{-1}\big(0.132\,\mathrm{Re}\,G_0 + 0.042\,\mathrm{Im}\,G_0 - 0.349\,\mathrm{Re}\,H_0 - 0.131\,\mathrm{Im}\,H_0\big)\,, \\ A_Q &= \xi^{-1}\big(-0.067\,\mathrm{Re}\,G_0 - 0.062\,\mathrm{Im}\,G_0 + 0.075\,\mathrm{Re}\,H_0 + 0.047\,\mathrm{Im}\,H_0\big)\,, \\ A_S &= \xi^{-1}\big(0.416\,\mathrm{Re}\,G_0 + 0.119\,\mathrm{Im}\,G_0 - 0.008\,\mathrm{Re}\,H_0 - 0.006\,\mathrm{Im}\,H_0\big)\,. \end{aligned} \tag{6.68}$$

In these relations G_0 and H_0 enter in units of $1\,\mathrm{GeV}^{-6}$ and $10^{-3}\,\mathrm{GeV}^{-2}$, respectively. Equation (6.68) reveals that especially the sextant asymmetry parameter A_S is sensitive to contributions generated by $\mathcal{M}_0^{\not C}$, while effects of $\mathcal{M}_2^{\not C}$ are surpressed. Separating for contributions of $\mathcal{M}_0^{\not C}$ or $\mathcal{M}_2^{\not C}$ to the central values of the asymmetry parameters, we find

$$A_{LR} = 1.1\,, \qquad A_Q = 1.4\,, \qquad A_S = 4.0\,, \tag{6.69}$$

for interference effects of $\mathcal{M}_1^C$ with $\mathcal{M}_0^{\not C}$, whereas the interference of $\mathcal{M}_1^C$ with $\mathcal{M}_2^{\not C}$ yields

$$A_{LR} = -8.7\,, \qquad A_Q = 2.7\,, \qquad A_S = -0.3\,. \tag{6.70}$$

Once more, all asymmetry parameters are given in units of 10^{-4}.

6.4.3 Taylor invariants and the Adler zero of $\mathcal{M}_1^C$

Analogous to the extraction of the C-violating Taylor invariants G_0 and H_0 of the amplitudes $\mathcal{M}_0^{\not C}$, we now want to discuss the C-conserving invariants of the SM part $\mathcal{M}_1^C$. First of all, the invariant F_0 used to fix normalization is given by

$$F_0 = 1.176(53) - 0.0094(14)\, i\,. \tag{6.71}$$

Note that only $\mathrm{Re}\, F_0$ is fixed by the imposed normalization condition, while $\mathrm{Im}\, F_0$ is allowed to vary freely, *cf.* sec. 6.3.1. Since $\mathrm{Im}\, F_0$ is exclusively generated by contributions of the dispersion integrals to eq. (6.34), it is roughly two orders of magnitude smaller than $\mathrm{Re}\, F_0$. For the real parts of the reduced coefficients f_i we find

$$\left.\begin{array}{rr|ccc} \mathrm{Re}\, f_1/\,\mathrm{GeV}^{-2} = & 4.34(15) & 1.00 & 0.24 & -0.13 \\ \mathrm{Re}\, f_2/\,\mathrm{GeV}^{-4} = & 12.99(52) & & 1.00 & 0.03 \\ \mathrm{Re}\, f_3/\,\mathrm{GeV}^{-4} = & 7.54(59) & & & 1.00 \end{array}\right| \,, \tag{6.72}$$

which are in good agreement with the prediction of one-loop ChPT (6.44). In contrast to the dispersive representation of ref. [152], which uses a subtraction scheme for $\mathcal{M}_1^C$ involving six independent subtraction constants, our minimalistic scheme (6.34) is extremely stiff. Therefore it does not allow for a large variation of the reduced Taylor invariants, *cf.* tab. 6.1. Similar to $\mathrm{Im}\, F_0$ the imaginary parts of the reduced invariants are found to be small

$$\mathrm{Im}\, f_1 = 0.193(29)\,\mathrm{GeV}^{-2}\,, \quad \mathrm{Im}\, f_2 = -0.006(85)\,\mathrm{GeV}^{-4}\,, \quad \mathrm{Im}\, f_3 = -0.128(39)\,\mathrm{GeV}^{-4}\,. \tag{6.73}$$

Finally, we want to consider the behavior of $\mathcal{M}_1^C$ at its soft-pion point, *i.e.*, in the limit where the four-momentum of one of the pions vanishes. Since the strong process $\eta \to \pi^i\pi^j + \pi^k(p^\mu)$ is of isospin breaking nature, it has to be mediated by the scalar quark operator $S_3 = \bar{q}\lambda^3 q$, *cf.* eq. (1.12). At the soft-pion point $p^\mu \to 0$ arguments of current algebra (*cf.* sec. 1.3) dictate the behavior of the T-matrix element (6.8)

$$\lim_{p^\mu \to 0} \mathcal{T}_C^{ijk}(s,t,u) \sim \langle \pi^i\pi^j + \pi^k(p^\mu) | \bar{q}\{\lambda^k, \lambda^3\}\gamma_5 q | \eta \rangle\,. \tag{6.74}$$

Since the anti-commutator on the right-hand side vanishes except if $k = 3$, the amplitude $\mathcal{M}_1^C$ exhibits a zero if the momentum of one of the charged pions vanishes. In terms of the Mandelstam variables we will find two Adler zeros at $s_A = t_A = 0$ and $s_A = u_A = 0$ connected by crossing symmetry. These zeros are protected by chiral $\mathrm{SU}(2)_L \times \mathrm{SU}(2)_R$ flavor symmetry, hence their positions are only subject to corrections of order M_π^2 if the pion mass is turned on again. At tree level the amplitude is given by [246]

$$\mathcal{M}_1^C(s,t,u) = \frac{3s - 4M_\pi^2}{M_\eta^2 - M_\pi^2}\,, \tag{6.75}$$

hence it exhibits a zero crossing at $s_A = \frac{4}{3}M_\pi^2$. A study of one-loop ChPT yields a slight shift of the Adler zero to $s_A \approx 1.4 M_\pi^2$ [233].

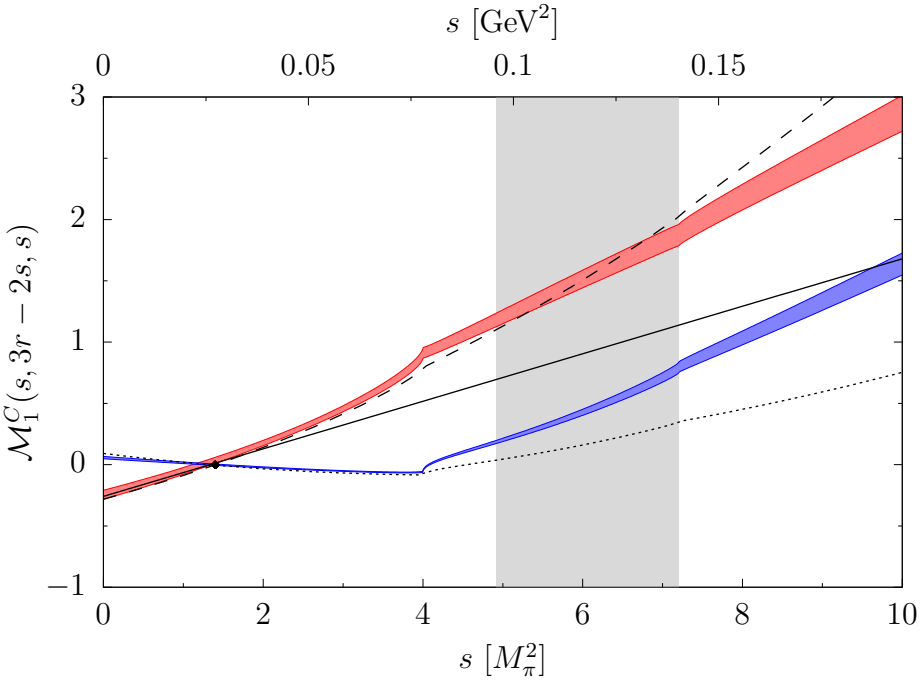

Fig. 6.5: Comparison of the dispersive amplitude $\mathcal{M}_1^C$ with the respective tree and one-loop level expressions obtained from ChPT along the critical line $s = u$. The real and imaginary parts of the dispersive amplitude are given by the red and blue bands, which cover the range of statistical and systematical uncertainties added in quadrature. The tree level result is depicted by the solid black line, while the one-loop real part is given by the dashed and the imaginary part by the dotted black lines. The black diamond denotes the position of the Adler zero in one-loop ChPT. The physically allowed region for the $\eta \to 3\pi$ decay is depicted by the gray area.

In fig. 6.5 the behavior of our dispersive representation for $\mathcal{M}_1^C$ along the critical line $s = u$ is compared to the tree level and one-loop predictions of ChPT. We extract the zero crossing of the dispersive representation at

$$\begin{array}{rl|cc} s_A/M_\pi^2 = & 1.29(13) & 1.00 & -0.85 \\ (s_A - t_A)/M_\pi^2 = & -0.057(15) & & 1.00 \end{array}, \tag{6.76}$$

which is in perfect agreement with the ChPT prediction. Nevertheless, we want to mention that the Adler zeros are shifted slightly away from the critical lines $s = t$ and $s = u$. The dominating error source in eq. (6.76) stems from the low- and high-energy uncertainties of the phase shift input, *cf.* fig. 6.1.

6.5 Summary and conclusion

We analyzed C- and CP-violating effects in $\eta \to \pi^+\pi^-\pi^0$ decays in a dispersion theoretical framework. In this framework the amplitude can be decomposed into three contributions $\mathcal{M}_1^C$, $\mathcal{M}_0^{\not C}$, and $\mathcal{M}_2^{\not C}$, describing the C-conserving $\Delta I = 1$ SM and C-violating $\Delta I = 0, 2$

BSM transitions, respectively. Analyticity and unitarity constrain these amplitudes by the dynamical information on the strong two-body $\pi\pi$ scattering phase shifts and a fixed number of subtraction constants determine the normalizations of $\mathcal{M}_1^C$, $\mathcal{M}_0^{\not{C}}$, and $\mathcal{M}_2^{\not{C}}$ as well as containing some information on the energy dependence of $\mathcal{M}_1^C$. Therefore our dispersive representation can be seen as superior compared to a simple phenomenological parameterization with an *a priori* unknown number of relevant coefficients. We demonstrated that our representation allows for a good description of the high-statistics measurement $\eta \to \pi^+\pi^-\pi^0$ DALITZ-plot distribution provided by the KLOE-2 collaboration [240]. Moreover, our framework allows us to disentangle of the individual $\Delta I = 0$ and $\Delta I = 2$ contributions systematically. To current precision of experimental data we are able to limit the patterns of C- and CP-violation in the DALITZ-plot distribution generated by interference effects of $\mathcal{M}_1^C$ with $\mathcal{M}_0^{\not{C}}$ and $\mathcal{M}_2^{\not{C}}$ to the per mille level. These in turn, allowed us to extract coupling strengths of the underlying effective isoscalar and isotensor BSM operators. In principle, an identification of these effective operators with fundamental BSM operators on the quark level, which is still pending, would allow to predict a scale for BSM physics [247–252]. We conclude that our framework opens a window on the systematic analysis of C- and CP-violation in $\eta \to \pi^+\pi^-\pi^0$ decays provided by future high-statistics experimental measurements [253–256].

Similar considerations could also be made for decays of the heavier η', which carries the same quantum numbers as the η. Thus, the $\eta' \to \pi^+\pi^-\pi^0$ transition is also mediated by the C-conserving $\Delta I = 1$ SM or C-violating $\Delta I = 0, 2$ BSM operators. Especially the increased phase space of this decay process might yield to a resonance enhancement of the isoscalar amplitude induced by the $\rho(770)$, which could be tested. However, compared to $\eta \to \pi^+\pi^-\pi^0$ the experimental data currently available on $\eta' \to \pi^+\pi^-\pi^0$ is rather limited [257], making it impossible to extract any meaningful bounds on C- and CP-violating operators at this point. Another possible decay of the η' that could be tested is $\eta' \to \pi^+\pi^-\eta$. Recently, a high-statistics measurement of this process has been performed by the BESIII collaboration [221]. Since this transition preserves G-parity, either isospin and C-conjugation symmetry are simultaneously conserved or violated. Therefore, decays of $\eta' \to \pi^+\pi^-\eta$ are sensitive to another class of C- and CP-violating BSM operators, mediating isospin-breaking $\Delta I = 1$ transitions. A combined dispersion theoretical analysis of C- and CP-violating transitions in η and η' decays is currently in preparation [258].

Part IV

Decays of vector mesons into three pions

Chapter 7

Quark-mass dependence in $\omega \to 3\pi$ decays[#1]

Despite tremendous progress in simulating QCD on space-time lattices using physical quark masses, many studies of complicated observables within lattice QCD are still performed with light quarks that are heavier than they are in the real world (*cf. e.g.* refs. [260, 261] for reviews). To extrapolate such simulations to the physical point, additional theoretical input is required, which should ideally be based on systematically improvable effective field theories. At low energies, the effective field theory that controls the quark-mass dependence by construction is ChPT [72, 73], which describes the interactions of the Nambu–Goldstone Bosons of spontaneous chiral symmetry breaking, the pions as well as kaons and the η, *cf.* ch. 1.

However, the vast majority of states in QCD are resonances, and to perform *chiral extrapolations* for these is less straightforward. A popular tool in this regard has been to employ unitarized versions of ChPT, such as the inverse amplitude method (IAM) [262–265]: a resummation of higher-order effects obeying S-matrix unitarity allows one to generate poles on unphysical Riemann sheets in the complex-energy plane, the signatures of resonances, *cf.* ch. 2. The IAM can be justified using dispersion theory; scattering amplitudes constructed via the IAM match smoothly on the ChPT expansion at low energies. In this manner, the properties of elastic resonances such as the $f_0(500)$ and the $\rho(770)$ in $\pi\pi$ as well as the $K_0^*(700)$ and $K^*(892)$ in πK scattering have been investigated with respect to their quark-mass dependence [266, 267].

Nevertheless, by far not all hadronic resonances appear in two-body scattering processes. The lightest resonance that decays only into a three-body final state (in QCD in the isospin limit) is the $\omega(782)$, with its dominant decay $\omega \to 3\pi$. Clearly, the quark-mass dependence of the ω cannot be assessed within an IAM-type formalism; it could at best be studied within the appropriate partial wave of the $3\pi \to 3\pi$ scattering process, and the formalism to study such processes on the lattice is currently under intense investigation [268–274]. In this chapter, we suggest an approach to assess the quark-mass dependence of the $\omega \to 3\pi$ decay amplitude based on Khuri–Treiman equations, *cf.* chs. 4 and 5. These equations require the two-body P-wave $\pi\pi$ scattering phase shift as

[#1] The contents of this chapter have been published in [259].

input, which we extract from the known quark-mass-dependent IAM partial wave. While we still need to rely on effective field theory ideas to describe the variation of the ω *mass* with the quark masses, the dispersive framework allows us to predict its quark-mass-dependent *width*. The idea to employ dispersion theory to extend the applicability of IAM-generated phase shifts is not new: it has already been applied to describe the pion vector form factor [275], as well as, in a formalism closely related to what we present here, to the reaction $\gamma\pi \to \pi\pi$ [144, 276].

The outline of this chapter is as follows: we recall the description of $\pi\pi$ scattering with the IAM formalism in sec. 7.1. The KHURI–TREIMAN formalism for $\omega \to 3\pi$ is described in sec. 7.2. Supplementary assumptions to describe the quark-mass dependence of the ω width are collected in sec. 7.3, before we show results in sec. 7.4. We summarize our findings in sec. 7.5.

7.1 *P*-wave $\pi\pi$ scattering and the ρ resonance in one-loop unitarized ChPT

Before starting with the discussion of the quark-mass dependence of the ω as a three-pion resonance, we briefly summarize the investigation of the quark-mass dependence in $\pi\pi \to \pi\pi$ scattering. The results of this section will be an essential input for the study of $\omega \to 3\pi$. We follow the formalism introduced in refs. [266, 277]. For the later purpose our investigation will focus on the $\rho(770)$ resonance, which appears as a pole in the P-wave scattering amplitude. The $\pi\pi \to \pi\pi$ rescattering will be treated as elastic in this whole section.

As discussed in sec. 2.3.1 the $\pi\pi$ scattering amplitude can be decomposed into partial-wave amplitudes t_ℓ^I of isospin I and angular momentum ℓ. We work with degenerated pion masses in the isospin limit, *i.e.*, $M_\pi \equiv M_{\pi^\pm} = M_{\pi^0}$.[#2] For center-of-mass energies $s > 4M_\pi^2$ and below any inelastic thresholds the partial-wave amplitude is given in terms of the scattering phase shift δ_ℓ^I soley,

$$t_\ell^I(s) = \sigma^{-1}(s)\, \sin\delta_\ell^I(s)\, \exp\left[i\delta_\ell^I(s)\right], \tag{7.1}$$

where $\sigma(s) = \sqrt{1 - 4M_\pi^2/s}$. Since we are interested in P-wave $\pi\pi$ scattering exclusively, we fix the quantum numbers $I = \ell = 1$ from now on.

In ChPT the pion mass is given in terms of the light-quark masses as an expansion $M_\pi^2 = 2B_0\hat{m} + \mathcal{O}(m_q^2)$, with its leading term known as the GMOR relation, *cf.* sec. 1.3.2. The GMOR relation implies that studying the quark-mass dependence is equivalent to an investigation of the pion-mass dependence. Hence from now on we will refer to the pion-mass dependence instead. Since we are interested in pion-mass-dependent quantities, it turns out to be useful to define parameters at the physical point as *e.g.* $\bar{M}_\pi \equiv M_\pi^{\text{phys}}$.

The ChPT power counting allows us to expand the P-wave $\pi\pi$ scattering amplitude up to next-to-leading order in terms of

$$t_{\text{ChPT}}(s) = t_2(s) + t_4(s) + \mathcal{O}(p^6), \tag{7.2}$$

[#2] A brief discussion of the isospin-breaking effects in $\omega \to 3\pi$ can be found in sec. 7.3.3.

where t_i denotes the contribution of chiral order p^i. Projecting the expression for the $\pi\pi$ scattering amplitude given in ref. [72] onto the P-wave yields

$$t_2(s) = \frac{s\sigma^2}{96\pi F^2}\,, \tag{7.3}$$

at tree-level and

$$t_4(s) = \frac{t_2(s)}{48\pi^2 F^2}\bigg[s\left(\bar{l}+\frac{1}{3}\right) - \frac{M_\pi^4}{2s}\Big(41 - 2L_\sigma\big(73-25\sigma^2\big) + 3L_\sigma^2\big(5-32\sigma^2+3\sigma^4\big)\Big) - \frac{15}{2}M_\pi^2\bigg] + i\sigma\, t_2(s)^2\,, \tag{7.4}$$

for the one-loop correction, where we made use of the abbreviation

$$L_\sigma = \frac{1}{\sigma^2}\left(\frac{1}{2\sigma}\log\frac{1+\sigma}{1-\sigma} - 1\right)\,. \tag{7.5}$$

The value for the pion decay constant in the chiral limit F is taken from the ratio $F_\pi/F = 1.064(7)$ [260, 278–282], where $F_\pi = 92.28(9)\,\mathrm{MeV}$ [117] is the pion decay constant at the physical point. For our purpose it is beneficial to work with F instead of F_π, since F is independent of M_π. We treat the combination of LECs $\bar{l} = \bar{l}_2 - \bar{l}_1$, which occurs in the ChPT expression at next-to-leading order, as a free parameter that will be fixed in the following. Note that $\bar{l}$ is also independent of M_π, since the individual mass dependences of $\bar{l}_1$ and $\bar{l}_2$ cancel [72].

This amplitude however cannot capture the effects of the ρ resonance, which we expect to be the dominant effect in the P-wave above the threshold region, since unitarity is only fulfilled perturbatively ($\mathrm{Im}\, t_4 = \sigma|t_2|^2$). Furthermore t_2 and t_4 are polynomials in s (up to cuts encoded in the σ dependence), thus the analytic structure of the standard ChPT expression t_{ChPT} does not allow for any poles on the second RIEMANN sheet.

In order to include the ρ resonance into our amplitude we will use the IAM. This method allows us to construct an amplitude that fulfills unitarity exactly. Up to next-to-leading order the IAM yields

$$t_{\mathrm{IAM}}(s) = \frac{t_2(s)^2}{t_2(s) - t_4(s)}\,, \tag{7.6}$$

which is equivalent to t_{ChPT} up to corrections of $\mathcal{O}(p^6)$. Note that crossing symmetry is now only fulfilled perturbatively.

7.1.1 Pole position and residue

The characteristic properties of the ρ resonance are encoded in the pole position and residue of the amplitude on the second RIEMANN sheet, *cf.* sec. 2.1.2. By analytic continuation the amplitude on the second sheet can be expressed in terms of the amplitude on the first sheet [283]. We employ the specific representation [284]

$$t^{\mathrm{II}}(s) = \frac{t^{\mathrm{I}}(s)}{1 - 2\hat{\sigma}(s)\, t^{\mathrm{I}}(s)}\,, \qquad \hat{\sigma}(s) = \sqrt{\frac{4M_\pi^2}{s} - 1}\,, \qquad \hat{\sigma}(s \pm i\epsilon) = \mp i\sigma(s)\,, \tag{7.7}$$

where t^{I} and t^{II} denote the amplitudes on the first and second sheets, respectively. Thus the pole position of the amplitude is determined by

$$1 - 2\hat{\sigma}(s_{\mathrm{pole}})\, t^{\mathrm{I}}(s_{\mathrm{pole}}) = 0\,, \tag{7.8}$$

where s_{pole} corresponds to

$$\sqrt{s_{\mathrm{pole}}} = M_\rho - \frac{i}{2}\Gamma_\rho\,. \tag{7.9}$$

This allows us to identify the mass M_ρ, as well as the decay width Γ_ρ of the ρ resonance (that is assumed to be a purely elastic resonance with a single decay channel $\pi\pi$). The location of the ρ pole at the physical pion mass stemming from two studies of $\pi\pi$ scattering with Roy-type dispersion relations [132, 285] is used to constrain the up to now undetermined LEC. This is done in the following way: we minimize the distance of the ρ pole position at the physical point of the IAM amplitude with respect to the most precise extraction of the pole position from the GKPY analysis[#3] of ref. [285]. This yields $\bar{l} = 5.73(8)$.

The pole position of the IAM at the physical point is then given by

$$\sqrt{s_{\mathrm{pole}}} = 0.7620(15)\,\mathrm{GeV} - i0.0778(11)\,\mathrm{GeV}\,, \tag{7.10}$$

which is in good agreement with refs. [266, 277] and the real part of the pole position coincides with refs. [132, 285] within the error bars. Nevertheless we observe a tension in the imaginary part, which is ~ 4 MeV ($\sim 2-3$ standard deviations) larger than the imaginary parts from the Roy analyses. Thus here we reach the limits of the one-loop IAM description with only one free parameter; for more elaborate studies with an $\mathcal{O}(p^6)$ IAM amplitude containing several LECs, *cf.* refs. [277, 286]. However, for the purposes of our study of $\omega \to 3\pi$, we consider the one-loop IAM a sufficiently reasonable description of $\pi\pi$ scattering.

Since the amplitude is not limited to the physical value of the pion mass, we are able to calculate M_ρ and Γ_ρ as a function of M_π. The trajectory of the pole position on the second Riemann sheet is displayed in fig. 7.1. As expected from its quark content, the mass of the ρ increases if the pion becomes heavier. This behavior can be described to good approximation as a linear function in M_π^2 given by

$$M_\rho(M_\pi^2) = M_\rho(0) + a\, M_\pi^2\,, \tag{7.11}$$

where $M_\rho(0)$ and a can be matched to the pion-mass-dependent pole trajectory extracted from eq. (7.8), which yields

$$M_\rho(0) = 0.7480(16)\,\mathrm{GeV}\,, \qquad a = 0.719(9)\,\mathrm{GeV}^{-1}\,. \tag{7.12}$$

Similar observations have been made by investigating chiral symmetry constraints [287].

The available phase space for the decay decreases with growing pion mass, since the ρ mass increases much more slowly than the pion mass [266]. Thus the width of the ρ

[#3] Note that all three determinations of the ρ pole position in refs. [132, 285] lead to compatible results for $\bar{l}$.

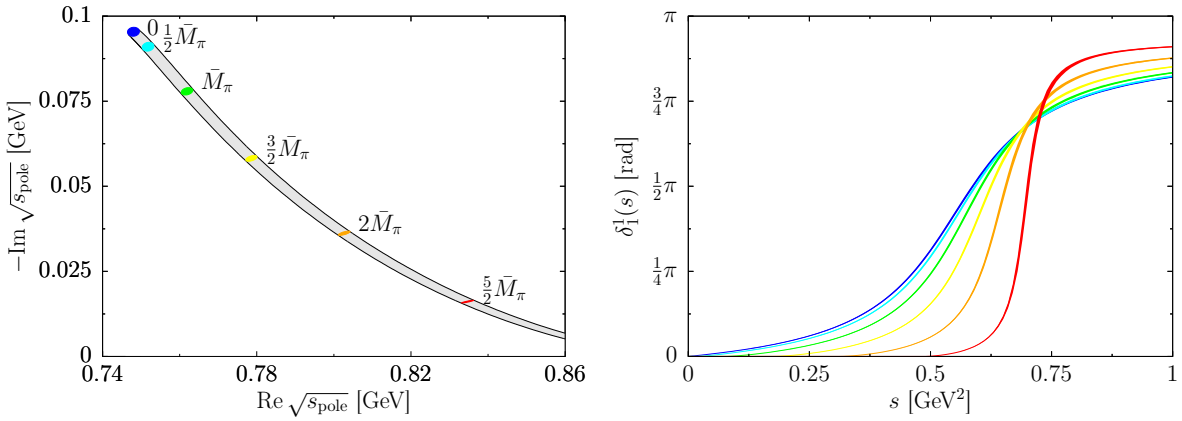

Fig. 7.1: Left: trajectory of the ρ pole position of t^{II} in the complex s plane as given in eq. (7.7) for different pion masses. The gray error band is generated by the uncertainty of F and $\bar{l}$. The colored ellipses mark the one-σ uncertainty regions of the pole position for the respective pion mass. Right: phase shift δ_1^1 of the IAM P-wave $\pi\pi$ scattering amplitude for different values of the pion mass using the same color coding as for the ρ pole trajectory. Again the error bands result from the uncertainty of F and $\bar{l}$.

becomes smaller for larger values of M_π. The coupling $g_{\rho\pi\pi}$ of the ρ to the $\pi\pi$ system is defined via the residue

$$g_{\rho\pi\pi}^2 = -48\pi \lim_{s\to s_{\mathrm{pole}}} \frac{s - s_{\mathrm{pole}}}{s - 4M_\pi^2}\, t^{\mathrm{II}}(s)\,, \tag{7.13}$$

where the normalization factors are chosen such that it coincides with the naive expression

$$\Gamma_\rho = \frac{|g_{\rho\pi\pi}|^2}{48\pi M_\rho^2}\left(M_\rho^2 - 4M_\pi^2\right)^{3/2}, \tag{7.14}$$

as obtained from a LAGRANGIAN-based narrow-width approximation or a vector-meson-dominance (VMD) model. Equation (7.13) yields a numerical value of $|g_{\rho\pi\pi}| = 6.12(4)$, which is in fair agreement with other determinations [277, 285]. Note that the coupling $g_{\rho\pi\pi}$ extracted from the IAM is pion-mass independent to very good approximation. Thus the pion-mass dependence of Γ_ρ is driven by the phase space factor only, *cf.* eq. (7.14), as confirmed by lattice QCD calculations [288].

7.1.2 Scattering phase shift

The $I = \ell = 1$ $\pi\pi$ system is one of the most widely-studied resonant scattering phase shifts in lattice QCD [288–299]. As defined in eq. (7.1) the scattering phase shift of the IAM amplitude can be extracted via $\delta_1^1(s) \equiv \arg t_1^1(s)$. The results for different values of the pion mass are shown in fig. 7.1. As expected, the slope of the phase shift becomes steeper for heavier pions, while the whole curve moves to the right (decreasing width and increasing mass of the ρ). This behavior is also observed by various lattice QCD calculations carried out at different pion masses [288–299]. At the physical pion mass

the phase shift is in perfect agreement with the ROY analyses of refs. [133, 134] in the low-energy regime up to $\sqrt{s} \sim 0.8\,\text{GeV}$.

Above this energy the ROY solutions are typically continued to an asymptotic value of π. The IAM amplitude on the other hand behaves like

$$\lim_{s\to\infty} t_{\text{IAM}}(s) = -\frac{3\pi}{6\bar{l} + 2 + 3\pi i} \tag{7.15}$$

in the high-energy limit, which depends only on the value of the LEC. Thus the phase of the IAM amplitude will not reach π for all reasonable values of $\bar{l}$. Nevertheless the phase shift gives a reasonable parametrization up to the ρ resonance region and thus will be used as a key ingredient for the dispersive representation of the $\omega \to 3\pi$ amplitude, as described in sec. 7.2. In order to test the effect of the discrepancy of the IAM compared to the ROY solution phase shifts, we will also use the parametrization

$$\delta_1^1(s) = \pi - \frac{\delta_a}{\delta_b + s/\Lambda^2} \tag{7.16}$$

to account for the correct asymptotic behavior. The parameters δ_a and δ_b are fixed by ensuring continuity of the phase shift and its derivative at some high-energy scale $\Lambda^2 \sim 1.2\,\text{GeV}^2$, at which we switch from the IAM to the asymptotic phase shift. Note that this high-energy continuation has no relevant influence on the $\omega \to 3\pi$ amplitude, since its effects can be fully absorbed by adjusting the unknown normalization of the amplitude, *cf.* eq. (7.32) below. Similarly, any hypothetical, subleading, pion-mass dependence in Λ^2 would be far too small to be of relevance.

7.2 Dispersive representation of the $\omega \to 3\pi$ amplitude

The dispersive framework to describe the $\omega \to 3\pi$ decay was already used in previous studies of this process [120, 121] as well as the closely related $\gamma^{(*)}\pi \to \pi\pi$ transition [300–304]. We define the T-matrix element for the $\omega_\lambda(p_1) \to \pi^i(p_2)\,\pi^j(p_3)\,\pi^k(p_4)$ decay as

$$\langle \pi^i(p_2)\pi^j(p_3)\pi^k(p_4)|iT|\omega_\lambda(p_1)\rangle = i(2\pi)^4\delta^{(4)}(p_1 - p_2 - p_3 - p_4)\,\epsilon^{ijk}\,\mathcal{H}_\lambda(s,t,u)\,, \tag{7.17}$$

where the helicity of the ω meson is labelled with λ and π^i denotes a pion state in the HERMITIAN basis, *cf.* eqs. (2.21) and (2.50). The totally antisymmetric LEVI-CIVITA tensor guarantees that the three pions couple to a state of total isospin $I = 0$, which in nature can only be realized by $\omega \to \pi^+\pi^-\pi^0$. In our convention the MANDELSTAM variables (*cf.* sec. 2.2.1) are defined according to

$$s = (p_2 + p_3)^2\,, \qquad t = (p_2 + p_4)^2\,, \qquad u = (p_3 + p_4)^2\,, \tag{7.18}$$

which fulfill the relation

$$M_\omega^2 + 3M_\pi^2 = s + t + u \equiv 3r\,. \tag{7.19}$$

In the s-channel CMS, t and u can be expressed as (2.30),

$$t(s, z_s) = u(s, -z_s) = \frac{1}{2}\big(3r - s + \kappa(s)\,z_s\big)\,, \tag{7.20}$$

where $z_s = \cos\theta_s$ is the scattering angle (2.31)

$$z_s = \cos\theta_s = \frac{t-u}{\kappa(s)}\,, \qquad \kappa(s) = \frac{\sqrt{\lambda(s,M_\pi^2,M_\pi^2)\,\lambda(s,M_\pi^2,M_\omega^2)}}{s}\,. \tag{7.21}$$

Similar expressions hold for the t- (2.36) and u-channels (2.38), respectively. The physical thresholds in the three channels are

$$s_{\rm thr} = t_{\rm thr} = u_{\rm thr} = 4M_\pi^2\,. \tag{7.22}$$

Since the transition $\omega \to 3\pi$ is of odd intrinsic parity, the helicity amplitude $\mathcal{H}_\lambda$ can be further decomposed into a kinematic prefactor and a scalar amplitude $\mathcal{M}$ containing the dynamical information (2.22),

$$\mathcal{H}_\lambda(s,t,u) = i\epsilon_{\mu\nu\alpha\beta}\, n_\lambda^\mu(p_1)\, p_2^\nu\, p_3^\alpha\, p_4^\beta\, \mathcal{M}(s,t,u)\,. \tag{7.23}$$

Here $n_\lambda^\mu(p_1)$ denotes the polarization vector of the ω meson. The helicity averaged squared modulus of the amplitude is given by

$$\frac{1}{4}\sum_\lambda |\mathcal{H}_\lambda(s,t,u)|^2 = \frac{1}{4}\Big[stu - M_\pi^2\big(M_\omega^2 - M_\pi^2\big)^2\Big]\,|\mathcal{M}(s,t,u)|^2\,, \tag{7.24}$$

where the expression in the square brackets is also known as the KIBBLE *cubic* [305].

BOSE symmetry demands the scalar amplitude $\mathcal{M}$ to be fully symmetric under pairwise interchange of the MANDELSTAM variables, *i.e.*,

$$\mathcal{M}(s,t,u) = \mathcal{M}(s,u,t) = \mathcal{M}(t,u,s) = \mathcal{M}(t,s,u) = \mathcal{M}(u,s,t) = \mathcal{M}(u,t,s)\,. \tag{7.25}$$

This symmetry reflects the fact that the process is invariant under the exchange of the pions. Accordingly, only odd partial-wave amplitudes f_ℓ^I are allowed to contribute to the process and the partial-wave decomposition for $\mathcal{M}$ in the s-channel reads

$$\mathcal{M}(s,z_s) = \sum_{\ell\ \text{odd}} P_\ell'(z_s)\,\kappa^\ell(s)\,f_\ell^1(s)\,, \qquad f_\ell^1(s) = \frac{1}{2}\int_{-1}^{1}\mathrm{d}z_s\,\big[P_{\ell-1}(z_s) - P_{\ell+1}(z_s)\big]\,\mathcal{M}(s,z_s)\,, \tag{7.26}$$

where P_ℓ' denotes the differentiated LEGENDRE polynomials, *cf.* app. A.2. As the available phase space in the $\omega \to 3\pi$ decay is rather small, the dominant contribution will come from the $I = \ell = 1$ partial wave (*cf.* ref. [120] for a discussion of potential F-wave contributions). Neglecting discontinuities from F- and higher partial waves, *i.e.*,[#4]

$$\mathrm{disc}_x\,\mathcal{M}(x,z_x) = \mathrm{disc}\,f_1^1(x) \tag{7.27}$$

for $x \in \{s,t,u\}$, the reconstruction theorem allows us to decompose the scalar amplitude into a sum of single-variable amplitudes

$$\mathcal{M}(s,t,u) = \mathcal{F}_1^1(s) + \mathcal{F}_1^1(t) + \mathcal{F}_1^1(u)\,, \tag{7.28}$$

[#4] Here and in the following relations that involve the discontinuity are always meant to be valid along the right-hand cut only, which starts at the two-pion threshold in the respective channel.

where $\mathcal{F}_1^1$ possesses only a right-hand cut, *cf.* sec. 4.2.3. Combining eqs. (7.26) and (7.28) the partial-wave amplitude f_1^1 is given by

$$f_1^1(s) = \mathcal{F}_1^1(s) + \hat{\mathcal{F}}_1^1(s)\,. \tag{7.29}$$

The right-hand cut of f_1^1 is contained in $\mathcal{F}_1^1$, while its left-hand cut contributions reside entirely in the projection $\hat{\mathcal{F}}_1^1$ of the crossed-channel single-variable amplitudes

$$\hat{\mathcal{F}}_1^1(s) = 3\big\langle (1-z_s^2)\,\mathcal{F}_1^1\big\rangle\,, \qquad \big\langle z_s^n \mathcal{F}_1^1\big\rangle = \frac{1}{2}\int_{-1}^{1} \mathrm{d}z_s\, z_s^n\, \mathcal{F}_1^1\big(t(s,z_s)\big)\,. \tag{7.30}$$

Restricting ourselves to elastic $\pi\pi$ final-state rescattering (7.1), the unitarity relation for the partial-wave amplitude f_1^1 is given in terms of the P-wave $\pi\pi$ scattering phase shift δ_1^1 only

$$\operatorname{disc} f_1^1(s) = 2i\, f_1^1(s)\, \sin\delta_1^1(s)\, \exp\big[-i\delta_1^1(s)\big]\,. \tag{7.31}$$

Inserting eq. (7.29) and noting that $\operatorname{disc} f_1^1(s) = \operatorname{disc}\mathcal{F}_1^1(s)$ along the right-hand cut results in an inhomogeneous Omnès problem for $\mathcal{F}_1^1$ with the inhomogeneity $\hat{\mathcal{F}}_1^1$, *cf.* sec. 3.2.2. Assuming the Froissart–Martin bound [161, 162], a solution of eq. (7.31) can be written in terms of a single subtraction constant α [120],

$$\mathcal{F}_1^1(s) = \Omega_1^1(s)\left[\alpha + \frac{s}{\pi}\int_{4M_\pi^2}^{\infty} \frac{\mathrm{d}x}{x}\frac{\hat{\mathcal{F}}_1^1(x)\,\sin\delta_1^1(x)}{|\Omega_1^1(x)|(x-s)}\right]. \tag{7.32}$$

Since eqs. (7.30) and (7.32) are linear in α, we introduce the basis amplitude $\mathcal{F}_1^1(s)|_{\alpha=1}$, *cf.* sec. 3.4. By definition this basis amplitude is constructed independently of the numerical value of α, which therefore can be determined *a posteriori*. As α serves as an overall normalization of the amplitude, at physical pion masses it is fixed to the decay width $\Gamma(\omega \to 3\pi)$, with the energy dependence of the amplitude or the Dalitz-plot distribution then being a theoretical prediction [120].

7.3 Decay width and pion-mass dependencies

In nature the by far dominant contribution to the total decay width of the ω meson stems from $\mathrm{BR}(\omega \to 3\pi) = 89.2(7)\%$. Besides that, the main subleading contributions are given by $\mathrm{BR}(\omega \to \pi\gamma) = 8.4(2)\%$ (electromagnetic) and $\mathrm{BR}(\omega \to \pi\pi) = 1.5(1)\%$ (isospin-breaking). Together these contributions account for more than 99% of the decay width at the physical point [117]. Accordingly the total decay width is fully driven by $\omega \to 3\pi$, as long as we restrict ourselves to strong interactions in the isospin limit.

Integrating eq. (7.24) over phase space the decay width $\Gamma_\omega \equiv \Gamma(\omega \to 3\pi)$ is obtained by

$$\Gamma_\omega = \frac{1}{1024\pi^3 M_\omega^3}\int \mathrm{d}s\,\mathrm{d}t\,\Big[stu - M_\pi^2\big(M_\omega^2 - M_\pi^2\big)^2\Big]|\mathcal{M}(s,t,u)|^2\,. \tag{7.33}$$

This expression has several M_π dependencies besides the explicit ones (integration boundaries and Mandelstam variables), which will be discussed in the following.

7.3.1 Pion-mass dependence of the ω mass

In contrast to the case of the ρ, for which we can derive the pion-mass dependence of the complete pole position in the P-wave $\pi\pi \to \pi\pi$ amplitude by means of the IAM, we are not in the position to do the same for the ω within some $3\pi \to 3\pi$ amplitude of the appropriate quantum numbers. We will discuss the complicated pion-mass dependence of the *width* of the ω, or the imaginary part of its pole in the complex plane, which is the main focus of this study, in the following; for the pion-mass dependence of its *mass*, the corresponding real part, we have to resort to symmetry arguments based on effective LAGRANGIANS. These will relate $M_\omega(M_\pi^2)$ to $M_\rho(M_\pi^2)$, which we have discussed in sec. 7.1.1.

We briefly recapitulate the analysis of the leading symmetry-breaking effects in the masses of the vector meson nonet [306–308]. Here, the vector mesons are treated as static matter fields; the effective LAGRANGIAN is organized in terms of increasing chiral dimension as well as using the expansion in the inverse number of colors N_C^{-1}. We neglect isospin breaking and electromagnetic effects [307], and ignore deviations from ideal mixing. In this approximation, the symmetry-breaking part of the effective LAGRANGIAN can be written as

$$\begin{aligned}\mathcal{L}_{\text{SB}} = \frac{\delta}{2}\langle W_\mu^\dagger\rangle\langle W^\mu\rangle + \frac{a}{2}\langle\chi\{W_\mu^\dagger, W^\mu\}\rangle + \frac{b}{4}\big(\langle\chi W_\mu^\dagger\rangle\langle W^\mu\rangle + \text{h.c.}\big) \\ + \frac{c}{2}\langle\chi\rangle\langle W_\mu^\dagger W^\mu\rangle + \mathcal{O}(m_q^2, N_C^{-2})\,,\end{aligned} \tag{7.34}$$

where

$$W_\mu = \begin{pmatrix} \frac{\rho_\mu^0}{\sqrt{2}} + \frac{\omega_\mu}{\sqrt{2}} & \rho_\mu^+ & K_\mu^{*+} \\ \rho_\mu^- & -\frac{\rho_\mu^0}{\sqrt{2}} + \frac{\omega_\mu}{\sqrt{2}} & K_\mu^{*0} \\ K_\mu^{*-} & \bar{K}_\mu^{*0} & \phi_\mu \end{pmatrix} \tag{7.35}$$

contains the (nonrelativistic) vector-meson fields, and $\chi = \text{diag}(M_\pi^2, M_\pi^2, 2M_K^2 - M_\pi^2)$ breaks SU(3) flavor symmetry due to the different quark masses. Among the terms in eq. (7.34), the quark-mass-independent operator $\propto \delta$ is N_C^{-1} suppressed and breaks nonet symmetry; the term $\propto a$ is chirally suppressed, but the dominant flavor-breaking term in the large-N_C limit; and the operators $\propto b$ and $\propto c$ are both chirally and N_C^{-1} suppressed. The term $\propto c$ leads to a common shift in all nonet masses and hence cannot be discerned from the common mass M_V using experimental data only; on account of the fact that we can show the operator $\propto b$ indeed to be strongly suppressed below, we will neglect the former in the following.

Equation (7.34) then leads to the vector-meson masses

$$\begin{aligned} M_\rho &= M_V + a\,M_\pi^2\,, & M_\phi &= M_V + \frac{\delta}{2} + \Big(a + \frac{b}{2}\Big)\big(2M_K^2 - M_\pi^2\big)\,, \\ M_\omega &= M_V + \delta + (a+b)M_\pi^2\,, & M_{K^*} &= M_V + a\,M_K^2\,, \end{aligned} \tag{7.36}$$

which allows us to extract the coupling constants according to

$$a = \frac{M_{K^*} - M_\rho}{M_K^2 - M_\pi^2}\,, \qquad b = \frac{M_\phi - 2M_{K^*} + \frac{3}{2}M_\rho - \frac{1}{2}M_\omega}{M_K^2 - M_\pi^2}\,, \qquad \delta = M_\omega - M_\rho - b\,M_\pi^2\,. \tag{7.37}$$

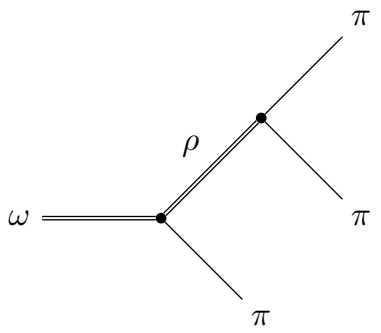

Fig. 7.2: VMD tree-level diagram for $\omega \to 3\pi$ given by a $\omega \to \rho\pi$ and a subsequent $\rho \to \pi\pi$ decay.

In particular the value for b depends quite sensitively on the precise values inserted for the masses of the broad ρ and K^* resonances; if we employ the real parts of their pole positions [285, 309], we find $a = 0.57(1)\,\mathrm{GeV}^{-1}$, $b = -0.045(20)\,\mathrm{GeV}^{-1}$, $\delta = 20(2)\,\mathrm{MeV}$.

We hence conclude that the formal N_C^{-1} suppression of b/a translates, in fact, into a numerical suppression by more than an order of magnitude; we will therefore neglect b, too. Furthermore, we observe that the determination of a based on SU(3) symmetry leads to an estimate that is about 20% smaller than the value deduced from the one-loop IAM representation, *cf.* eq. (7.12). As we expect that SU(3) breaking effects ought to affect the relation between ρ and ω observables less, we use the arguments above to employ a pion-mass dependence of M_ω that equals the one of M_ρ up to the constant offset δ, hence

$$M_\omega(M_\pi^2) = \bar{M}_\omega + \frac{0.719(9)}{\mathrm{GeV}}\left(M_\pi^2 - \bar{M}_\pi^2\right), \qquad M_\omega(0) = 0.7686(20)\,\mathrm{GeV}\,. \tag{7.38}$$

At higher orders in the chiral expansion, Nambu–Goldstone Boson loops induce nonanalytic dependencies of the vector meson masses of the form $\mathcal{O}(m_q^{3/2})$ and $\mathcal{O}(m_q^2 \log m_q)$, which have been studied extensively in the literature [306–308, 310–312]; such terms will obviously break the similarity in $M_\rho(M_\pi^2)$ and $M_\omega(M_\pi^2)$ due to the different coupling of ρ and ω to pions. We ignore such terms in the present study solely based on the observation in sec. 7.1.1 that a linear dependence of M_ρ on M_π^2 is sufficient to describe the behavior of the ρ pole of the $\mathcal{O}(p^4)$ IAM amplitude.

7.3.2 The subtraction constant

As derived in sec. 7.2, we require one subtraction constant in the dispersive representation of the $\omega \to 3\pi$ decay amplitude in order to maintain a convergent integral representation. Since this subtraction constant is not fixed by unitarity (and, for the process at hand, cannot be matched to ChPT as for other processes such as $\gamma\pi \to \pi\pi$ [144, 276, 300]), we need to fix its pion-mass dependence in a different way.

In sec. 7.1 we have recounted that the coupling $g_{\rho\pi\pi}$ at the $\rho \to \pi\pi$ vertex is (essentially) pion-mass independent and in good agreement with a narrow-width formula or a VMD model. In an isobar model of subsequent two-body decays, $\omega \to 3\pi$ is typically understood in terms of processes $\omega \to \rho\pi$, followed by $\rho \to \pi\pi$ decays, *cf.* fig. 7.2 and

e.g. refs. [313–315]. Reducing the dispersive representation eq. (7.32) to such a simplified picture, we find the subtraction constant α in one-to-one correspondence with the product of coupling constants $g_{\omega\rho\pi} \times g_{\rho\pi\pi}$. We therefore conjecture that, by analogy, it is reasonable to assume $g_{\omega\rho\pi}$, and hence α, to be also pion-mass independent, and we fix the subtraction constant to the decay width Γ_ω at the physical point.

7.3.3 Isospin-breaking effects

Up to now all calculations have been carried out under the assumption of isospin symmetry ($M_\pi \equiv M_{\pi^\pm} = M_{\pi^0}$). We now want to briefly discuss the influence of isospin breaking effects in $\omega \to 3\pi$; a more detailed discussion can be found in ref. [316]. It is well known that in the context of precision analyses of $\eta \to 3\pi$, in particular comparing $\eta \to \pi^+\pi^-\pi^0$ and $\eta \to 3\pi^0$, taking into account the pion-mass difference for the available phase space at least is mandatory [152, 201, 202, 233]. In this section, we therefore only investigate isospin breaking in the kinematical contribution, ignoring all dynamical effects (*i.e.* using $\mathcal{M}(s,t,u) = const.$), expecting this to be the dominant change.

The pion-mass difference

$$\Delta_\pi = \left(M_{\pi^\pm}^2 - M_{\pi^0}^2\right) = 1.26116(15) \times 10^{-3}\,\mathrm{GeV}^2 \tag{7.39}$$

originates from two sources: electromagnetic effects and the difference of the up- and down-quark masses, *cf.* secs. 1.3.2 and 1.3.3. At leading-order in ChPT (for three flavors), the latter can be evaluated to

$$\Delta_\pi^{\mathrm{QCD}} = \frac{(m_u - m_d)^2}{8\hat{m}(m_s - \hat{m})} M_\pi^2 \approx 3 \times 10^{-5}\,\mathrm{GeV}^2\,, \tag{7.40}$$

hence this effect is very small: the pion-mass difference is dominantly caused by electromagnetism, and we neglect the effect of the difference of the light quark masses completely. Consequently, as long as we neglect higher-order corrections of $\mathcal{O}(e^2 m_q)$, the pion-mass difference Δ_π stays constant when varying M_π. This allows us to relate the neutral pion mass to the charged one according to

$$M_{\pi^0}(M_{\pi^\pm}^2) = \sqrt{M_{\pi^\pm}^2 - \Delta_\pi}\,. \tag{7.41}$$

Obviously, below a minimal charged pion mass given by $M_{\pi^\pm} = \sqrt{\Delta_\pi} \approx 35.5\,\mathrm{MeV}$ this relation breaks down.

It turns out that isospin breaking in the kinematical dependence of Γ_ω as given in eq. (7.33) when tuning the charged pion mass gives only a tiny correction to Γ_ω of less than 2%. Due to the connection of the pion masses in eq. (7.41) it is easy to see that the effect of isospin breaking becomes smaller when increasing the mass of the pions; on the other hand, since the ratio of the ω mass to the pion masses becomes larger when approaching the chiral limit, the increasing isospin-breaking effects are lifted by the ω mass. Thus using the isospin limit is entirely justified for our purposes.

7.4 Results

In this section we discuss the final results of our dispersive representation of $\omega \to 3\pi$. First of all we want to compare the resulting pion-mass-dependent OMNÈS function or two-body final-state interaction[#5] (two-body FSI) to the single-variable amplitude (three-body FSI) to study the dynamical effects generated by the interaction with the third pion as depicted in fig. 7.3.

Besides pion masses close to the chiral limit, the three-body FSI leads to an enhancement of the modulus of the single-variable amplitude compared to the OMNÈS function. While the peak position in the absolute values (due to the ρ resonance) is essentially identical for two- and three-body FSI at a given value of M_π, the phases behave rather differently. The OMNÈS function fulfills WATSON's theorem and thus its phase is identical to the IAM $\pi\pi$ scattering phase shift. Due to the dynamical effects stemming from the interaction with the third pion (and the generation of a three-pion cut), this does not hold for the single-variable amplitude, *cf.* sec. 7.2. Thus the argument of the single-variable function is shifted compared to the input IAM phase. The lower and upper phase-space boundaries are marked by dashed vertical lines, and hence denote the kinematical range directly accessible in the decay. Already here we want to point out that mainly the tails of the ρ resonance will only contribute to the dynamics when increasing M_π, *cf.* fig. 7.5.

In order to study the dynamical effects on the decay width we consider three different scenarios: first we consider only kinematic contributions to the decay width (all pion–pion dynamics are disregarded, *i.e.*, $\delta_1^1(s) = 0$, and thus $\mathcal{M}(s,t,u) = const.$), secondly we allow for two-body rescattering effects (meaning $\mathcal{M}(s,t,u) \propto \Omega_1^1(s) + \Omega_1^1(t) + \Omega_1^1(u)$), and third the full three-body dynamics are taken into account. A comparison of the different cases is displayed in fig. 7.4.

First of all we notice that the $\omega \to 3\pi$ width decreases with increasing pion mass. This is not surprising since the mass of the three pions is increasing faster than the mass of the ω (7.38). Hence the phase space shrinks for larger pion masses as depicted in fig. 7.5. For $M_\pi > \frac{1}{3}M_\omega \approx 1.96\bar{M}_\pi$ the masses of the three pions exceed the ω mass, thus the reaction $\omega \to 3\pi$ is no longer allowed and the ω becomes stable with respect to the considered decay channel (*i.e.*, in QCD in the isospin limit).

We now study the effects of the two- and three-body dynamics. First of all we notice that the kinematical prefactor given in eq. (7.24) vanishes at the phase space boundaries in all directions. This leads to a stronger weighting of the inner region compared to the outskirts of the phase space when evaluating the integral eq. (7.33). Secondly, the dynamics are mainly governed by the ρ resonance in the respective two-body channels, leading to a three-band structure (one for each channel) in the amplitude $\mathcal{M}(s,t,u)$. The peak position and width of these bands will be determined by the respective two- and three-body FSI effects and the information of the scattering phase input from the IAM. We conclude that strong imprints of the ρ as a dynamical effect will only affect the decay width close to the chiral limit, since the ρ is only allowed to go on-shell within the phase space boundaries for $M_\pi < 0.15\bar{M}_\pi$. This effect is even reinforced by the increasing mass

[#5] Here the third pion will act as spectator, meaning $\hat{\mathcal{F}}_1^1(s) = 0$, thus the single-variable amplitude equals the OMNÈS function in this case, *cf.* eq. (7.32).

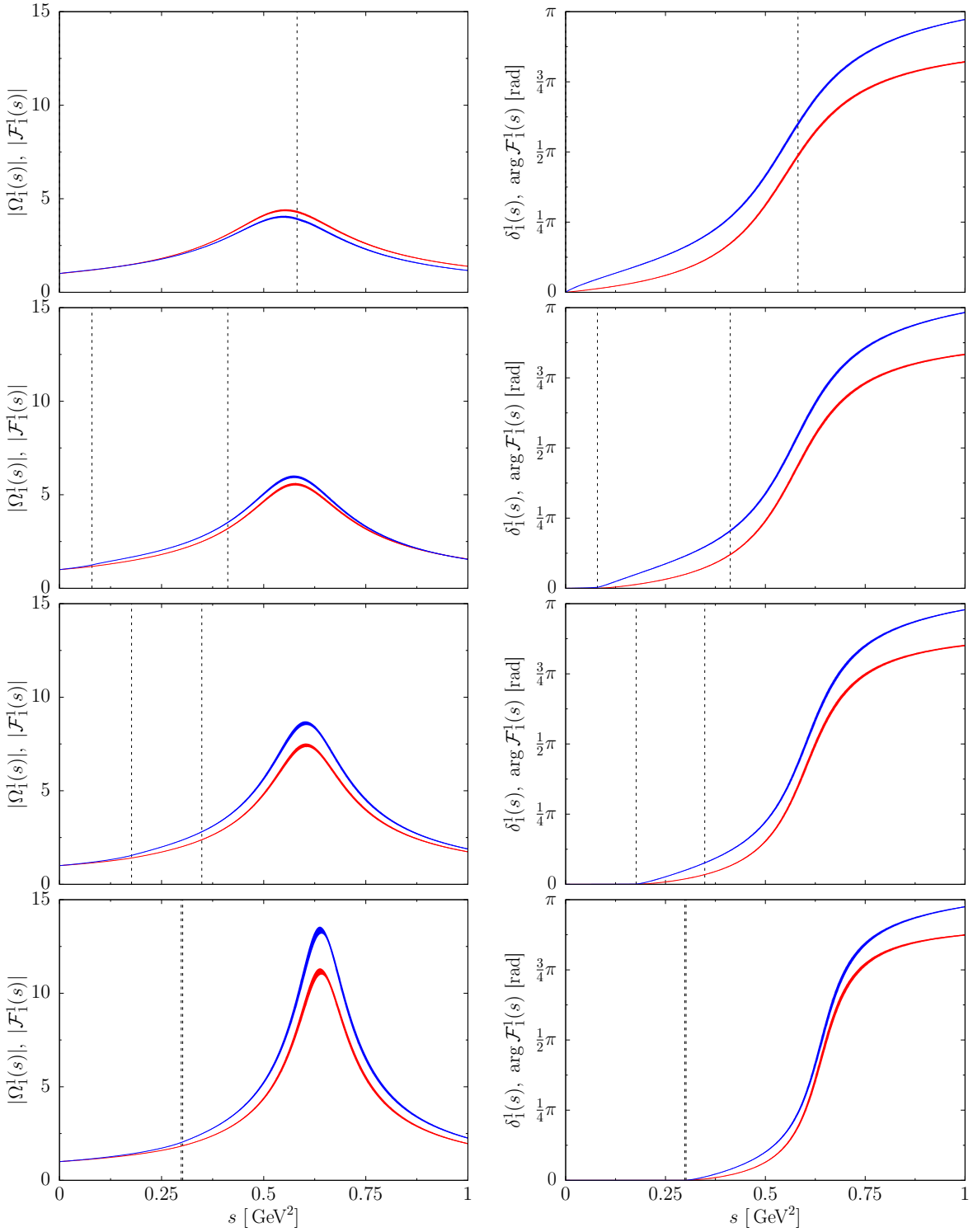

Fig. 7.3: Comparison of the absolute value (left column) and phase motion (right column) of Ω_1^1 (red) and $\mathcal{F}_1^1$ with $\alpha = 1$ (blue) for various pion masses: first row $M_\pi = 0$, second row $M_\pi = \bar{M}_\pi$, third row $M_\pi = \frac{3}{2}\bar{M}_\pi$, and last row $M_\pi = 1.96\bar{M}_\pi \approx \frac{1}{3}M_\omega(M_\pi^2)$. The dashed black lines mark the pion-mass-dependent lower and upper phase-space boundaries for the $\omega \to 3\pi$ decay given by $4M_\pi^2$ and $(M_\omega - M_\pi)^2$, respectively. The error bands are generated by taking the uncertainties of the IAM phase shift δ_1^1 and $M_\omega(M_\pi^2)$ into account, *cf.* fig. 7.1 and eq. (7.38). The latter only affects $\mathcal{F}_1^1$.

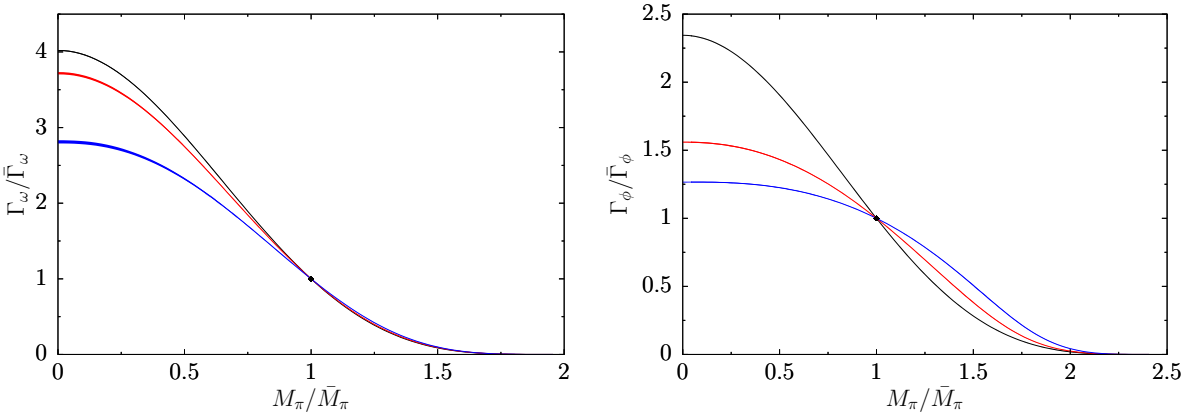

Fig. 7.4: Pion-mass-dependent decay width for $\omega \to 3\pi$ (left) and $\phi \to 3\pi$ (right) shown for three different cases: kinematic contribution only (black), considering two-body FSI (red), and full three-body FSI (blue). The physical point is marked by the black diamond. The error bands are generated by taking the uncertainties of the IAM phase shift $\delta_1^1(s)$ and $M_\omega(M_\pi^2)$ into account (M_ϕ is considered to be pion-mass independent), *cf.* fig. 7.1 and eq. (7.38).

of the ρ and its decreasing width with growing pion mass, as investigated in sec. 7.1. Thus the main contributions to the ω width will come from the tail of the ρ resonances at low pion masses, *cf.* fig. 7.5.

This is consistent with the result given in fig. 7.4. We observe that the impact of the two- and three-body dynamics on the decay width is very strong close to the chiral limit, where it leads to a reduction of the decay width compared to the one of pure kinematics. The damping due to the three-body dynamics is four times stronger than the influence of the two-body effects and results in a width smaller by about one third than the purely kinematic effects. In the chiral limit we find

$$\Gamma_\omega(0) = 4.02(1)\,\bar{\Gamma}_\omega = 30.4(1)\,\text{MeV}\,, \tag{7.42}$$

for the decay width when allowing for kinematic effects only,

$$\Gamma_\omega(0) = 3.72(2)\,\bar{\Gamma}_\omega = 28.1(1)\,\text{MeV}\,, \tag{7.43}$$

when considering two-body dynamics, and

$$\Gamma_\omega(0) = 2.81(2)\,\bar{\Gamma}_\omega = 21.3(2)\,\text{MeV}\,, \tag{7.44}$$

when accounting for three-body dynamics. Here we used $\bar{\Gamma}_\omega \equiv \bar{\Gamma}(\omega \to 3\pi) = 7.57(9)\,\text{MeV}$ for the decay width at the physical point [117]. Since the subtraction constant of all three curves is fixed at the physical point, the difference between them shrinks when approaching this point. Above the behavior is opposite, here the two- and three-body dynamics generate a decay width that is larger than the one obtained from pure kinematic effects. Since the phase space at the physical point and above does not allow for on-shell ρ mesons in the respective two-body systems, the influence of the dynamical effects above

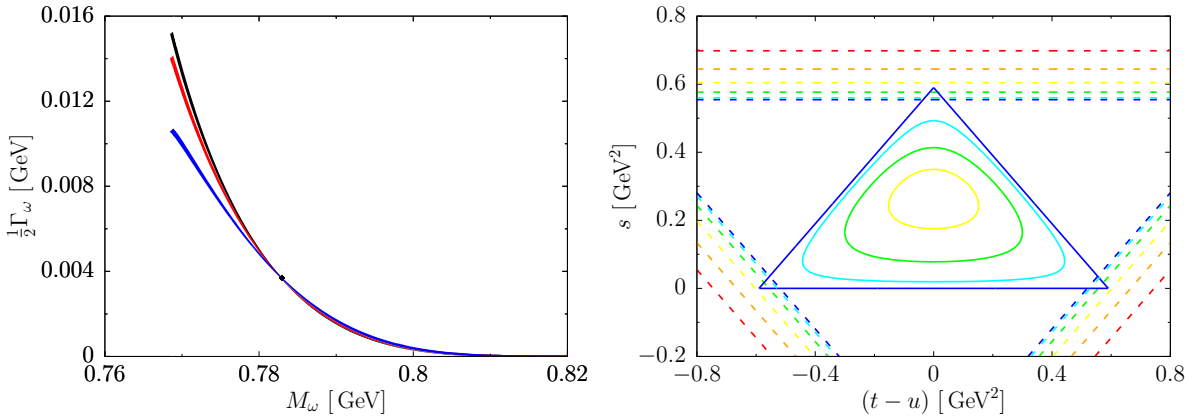

Fig. 7.5: Left: trajectory of the pion-mass-dependent ω mass and width in the complex-energy plane of $3\pi \to 3\pi$ scattering for the three investigated scenarios: pure kinematics (black), two-body FSI (red), and full three-body FSI (blue). This plot can be compared with the one for the ρ resonance, *cf.* fig. 7.1. The physical point is marked by the black diamond. The error bands are generated by taking the uncertainties of the IAM phase shift $\delta(s)$, $M_\omega(M_\pi^2)$, and $\bar{\Gamma}_\omega$ into account, *cf.* fig. 7.1, eq. (7.38), and ref. [117]. Right: pion-mass-dependent phase space boundaries of $\omega \to 3\pi$ (solid lines) and position of the "on-shell" ρ in the respective s-, t-, and u-channels (dashed lines). The color coding is kept identical to fig. 7.1 with the following pion masses: 0 (blue), $\frac{1}{2}\bar{M}_\pi$ (cyan), $\bar{M}_\pi$ (green), $\frac{3}{2}\bar{M}_\pi$ (yellow), $2\bar{M}_\pi$ (orange), and $\frac{5}{2}\bar{M}_\pi$ (red). For the last two the phase space already vanishes, and thus the ω becomes stable with respect to the investigated decay mode.

this point is very small. Thus the two- and three-body FSI curves do not differ strongly from the curve of pure kinematics.

Considering eq. (7.9) we are in the position to predict a pion-mass-dependent trajectory of the ω pole position in the complex-energy plane of $3\pi \to 3\pi$ scattering similar to the ρ resonance in fig. 7.1. A plot of this pole trajectory is given in fig. 7.5. Note that, strictly speaking, our formalism does not determine such a complex pole position: rather, we have discussed mass (via effective Lagrangians) and width (via the Khuri–Treiman formalism) individually. Given the smallness of the width of the ω, we regard the error committed thereby as negligible, although this may not obviously be so in the general case of an arbitrary 3π resonance.

Since dynamical effects in the investigated process are limited due to the small phase space, we want to emphasize that the dispersive representation derived in sec. 7.2 is valid for general $V \to 3\pi$ decays, with V denoting an arbitrary isoscalar vector meson, at least to the extent that the elastic approximation in the pion–pion rescattering is justifiable. Thus we are able to describe $\phi \to 3\pi$ by just replacing the decay mass according to $M_\omega \mapsto M_\phi$ within the same formalism [120, 121]. With a mass of 1019 MeV [117] its decay allows for much richer dynamics due to the larger phase space, in particular the three ρ bands are visible inside the Dalitz plot [317, 318]. In the quark-model picture, the ϕ can be understood as a pure $s\bar{s}$ state, thus its mass does not depend on the pion mass at leading order. This follows from eq. (7.36) when using the GMOR relation to relate

$M_K^2 = B(\hat{m} + m_s) + \mathcal{O}(m_q^2)$. The results for the pion-mass-dependent partial decay width $\Gamma_\phi \equiv \Gamma(\phi \to 3\pi)$ are displayed in fig. 7.4. Since the ρ is allowed to go on-shell up to a maximal pion mass of $M_\pi \approx 1.7\bar{M}_\pi$, the dynamical imprints are much stronger compared to the case of the $\omega \to 3\pi$ even above the physical point.

Overall, given how subtle rescattering effects beyond two-body rescattering are usually thought to be (and more often than not neglected altogether in experimental Dalitz plot analyses), it is remarkable to see that in both cases studied here, $\omega \to 3\pi$ and $\phi \to 3\pi$, the three-body FSI effects tend to affect the quark-mass dependence of the (partial) widths about as strongly as the two-body FSI.

We wish to add a few caveats concerning the precision of the predictions shown in this section. Error bands are estimated solely based on the uncertainty within the one-loop IAM phase shift input, as well as the one in $M_\omega(M_\pi^2)$, which is nonetheless based on the large-N_C expansion and leading-order symmetry breaking in the quark masses. We do not attempt to quantify corrections due to higher orders in either case, and refer to ref. [286] for future work concerning an improved pion-mass-dependent phase shift. Furthermore, a high-precision measurement of the $\phi \to 3\pi$ Dalitz plot [317] revealed the need to include a *second* subtraction in the dispersive representation of the decay amplitude [120], which has also not been considered here; experimental data on the $\omega \to 3\pi$ Dalitz plot is not conclusive in this respect yet [319].

7.5 Summary

We have investigated the pion-mass (and hence the quark-mass) dependence of the $\omega \to 3\pi$ decay width, generalizing previous studies of two-pion resonances based on the inverse amplitude method. To this end, we have employed a dispersive formalism, based on Khuri–Treiman equations, that uses inverse-amplitude-method phase shifts as input. The pion-mass dependence of the ω mass is estimated using a symmetry relation based on chiral perturbation theory for vector mesons. Deviations from phase space behavior alone, induced by the pion-mass-dependent decay amplitude, are clearly visible, although suppressed for larger-than-physical pion masses due to the smallness of phase space. We have demonstrated for the decay of the heavier ϕ into three pions that this need not be the case in general. Remarkably, a simple description of the decays in terms of two-body rescattering alone does not yield a good approximation to the full pion-mass dependence seen.

The three-pion decays of the lightest isoscalar vector mesons only serve as a paradigm case for the investigation of three-body resonances; extensions to other, similar decays within the same formalism ought to be tested in the future.

Summary and outlook

In this thesis we studied the phenomenology of strong interactions in hadronic three-body decays at low energies exemplary in the analyses of the charged and neutral mode $\eta' \to \pi\pi\eta$ DALITZ-plot distributions, C- and CP-violating patterns in $\eta \to \pi^+\pi^-\pi^0$, and the quark-mass dependence of $\omega \to 3\pi$. With the presented KHURI–TREIMAN type dispersive framework based on the fundamental principles of analyticity and unitarity, we were able to perform a resummation of the leading $\pi\pi$ and $\pi\eta$ final-state rescattering effects. In this way we consistently accounted for the rescattering effects among all three decay products, which have been proven to be vital in hadronic final-state interactions at low energies. The dispersive integral equations have been solved numerically by iteration until sufficient convergence was reached. As a result, the dispersive framework allowed us to describe the considered hadronic three-body decay processes in terms of holomorphic functions, which are also valid outside of the experimentally accessible physical decay region.

To conclude this thesis, we want to address the question where to go next. Considering strong three-body decay processes in the η and η' sector, only three decay modes are kinematically allowed: one isospin conserving $\eta' \to \pi\pi\eta$ as well as two isospin breaking $\eta/\eta' \to 3\pi$ modes. Under the assumption of elastic final-state rescattering, the analytic structure of the respective amplitudes will be fixed by two-body unitarity for $\pi\pi$ and $\pi\eta$ intermediate states uniquely. However, a $\eta' \to \pi\pi\eta$ decay followed by $\pi\eta \to \pi\pi$ rescattering yields an inelastic contribution to the unitarity relation of $\eta' \to 3\pi$ within the physical boundaries of the DALITZ plot. In order to take this effect properly into account, the dispersion relations of all three amplitudes have to consistently fulfill the constraints of unitarity for $\pi\pi$ and $\pi\eta$ intermediate states. The work on this extension is currently in progress [199], including an update of the $\eta' \to \pi\pi\eta$ analysis based on the latest version of the $\pi\eta$ scattering phase shift from the Orsay group [136] and the high-statistics DALITZ-plot distributions from the A2 and BESIII collaborations [220, 221].

In analogy to the analysis of C- and CP-violating transitions in $\eta \to \pi^+\pi^-\pi^0$ presented in this thesis, we are currently extending the dispersive framework to study these kind of transitions in $\eta' \to \pi^+\pi^-\eta$ as well [258]. Due to the different isospin structure of the three-body final state, this decay is sensitive to a different BSM operator with isovector quantum numbers. An essential future extension of the analysis, which still has to be completed for both $\eta \to \pi^+\pi^-\pi^0$ and $\eta' \to \pi^+\pi^-\eta$, is the construction of operators mediating such C- and CP-violating transitions in ChPT that can be matched with our dispersion relations. Furthermore, to predict a scale for BSM physics an identification of these effective operators with fundamental quark-level operators is needed [252].

Finally, we want to mention further possible applications of KHURI–TREIMAN techniques in the analysis of three-body rescattering effects of pions at low and intermediate energies. The diffractive $\pi^- p \to \pi^+\pi^-\pi^- p$ reaction studied at the COMPASS experiment offers a nice testing ground to study final-state interactions of the three-pion system with isovector quantum numbers [320, 321]. As a first step we propose an analysis of the spin-exotic $I^G(J^{PC}) = 1^-(1^{-+})$ three-pion mode associated with the $\pi_1(1600)$ resonance, since this mode shows rather simple decay dynamics consisting of two interfering P-waves in the two-body $\pi\pi$ subsystems [322]. Similarly to the $I^G(J^{PC}) = 0^-(1^{--})$ three-pion mode in $\omega \to 3\pi$ decays, elastic two-body unitarity demands the dynamics of $\pi_1(1600) \to 3\pi$ decays to be dominated by $\rho(770)$ contributions at low energies. In order to gain a better understanding of three-body unitarity effects induced by the crossed-channel $\rho(770)$ interference in the KHURI–TREIMAN formalism, a comparison of the resulting single-variable amplitudes for the isoscalar and isovector three-pion modes at different invariant energies seems promising. For the future, extensions to other isovector three-pion modes investigated by the COMPASS collaboration are planned. In this way, the KHURI–TREIMAN formalism has the potential to systematically improve on new amplitude analyses of hadronic three-body decays.

Appendices

Appendix A

Mathematical formulae

A.1 Properties of the Gell-Mann matrices

In the lowest-dimensional representation of SU(3) the eight generators are given in terms of 3×3 complex matrices λ^a. These HERMITIAN and traceless GELL-MANN matrices [38] are given by

$$\begin{aligned}
\lambda^1 &= \begin{pmatrix} 0 & 1 & 0 \\ 1 & 0 & 0 \\ 0 & 0 & 0 \end{pmatrix}, \qquad \lambda^2 = \begin{pmatrix} 0 & -i & 0 \\ i & 0 & 0 \\ 0 & 0 & 0 \end{pmatrix}, \qquad \lambda^3 = \begin{pmatrix} 1 & 0 & 0 \\ 0 & -1 & 0 \\ 0 & 0 & 0 \end{pmatrix}, \\
\lambda^4 &= \begin{pmatrix} 0 & 0 & 1 \\ 0 & 0 & 0 \\ 1 & 0 & 0 \end{pmatrix}, \qquad \lambda^5 = \begin{pmatrix} 0 & 0 & -i \\ 0 & 0 & 0 \\ i & 0 & 0 \end{pmatrix}, \\
\lambda^6 &= \begin{pmatrix} 0 & 0 & 0 \\ 0 & 0 & 1 \\ 0 & 1 & 0 \end{pmatrix}, \qquad \lambda^7 = \begin{pmatrix} 0 & 0 & 0 \\ 0 & 0 & -i \\ 0 & i & 0 \end{pmatrix}, \qquad \lambda^8 = \frac{1}{\sqrt{3}} \begin{pmatrix} 1 & 0 & 0 \\ 0 & 1 & 0 \\ 0 & 0 & -2 \end{pmatrix},
\end{aligned} \tag{A.1}$$

and obey, in analogy to the 2×2 PAULI matrices of SU(2), the commutation, anticommutation and orthogonality relations

$$[\lambda^a, \lambda^b] = 2i\, f_{abc}\, \lambda^c\,, \qquad \{\lambda^a, \lambda^b\} = \tfrac{4}{3}\delta_{ab} + 2d_{abc}\, \lambda^c\,, \qquad \mathrm{tr}(\lambda^a \lambda^b) = 2\delta_{ab}\,. \tag{A.2}$$

The completely antisymmetric real structure constants f_{abc} can be expressed as

$$f_{abc} = -\tfrac{1}{4} i\, \mathrm{tr}\big([\lambda^a, \lambda^b]\lambda^c\big)\,, \tag{A.3}$$

leading to

$$\begin{aligned}
&f_{123} = 1\,, \\
&f_{147} = -f_{156} = f_{246} = f_{257} = f_{345} = -f_{367} = \tfrac{1}{2}\,, \\
&f_{458} = f_{678} = \tfrac{\sqrt{3}}{2}\,,
\end{aligned} \tag{A.4}$$

where other combinations not listed above are zero. A similar identity is found for the completely symmetric real constants d_{abc} given by

$$d_{abc} = \tfrac{1}{4}\,\mathrm{tr}\big(\{\lambda^a, \lambda^b\}\lambda^c\big)\,, \tag{A.5}$$

fixes

$$\begin{aligned} &d_{118} = d_{228} = d_{338} = -d_{888} = \tfrac{1}{\sqrt{3}}\,, \\ &d_{448} = d_{558} = d_{668} = d_{778} = -\tfrac{1}{2\sqrt{3}}\,, \\ &d_{146} = d_{157} = -d_{247} = d_{256} = d_{344} = d_{355} = -d_{366} = d_{377} = \tfrac{1}{2}\,. \end{aligned} \tag{A.6}$$

Again, all combinations not listed above are zero.

One may define a ninth 3×3 matrix [38]

$$\lambda^0 = \sqrt{\frac{2}{3}} \begin{pmatrix} 1 & 0 & 0 \\ 0 & 1 & 0 \\ 0 & 0 & 1 \end{pmatrix}\,, \tag{A.7}$$

which extends SU(3) to U(3) symmetry. The new matrix is chosen in such a way that the relations

$$[\lambda^a, \lambda^b] = 2i\, f_{abc}\, \lambda^c\,, \qquad \{\lambda^a, \lambda^b\} = 2d_{abc}\, \lambda^c\,, \qquad \mathrm{tr}(\lambda^a \lambda^b) = 2\delta_{ab}\,, \tag{A.8}$$

hold for all nine λ^a. Hence, f_{abc} is defined as before with the exception that it vanishes if one index is zero. Similarly, d_{abc} will be given as before except for additional nonzero elements whenever one index is zero and the two other indices will be identical

$$d_{000} = d_{011} = d_{022} = d_{033} = d_{044} = d_{055} = d_{066} = d_{077} = d_{088} = \sqrt{\tfrac{2}{3}}\,. \tag{A.9}$$

Supplemented by this unit matrix, an arbitrary 3×3 matrix M can be constructed according to

$$M = M_a\, \lambda^a\,, \tag{A.10}$$

where summation index a now runs from 0 to 8 and the complex coefficients M_a may be given by

$$M_a = \tfrac{1}{2}\,\mathrm{tr}(M\,\lambda^a)\,. \tag{A.11}$$

A.2 Properties of the Legendre polynomials

The Legendre polynomials $P_\ell(z)$ with $\ell \in \mathbb{N}_0$ and $z \in [-1, 1]$, used in the partial-wave expansion of $2 \to 2$ scattering processes involving only particles of spin zero, are a set of linearly independent functions. Hence, these polynomials fulfil the orthogonality relation

$$\int_{-1}^{1} \mathrm{d}z\, P_\ell(z)\, P_{\ell'}(z) = \frac{2}{2\ell + 1}\, \delta_{\ell\ell'}\,, \tag{A.12}$$

which allows for a projection of an amplitude onto distinct partial waves. Under sign flip of the argument $z \mapsto -z$ the LEGRENDRE polynomials obey

$$P_\ell(-z) = (-)^\ell \, P_\ell(z) \,. \tag{A.13}$$

Furthermore, if the angles $z \equiv \cos\theta$ fulfil

$$\cos\theta'' = \cos\theta \, \cos\theta' + \sin\theta \, \sin\theta' \cos(\phi - \phi') \,, \tag{A.14}$$

the identity

$$\int \mathrm{d}\Omega' \, P_{\ell'}(z') \, P_{\ell''}(z'') = \frac{4\pi \, \delta_{\ell'\ell''}}{2\ell' + 1} P_{\ell'}(z) \,, \tag{A.15}$$

holds, which can be proven by using the addition theorem for the spherical harmonics

$$P_\ell(z_s'') = \frac{4\pi}{2\ell + 1} \sum_{m=-\ell}^{\ell} Y_{\ell m}(\theta, \phi) \, Y_{\ell m}^*(\theta', \phi') \,. \tag{A.16}$$

The first three LEGENDRE polynomials are given by

$$P_0(z) = 1 \,, \qquad P_1(z) = z \,, \qquad P_2(z) = \frac{1}{2}(3z^2 - 1) \,. \tag{A.17}$$

When dealing with derivatives of the LEGRENDRE polynomials P_ℓ' the following orthogonality relation will hold:

$$\int_{-1}^{1} \mathrm{d}z \, \big[P_{\ell-1}(z) - P_{\ell+1}(z)\big] \, P_{\ell'}(z) = 2\delta_{\ell\ell'} \,. \tag{A.18}$$

A.3 Identities for complex numbers

Any given arbitrary complex number $z \in \mathbb{C}$ can be given in two different ways: a CARTESIAN representation

$$z = \mathrm{Re}\, z + i \, \mathrm{Im}\, z \,, \tag{A.19}$$

and a polar representation

$$z = |z| \exp(i \arg z) = |z| \cos(\arg z) + i \, |z| \sin(\arg z) \,, \tag{A.20}$$

where the second equivalence is known as EULER's formula. Comparing eqs. (A.19) and (A.20) yields the identities

$$\mathrm{Re}\, z = z \cos(\arg z) \exp(-i \arg z) \,, \qquad \mathrm{Im}\, z = z \sin(\arg z) \exp(-i \arg z) \,. \tag{A.21}$$

A.4 Identities for polynomials

For $x, s \in \mathbb{C}$ and $n \in \mathbb{N}_0$ the following identity will hold

$$x^n - s^n = (x - s) \sum_{k=0}^{n-1} s^{n-k-1} \, x^k \, . \tag{A.22}$$

If a polynomial P_n of degree n is given by

$$P_n(x) = \sum_{k=0}^{n} c_k \, x^k \, , \tag{A.23}$$

with $c_j \in \mathbb{C}$, eq. (A.22) allows us to rewrite

$$P_n(x) - P_n(s) = (x - s) \sum_{k=1}^{n} c_k \sum_{j=0}^{k-1} s^{k-j-1} \, x^j \, . \tag{A.24}$$

Let Q_n denote another polynomial of degree n given by

$$Q_n(s) = \prod_{k=1}^{n} (s - s_k) \, , \tag{A.25}$$

with $s_k \in \mathbb{C}$, then

$$\frac{Q_n(a - s)}{Q_n(a - x)} = \frac{Q_n(s)}{Q_n(x)} + (x - s) \, q_{n-1}^x(s) \, , \tag{A.26}$$

holds for $a \in \mathbb{C}$ and q_{n-1}^x denotes another polynomial in s of degree $n-1$ whose coefficients are of order $\mathcal{O}(x^{-n-1})$. A formal proof of this relation can be found in [144].

Appendix B

Dalitz-plot expansion of $1 \to 3$ decay amplitudes

First invented to study the decay region of $K \to 3\pi$ [122–124], it has become common to present the Dalitz-plot expansion of the T-matrix element in terms of dimensionless kinematical variables when analysing three-body decays, *cf.* chs. 5 and 6. These so-called Dalitz-plot variables, describing the kinematics in the decay region of the analysed process, can be related to the Mandelstam variables discussed in sec. 2.2.1.

The construction of the Dalitz-plot variables can be realized in the following way: we begin by choosing the rest frame of the decaying particle defined in eq. (2.41), *i.e.*, $p_1^0 = M_1$ and $|\mathbf{p}_1| = 0$. The total kinetic energy available for the decay is given by

$$Q_1 = T_2 + T_3 + T_4 = M_1 - M_2 - M_3 - M_4 \,, \tag{B.1}$$

where $T_i = p_i^0 - M_i$ define the kinetic energies carried by the three decay products. Similarly to the sum of the Mandelstam variables (2.25), eq. (B.1) tells us directly that the sum of the three kinetic energies T_i for a given decay is fixed. In analogy to the construction of the Mandelstam diagram, we construct an equilateral triangle in the plane of rescaled kinetic energies $\varepsilon_i = 3T_i/Q_i$ rendering them dimensionless. Since the perpendicular distances from each side will be identified with the respective energies ε_i, eq. (B.1) directly fixes the height of the triangle to a value three. Any given kinematical configuration of the considered three-body decay process (2.41) can be identified uniquely as a point in the ε_i-plane bounded by the triangle. The constructed triangle encloses a unit circle whose center is located at the point of equal ε_i. Now we introduce a set of two linear-independent Dalitz-plot variables [122–124]

$$x \equiv \sqrt{3}\,\frac{T_4 - T_3}{Q_1} \,, \qquad y \equiv \frac{2T_2 - T_3 - T_4}{Q_1} \,, \tag{B.2}$$

which are defined such that the origin[#1] of the new coordinate system $x = y = 0$ coincides with the center of the unit circle and the additional condition $x^2 + y^2 = 1$ on its perimeter

[#1] It follows directly that the center of the Mandelstam diagram at $s = t = u = r$ will coincide with the Daliz-plot center only in the special case of equal mass decay products.

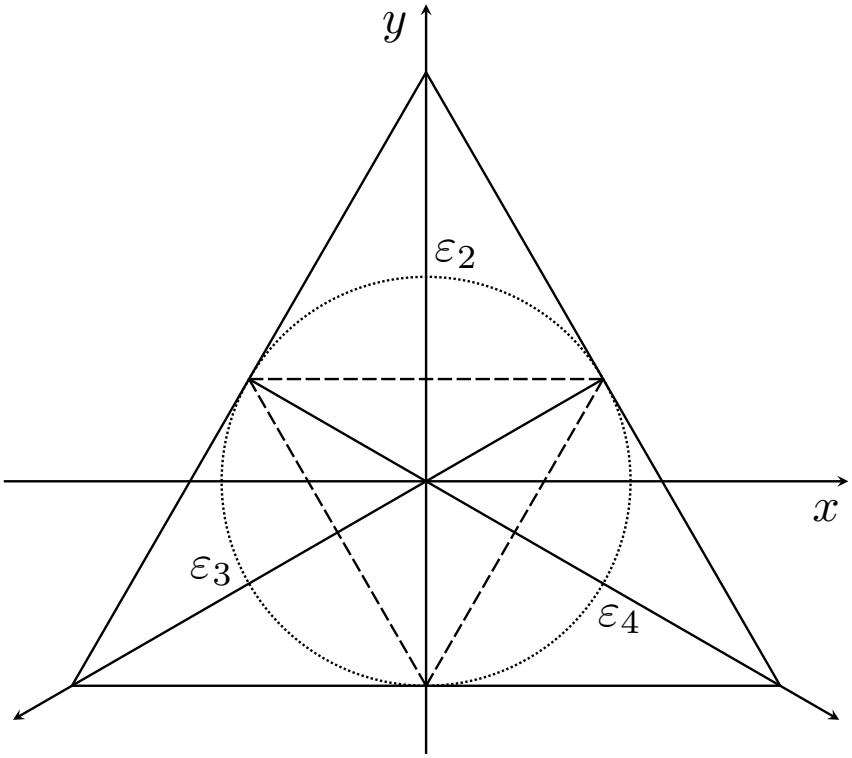

Fig. B.1: Geometry of the DALITZ-plot plane spanned by the perpendicular DALITZ-plot variables x and y, defined in terms of the rescaled dimensionless kinetic energies ε_i of the three decay products (B.2). The outer equilateral triangle defines the universal bounds on x and y for a general three-body decay process. The restrictions for the non- and ultra-relativistic limits are depicted by the dotted unit circle and the dashed inner triangle, respectively.

will hold. From eqs. (2.23) and (2.24) follows that the energies of the three decay products in terms of the MANDELSTAM variables are given by

$$p_2^0 = \frac{M_1^2 + M_2^2 - s}{2M_1}\,, \qquad p_3^0 = \frac{M_1^2 + M_3^2 - t}{2M_1}\,, \qquad p_4^0 = \frac{M_1^2 + M_4^2 - u}{2M_1}\,, \tag{B.3}$$

which allows us to rewrite the DALITZ-plot variables in eq. (B.2) according to

$$x = \frac{\sqrt{3}}{2M_1\,Q_1}\big(t - u + 2M_1(M_3 - M_4) - \Delta_{34}\big)\,, \qquad y = \frac{3}{2M_1\,Q_1}\big((M_1 - M_2)^2 - s\big) - 1\,. \tag{B.4}$$

The DALITZ-plot variables of any given three-body decay process will at least be bounded by the outer triangle.[#2] In the special case of decay products of equal mass, the limits are further restricted to the inner of the unit circle. Since a decay with identical

[#2] Dealing with three-body decays involving the decay products with different masses, it might be convenient to rescale the DALITZ-plot variables by some fraction of these masses, *cf.* ch. 5. However, it needs to be mentioned that such a rescaling directly contradicts the underlying symmetry of these variables.

reaction products will be symmetric under exchange of the kinetic energies, the three perpendicular ε_i-axes reveal the sixfold symmetry of such a process. Therefore the information on the T-matrix element in one of the six sub-triangles generates the complete DALITZ plot by mirroring along the symmetry axes. Additionally, we want to mention the constraints on x and y in the *non-* and *ultra-relativistic limit*: the former limit will result in a unit circle, while latter limit leads to an equilateral triangle whose tips will touch the unit circle. A sketch of the geometric considerations made so far is depicted in fig. B.1.

In case of three-body decay process that is free of any dominant resonance structures in the DALITZ-plot distribution, it is convenient to expand the modulus square of the T-matrix element in terms of the DALITZ-plot variables x and y. At the DALITZ-plot center the most general expansion is given by

$$\begin{aligned}\left|\mathcal{T}_{fi}(x,y)\right|^2 = |\mathcal{N}|^2(1 + a\,y + b\,y^2 + c\,x + d\,x^2 + e\,x\,y \\ + f\,y^3 + g\,x^2\,y + h\,x\,y^2 + l\,x^3 + ...)\,.\end{aligned} \tag{B.5}$$

where the real coefficients a, b, c, d, e, f, g, h, and l are the so-called DALITZ-plot parameters and $\mathcal{N}$ defines the normalization of the matrix element. Considering the case of two identical particles in the final state, the squared modulus of the amplitude is symmetric under exchange of the corresponding momenta, *cf.* sec. 2.2.1. Conventionally the kinematic variables will be defined such that the expansion in eq. (B.5) has to be even under reflection of $x \to -x$, hence all DALITZ-plot parameters of odd powers of x have to vanish and eq. (B.5) simplifies to

$$\left|\mathcal{T}_{fi}(x,y)\right|^2 = |\mathcal{N}|^2(1 + a\,y + b\,y^2 + d\,x^2 + f\,y^3 + g\,x^2\,y + ...)\,. \tag{B.6}$$

Finally, we want to mention that for three-body decay processes with three identical decay products commonly two additional polar variables are defined at the DALITZ-plot center

$$z \equiv x^2 + y^2\,, \qquad \phi \equiv \arg(x + iy)\,, \tag{B.7}$$

which account for the underlying symmetry of this configuration. Thus, the new DALITZ-plot variable z can only depend on the squares of the MANDELSTAM variables given by

$$z = \frac{3}{2M_1^2\,Q_1^2}\,(s^2 + t^2 + u^2 - 3r^2)\,. \tag{B.8}$$

Accordingly the DALITZ-plot expansion of the squared absolute value of the T-matrix element

$$\begin{aligned}\left|\mathcal{T}_{fi}(z,\phi)\right|^2 = |\mathcal{N}|^2(1 + 2\alpha\,z + 2\beta\,z^{3/2}\sin 3\phi + 2\gamma\,z^2 \\ + 2\delta\,z^{5/2}\sin 3\phi + 2\varepsilon\,z^3 + 2\zeta\,z^3\cos 6\phi + ...)\,,\end{aligned} \tag{B.9}$$

defines the DALITZ-plot parameters α, β, γ, δ, ε, and ζ.

Appendix C

Supplementary notes on $\eta' \to \pi\pi\eta$ decays

C.1 Construction of $\pi^0\pi^0$ and $\pi^0\eta$ phase shifts

The scalar form factors of neutral and charged pions including isospin-breaking effects have been calculated in the framework of a nonrelativistic effective field theory (NREFT) in ref. [323] (*cf.* also refs. [324, 325] for details on the NREFT formalism). We use a simplified version of this result: we only retain the correct thresholds of the two channels ($\pi^0\pi^0$ and $\pi^+\pi^-$), but disregard isospin-violating corrections in the polynomials that describe the effective-range expansion of the scattering partial wave and the low-energy form factor expansion. In this way, we retain all the nonanalytic effects due to the pion mass difference that scale like $\sqrt{M_\pi^2 - M_{\pi^0}^2}$ near the two-pion thresholds, but neglect regular isospin violation in the form factor of order $M_\pi^2 - M_{\pi^0}^2$, which can be calculated in chiral perturbation theory [326, 327]. In this approximation, the phase of F_S^0 is given by

$$\arg F_S^0(s) = \arg\left[1 - i\sigma_0 v_0 - \frac{2}{3} i \frac{(v_0 - v_2)(\sigma - \sigma_0)}{1 - i\sigma v_2}\right]^{-1}, \tag{C.1}$$

where $\sigma = \sigma_\pi(s)$ as defined in sec. 2.3.1, and $\sigma_0 = \sqrt{1 - 4M_{\pi^0}^2/s}$. The polynomials v_I for isospin $I = 0, 2$ are related to the S-wave effective-range expansions,

$$v_I(s) = a_0^I + \mathcal{O}(s - 4M_\pi^2)\,, \tag{C.2}$$

where a_0^I are the S-wave $\pi\pi$ scattering lengths. They can be expressed in terms of the phase shifts of corresponding isospin according to

$$v_I(s) = \sigma^{-1}(s) \tan\delta_0^I(s)\,. \tag{C.3}$$

In order to continue eqs. (C.1) and (C.3) to the region $4M_{\pi^0}^2 \leq s < 4M_\pi^2$, we employ an effective-range expansion adapted to the phase shifts used for the v_I, and the analytic continuation $\sigma \mapsto +i\sqrt{-\sigma^2}$.

The resulting phase is shown in fig. C.1 and compared to δ_0^0, the phase shift in the isospin limit. We see that $\arg F_S^0$ starts at $s = 4M_{\pi^0}^2$, and has a sharp cusp at $s = 4M_\pi^2$, as

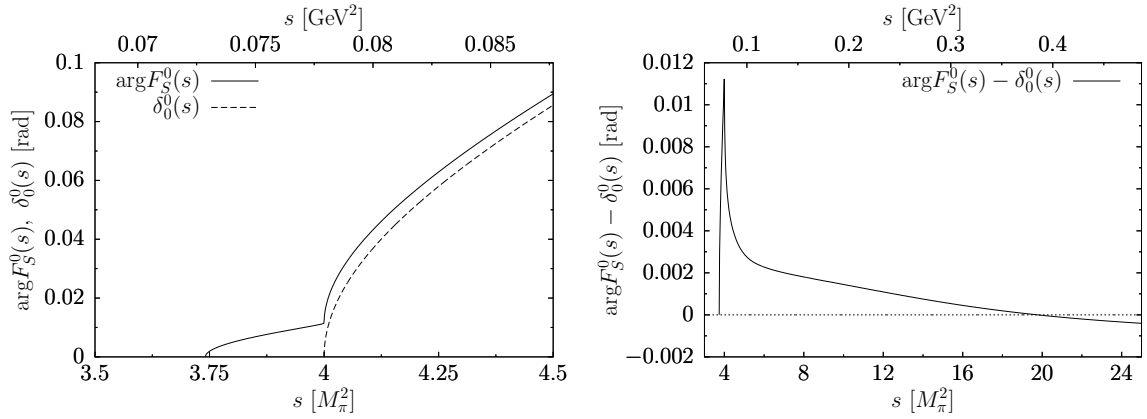

Fig. C.1: Left panel: Comparison of $\arg F_S^0$ (solid line), the phase of the neutral-pion scalar form factor including the effects of different $\pi^0\pi^0$ and $\pi^+\pi^-$ thresholds, to the isospin-symmetric phase shift δ_0^0 (dashed line). Right panel: the difference of $\arg F_S^0$ and δ_0^0 over a larger range in s.

anticipated. The difference of $\arg F_S^0$ and δ_0^0 quickly becomes tiny away from the threshold region, and in fact crosses 0 around $s = 0.4\,\mathrm{GeV}^2$. We neglect the isospin-violating phase difference above this point, and use the isospin-symmetric phase shift at higher energies.

We adapt the $\pi\eta$ phase from ref. [135] for $\pi^0\eta$ scattering in a simpler manner. In this case, there are no different channels coupling/no additional cusps introduced, hence we just need to account for the slightly lower threshold. We achieve this by a linear mapping of the elastic regions $[(M_{\pi^0}+M_\eta)^2, 4M_K^2] \mapsto [(M_\pi+M_\eta)^2, 4M_K^2]$, such that the $\pi^0\eta$ scattering phase shift $\tilde{\delta}_0^1$ is defined as

$$\tilde{\delta}_0^1(t) = \delta_0^1\big(\tilde{t}(t)\big)\,, \qquad \tilde{t}(t) = 4M_K^2 - \frac{4M_K^2 - (M_\pi+M_\eta)^2}{4M_K^2 - (M_{\pi^0}+M_\eta)^2}\,(4M_K^2 - t)\,. \tag{C.4}$$

Above the $\bar{K}K$ threshold, we set $\tilde{\delta}_0^1$ equal to δ_0^1. As the $\pi\eta$ phase shift rises only slowly before the onset of the $a_0(980)$ resonance, the isospin-breaking shift is small compared to the uncertainty in the phase shift itself already rather close to threshold.

C.2 Matching equations

In the case of RChT, the matching procedure to the dispersive representation is straightforward: an obvious decomposition of the amplitude (5.65) is

$$\begin{aligned}
\mathcal{F}_0^{0,\mathrm{RChT}}(s) &= c_{qq}\,\frac{M_S^2}{M_S^2 - s}\left[\frac{M_S^2}{F_\pi^2}\left(\frac{\xi}{M_S^4} + \frac{\psi}{M_S^2} + c_d^2\right) + \rho - \frac{c_d^2\,\Delta}{F_\pi^2\,M_S^2} - \rho\,\frac{s}{M_S^2}\right], \\
\mathcal{G}_0^{1,\mathrm{RChT}}(t) &= c_{qq}\,\frac{M_S^2}{M_S^2 - t}\,\frac{M_S^2}{F_\pi^2}\left(\frac{\xi}{M_S^4} + \frac{\psi}{M_S^2} + c_d^2\right),
\end{aligned} \tag{C.5}$$

which is compatible with the required asymptotic behavior. In order also to match the TAYLOR expansion in (5.26), we have to apply a transformation (5.23) with $c_2 = 0$ and

$$c_1 = 2c_{qq}\,\frac{M_S^2}{F_\pi^2}\,A\,, \qquad A \equiv \frac{\xi}{M_S^4} + \frac{\psi}{M_S^2} + c_d^2\,. \tag{C.6}$$

Matching the TAYLOR coefficients to the dispersive representation leads to the subtraction constants

$$\begin{aligned}
\alpha^{\mathrm{RChT}} &= c_{qq}\left[\rho + \frac{3M_S^2}{F_\pi^2}\left(A - \frac{c_d^2\,\Delta}{3M_S^4}\right)\right],\\
\beta^{\mathrm{RChT}} &= c_{qq}\left[\frac{M_{\eta'}^2}{F_\pi^2}\left(A - \frac{c_d^2\,\Delta}{M_S^4}\right) - \omega_0^0\left(\frac{3M_{\eta'}^2\,M_S^2}{F_\pi^2}\left(A - \frac{c_d^2\,\Delta}{3M_S^4}\right) + \rho\,M_{\eta'}^2\right)\right],\\
\gamma^{\mathrm{RChT}} &= c_{qq}\,\frac{M_{\eta'}^2}{F_\pi^2}\,A\,.
\end{aligned} \tag{C.7}$$

The RChT amplitude can also be matched to the representation (5.24) with four subtraction constants. In this case, eq. (C.5) has to be transformed according to (5.23) with

$$c_1 = 2c_{qq}\frac{M_S^2 + r}{F_\pi^2}A\,, \quad c_2 = -c_{qq}\,\frac{M_{\eta'}^2}{F_\pi^2}\,A\,. \tag{C.8}$$

The matching equations for this case are given by

$$\begin{aligned}
\alpha_0^{\mathrm{RChT}} &= c_{qq}\left[\rho + \frac{3}{F_\pi^2}\left(\left(M_S^2 + r\right)A - \frac{c_d^2\,\Delta}{3M_S^2}\right)\right],\\
\beta_0^{\mathrm{RChT}} &= -c_{qq}\left[\frac{c_d^2\,\Delta\,M_{\eta'}^2}{F_\pi^2\,M_S^4} + \omega_0^0\,\frac{3M_{\eta'}^2}{F_\pi^2}\left(\left(M_S^2 + r\right)A - \frac{c_d^2\,\Delta}{3M_S^2}\right) + M_{\eta'}^2\,\omega_0^0\,\rho\right],\\
\gamma_0^{\mathrm{RChT}} &= c_{qq}\Bigg[-\tilde{\omega}_0^0\,\frac{3M_{\eta'}^4}{2F_\pi^2}\left(\left(M_S^2 + r\right)A - \frac{c_d^2\,\Delta}{3M_S^2}\right)\\
&\qquad + \frac{M_{\eta'}^4}{F_\pi^2\,M_S^2}\left(A + \frac{c_d^2\,\Delta\,(M_S^2\,\omega_0^0 - 1)}{M_S^4}\right) - \frac{M_{\eta'}^4}{2}\,\tilde{\omega}_0^0\,\rho\Bigg],\\
\gamma_1^{\mathrm{RChT}} &= c_{qq}\,\frac{M_{\eta'}^4}{F_\pi^2\,M_S^2}\,A\,.
\end{aligned} \tag{C.9}$$

In the case of NLO large-N_C ChPT, an obvious decomposition of the amplitude (5.62) is

$$\mathcal{F}_{0,\mathrm{NLO}}^{0,\mathrm{ChPT}}(s) = B + C\frac{s^2}{M_{\eta'}^4}\,, \qquad \mathcal{G}_{0,\mathrm{NLO}}^{1,\mathrm{ChPT}}(t) = C\frac{t^2}{M_{\eta'}^4}\,, \tag{C.10}$$

where we defined

$$B \equiv c_{qq}\left[\frac{M_\pi^2}{2} - \frac{2\,(3L_2+L_3)}{F_\pi^2}\left(M_{\eta'}^4 + M_\eta^4 + 2M_\pi^4\right)\right.$$
$$\left. - \frac{2L_5}{F_\pi^2}\left(M_{\eta'}^2 + M_\eta^2 + 2M_\pi^2\right)M_\pi^2 + \frac{24L_8}{F_\pi^2}\,M_\pi^4 + \frac{2}{3}\Lambda_2\,M_\pi^2\right] + c_{sq}\,\frac{\sqrt{2}}{3}\Lambda_2\,M_\pi^2\,,$$
$$C \equiv c_{qq}\,\frac{2\,(3L_2+L_3)}{F_\pi^2}\,M_{\eta'}^4\,. \tag{C.11}$$

In this case, it is not possible to match to the representation (5.26), because NLO large-N_C ChPT is not compatible with the assumed asymptotic behavior. However, it can be matched directly to the representation (5.24), as both the asymptotics and the Taylor expansion agree, leading to

$$\alpha_0^{\text{ChPT}} = B\,, \qquad \beta_0^{\text{ChPT}} = -B\,M_{\eta'}^2\,\omega_0^0\,, \qquad \gamma_0^{\text{ChPT}} = C - \frac{\tilde{\omega}_0^0}{2}\,B\,M_{\eta'}^4\,, \qquad \gamma_1^{\text{ChPT}} = C\,. \tag{C.12}$$

Bibliography

[1] S. L. Glashow, *Partial Symmetries of Weak Interactions*, Nucl. Phys. **22**, 579–588 (1961).

[2] A. Salam and J. C. Ward, *Electromagnetic and weak interactions*, Phys. Lett. **13**, 168–171 (1964).

[3] S. Weinberg, *A Model of Leptons*, Phys. Rev. Lett. **19**, 1264–1266 (1967).

[4] G. 't Hooft and M. J. G. Veltman, *Regularization and Renormalization of Gauge Fields*, Nucl. Phys. B **44**, 189–213 (1972).

[5] H. Fritzsch, M. Gell-Mann, and H. Leutwyler, *Advantages of the Color Octet Gluon Picture*, Phys. Lett. B **47**, 365–368 (1973).

[6] F. Englert and R. Brout, *Broken Symmetry and the Mass of Gauge Vector Mesons*, Phys. Rev. Lett. **13**, 321–323 (1964).

[7] P. W. Higgs, *Broken Symmetries and the Masses of Gauge Bosons*, Phys. Rev. Lett. **13**, 508–509 (1964).

[8] G. S. Guralnik, C. R. Hagen, and T. W. B. Kibble, *Global Conservation Laws and Massless Particles*, Phys. Rev. Lett. **13**, 585–587 (1964).

[9] G. Aad *et al.* [ATLAS Collaboration], *Observation of a new particle in the search for the Standard Model Higgs boson with the ATLAS detector at the LHC*, Phys. Lett. B **716**, 1–29 (2012) [arXiv:1207.7214 [hep-ex]].

[10] S. Chatrchyan *et al.* [CMS Collaboration], *Observation of a New Boson at a Mass of 125 GeV with the CMS Experiment at the LHC*, Phys. Lett. B **716**, 30–61 (2012) [arXiv:1207.7235 [hep-ex]].

[11] N. N. Khuri and S. B. Treiman, *Pion-Pion Scattering and $K^{\pm} \to 3\pi$ Decay*, Phys. Rev. **119**, 1115–1121 (1960).

[12] C.-N. Yang and R. L. Mills, *Conservation of Isotopic Spin and Isotopic Gauge Invariance*, Phys. Rev. **96**, 191–195 (1954).

[13] S. Weinberg, *Nonabelian Gauge Theories of the Strong Interactions*, Phys. Rev. Lett. **31**, 494–497 (1973).

[14] P. A. Zyla *et al.* [Particle Data Group], *Review of Particle Physics*, Prog. Theor. Exp. Phys. **2020**, 083C01 (2020).

[15] J. Greensite, *An introduction to the confinement problem.* Lect. Notes Phys. **821**. Springer, Heidelberg, Germany, (2011).

[16] A. Jaffe and E. Witten, *Quantum Yang–Mills theory*, Clay Mathematics Institute, Peterborough (NH), United States, (2000).

[17] D. J. Gross and F. Wilczek, *Ultraviolet Behavior of Nonabelian Gauge Theories*, Phys. Rev. Lett. **30**, 1343–1346 (1973).

[18] D. J. Gross and F. Wilczek, *Asymptotically Free Gauge Theories. I*, Phys. Rev. D **8**, 3633–3652 (1973).

[19] D. J. Gross and F. Wilczek, *Asymptotically Free Gauge Theories. II*, Phys. Rev. D **9**, 980–993 (1974).

[20] H. D. Politzer, *Reliable Perturbative Results for Strong Interactions?*, Phys. Rev. Lett. **30**, 1346–1349 (1973).

[21] H. D. Politzer, *Asymptotic Freedom: An Approach to Strong Interactions*, Phys. Rept. **14**, 129–180 (1974).

[22] D. J. Gross, *Twenty five years of asymptotic freedom*, Nucl. Phys. B Proc. Suppl. **74**, 426–446 (1999) [arXiv:hep-th/9809060].

[23] R. J. Crewther, *Nonperturbative evaluation of the anomalies in low-energy theorems*, Phys. Rev. Lett. **28**, 1421 (1972).

[24] M. S. Chanowitz and J. R. Ellis, *Canonical Trace Anomalies*, Phys. Rev. D **7**, 2490–2506 (1973).

[25] J. C. Collins, A. Duncan, and S. D. Joglekar, *Trace and Dilatation Anomalies in Gauge Theories*, Phys. Rev. D **16**, 438–449 (1977).

[26] K. Fujikawa, *Energy Momentum Tensor in Quantum Field Theory*, Phys. Rev. D **23**, 2262 (1981).

[27] J. F. Donoghue, E. Golowich, and B. R. Holstein, *Dynamics of the standard model*, vol. 2 of *Cambridge Monographs on Particle Physics, Nuclear Physics and Cosmology.* Cambridge Univ. Press, Cambridge, United Kingdom, (2014).

[28] M. Hoferichter, C. Ditsche, B. Kubis, and U.-G. Meißner, *Dispersive analysis of the scalar form factor of the nucleon*, JHEP **06**, 063 (2012) [arXiv:1204.6251 [hep-ph]].

[29] M. Hoferichter, J. Ruiz de Elvira, B. Kubis, and U.-G. Meißner, *High-Precision Determination of the Pion-Nucleon σ Term from Roy-Steiner Equations*, Phys. Rev. Lett. **115**, 092301 (2015) [arXiv:1506.04142 [hep-ph]].

[30] M. Hoferichter, J. Ruiz de Elvira, B. Kubis, and U.-G. Meißner, *Remarks on the pion–nucleon σ-term*, Phys. Lett. B **760**, 74–78 (2016) [arXiv:1602.07688 [hep-lat]].

[31] J. Ruiz de Elvira, M. Hoferichter, B. Kubis, and U.-G. Meißner, *Extracting the σ-term from low-energy pion-nucleon scattering*, J. Phys. G **45**, 024001 (2018) [arXiv:1706.01465 [hep-ph]].

[32] Y. Nambu and G. Jona-Lasinio, *Dynamical Model of Elementary Particles Based on an Analogy with Superconductivity. I*, Phys. Rev. **122**, 345–358 (1961).

[33] Y. Nambu and G. Jona-Lasinio, *Dynamical Model of Elementary Particles Based on an Analogy with Superconductivity. II*, Phys. Rev. **124**, 246–254 (1961).

[34] J. Goldstone, *Field Theories with Superconductor Solutions*, Nuovo Cim. **19**, 154–164 (1961).

[35] J. Goldstone, A. Salam, and S. Weinberg, *Broken Symmetries*, Phys. Rev. **127**, 965–970 (1962).

[36] M. Gell-Mann, *The Eightfold Way: A Theory of strong interaction symmetry*, CTSL-20, TID-12608 (1961).

[37] Y. Ne'eman, *Derivation of strong interactions from a gauge invariance*, Nucl. Phys. **26**, 222–229 (1961).

[38] M. Gell-Mann, *Symmetries of baryons and mesons*, Phys. Rev. **125**, 1067–1084 (1962).

[39] M. Gell-Mann, *A Schematic Model of Baryons and Mesons*, Phys. Lett. **8**, 214–215 (1964).

[40] G. Zweig, *An SU(3) model for strong interaction symmetry and its breaking: I*, CERN-TH-401 (1964).

[41] G. Zweig, *An SU(3) model for strong interaction symmetry and its breaking: II*, CERN-TH-412 (1964).

[42] M. Gell-Mann and Y. Ne'eman, *The Eightfold Way*. W. A. Benjamin Inc., New York City (NY), United States, (1964).

[43] S. L. Adler and R. F. Dashen, *Current Algebras and Applications to Particle Physics*. W. A. Benjamin Inc., New York City (NY), United States, (1968).

[44] V. de Alfaro, S. Fubini, G. Furlan, and C. Rossetti, *Currents in Hadron Physics*. North-Holland Publ., Amsterdam, The Netherlands, (1973).

[45] D. B. Lichtenberg, *Unitary Symmetry and Elementary Particles*. Academic Press, Cambridge (MA), United States, (1978).

[46] T. P. Cheng and L. F. Li, *Gauge Theory of Elementary Particle Physics: Problems and Solutions*. Oxford Univ. Press, Oxford, United Kingdom, (1984).

[47] S. Scherer and M. R. Schindler, *A Primer for Chiral Perturbation Theory*. Lect. Notes Phys. **830**. Springer, Heidelberg, Germany, (2012).

[48] P. B. Pal, *An Introductory Course of Particles Physics*. CRC Press Taylor & Francis Group, Abingdon-on-Thames, United Kingdom, (2014).

[49] K. Ottnad, B. Kubis, U.-G. Meißner, and F. K. Guo, *New insights into the neutron electric dipole moment*, Phys. Lett. B **687**, 42–47 (2010) [arXiv:0911.3981 [hep-ph]].

[50] S. L. Adler, *Axial vector vertex in spinor electrodynamics*, Phys. Rev. **177**, 2426–2438 (1969).

[51] S. L. Adler and W. A. Bardeen, *Absence of higher order corrections in the anomalous axial vector divergence equation*, Phys. Rev. **182**, 1517–1536 (1969).

[52] W. A. Bardeen, *Anomalous Ward identities in spinor field theories*, Phys. Rev. **184**, 1848–1857 (1969).

[53] J. S. Bell and R. Jackiw, *A PCAC puzzle:* $\pi^0 \to \gamma\gamma$ *in the* σ *model*, Nuovo Cim. A **60**, 47–61 (1969).

[54] G. 't Hooft, *Symmetry Breaking Through Bell-Jackiw Anomalies*, Phys. Rev. Lett. **37**, 8–11 (1976).

[55] H. Weyl, *Quantum mechanics and group theory*, Z. Phys. **46**, 1 (1927).

[56] E. P. Wigner, *Gruppentheorie und ihre Anwendung auf die Quantenmechanik der Atomspektren*. Vieweg Verlag, Braunschweig, Germany, (1931).

[57] C. Vafa and E. Witten, *Restrictions on Symmetry Breaking in Vector-Like Gauge Theories*, Nucl. Phys. B **234**, 173–188 (1984).

[58] J. J. de Swart, *The Octet model and its Clebsch-Gordan coefficients*, Rev. Mod. Phys. **35**, 916–939 (1963), [Erratum: Rev.Mod.Phys. 37, 326–326 (1965)].

[59] H. J. Lipkin, *Unitarity symmetry for pedestrians (or I-spin, U-spin, V-all spin for I-spin)*. Univ. of Michigan Library, Ann Arbor (MI), United States, (1964). [PRINT-63-465, ANL-6942].

[60] T. Nakano and K. Nishijima, *Charge Independence for V-particles*, Prog. Theor. Phys. **10**, 581–582 (1953).

[61] K. Nishijima, *Charge Independence Theory of V Particles*, Prog. Theor. Phys. **13**, 285–304 (1955).

[62] M. Gell-Mann, *The interpretation of the new particles as displaced charge multiplets*, Nuovo Cim. **4**, 848–866 (1956).

[63] A. Bramon, R. Escribano, and M. D. Scadron, *The η-η' mixing angle revisited*, Eur. Phys. J. C **7**, 271–278 (1999) [arXiv:hep-ph/9711229].

[64] M. L. Goldberger and S. B. Treiman, *Conserved Currents in the Theory of Fermi Interactions*, Phys. Rev. **110**, 1478–1479 (1958).

[65] M. Gell-Mann, *The Symmetry group of vector and axial vector currents*, Phys. Phys. Fiz. **1**, 63–75 (1964).

[66] S. L. Adler, *Consistency conditions on the strong interactions implied by a partially conserved axial-vector current. I*, Phys. Rev. **137**, B1022–B1033 (1965).

[67] S. L. Adler, *Consistency conditions on the strong interactions implied by a partially conserved axial-vector current. II*, Phys. Rev. **139**, B1638–B1643 (1965).

[68] S. Weinberg, *Pion scattering lengths*, Phys. Rev. Lett. **17**, 616–621 (1966).

[69] S. Weinberg, *Phenomenological Lagrangians*, Physica A **96**, 327–340 (1979).

[70] H. Leutwyler, *On the foundations of chiral perturbation theory*, Ann. Phys. **235**, 165–203 (1994) [arXiv:hep-ph/9311274].

[71] E. D'Hoker and S. Weinberg, *General effective actions*, Phys. Rev. D **50**, R6050–R6053 (1994) [arXiv:hep-ph/9409402].

[72] J. Gasser and H. Leutwyler, *Chiral Perturbation Theory to One Loop*, Annals Phys. **158**, 142 (1984).

[73] J. Gasser and H. Leutwyler, *Chiral Perturbation Theory: Expansions in the Mass of the Strange Quark*, Nucl. Phys. B **250**, 465–516 (1985).

[74] H. Lehmann, K. Symanzik, and W. Zimmermann, *On the formulation of quantized field theories*, Nuovo Cim. **1**, 205–225 (1955).

[75] S. Aoki *et al.* [FLAG Collaboration], *FLAG Review 2019*, Eur. Phys. J. C **80**, 113 (2020) [arXiv:1902.08191 [hep-lat]].

[76] P. Güttinger, *Das Verhalten von Atomen im magnetischen Drehfeld*, Z. Phys. **73**, 169–184 (1932).

[77] W. Pauli, *Die allgemeinen Prinzipien der Wellenmechanik*, Handbuch der Physik **24**, 82–272 (1933).

[78] H. Hellmann, *Einführung in die Quantenchemie*. Deuticke-Verlag, Wien, Austria, (1937).

[79] R. P. Feynman, *Forces in Molecules*, Phys. Rev. **56**, 340–343 (1939).

[80] M. Gell-Mann, R. J. Oakes, and B. Renner, *Behavior of current divergences under* $SU(3) \times SU(3)$, Phys. Rev. **175**, 2195–2199 (1968).

[81] S. Okubo, *Note on unitary symmetry in strong interactions*, Prog. Theor. Phys. **27**, 949–966 (1962).

[82] S. Okubo, *Note on Unitary Symmetry in Strong Interaction. II: Excited States of Baryons*, Prog. Theor. Phys. **28**, 24–32 (1962).

[83] S. Weinberg, *The Problem of Mass*, Trans. New York Acad. Sci. **38**, 185–201 (1977).

[84] J. Gasser and H. Leutwyler, *Quark Masses*, Phys. Rept. **87**, 77–169 (1982).

[85] J. M. Gérard, *The Light Quark Current Mass Ratios and* $\eta - \eta'$ *Mixing*, Mod. Phys. Lett. A **5**, 391 (1990).

[86] H. Leutwyler, m_u *is not equal to zero*, Nucl. Phys. B **337**, 108–118 (1990).

[87] J. F. Donoghue, B. R. Holstein, and D. Wyler, *Mass ratios of the light quarks*, Phys. Rev. Lett. **69**, 3444–3447 (1992).

[88] H. Leutwyler, *The Ratios of the light quark masses*, Phys. Lett. B **378**, 313–318 (1996) [arXiv:hep-ph/9602366].

[89] T. Das, G. S. Guralnik, V. S. Mathur, F. E. Low, and J. E. Young, *Electromagnetic mass difference of pions*, Phys. Rev. Lett. **18**, 759–761 (1967).

[90] R. F. Dashen, *Chiral SU(3)×SU(3) as a symmetry of the strong interactions*, Phys. Rev. **183**, 1245–1260 (1969).

[91] J. S. Schwinger, *On Quantum electrodynamics and the magnetic moment of the electron*, Phys. Rev. **73**, 416–417 (1948).

[92] J. S. Schwinger, *Quantum electrodynamics. I. A covariant formulation*, Phys. Rev. **74**, 1439 (1948).

[93] J. S. Schwinger, *Quantum electrodynamics. II. Vacuum polarization and selfenergy*, Phys. Rev. **75**, 651 (1948).

[94] J. S. Schwinger, *Quantum electrodynamics. III. The electromagnetic properties of the electron: Radiative corrections to scattering*, Phys. Rev. **76**, 790–817 (1949).

[95] H. Fukuda, Y. Miyamoto, and S. Tomonaga, *A Self-Consistent Subtraction Method in the Quantum Field Theory. II-1*, Prog. Theor. Phys. **4**, 47–59 (1949).

[96] R. P. Feynman, *Relativistic cutoff for quantum electrodynamics*, Phys. Rev. **74**, 1430–1438 (1948).

[97] R. P. Feynman, *Space - time approach to quantum electrodynamics*, Phys. Rev. **76**, 769–789 (1949).

[98] F. J. Dyson, *The Radiation theories of Tomonaga, Schwinger, and Feynman*, Phys. Rev. **75**, 486–502 (1949).

[99] F. J. Dyson, *The S-matrix in quantum electrodynamics*, Phys. Rev. **75**, 1736–1755 (1949).

[100] L. D. Landau, *On analytic properties of vertex parts in quantum field theory*, Nucl. Phys. **13**, 181–192 (1959).

[101] G. F. Chew, *S-Matrix Theory of Strong Interactions without Elementary Particles*, Rev. Mod. Phys. **34**, 394–401 (1962).

[102] H. P. Stapp, *Derivation of the CPT Theorem and the Connection between Spin and Statistics from Postulates of the S-Matrix Theory*, Phys. Rev. **125**, 2139 (1962).

[103] J. Gunson, *Unitarity and On-Mass-Shell Analyticity as a Basis for S-Matrix Theories. I*, J. Math. Phys. **6**, 827–844 (1965).

[104] J. Gunson, *Unitarity and On-Mass-Shell Analyticity as a Basis for S-Matrix Theories. II*, J. Math. Phys. **6**, 845–851 (1965).

[105] J. Gunson, *Unitarity and On-Mass-Shell Analyticity as a Basis for S-Matrix Theories. III*, J. Math. Phys. **6**, 852–858 (1965).

[106] D. Rickles, *A brief history of string theory: From dual models to M-theory*. The frontiers collection. Springer, Heidelberg, Germany, (2014).

[107] R. J. Eden, P. V. Landshoff, D. I. Olive, and J. C. Polkinghorne, *The analytic S-matrix*. Cambridge Univ. Press, Cambridge, United Kingdom, (1966).

[108] A. D. Martin and T. D. Spearman, *Elementary Particle Theory*. North-Holland Publ., Amsterdam, The Netherlands, (1970).

[109] S. Weinberg, *The Quantum theory of fields. Vol. 1: Foundations*. Cambridge Univ. Press, Cambridge, United Kingdom, (2005).

[110] M. E. Peskin and D. V. Schroeder, *An Introduction to quantum field theory*. Addison-Wesley, Reading (MA), United States, (1995).

[111] H. M. Nussenzveig, *Causality and dispersion relations*, vol. 95. Academic Press, Cambridge (MA), United States, (1972).

[112] S. Dyatlov and M. Zworski, *Mathematical Theory of Scattering Resonances*. American Mathematical Society, Providence (RI), United States, (2019).

[113] R. Omnès, *Introduction to Particle Physics*. Wiley-Interscience – John Wiley & Sons Ltd., New York City (NY), United States, (1970).

[114] I. T. Todorov, *Analytic Properties of Feynman Diagrams in Quantum Field Theory*. Pergamon Press, Oxford, United Kingdom, (1971).

[115] D. Iagolnitzer, *Scattering in Quantum Field Theories – The Axiomatic and Constructive Approaches*. Princeton Univ. Press, Princeton (NJ), United States, (1971).

[116] C. Hanhart, J. R. Pelaéz, and G. Ríos, *Remarks on pole trajectories for resonances*, Phys. Lett. B **739**, 375–382 (2014) [arXiv:1407.7452 [hep-ph]].

[117] M. Tanabashi *et al.* [Particle Data Group], *Review of Particle Physics*, Phys. Rev. D **98**, 030001 (2018).

[118] M. Gell-Mann and M. L. Goldberger, *Scattering of low-energy photons by particles of spin* $1/2$, Phys. Rev. **96**, 1433–1438 (1954).

[119] F. Niecknig, *Dispersive analysis of charmed meson decays*, PhD thesis, Bonn U., HISKP (2016).

[120] F. Niecknig, B. Kubis, and S. P. Schneider, *Dispersive analysis of* $\omega \to 3\pi$ *and* $\phi \to 3\pi$ *decays*, Eur. Phys. J. C **72**, 2014 (2012) [arXiv:1203.2501 [hep-ph]].

[121] I. V. Danilkin, C. Fernández-Ramírez, P. Guo, V. Mathieu, D. Schott, M. Shi, and A. P. Szczepaniak, *Dispersive analysis of* $\omega/\phi \to 3\pi, \pi\gamma^*$, Phys. Rev. D **91**, 094029 (2015) [arXiv:1409.7708 [hep-ph]].

[122] R. H. Dalitz, *On the analysis of* τ*-meson data and the nature of the* τ*-meson*, Phil. Mag. Ser. 7 **44**, 1068–1080 (1953).

[123] E. Fabri, *A study of* τ*-meson decay*, Nuovo Cim. **11**, 479–491 (1954).

[124] S. Weinberg, *New Test for* $\Delta I = 1/2$ *in* K^+ *Decay*, Phys. Rev. Lett. **4**, 87–89 (1960), [Erratum: Phys.Rev.Lett. 4, 585 (1960)].

[125] D. I. Olive, *Unitarity and the evaluation of discontinuities*, Nuovo Cim. **26**, 73–102 (1962).

[126] I. J. R. Aitchison and R. J. A. Golding, *Relativistic Three Pion Dynamics in the omega Channel*, J. Phys. G **4**, 43 (1978).

[127] A. V. Anisovich and H. Leutwyler, *Dispersive analysis of the decay* $\eta \to 3\pi$, Phys. Lett. B **375**, 335–342 (1996) [arXiv:hep-ph/9601237].

[128] E. U. Condon and G. H. Shortley, *The Theory of Atomic Spectra*. Cambridge Univ. Press, Cambridge, United Kingdom, (1935).

[129] H. F. Jones, *Groups, representations and physics*. IOP Publishing, Bristol, United Kingdom, (1990).

[130] G. F. Chew and S. Mandelstam, *Theory of low-energy pion pion interactions*, Phys. Rev. **119**, 467–477 (1960).

[131] S. Ropertz, C. Hanhart, and B. Kubis, *A new parametrization for the scalar pion form factors*, Eur. Phys. J. C **78**, 1000 (2018) [arXiv:1809.06867 [hep-ph]].

[132] G. Colangelo, J. Gasser, and H. Leutwyler, *$\pi\pi$ scattering*, Nucl. Phys. B **603**, 125–179 (2001) [arXiv:hep-ph/0103088].

[133] I. Caprini, G. Colangelo, and H. Leutwyler, *Regge analysis of the $\pi\pi$ scattering amplitude*, Eur. Phys. J. C **72**, 1860 (2012) [arXiv:1111.7160 [hep-ph]].

[134] R. García-Martín, R. Kamiński, J. R. Pelaéz, J. Ruiz de Elvira, and F. J. Ynduráin, *Pion-pion scattering amplitude. IV. Improved analysis with once subtracted Roy-like equations up to 1100 MeV*, Phys. Rev. D **83**, 074004 (2011) [arXiv:1102.2183 [hep-ph]].

[135] M. Albaladejo and B. Moussallam, *Form factors of the isovector scalar current and the $\eta\pi$ scattering phase shifts*, Eur. Phys. J. C **75**, 488 (2015) [arXiv:1507.04526 [hep-ph]].

[136] J. Lu and B. Moussallam, *The $\pi\eta$ interaction and a_0 resonances in photon–photon scattering*, Eur. Phys. J. C **80**, 436 (2020) [arXiv:2002.04441 [hep-ph]].

[137] F.-K. Guo, B. Kubis, and A. Wirzba, *Anomalous decays of η' and η into four pions*, Phys. Rev. D **85**, 014014 (2012) [arXiv:1111.5949 [hep-ph]].

[138] J. Plenter, *Decay of η' into four Pions and its Impact on the Doubly-virtual η' Transition Form Factor*, Master's thesis, Bonn U., HISKP (2017).

[139] S. Holz, *Factorization breaking effects in the doubly-virtual η' transition form factor*, Master's thesis, Bonn U., HISKP (2018).

[140] J. Wess and B. Zumino, *Consequences of anomalous Ward identities*, Phys. Lett. B **37**, 95–97 (1971).

[141] E. Witten, *Global Aspects of Current Algebra*, Nucl. Phys. B **223**, 422–432 (1983).

[142] G. Barton, *Introduction to dispersion techniques in field theory.* W. A. Benjamin Inc., New York City (NY), United States, (1965).

[143] N. M. Queen and G. Violini, *Dispersion theory in high-energy physics.* Macmillan Press Ltd., London, United Kingdom, (1974).

[144] M. L. B. Niehus, *Quark mass dependence of $\gamma\pi \to \pi\pi$*, Master's thesis, Bonn U., HISKP (2017).

[145] M. Sugawara and A. Kanazawa, *Subtractions in Dispersion Relations*, Phys. Rev. **123**, 1895–1902 (1961).

[146] R. Omnès, *On the Solution of certain singular integral equations of quantum field theory*, Nuovo Cim. **8**, 316–326 (1958).

[147] N. I. Muskhelishvili, *Singular integral equations*. Wolters-Noordhoff Publishing, Groningen, The Netherlands, (1958).

[148] K. Kampf, M. Knecht, J. Novotný, and M. Zdráhal, *Analytical dispersive construction of $\eta \to 3\pi$ amplitude: first order in isospin breaking*, Phys. Rev. D **84**, 114015 (2011) [arXiv:1103.0982 [hep-ph]].

[149] P. Guo, I. V. Danilkin, D. Schott, C. Fernández-Ramírez, V. Mathieu, and A. P. Szczepaniak, *Three-body final state interaction in $\eta \to 3\pi$*, Phys. Rev. D **92**, 054016 (2015) [arXiv:1505.01715 [hep-ph]].

[150] G. Colangelo, S. Lanz, H. Leutwyler, and E. Passemar, *$\eta \to 3\pi$: Study of the Dalitz plot and extraction of the quark mass ratio Q*, Phys. Rev. Lett. **118**, 022001 (2017) [arXiv:1610.03494 [hep-ph]].

[151] M. Albaladejo and B. Moussallam, *Extended chiral Khuri–Treiman formalism for $\eta \to 3\pi$ and the role of the $a_0(980)$, $f_0(980)$ resonances*, Eur. Phys. J. C **77**, 508 (2017) [arXiv:1702.04931 [hep-ph]].

[152] G. Colangelo, S. Lanz, H. Leutwyler, and E. Passemar, *Dispersive analysis of $\eta \to 3\pi$*, Eur. Phys. J. C **78**, 947 (2018) [arXiv:1807.11937 [hep-ph]].

[153] P. Guo, I. V. Danilkin, and A. P. Szczepaniak, *Dispersive approaches for three-particle final state interaction*, Eur. Phys. J. A **51**, 135 (2015) [arXiv:1409.8652 [hep-ph]].

[154] T. Isken, B. Kubis, S. P. Schneider, and P. Stoffer, *Dispersion relations for $\eta' \to \eta\pi\pi$*, Eur. Phys. J. C **77**, 489 (2017) [arXiv:1705.04339 [hep-ph]].

[155] F. Niecknig and B. Kubis, *Dispersion-theoretical analysis of the $D^+ \to K^-\pi^+\pi^+$ Dalitz plot*, JHEP **10**, 142 (2015) [arXiv:1509.03188 [hep-ph]].

[156] F. Niecknig and B. Kubis, *Consistent Dalitz plot analysis of Cabibbo-favored $D^+ \to \bar{K}\pi\pi^+$ decays*, Phys. Lett. B **780**, 471–478 (2018) [arXiv:1708.00446 [hep-ph]].

[157] S. Lanz, *Determination of the quark mass ratio Q from $\eta \to 3\pi$*, PhD thesis, Bern U. (2011), arXiv:1809.10110 [hep-ph].

[158] S. P. Schneider, *Analysis tools for precision studies of hadronic three-body decays and transition form factors*, PhD thesis, Bonn U., HISKP (2012).

[159] H. Leutwyler, private communication.

[160] G. Höhler, *Pion Nucleon Scattering. Part 2: Methods and Results of Phenomenological Analyses*. Landolt-Börnstein - Group I Elementary Particles, Nuclei and Atoms. Springer, Heidelberg, Germany, (1983).

[161] M. Froissart, *Asymptotic behavior and subtractions in the Mandelstam representation*, Phys. Rev. **123**, 1053–1057 (1961).

[162] A. Martin, *Unitarity and high-energy behavior of scattering amplitudes*, Phys. Rev. **129**, 1432–1436 (1963).

[163] J. Stern, H. Sazdjian, and N. H. Fuchs, *What π-π scattering tells us about chiral perturbation theory*, Phys. Rev. D **47**, 3814–3838 (1993) [arXiv:hep-ph/9301244].

[164] M. Knecht, B. Moussallam, J. Stern, and N. H. Fuchs, *The Low-energy $\pi\pi$ amplitude to one and two loops*, Nucl. Phys. B **457**, 513–576 (1995) [arXiv:hep-ph/9507319].

[165] B. Ananthanarayan and P. Büttiker, *Comparison of πK scattering in SU(3) chiral perturbation theory and dispersion relations*, Eur. Phys. J. C **19**, 517–528 (2001) [arXiv:hep-ph/0012023].

[166] M. Zdráhal and J. Novotný, *Dispersive Approach to Chiral Perturbation Theory*, Phys. Rev. D **78**, 116016 (2008) [arXiv:0806.4529 [hep-ph]].

[167] M. Jacob and G. C. Wick, *On the General Theory of Collisions for Particles with Spin*, Annals Phys. **7**, 404–428 (1959).

[168] R. Kaiser and H. Leutwyler, *Large N_C in chiral perturbation theory*, Eur. Phys. J. C **17**, 623–649 (2000) [arXiv:hep-ph/0007101].

[169] R. Escribano, P. Masjuan, and J. J. Sanz-Cillero, *Chiral dynamics predictions for $\eta' \to \eta\pi\pi$*, JHEP **05**, 094 (2011) [arXiv:1011.5884 [hep-ph]].

[170] Riazuddin and S. Oneda, *Some remarks on the $(3, 3^*) \times (3^*, 3)$ breaking of chiral symmetry*, Phys. Rev. Lett. **27**, 548–552 (1971).

[171] N. G. Deshpande and T. N. Truong, *Resolution of the $\eta' \to \eta\pi\pi$ Puzzle*, Phys. Rev. Lett. **41**, 1579 (1978).

[172] C. A. Singh and J. Pasupathy, *On the Decay Modes of the Meson $\eta'(958)$ and Chiral Symmetry Breaking*, Phys. Rev. Lett. **35**, 1193–1195 (1975), [Erratum: Phys. Rev. Lett. **35**, 1748 (1975)].

[173] A. H. Fariborz and J. Schechter, *$\eta' \to \eta\pi\pi$ decay as a probe of a possible lowest lying scalar nonet*, Phys. Rev. D **60**, 034002 (1999) [arXiv:hep-ph/9902238].

[174] N. Beisert and B. Borasoy, *The $\eta' \to \eta\pi\pi$ decay in U(3) chiral perturbation theory*, Nucl. Phys. A **705**, 433–454 (2002) [arXiv:hep-ph/0201289].

[175] N. Beisert and B. Borasoy, *Hadronic decays of η and η' with coupled channels*, Nucl. Phys. A **716**, 186–208 (2003) [arXiv:hep-ph/0301058].

[176] B. Borasoy and R. Nißler, *Hadronic η and η' decays*, Eur. Phys. J. A **26**, 383–398 (2005) [arXiv:hep-ph/0510384].

[177] R. Nißler, *Topics in three flavor chiral dynamics*, PhD thesis, Bonn U., HISKP (2007).

[178] B. Kubis and S. P. Schneider, *The Cusp effect in $\eta' \to \eta\pi\pi$ decays*, Eur. Phys. J. C **62**, 511–523 (2009) [arXiv:0904.1320 [hep-ph]].

[179] A. M. Blik *et al.* [GAMS-4π Collaboration], *Measurement of the matrix element for the decay $\eta' \to \eta\pi^0\pi^0$ with the GAMS-4π spectrometer*, Phys. Atom. Nucl. **72**, 231–236 (2009), [Yad. Fiz. **72**, 258 (2009)].

[180] S. P. Schneider and B. Kubis, *Cusps in $\eta' \to \eta\pi\pi$ decays*, PoS **CD09**, 120 (2009) [arXiv:0910.0200 [hep-ph]].

[181] S. P. Schneider, *The cusp effect in $\eta' \to \eta\pi\pi$ decays*, Diploma thesis, Bonn U., HISKP (2009).

[182] V. Dorofeev *et al.*, *Study of $\eta' \to \eta\pi^+\pi^-$ Dalitz plot*, Phys. Lett. B **651**, 22–26 (2007) [arXiv:hep-ph/0607044].

[183] M. Ablikim *et al.* [BESIII Collaboration], *Measurement of the Matrix Element for the Decay $\eta' \to \eta\pi^+\pi^-$*, Phys. Rev. D **83**, 012003 (2011) [arXiv:1012.1117 [hep-ex]].

[184] G. R. Kalbfleisch, $\eta'(958)$ *branching ratio, linear matrix element, and dipion phase shift*, Phys. Rev. D **10**, 916 (1974).

[185] R. A. Briere *et al.* [CLEO Collaboration], *Rare decays of the η'*, Phys. Rev. Lett. **84**, 26–30 (2000) [arXiv:hep-ex/9907046].

[186] J. Kambor, C. Wiesendanger, and D. Wyler, *Final state interactions and Khuri–Treiman equations in $\eta \to 3\pi$ decays*, Nucl. Phys. B **465**, 215–266 (1996) [arXiv:hep-ph/9509374].

[187] M. Walker, $\eta \to 3\pi$, Diploma thesis, Bern U. (1998).

[188] T. Isken, *Dispersive analysis of $\eta' \to 3\pi$ decays*, Master's thesis, Bonn U., HISKP (2015).

[189] V. Bernard, N. Kaiser, and U.-G. Meißner, *$\pi\eta$ scattering in QCD*, Phys. Rev. D **44**, 3698–3701 (1991).

[190] C. Adolph *et al.* [COMPASS Collaboration], *Odd and even partial waves of $\eta\pi^-$ and $\eta'\pi^-$ in $\pi^- p \to \eta'\pi^- p$ at 191 GeV/c*, Phys. Lett. B **740**, 303–311 (2015) [arXiv:1408.4286 [hep-ex]].

[191] D. Schott [CLAS Collaboration], *The search for exotic mesons in $\eta\pi^-$ from photoproduction with CLAS*, PoS **ConfinementX**, 106 (2012).

[192] S. Gonzàlez-Solís and E. Passemar, *$\eta' \to \eta\pi\pi$ decays in unitarized resonance chiral theory*, Eur. Phys. J. C **78**, 758 (2018) [arXiv:1807.04313 [hep-ph]].

[193] J. F. Donoghue, J. Gasser, and H. Leutwyler, *The Decay of a Light Higgs Boson*, Nucl. Phys. **B343**, 341–368 (1990).

[194] B. Ananthanarayan, I. Caprini, G. Colangelo, J. Gasser, and H. Leutwyler, *Scalar form-factors of light mesons*, Phys. Lett. B **602**, 218–225 (2004) [arXiv:hep-ph/0409222].

[195] J. T. Daub, C. Hanhart, and B. Kubis, *A model-independent analysis of final-state interactions in* $\bar{B}^0_{d/s} \to J/\psi\pi\pi$, JHEP **02**, 009 (2016) [arXiv:1508.06841 [hep-ph]].

[196] G. Colangelo, E. Passemar, and P. Stoffer, *A dispersive treatment of* $K_{\ell 4}$ *decays*, Eur. Phys. J. C **75**, 172 (2015) [arXiv:1501.05627 [hep-ph]].

[197] C. Patrignani *et al.* [Particle Data Group], *Review of Particle Physics*, Chin. Phys. C **40**, 100001 (2016).

[198] A. Kupść, private communication.

[199] T. Isken, B. Kubis, A. Kupść, and P. Stoffer, *Strong three-body decays of* η *and* η' *mesons*, in preparation.

[200] S. Descotes-Genon and B. Moussallam, *Analyticity of* $\eta\pi$ *isospin-violating form factors and the* $\tau \to \eta\pi\nu$ *second-class decay*, Eur. Phys. J. C **74**, 2946 (2014) [arXiv:1404.0251 [hep-ph]].

[201] C. Ditsche, B. Kubis, and U.-G. Meißner, *Electromagnetic corrections in* $\eta \to 3\pi$ *decays*, Eur. Phys. J. C **60**, 83–105 (2009) [arXiv:0812.0344 [hep-ph]].

[202] S. P. Schneider, B. Kubis, and C. Ditsche, *Rescattering effects in* $\eta \to 3\pi$ *decays*, JHEP **1102**, 028 (2011) [arXiv:1010.3946 [hep-ph]].

[203] P. Budini and L. Fonda, *Pion-Pion Interaction from Threshold Anomalies in* K^+ *Decay*, Phys. Rev. Lett. **6**, 419 (1961).

[204] N. Cabibbo, *Determination of the* $a_0 - a_2$ *pion scattering length from* $K^+ \to \pi^+\pi^0\pi^0$ *decay*, Phys. Rev. Lett. **93**, 121801 (2004) [arXiv:hep-ph/0405001].

[205] M. Bissegger, A. Fuhrer, J. Gasser, B. Kubis, and A. Rusetsky, *Cusps in* $K_L \to 3\pi$ *decays*, Phys. Lett. B **659**, 576–584 (2008) [arXiv:0710.4456 [hep-ph]].

[206] P. Guo, *A coupled-channel formalism for three-body final state interaction*, Mod. Phys. Lett. A **31**, 1650058 (2016) [arXiv:1506.00042 [hep-ph]].

[207] J. A. Cronin, *Phenomenological model of strong and weak interactions in chiral U(3)×U(3)*, Phys. Rev. **161**, 1483–1494 (1967).

[208] J. Schwinger, *Chiral Transformations*, Phys. Rev. **167**, 1432–1436 (1968).

[209] P. Di Vecchia, F. Nicodemi, R. Pettorino, and G. Veneziano, *Large N, Chiral Approach to Pseudoscalar Masses, Mixings and Decays*, Nucl. Phys. B **181**, 318–334 (1981).

[210] S. Fajfer and J.-M. Gérard, *Hadronic Decays of η and η' in the Large N Limit*, Z. Phys. C **42**, 431 (1989).

[211] P. Herrera-Siklódy, *η and η' hadronic decays in $U(3)_L \times U(3)_R$ chiral perturbation theory* [arXiv:hep-ph/9902446].

[212] J. Schechter and Y. Ueda, *General treatment of the breaking of chiral symmetry and scale invariance in the SU(3) sigma model*, Phys. Rev. D **3**, 2874–2893 (1971), [Erratum: Phys. Rev. D **8**, 987 (1973)].

[213] H. Leutwyler, *On the $1/N$-expansion in chiral perturbation theory*, Nucl. Phys. Proc. Suppl. **64**, 223–231 (1998) [arXiv:hep-ph/9709408].

[214] R. Kaiser and H. Leutwyler, *Pseudoscalar decay constants at large N_C*, Proc. Workshop "Nonperturbative Methods in Quantum Field Theory," U. Adelaide, Australia 15–29 (1998) [arXiv:hep-ph/9806336].

[215] R. Escribano, private communication.

[216] R. Escribano, S. Gonzàlez-Solís, P. Masjuan, and P. Sanchez-Puertas, *η' transition form factor from space- and timelike experimental data*, Phys. Rev. D **94**, 054033 (2016) [arXiv:1512.07520 [hep-ph]].

[217] J. Bijnens and G. Ecker, *Mesonic low-energy constants*, Ann. Rev. Nucl. Part. Sci. **64**, 149–174 (2014) [arXiv:1405.6488 [hep-ph]].

[218] G. Ecker, J. Gasser, A. Pich, and E. de Rafael, *The Role of Resonances in Chiral Perturbation Theory*, Nucl. Phys. B **321**, 311–342 (1989).

[219] G. Ecker, J. Gasser, H. Leutwyler, A. Pich, and E. de Rafael, *Chiral lagrangians for massive spin-1 fields*, Phys. Lett. B **223**, 425–432 (1989).

[220] P. Adlarson *et al.* [A2 Collaboration], *Measurement of the decay $\eta' \to \pi^0\pi^0\eta$ at MAMI*, Phys. Rev. D **98**, 012001 (2018) [arXiv:1709.04230 [hep-ex]].

[221] M. Ablikim *et al.* [BESIII Collaboration], *Measurement of the matrix elements for the decays $\eta' \to \eta\pi^+\pi^-$ and $\eta' \to \eta\pi^0\pi^0$*, Phys. Rev. D **97**, 012003 (2018) [arXiv:1709.04627 [hep-ex]].

[222] P. Nuhn, *Untersuchung von η'-Zerfällen mit dem Crystal-Barrel/TAPS-Detektor an ELSA*, Diploma thesis, Bonn U., HISKP (2012).

[223] T. D. Lee, *Possible C-Noninvariant Effects in the 3π Decay Modes of η^0 and ω^0*, Phys. Rev. **139**, B1415–B1420 (1965).

[224] J. Prentki and M. J. G. Veltman, *Possibility of CP violation in semistrong interactions*, Phys. Lett. **15**, 88–90 (1965).

[225] M. Nauenberg, *The $\eta \to \pi^+\pi^-\pi^0$ decay with C-violation*, Phys. Lett. **17**, 329–331 (1965).

[226] B. Barrett, M. Jacob, M. Nauenberg, and T. N. Truong, *Consequences of C-Violating Interactions in η^0 and X^0 Decays*, Phys. Rev. **141**, 1342–1349 (1966).

[227] N. Cabibbo, *Unitary Symmetry and Leptonic Decays*, Phys. Rev. Lett. **10**, 531–533 (1963).

[228] M. Kobayashi and T. Maskawa, *CP Violation in the Renormalizable Theory of Weak Interaction*, Prog. Theor. Phys. **49**, 652–657 (1973).

[229] D. G. Sutherland, *Current algebra and the decay $\eta \to 3\pi$*, Phys. Lett. **23**, 384–385 (1966).

[230] J. S. Bell and D. G. Sutherland, *Current algebra and $\eta \to 3\pi$*, Nucl. Phys. B **4**, 315–325 (1968).

[231] D. J. Gross, S. B. Treiman, and F. Wilczek, *Light Quark Masses and Isospin Violation*, Phys. Rev. D **19**, 2188 (1979).

[232] P. Langacker and H. Pagels, *Light Quark Mass Spectrum in Quantum Chromodynamics*, Phys. Rev. D **19**, 2070 (1979).

[233] J. Gasser and H. Leutwyler, *$\eta \to 3\pi$ to One Loop*, Nucl. Phys. B **250**, 539–560 (1985).

[234] J. Bijnens and J. Gasser, *Eta decays at and beyond p^4 in chiral perturbation theory*, Phys. Scripta T **99**, 34–44 (2002) [arXiv:hep-ph/0202242].

[235] J. Bijnens and K. Ghorbani, *$\eta \to 3\pi$ at Two Loops In Chiral Perturbation Theory*, JHEP **11**, 030 (2007) [arXiv:0709.0230 [hep-ph]].

[236] R. Baur, J. Kambor, and D. Wyler, *Electromagnetic corrections to the decays $\eta \to 3\pi$*, Nucl. Phys. B **460**, 127–142 (1996) [arXiv:hep-ph/9510396].

[237] L. Gan, B. Kubis, E. Passemar, and S. Tulin, *Precision tests of fundamental physics with η and η' mesons* [arXiv:2007.00664 [hep-ph]].

[238] J. G. Layter, J. A. Appel, A. Kotlewski, W.-Y. Lee, S. Stein, and J. J. Thaler, *Measurement of the charge asymmetry in the decay $\eta \to \pi^+\pi^-\pi^0$*, Phys. Rev. Lett. **29**, 316–319 (1972).

[239] F. Ambrosino *et al.* [KLOE Collaboration], *Determination of $\eta \to \pi^+\pi^-\pi^0$ Dalitz plot slopes and asymmetries with the KLOE detector*, JHEP **05**, 006 (2008) [arXiv:0801.2642 [hep-ex]].

[240] A. Anastasi *et al.* [KLOE-2 Collaboration], *Precision measurement of the $\eta \to \pi^+\pi^-\pi^0$ Dalitz plot distribution with the KLOE detector*, JHEP **05**, 019 (2016) [arXiv:1601.06985 [hep-ex]].

[241] J. H. Christenson, J. W. Cronin, V. L. Fitch, and R. Turlay, *Evidence for the 2π Decay of the K_2^0 Meson*, Phys. Rev. Lett. **13**, 138–140 (1964).

[242] T. D. Lee and L. Wolfenstein, *Analysis of CP-Noninvariant Interactions and the K_1^0, K_2^0 System*, Phys. Rev. **138**, B1490–B1496 (1965).

[243] S. Gardner and J. Shi, *Patterns of CP violation from mirror symmetry breaking in the $\eta \to \pi^+\pi^-\pi^0$ Dalitz plot*, Phys. Rev. D **101**, 115038 (2020) [arXiv:1903.11617 [hep-ph]].

[244] A. V. Anisovich, *Dispersion relation technique for three-pion system and the P-wave interaction in $\eta \to 3\pi$ decay*, Phys. Atom. Nucl. **58**, 1383–1397 (1995).

[245] S. Prakhov *et al.* [A2 Collaboration], *High-statistics measurement of the $\eta \to 3\pi^0$ decay at the Mainz Microtron*, Phys. Rev. C **97**, 065203 (2018) [arXiv:1803.02502 [hep-ex]].

[246] H. Osborn and D. J. Wallace, *η-X mixing, $\eta \to 3\pi$ and chiral lagrangians*, Nucl. Phys. B **20**, 23–44 (1970).

[247] I. B. Khriplovich, *What do we know about T odd but P even interaction?*, Nucl. Phys. B **352**, 385–401 (1991).

[248] R. S. Conti and I. B. Khriplovich, *New limits on T odd, P even interactions*, Phys. Rev. Lett. **68**, 3262–3265 (1992).

[249] J. Engel, P. H. Frampton, and R. P. Springer, *Effective Lagrangians and parity conserving time reversal violation at low-energies*, Phys. Rev. D **53**, 5112–5114 (1996) [arXiv:nucl-th/9505026].

[250] M. J. Ramsey-Musolf, *Electric dipole moments and the mass scale of new T violating, P conserving interactions*, Phys. Rev. Lett. **83**, 3997–4000 (1999) [arXiv:hep-ph/9905429], [Erratum: Phys.Rev.Lett. 84, 5681 (2000)].

[251] A. Kurylov, G. C. McLaughlin, and M. J. Ramsey-Musolf, *Constraints on T odd, P even interactions from electric dipole moments, revisited*, Phys. Rev. D **63**, 076007 (2001) [arXiv:hep-ph/0011185].

[252] J. Shi, *Theoretical Studies of C and CP Violation in $\eta \to \pi^+\pi^-\pi^0$ Decay*, PhD thesis, Kentucky U. (2017).

[253] C. Gatto, B. Fabela Enriquez, and M. I. Pedraza Morales [REDTOP Collaboration], *The REDTOP project: Rare Eta Decays with a TPC for Optical Photons*, PoS **ICHEP2016**, 812 (2016).

[254] L. Gan, *Test Fundamental Symmetries via Precision Measurements of π^0, η, and η' Decays*, JPS Conf. Proc. **13**, 020063 (2017).

[255] C. Gatto [REDTOP Collaboration], *The REDTOP experiment* [arXiv:1910.08505 [physics.ins-det]].

[256] J. Beacham *et al.*, *Physics Beyond Colliders at CERN: Beyond the Standard Model Working Group Report*, J. Phys. G **47**, 010501 (2020) [arXiv:1901.09966 [hep-ex]].

[257] M. Ablikim *et al.* [BESIII Collaboration], *Amplitude Analysis of the Decays $\eta' \to \pi^+\pi^-\pi^0$ and $\eta' \to \pi^0\pi^0\pi^0$*, Phys. Rev. Lett. **118**, 012001 (2017) [arXiv:1606.03847 [hep-ex]].

[258] H. Akdag, T. Isken, and B. Kubis, *Patterns of C- and CP-violation in hadronic η and η' three-body decays*, in preparation.

[259] M. Dax, T. Isken, and B. Kubis, *Quark-mass dependence in $\omega \to 3\pi$ decays*, Eur. Phys. J. C **78**, 859 (2018) [arXiv:1808.08957 [hep-ph]].

[260] S. Aoki *et al.* [FLAG Collaboration], *Review of lattice results concerning low-energy particle physics*, Eur. Phys. J. C **77**, 112 (2017) [arXiv:1607.00299 [hep-lat]].

[261] R. A. Briceño, J. J. Dudek, and R. D. Young, *Scattering processes and resonances from lattice QCD*, Rev. Mod. Phys. **90**, 025001 (2018) [arXiv:1706.06223 [hep-lat]].

[262] T. N. Truong, *Remarks on the unitarization methods*, Phys. Rev. Lett. **67**, 2260–2263 (1991).

[263] A. Dobado and J. R. Peláez, *A Global fit of $\pi\pi$ and πK elastic scattering in ChPT with dispersion relations*, Phys. Rev. D **47**, 4883–4888 (1993) [arXiv:hep-ph/9301276].

[264] A. Dobado and J. R. Peláez, *The Inverse amplitude method in chiral perturbation theory*, Phys. Rev. D **56**, 3057–3073 (1997) [arXiv:hep-ph/9604416].

[265] A. Gómez Nicola, J. R. Peláez, and G. Ríos, *The Inverse Amplitude Method and Adler Zeros*, Phys. Rev. D **77**, 056006 (2008) [arXiv:0712.2763 [hep-ph]].

[266] C. Hanhart, J. R. Peláez, and G. Ríos, *Quark mass dependence of the rho and sigma from dispersion relations and Chiral Perturbation Theory*, Phys. Rev. Lett. **100**, 152001 (2008) [arXiv:0801.2871 [hep-ph]].

[267] J. Nebreda and J. R. Peláez., *Strange and non-strange quark mass dependence of elastic light resonances from $SU(3)$ Unitarized Chiral Perturbation Theory to one loop*, Phys. Rev. D **81**, 054035 (2010) [arXiv:1001.5237 [hep-ph]].

[268] K. Polejaeva and A. Rusetsky, *Three particles in a finite volume*, Eur. Phys. J. A **48**, 67 (2012) [arXiv:1203.1241 [hep-lat]].

[269] R. A. Briceño and Z. Davoudi, *Three-particle scattering amplitudes from a finite volume formalism*, Phys. Rev. D **87**, 094507 (2013) [arXiv:1212.3398 [hep-lat]].

[270] M. T. Hansen and S. R. Sharpe, *Relativistic, model-independent, three-particle quantization condition*, Phys. Rev. D **90**, 116003 (2014) [arXiv:1408.5933 [hep-lat]].

[271] M. T. Hansen and S. R. Sharpe, *Expressing the three-particle finite-volume spectrum in terms of the three-to-three scattering amplitude*, Phys. Rev. D **92**, 114509 (2015) [arXiv:1504.04248 [hep-lat]].

[272] H.-W. Hammer, J.-Y. Pang, and A. Rusetsky, *Three-particle quantization condition in a finite volume: 1. The role of the three-particle force*, JHEP **1709**, 109 (2017) [arXiv:1706.07700 [hep-lat]].

[273] H.-W. Hammer, J.-Y. Pang, and A. Rusetsky, *Three particle quantization condition in a finite volume: 2. general formalism and the analysis of data*, JHEP **1710**, 115 (2017) [arXiv:1707.02176 [hep-lat]].

[274] M. Mai and M. Döring, *Three-body Unitarity in the Finite Volume*, Eur. Phys. J. A **53**, 240 (2017) [arXiv:1709.08222 [hep-lat]].

[275] F.-K. Guo, C. Hanhart, F. J. Llanes-Estrada, and U.-G. Meißner, *Quark mass dependence of the pion vector form factor*, Phys. Lett. B **678**, 90–96 (2009) [arXiv:0812.3270 [hep-ph]].

[276] M. Niehus, M. Hoferichter, and B. Kubis, *Quark mass dependence of* $\gamma^*\pi \to \pi\pi$, PoS **CD2018**, 076 (2019) [arXiv:1902.10150 [hep-ph]].

[277] J. R. Peláez and G. Ríos, *Chiral extrapolation of light resonances from one and two-loop unitarized Chiral Perturbation Theory versus lattice results*, Phys. Rev. D **82**, 114002 (2010) [arXiv:1010.6008 [hep-ph]].

[278] A. Bazavov *et al.* [MILC Collaboration], *Results for light pseudoscalar mesons*, PoS LATTICE **2010**, 074 (2010) [arXiv:1012.0868 [hep-lat]].

[279] S. R. Beane *et al.*, $SU(2)$ *Low-Energy Constants from Mixed-Action Lattice QCD*, Phys. Rev. D **86**, 094509 (2012) [arXiv:1108.1380 [hep-lat]].

[280] S. Borsányi, S. Dürr, Z. Fodor, S. Krieg, A. Schäfer, E. E. Scholz, and K. K. Szabó, $SU(2)$ *chiral perturbation theory low-energy constants from* $2+1$ *flavor staggered lattice simulations*, Phys. Rev. D **88**, 014513 (2013) [arXiv:1205.0788 [hep-lat]].

[281] S. Dürr *et al.* [BMW Collaboration], *Lattice QCD at the physical point meets* $SU(2)$ *chiral perturbation theory*, Phys. Rev. D **90**, 114504 (2014) [arXiv:1310.3626 [hep-lat]].

[282] T. Blum *et al.* [RBC, UKQCD Collaboration], *Domain wall QCD with physical quark masses*, Phys. Rev. D **93**, 074505 (2016) [arXiv:1411.7017 [hep-lat]].

[283] V. N. Gribov, *Strong interactions of hadrons at high energies: Gribov lectures on theoretical physics*, vol. 27. Cambridge Univ. Press, Cambridge, United Kingdom, (2012).

[284] B. Moussallam, *Couplings of light $I = 0$ scalar mesons to simple operators in the complex plane*, Eur. Phys. J. C **71**, 1814 (2011) [arXiv:1110.6074 [hep-ph]].

[285] R. García-Martín, R. Kamiński, J. R. Peláez, and J. Ruiz de Elvira, *Precise determination of the $f_0(600)$ and $f_0(980)$ pole parameters from a dispersive data analysis*, Phys. Rev. Lett. **107**, 072001 (2011) [arXiv:1107.1635 [hep-ph]].

[286] M. Niehus, M. Hoferichter, B. Kubis, and J. Ruiz de Elvira, *Two-Loop Analysis of the Pion Mass Dependence of the ρ Meson*, Phys. Rev. Lett. **126**, 102002 (2021) [arXiv:2009.04479 [hep-ph]].

[287] P. C. Bruns and M. Mai, *Chiral symmetry constraints on resonant amplitudes*, Phys. Lett. B **778**, 43–47 (2018) [arXiv:1707.08983 [hep-lat]].

[288] C. Alexandrou *et al.*, *P-wave $\pi\pi$ scattering and the ρ resonance from lattice QCD*, Phys. Rev. D **96**, 034525 (2017) [arXiv:1704.05439 [hep-lat]].

[289] S. Aoki *et al.* [CP-PACS Collaboration], *Lattice QCD Calculation of the rho Meson Decay Width*, Phys. Rev. D **76**, 094506 (2007) [arXiv:0708.3705 [hep-lat]].

[290] X. Feng, K. Jansen, and D. B. Renner, *Resonance Parameters of the ρ Meson from Lattice QCD*, Phys. Rev. D **83**, 094505 (2011) [arXiv:1011.5288 [hep-lat]].

[291] S. Aoki *et al.* [CS Collaboration], *ρ Meson Decay in 2+1 Flavor Lattice QCD*, Phys. Rev. D **84**, 094505 (2011) [arXiv:1106.5365 [hep-lat]].

[292] C. B. Lang, D. Mohler, S. Prelovsek, and M. Vidmar, *Coupled channel analysis of the rho meson decay in lattice QCD*, Phys. Rev. D **84**, 054503 (2011) [arXiv:1105.5636 [hep-lat]], [Erratum: Phys. Rev. D **89**, 059903 (2014)].

[293] J. J. Dudek, R. G. Edwards, and C. E. Thomas [Hadron Spectrum Collaboration], *Energy dependence of the ρ resonance in $\pi\pi$ elastic scattering from lattice QCD*, Phys. Rev. D **87**, 034505 (2013) [arXiv:1212.0830 [hep-ph]], [Erratum: Phys. Rev. D **90**, 099902 (2014)].

[294] C. Pelissier and A. Alexandru, *Resonance parameters of the rho-meson from asymmetrical lattices*, Phys. Rev. D **87**, 014503 (2013) [arXiv:1211.0092 [hep-lat]].

[295] G. S. Bali *et al.* [RQCD Collaboration], *ρ and K^* resonances on the lattice at nearly physical quark masses and $N_f = 2$*, Phys. Rev. D **93**, 054509 (2016) [arXiv:1512.08678 [hep-lat]].

[296] D. J. Wilson, R. A. Briceño, J. J. Dudek, R. G. Edwards, and C. E. Thomas, *Coupled $\pi\pi, K\bar{K}$ scattering in P-wave and the ρ resonance from lattice QCD*, Phys. Rev. D **92**, 094502 (2015) [arXiv:1507.02599 [hep-ph]].

[297] J. Bulava, B. Fahy, B. Hörz, K. J. Juge, C. Morningstar, and C. H. Wong, *$I = 1$ and $I = 2$ $\pi - \pi$ scattering phase shifts from $N_\mathrm{f} = 2 + 1$ lattice QCD*, Nucl. Phys. B **910**, 842–867 (2016) [arXiv:1604.05593 [hep-lat]].

[298] B. Hu, R. Molina, M. Döring, M. Mai, and A. Alexandru, *Chiral extrapolations of the $\rho(770)$ meson in $N_f = 2 + 1$ lattice QCD simulations*, Phys. Rev. D **96**, 034520 (2017) [arXiv:1704.06248 [hep-lat]].

[299] C. Andersen, J. Bulava, B. Hörz, and C. Morningstar, *The $I = 1$ pion-pion scattering amplitude and timelike pion form factor from $N_\mathrm{f} = 2 + 1$ lattice QCD*, Nucl. Phys. B **939**, 145–173 (2019) [arXiv:1808.05007 [hep-lat]].

[300] M. Hoferichter, B. Kubis, and D. Sakkas, *Extracting the chiral anomaly from $\gamma\pi \to \pi\pi$*, Phys. Rev. D **86**, 116009 (2012) [arXiv:1210.6793 [hep-ph]].

[301] M. Hoferichter, B. Kubis, S. Leupold, F. Niecknig, and S. P. Schneider, *Dispersive analysis of the pion transition form factor*, Eur. Phys. J. C **74**, 3180 (2014) [arXiv:1410.4691 [hep-ph]].

[302] M. Hoferichter, B. Kubis, and M. Zanke, *Radiative resonance couplings in $\gamma\pi \to \pi\pi$*, Phys. Rev. D **96**, 114016 (2017) [arXiv:1710.00824 [hep-ph]].

[303] M. Hoferichter, B.-L. Hoid, B. Kubis, S. Leupold, and S. P. Schneider, *Pion-pole contribution to hadronic light-by-light scattering in the anomalous magnetic moment of the muon*, Phys. Rev. Lett. **121**, 112002 (2018) [arXiv:1805.01471 [hep-ph]].

[304] M. Hoferichter, B.-L. Hoid, B. Kubis, S. Leupold, and S. P. Schneider, *Dispersion relation for hadronic light-by-light scattering: pion pole*, JHEP **10**, 141 (2018) [arXiv:1808.04823 [hep-ph]].

[305] T. W. B. Kibble, *Kinematics of General Scattering Processes and the Mandelstam Representation*, Phys. Rev. **117**, 1159–1162 (1960).

[306] E. E. Jenkins, A. V. Manohar, and M. B. Wise, *Chiral perturbation theory for vector mesons*, Phys. Rev. Lett. **75**, 2272–2275 (1995) [arXiv:hep-ph/9506356].

[307] J. Bijnens and P. Gosdzinsky, *Electromagnetic contributions to vector meson masses and mixings*, Phys. Lett. B **388**, 203–210 (1996) [arXiv:hep-ph/9607462].

[308] J. Bijnens, P. Gosdzinsky, and P. Talavera, *Vector meson masses in chiral perturbation theory*, Nucl. Phys. B **501**, 495–517 (1997) [arXiv:hep-ph/9704212].

[309] J. R. Peláez, A. Rodas, and J. Ruiz de Elvira, *Strange resonance poles from $K\pi$ scattering below 1.8 GeV*, Eur. Phys. J. C **77**, 91 (2017) [arXiv:1612.07966 [hep-ph]].

[310] P. C. Bruns and U.-G. Meißner, *Infrared regularization for spin-1 fields*, Eur. Phys. J. C **40**, 97–119 (2005) [arXiv:hep-ph/0411223].

[311] P. C. Bruns, L. Greil, and A. Schäfer, *Chiral behavior of vector meson self energies*, Phys. Rev. D **88**, 114503 (2013) [arXiv:1309.3976 [hep-ph]].

[312] R. Bavontaweepanya, X.-Y. Guo, and M. F. M. Lutz, *On the chiral expansion of vector meson masses*, Phys. Rev. D **98**, 056005 (2018) [arXiv:1801.10522 [hep-ph]].

[313] M. Gell-Mann, D. Sharp, and W. G. Wagner, *Decay rates of neutral mesons*, Phys. Rev. Lett. **8**, 261 (1962).

[314] F. Klingl, N. Kaiser, and W. Weise, *Effective Lagrangian approach to vector mesons, their structure and decays*, Z. Phys. A **356**, 193–206 (1996) [arXiv:hep-ph/9607431].

[315] S. Leupold and M. F. M. Lutz, *Hadronic three-body decays of light vector mesons*, Eur. Phys. J. A **39**, 205–212 (2009) [arXiv:0807.4686 [hep-ph]].

[316] M. Dax, *Pion mass dependence of the partial decay width of* $\omega \to 3\pi$, Bachelor's thesis, Bonn U., HISKP (2017).

[317] A. Aloisio *et al.* [KLOE Collaboration], *Study of the decay* $\phi \to \pi^+\pi^-\pi^0$ *with the KLOE detector*, Phys. Lett. B **561**, 55–60 (2003) [arXiv:hep-ex/0303016], [Erratum: Phys. Lett. B **609**, 449 (2005)].

[318] R. R. Akhmetshin *et al.*, *Study of* $\phi \to \pi^+\pi^-\pi^0$ *with CMD-2 detector*, Phys. Lett. B **642**, 203–209 (2006).

[319] P. Adlarson *et al.* [WASA-at-COSY Collaboration], *Measurement of the* $\omega \to \pi^+\pi^-\pi^0$ *Dalitz plot distribution*, Phys. Lett. B **770**, 418–425 (2017) [arXiv:1610.02187 [nucl-ex]].

[320] C. Adolph *et al.* [COMPASS Collaboration], *Resonance Production and* $\pi\pi$ *S-wave in* $\pi^- + p \to \pi^-\pi^-\pi^+ + p_{recoil}$ *at 190 GeV/c*, Phys. Rev. D **95**, 032004 (2017) [arXiv:1509.00992 [hep-ex]].

[321] M. Aghasyan *et al.* [COMPASS Collaboration], *Light isovector resonances in* $\pi^- p \to \pi^-\pi^-\pi^+ p$ *at 190 GeV/c*, Phys. Rev. D **98**, 092003 (2018) [arXiv:1802.05913 [hep-ex]].

[322] F. Krinner [COMPASS Collaboration], *Recent progress in the partial-wave analysis of the diffractively produced* $\pi^-\pi^+\pi^-$ *final state at COMPASS*, EPJ Web Conf. **199**, 02003 (2019) [arXiv:1808.09207 [hep-ex]].

[323] G. Colangelo, J. Gasser, and A. Rusetsky, *Isospin breaking in* K_{l4} *decays*, Eur. Phys. J. C **59**, 777–793 (2009) [arXiv:0811.0775 [hep-ph]].

[324] G. Colangelo, J. Gasser, B. Kubis, and A. Rusetsky, *Cusps in* $K \to 3\pi$ *decays*, Phys. Lett. B **638**, 187–194 (2006) [arXiv:hep-ph/0604084].

[325] J. Gasser, B. Kubis, and A. Rusetsky, *Cusps in $K \to 3\pi$ decays: a theoretical framework*, Nucl. Phys. B **850**, 96–147 (2011) [arXiv:1103.4273 [hep-ph]].

[326] B. Kubis and U.-G. Meißner, *Virtual photons in the pion form-factors and the energy momentum tensor*, Nucl. Phys. A **671**, 332–356 (2000) [arXiv:hep-ph/9908261], [Erratum: Nucl. Phys. A **692**, 647 (2001)].

[327] S. Descotes-Genon and M. Knecht, *Two-loop representations of low-energy pion form factors and $\pi\pi$ scattering phases in the presence of isospin breaking*, Eur. Phys. J. C **72**, 1962 (2012) [arXiv:1202.5886 [hep-ph]].

Acknowledgements

After more than half a decade as a PhD student with all its ups and downs, the end is now in sight. Reaching this point would not have been possible without the support of many people, and therefore I want to express my deep gratitude to everyone who was (directly or indirectly) involved in the completion of this thesis.

Firstly, I would like to thank my thesis advisor, Bastian Kubis, for his outstanding supervision and continuous support during my PhD studies. I am grateful for countless fruitful discussions, his patience and constant optimism, especially when unexpected complications arose. It has been a great pleasure to work with him and benefit from his vast experience and knowledge. Secondly, I want to thank him for his encouragement to participate in numerous international conferences and workshops, giving me the opportunity to present my work to other experts in the field.

Furthermore, I thank Ulf-G. Meißner for being the second advisor of my PhD thesis and for supporting my attendance of conferences and workshops.

It has been an enriching experience to collaborate with Peter Stoffer and I am deeply grateful for all enlightening discussions and the rewarding teamwork. Additionally, I enjoyed many informative and helpful discussions with Gilberto Colangelo, Stefan Leupold, Jan Lüdtke, Bachir Moussallam, Judith Plenter, and many others at various occasions. I further thank Patrik Adlarson, Andrzej Kupść, and Sergey Prakhov for providing me with unpublished data and detailed explanations on the experimental analyses.

A very special thanks go to my office mates Bai-Long Hoid, Simon Holz, and Jonathan Lozano de la Parra. I will certainly miss our daily tea/coffee breaks and spontaneous dinner hang-outs. Thanks go to Ingrid and Maximilian Dax, Frederic Noël, Stefan Ropertz, and Dominik Stamen for the regular board game evenings, which were always fun and a welcome distraction. I owe thanks to Malwin Niehus for being a great travel companion, who was always up for touristic activities after the daily business of physics conferences. Thanks to Hakan Akdag, Christa Börsch, Christoph Hanhart, Christian Jost, Yannis Korte, Barbara Kraus, Stephan Kürten, Bernard Metsch, Johann Ostmeyer, Janak Prahbu, Martin Ueding, Markus Werner, Marvin Zanke, Falk Zimmermann, and other colleagues from the HISKP theory group for their help and very enjoyable working atmosphere.

Finally, I would like to thank my parents, brothers, and friends for their continuous support. Without their backing, I would not have been able to overcome the unavoidable low-points during the completion of this thesis.

Partial financial support by DFG and NSFC through funds provided to the Sino–German CRC 110 “Symmetries and the Emergence of Structure in QCD” (DFG Grant

No. TRR110 and NSFC Grant No. 11621131001), and by the Bonn–Cologne Graduate School of Physics and Astronomy is gratefully acknowledged.